EKMAGEION

Thesis by

Michael H. B. Stowell

In Partial Fulfillment of the Requirements

for the Degree of

Doctor of Philosophy

California Institute of Technology

Pasadena, California

Jan 7 1997

1997

Michael H. B. Stowell

Absolutely no rights reserved

Acknowledgments

Any scientific endeavor is a collaborative effort which relies upon the knowledge of the past as well as the present. The work that is presented herein has foremost been a collaboration with my advisors, Doug and Sunney, who allowed me to pursue my scientific interests wherever they led me and always offered encouragement and insight. I will always cherish my times at Caltech for the intellectually stimulating atmosphere that my two advisors provided me. It was a great privilege to have worked with two people who I consider not only brilliant scientific collaborators and mentors but also great friends.

This thesis is divided into two sections, and the second section is a specific tribute to the many brilliant collaborators that I have had the privilege to work with during my Ph.D. career at Caltech, and is a true testimony to the great benefits of scientific collaboration for the sake of knowledge. All the work presented herein could not have taken place with out the efforts of these individuals. Randy Larsen and Jay Winkler were responsible for my interests in studying electron transfer kinetics. Ted DiMagno continued my education on laser spectroscopy and rapid electron transfer studies and methodologies. Ron Rock, Guanyang Wang, and Eric Carriera have been essential to my synthetic efforts and always offered useful and insightful suggestions. Fascinating new results on nitrogenase have been the result of intellectually stimulating collaboration with John Peters, who has tried to teach me everything about nitrogenase but I still don't get it. Work on developing simple methods for MIR phasing with xenon have been performed with Mike Soltis, who is always willing to try out new ideas. Recent studies on succinate:quinone oxidoreductase have been spearheaded by Reggie Waldeck along with Hung-Kay Lee and Shao-Ching Hung and they have taught me alot about EPR. Tim McPhillips, Ed Abresch and George Feher were essential to the crystallographic studies on the photosynthetic reaction center. Siegfried Musser has been my intellectual sounding board for much of my career at Caltech and his sharp mind and insightful comments have been a great attribute,

not only to our collaborative efforts on the cytochrome bo_3 complex, but also to my other research efforts as well. His input will surely be missed in my future scientific endeavors.

I would also like to thank Leemor Joshua-Tor, Arthur Chirino, and Barbara Hsu, for helping me understand protein crystallography. Robert Spencer and Geoff Chang for their SQR cloning efforts and their shared enthusiasm for membrane protein structure. Sean Elliot for explaining the intricacies of pMMO. Jamie Schlessman for insights into the nitrogenase system. Brian Shultz for discussions on the mechanism of the cytochrome bo_3 complex. Salem Fahem for helpful discussions on structure solution by molecular replacement. Ben Ramirez for interesting discussions and the ever important organization of the BI social hour. Yaoying Su for correcting my illconcieved ideas about protein folding. Mike Day for introducing me to SHELX and small molecule crystallography. Dennis Anderson for help with NMR spectroscopy. Michael Weiner and Gil Prive for helpful discussions on membrane protein crystallization. Brian Ackrell and Gary Ceccini for support on the SQR project. Dan Vaughn for helpful crystallographic discussions and good humor. Ray, Guy, Tony and Mike for help in the shops. All the members of the Chan and Rees labs for there help over the years. My family for their support. And lastly, old broad shoulders and the philosopher kings for suggesting it all in the first place.

Abstract

Membrane proteins compose roughly 30% of the proteins in a living organism. Furthermore, they are the essential link between the outside world and the cell. A large number of important processes occur in the biological membranes; these include the production of cellular energy, the transmission of nerve impulses, and the perception of light and sound. Knowledge of how these systems are constructed and how they function is critical to understanding the biological world around us as well as ourselves. The studies presented herein were aimed at gaining an understanding of such systems through the combination of both structural and functional analysis of these systems. The results presented here are the author's efforts to understand such systems and in the process develop methods and techniques which help others understand such systems or related ones. This thesis is divided into two sections. The first section is devoted solely to the investigation of membrane proteins. An introductory discussion on the structure and stability of membrane proteins is presented followed by studies on the photosynthetic reaction center, succinate:quinone oxidoreductase, cytochrome c oxidase, and the development of methods for studying rapid electron transfer in ubiquinone:cytochrome-c oxidoreductases and ubiquinol oxidases. The second section is a compilation of theoretical, methodological, synthetic, and biophysical studies. These include the development of MIRAS phasing methods using xenon gas, facile synthetic methods for benzoin compounds, development of universal photoreduction compounds, theoretical models for proton pumping mechanisms in ubiquinol oxidases, and structural studies on a leucine-rich repeat variant protein.

Contents

Section I

Section II

Chapter I

Introduction: Structure and Stability of Membrane Proteins

Reprinted from Advances in Protein Chemistry

STRUCTURE AND STABILITY OF MEMBRANE PROTEINS

By MICHAEL H. B. STOWELL and DOUGLAS C. REES

Division of Chemistry and Chemical Engineering, California Institute of Technology, Pasadena, California 91125

I. Introduction

It is a fundamental tenet of present-day structural biology that the unique tertiary structures of proteins reflect the strongly stabilizing influence of hydrophobic interactions (Kauzmann, 1959; Tanford, 1980; Baldwin, 1986; Dill, 1990). According to this view, protein folding is driven by the positioning of apolar residues in the protein interior, where they are shielded from exposure to the aqueous solution by surrounding polar residues. Relative to the unfolded state, the native state of a protein will be stabilized by the sequestering of nonpolar residues from the aqueous environment; estimates of the contribution of these hydrophobic interactions to protein stability obtained from calorimetry (Baldwin, 1986) and transfer experiments of amino acid analogs (Tanford, 1980) are in the range of a few hundred kilocalories/mole. Because water-soluble proteins are stable by only ~15 kcal/mol relative to the unfolded state (Privalov, 1979; Privalov and Gill, 1988), hydrophobic effects are

ADVANCES IN PROTEIN CHEMISTRY, Vol. 46

Copyright © 1995 by Academic Press, Inc.
All rights of reproduction in any form reserved.

expected to provide an indispensable contribution to protein stability. Accordingly, if hydrophobic effects could be somehow "turned off," one would predict that stable tertiary protein structures could not possibly be formed. As a corollary, it would also seem that proteins could only adopt stable tertiary structures in an aqueous environment, because by definition, hydrophobic effects cannot exist in the absence of water. Despite such predictions, however, many proteins do adopt stable tertiary structures in predominantly nonaqueous environments. Examples of such proteins include membrane proteins, which fold with the bulk of their tertiary structure located within the nonpolar environment of the lipid bilayer, as well as nonmembrane proteins, such as the plant seed proteins crambin and zein, which are quite soluble and stable in nonaqueous solvents (Llinás *et al.*, 1980). Because these proteins exist in primarily apolar environments, the contribution of the hydrophobic effect to their stability is expected to be greatly diminished (Engelman, 1982). Thus, the critical question arises: If the hydrophobic theory of protein stability is correct, how is it possible for stable proteins to exist in nonaqueous environments where hydrophobic effects should be quantitatively less significant? This question will be addressed in light of the available structural and stability data on integral membrane proteins, emphasizing a comparison of these properties to those of better characterized water-soluble proteins.

II. Membrane Protein Structure

The past few decades have witnessed four important developments in the structural analysis of membrane proteins: (1) The 7-Å resolution structure of bacteriorhodopsin (BR) determined by Henderson and Unwin (1975), followed by the subsequent high-resolution structural analysis at 3.5 Å resolution (Henderson *et al.*, 1990). (2) The 2.3-Å resolution structure of the photosynthetic reaction center (RC) from *Rhodopseudomonas viridis* (Deisenhofer *et al.*, 1984, 1985; Deisenhofer and Michel, 1989), and the homologous reaction center from *Rhodobacter sphaeroides* (Allen *et al.*, 1986, 1987; Chang *et al.*, 1986, 1991; Ermler *et al.*, 1992). (3) The 1.8-Å resolution structure of the outer membrane protein, porin (POR) from *Rhodobacter capsulatus* (Weiss *et al.*, 1990), and the homologous *Escherichia coli* porin structures (Cowan *et al.*, 1992). (4) Finally, and most recently, the structure of the light-harvesting complex from photosystem II (LHCII), determined at 3.4 Å resolution by Kühlbrandt and coworkers (Kühlbrandt *et al.*, 1994). Each of these landmarks in membrane protein structure analysis will be briefly discussed, with an emphasis on their implications for membrane protein stability.

BR is present in the purple membrane of the salt-loving *Halobacterium halobium,* where it functions as a light-driven proton pump. The initial structural investigation of BR at 7 Å resolution revealed seven rodlike features that were identified as transmembrane-spanning α helices (Henderson and Unwin, 1975). This groundbreaking work established the significance of the α helix as an important structural element of integral membrane proteins, and catalyzed efforts both to understand the important elements of membrane protein folding and to predict the topologies of membrane proteins based on sequence analysis (Engelman *et al.,* 1980; Kyte and Doolittle, 1982; Eisenberg *et al.,* 1984; Engelman *et al.,* 1986). Those efforts directed toward the sequence-based identification of potential membrane-spanning α-helical segments have been relatively fruitful and are routinely used today in the analysis of membrane protein sequences.

BR forms a trimer in the membrane, with each monomer composed of seven transmembrane-spanning α helices that contain 20–25 amino acids/helix. The helices are designated A through G, in order of appearance in the amino acid sequence. The topology of the monomer can be described as an up–down multihelical bundle, with segments adjacent in the sequence located nearby in the structure, thus minimizing the length of the loop regions. The contact surfaces in the BR trimer are formed between each monomer and the adjacent monomers in a head-to-tail fashion (Fig. 1). The intermonomer contacts form a loose network of hydrogen bonds and hydrophobic interactions generated primarily by contacts between helix B from one monomer and helices E′ and D′ of the neighboring monomer. There are no intermolecular contacts about the threefold trimer axis, which results in a sizable cavity in the central core of the trimer. The external surface of the trimer is very hydrophobic, with the majority of exposed residues consisting of nonpolar, aliphatic residues. Transfer free energy calculations (Yeates *et al.,* 1987; Rees *et al.,* 1994) estimate the thickness of the bilayer-spanning region of BR to be 35 Å. Tryptophan residues, the most abundant aromatic amino acid in BR, are clustered primarily within the interior of a single monomer, whereas tyrosine residues participate in a number of hydrogen-bonding interactions at the monomer–monomer interface. There is a distinctive ring of aromatic residues (Fig. 2) located at the presumed water–bilayer interface, as is observed in both the RC and POR structures (see below). The BR core may be divided into two regions, the interior of the proton channel (which includes the retinal chromophore Schiff base) and a hydrophobic core (which also serves as the

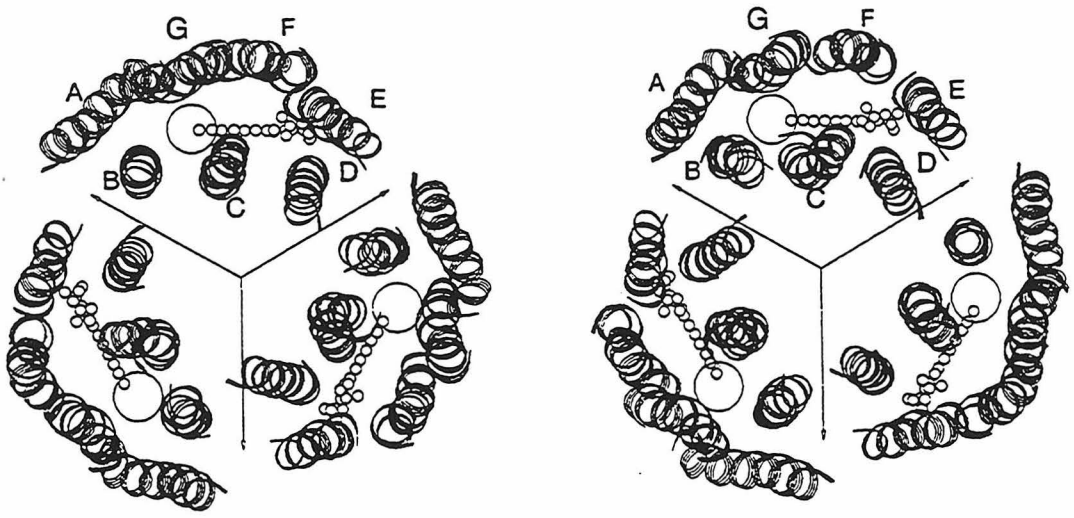

FIG. 1. Stereoview of bacteriorhodopsin. Helices A through G are labeled and the retinal chromophore is illustrated in ball and stick form. The approximate location of the proton channel is indicated by the circle that encloses the retinal chromophore Schiff base. Coordinate set 1BRD of the Brookhaven Protein Data Bank (Bernstein *et al.*, 1977) was used for this figure.

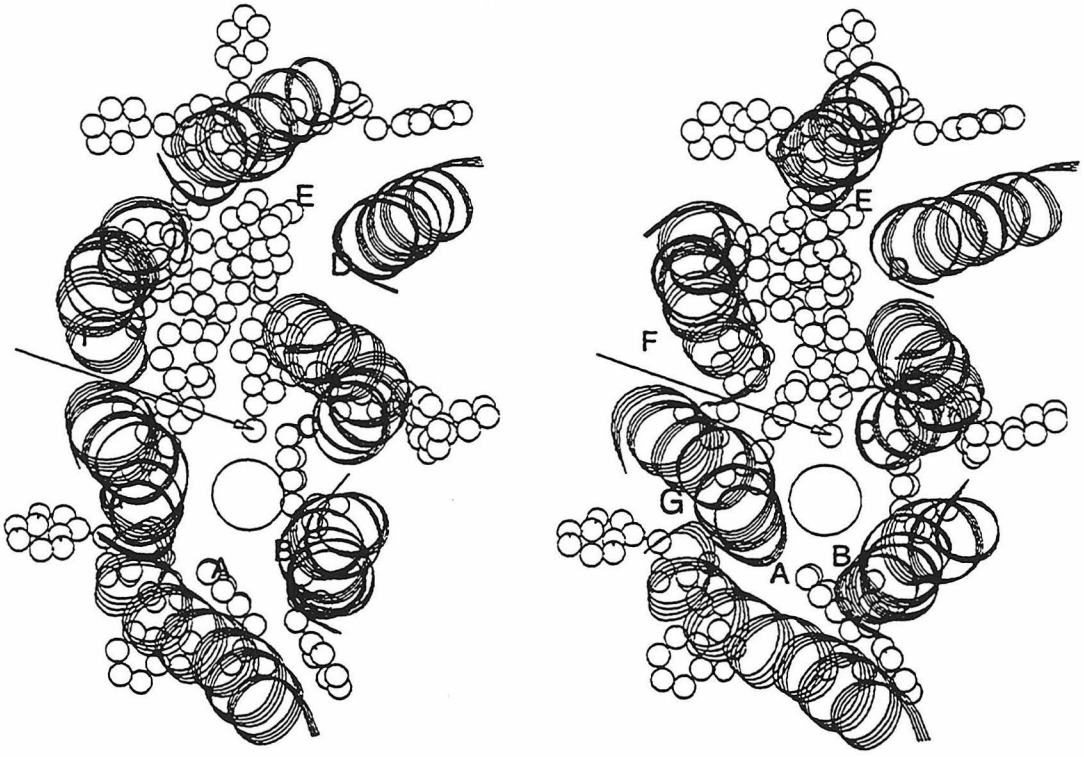

FIG. 2. Stereoview of a single bacteriorhodopsin monomer showing the location of the hydrophobic aromatic residues, depicted in ball and stick format. A ring of aromatic residues surrounds the bacteriorhodopsin monomer. A large number of tryptophan residues comprise the hydrophobic core located adjacent to the proton channel, approximated by the circle. The retinal chromophore Schiff base is located at the arrow.

pocket for the retinal chromophore) (Fig. 2). The hydrophilic region undoubtedly reflects the proton pumping function of BR and represents the only hydrophilic part of the protein interior. The hydrophobic core comprises the major part of the internal volume, however, so that overall the BR interior is similar in nature to the hydrophobic core of water-soluble proteins (Rees *et al.*, 1989a).

B. Photosynthetic Reaction Center

Photosynthetic reaction centers are integral membrane proteins responsible for the primary step in photosynthesis, the conversion of photochemical energy into electrochemical energy. The RC from *Rps. viridis* was the first membrane protein structure to be determined at atomic resolution and unambiguously demonstrated than an α helix could span the membrane bilayer. The structure also provided detailed insights into the folding pattern and molecular interactions of the RC, and provided a structural model for the spatial organization of the cofactors participating in the light-driven electron transfer reactions. The RCs from both *Rps. viridis* and *Rb. sphaeroides* are composed of three separate membrane-spanning subunits designated L, M, and H. A central feature

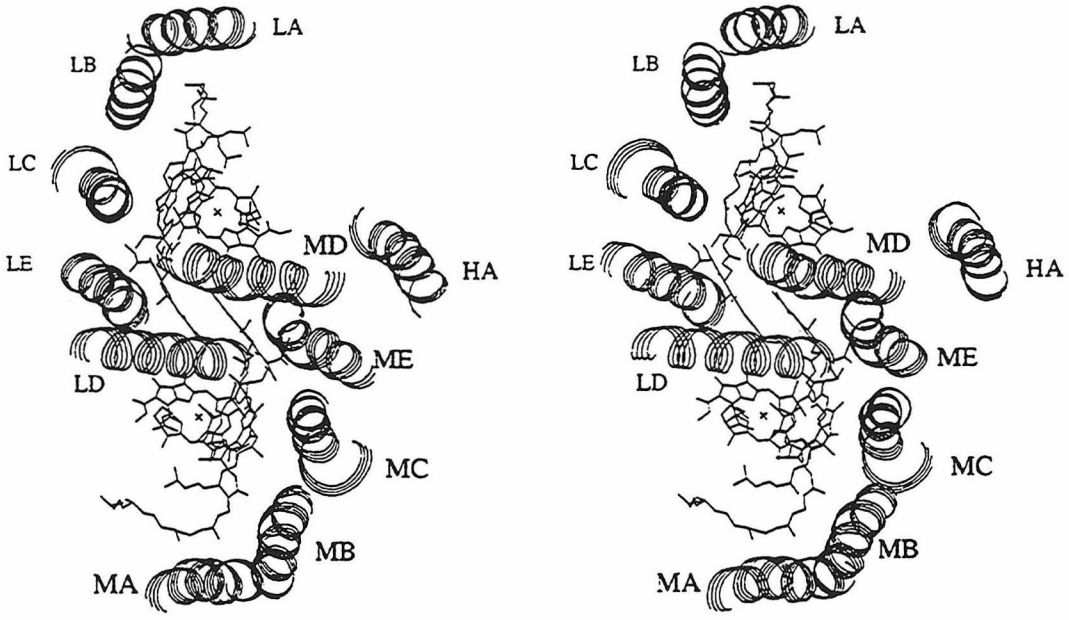

FIG. 3. Stereoview of the *Rb. sphaeroides* RC viewed down the pseudo-twofold axis. The helices are labeled according to the text and the chromophores are depicted in stick format. The central core of the protein is composed of helices LE, LD, ME, and MD, which surround the bacteriochlorophyll special pair. Coordinate set 4RCR of the Brookhaven Protein Data Bank (Bernstein *et al.*, 1977) was used for this figure.

of the RC structure is the presence of 11 hydrophobic α helices, each containing approximately 20–30 residues. The L and M subunits are homologous, and contain five transmembrane helices each. These helices are designated A through E in order of appearance in the protein sequence, prefixed with either L or M to designate the particular subunit. The H subunit contains a single transmembrane helix (HA) and adopts the majority of its fold outside the membrane bilayer (Figs. 3 and 4). Helices in the L or M subunits are arranged in a single layer. As with BR, helices adjacent in sequence tend to be adjacent in the structure, with the consequence that the majority of helix–helix interactions are antiparallel. The photosynthetic cofactors are predominantly positioned between the helices. The core of the RC is similar in hydrophobicity to the interior of water-soluble proteins, whereas the external surface is more hydrophobic (Rees *et al.*, 1989a). This characteristic difference

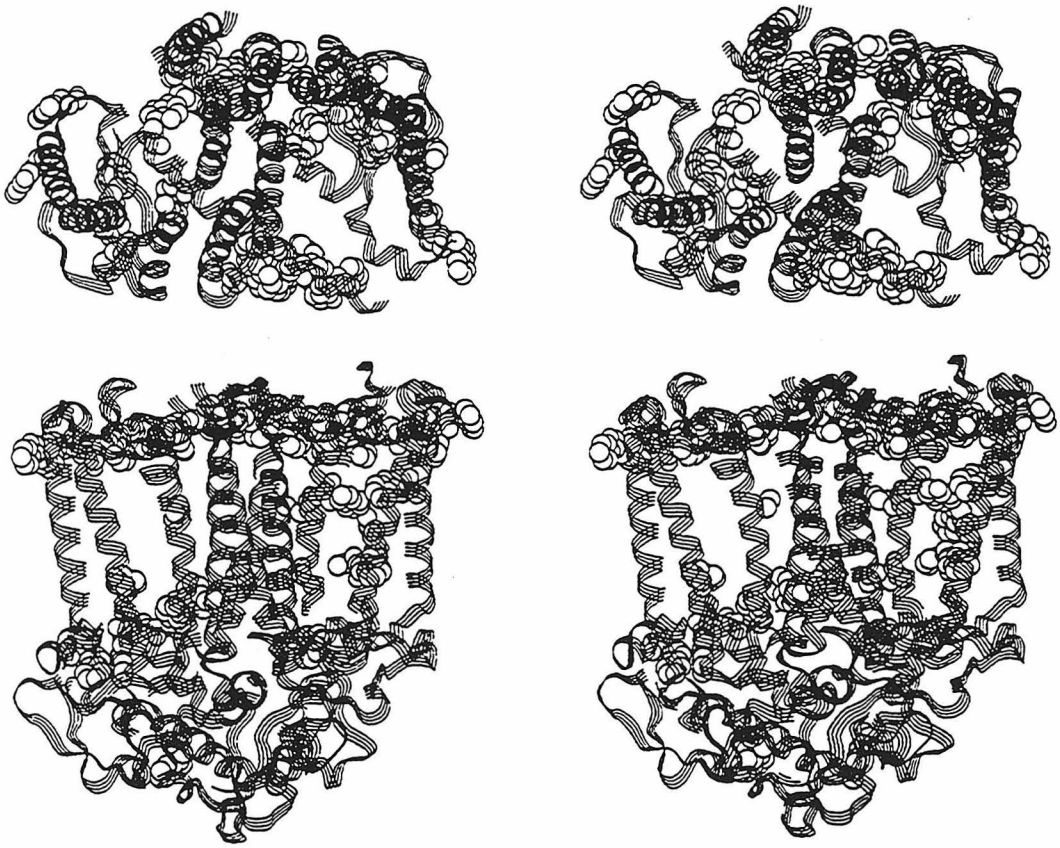

FIG. 4. Stereoview of the *Rb. sphaeroides* RC showing the ring of tryptophan residues located at the water–lipid interface. The top figure is viewed from the special pair toward the nonheme iron; the bottom figure is viewed in the plane of the membrane bilayer. The extramembranous portion of subunit H is evident in the bottom stereopair.

in hydrophobicity between the inner and outer surfaces of the helices generates an amphipathic pattern that can be detected by analysis of the protein sequence. Around the RC, there is a prominent ring of tryptophan residues localized at the presumed water bilayer interface (Fig. 4) (Deisenhofer and Michel, 1989; Schiffer *et al.*, 1992; Cowan, 1993), which may serve as a polarizable "buffer" between the high dielectric media of water and the low dielectric media of the membrane bilayer, or to help maintain the position of the protein in the bilayer.

C. Matrix Porin

Although the first membrane protein structures to be determined, BR and RC, are composed primarily of α helices, the structure of the outer membrane protein porin demonstrated that this folding topology is not a universal property of membrane proteins. The most striking feature of the porin structure is the formation of a 16-stranded, antiparallel β-barrel structure that traverses the membrane (Weiss *et al.*, 1991; Cowan, 1993). The inside of the β barrel forms an aqueous pore through which metabolites can pass. Because sequential residues along a β strand are oriented toward alternate sides of the β sheet, the barrel contains residues that, to first order, are hydrophobic on the external membrane-facing side and hydrophilic on the pore side (Fig. 5). It would seem that porin truly satisfies the requirements of an "inside-out" protein (Engelman

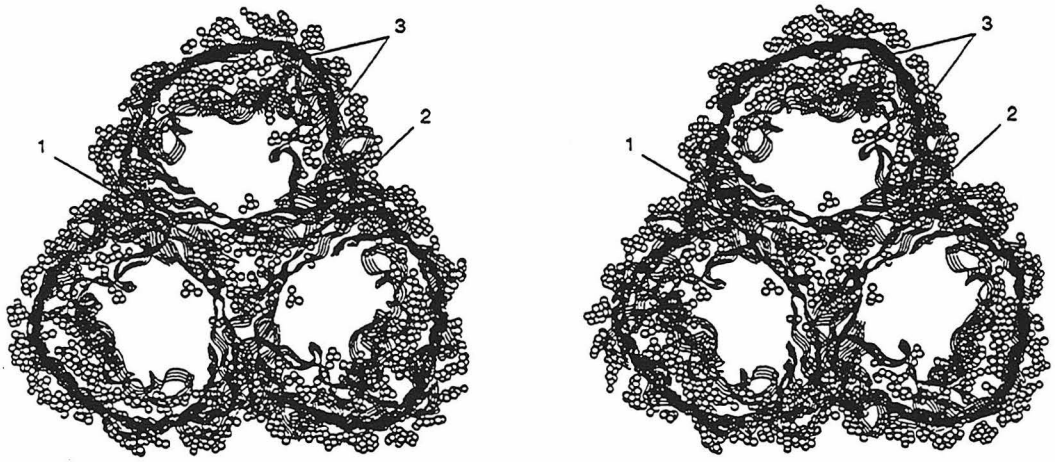

FIG. 5. Stereoview of the *Rb. capsulatus* porin viewed down the threefold trimer axis. Hydrophobic residues are shown in ball and stick format. The three hydrophobic core regions are labeled: 1, the hydrophobic core of the trimer axis; 2, the hydrophobic monomer–monomer interface; and 3 the hydrophobic core formed by the extended loop L3. Coordinate set 1POR of the Brookhaven Protein Data Bank (Bernstein *et al.*, 1977) was used for this figure.

and Zaccai, 1980), with a hydrophobic exterior and with the identification of the internal aqueous pore as forming the polar interior. Important aspects of the porin structure are the trimeric nature and an extended two-stranded sheet in the interior of the β barrel (designated L3, Fig. 5), which together give porin a tripartite hydrophobic organization consisting of an external membrane-facing side, a central mostly hydrophobic core, and a hydrophilic inner surface that forms the aqueous channel. The trimer contacts of porin comprise approximately 35–40% of the exposed surface of the molecule, whereas the two-stranded internal β sheet provides about 25% of the exposed internal surface. The trimer contact regions are tightly packed, with regions of stacked aromatic residues as well as interdigitated aliphatic residues. The extended two-stranded loop, designated L3, along with the internal surface of the monomer barrel, also generates a tightly packed hydrophobic core (Fig.

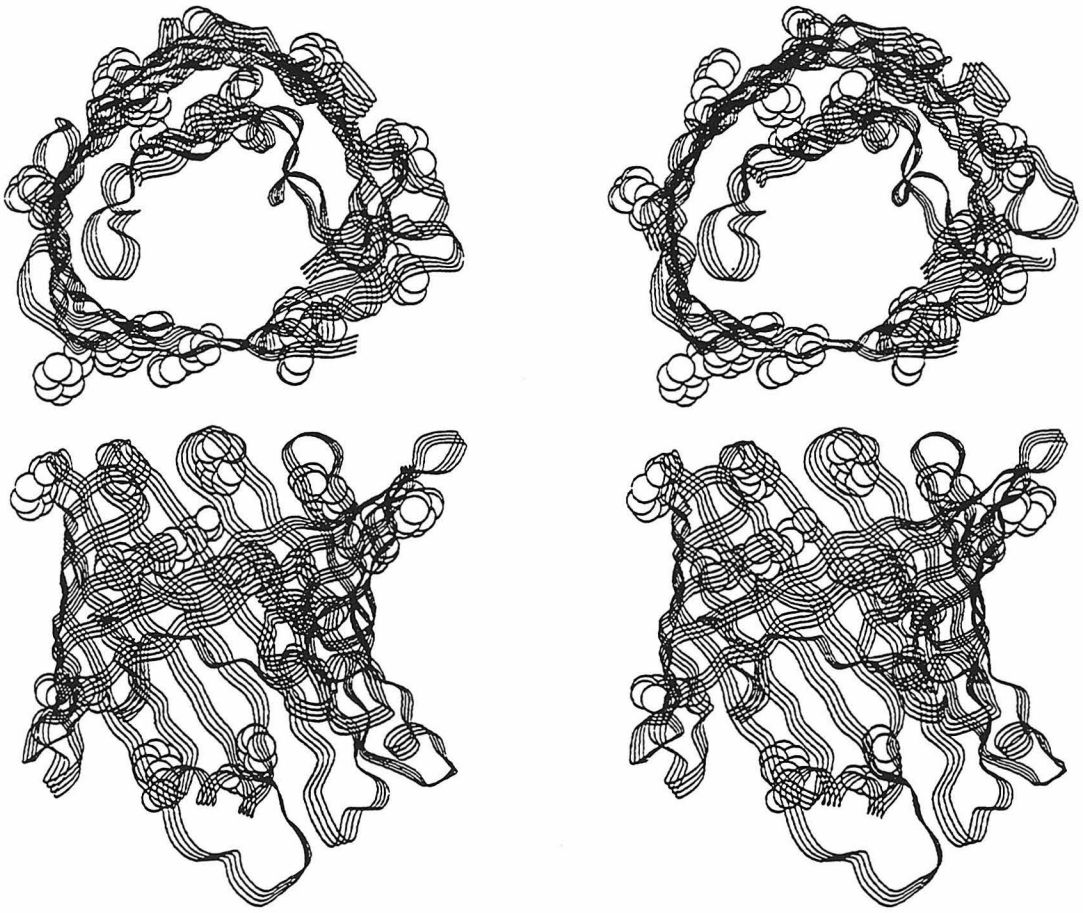

FIG. 6. Stereoview of the *Rb. capsulatus* porin illustrating the ring of phenylalanine residues located at the water–lipid interface. The top figure is viewed normal to the membrane bilayer; the bottom figure is viewed in the plane of the membrane bilayer.

5). Thus, porin would appear to have a discontinuous hydrophobic core. The relative instability of porin monomers compared to porin trimers (Rosenbusch, 1974) would be explained if the trimer interactions do indeed form a hydrophobic core of this protein and are therefore partly responsible for the stability of porin. As with the RC, a very pronounced ring of aromatic residues (tyrosine in this case) is located at the presumed water–lipid interface (Fig. 6).

D. Light-Harvesting Complex II of Photosystem II

The LHCII is an important element of photosystem II (PSII), which is responsible for the funneling of photons to the reaction center of PSII. LHCII is composed of an approximately 25-kDa polypeptide together with a minimum of 12 chlorophyll and 2 carotenoid (lutein) molecules. LHCII contains three transmembrane helices and adopts a trimeric structure in the chloroplast membrane. The structure of LHCII has been determined at 3.4 Å resolution by electron crystallography (Kühlbrandt *et al.*, 1994). This structure has several important features with interesting ramifications for membrane protein structure and stability. The LHCII polypeptide contains three transmembrane helices, A, B, and C. There is also a small fourth helix, designated D, which is positioned perpendicular to the membrane normal. Helix A and helix B form a left-handed supercoil in the central core of the complex (Fig. 7). This supercoil is stabilized by a set of ion pairs between Arg^{70}-Glu^{165} and Glu^{65}- Arg^{185}. Additionally, two lutein molecules bind to the grooves of the supercoil, so that the A and B helices and the two luteins form a pseudo "four-helix" bundle at the central core of the complex. The important structural role of the luteins is evidenced by the observation that their presence is essential to the stability of the LHCII and is required for the protein to fold into a stable tertiary structure (Paulsen *et al.*, 1993). Helix C is somewhat removed from the internal core formed by the A and B helices, and exhibits the most sequence variability of the three transmembrane helices. Given the large number of bound chlorophylls, residues in the A and B helices do not actually contact the membrane. Consequently, helix C is the only polypeptide segment of LHCII that has substantial interactions with the membrane bilayer. Overall, less than 36% of the LHCII polypeptide is within the membrane bilayer region, resulting in the presence of equal masses of polypeptide and chromophore within the membrane bilayer. Furthermore, a large portion of the interaction of the complex with the membrane bilayer is mediated by the chlorophylls, and not protein, because only helix C maintains contact with the bilayer. This is a very different situation from that observed with either

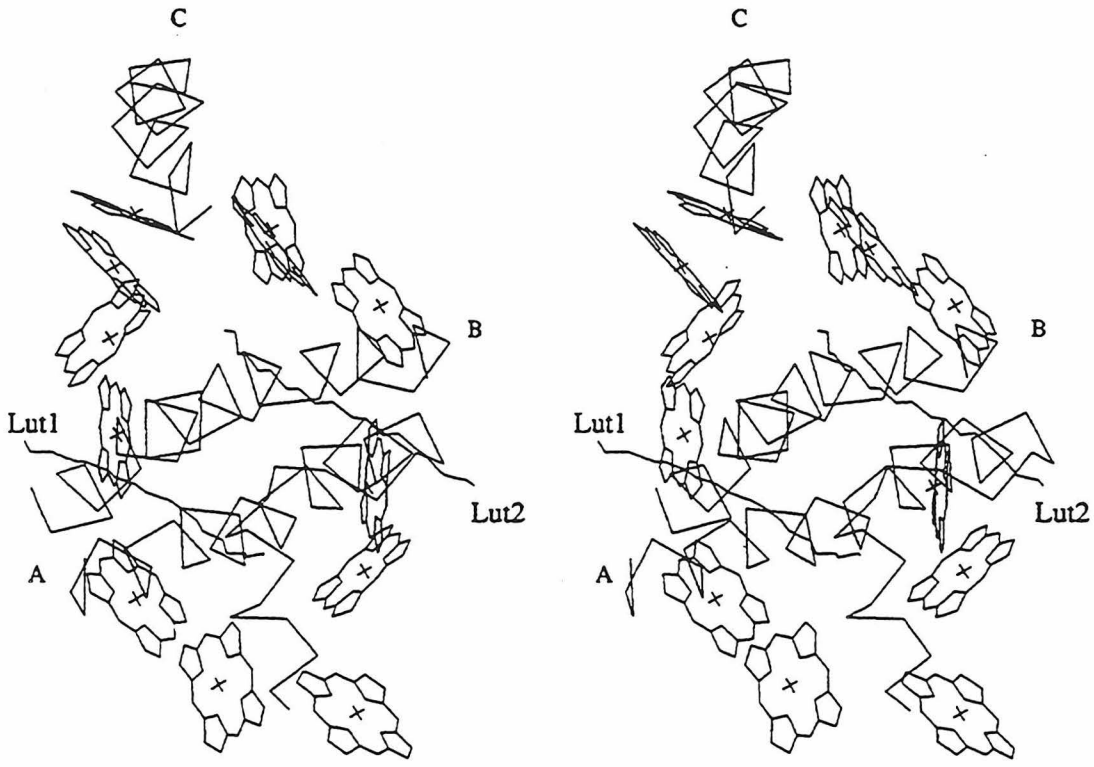

FIG. 7. Stereoview of LHCII viewed normal to the membrane bilayer. The helices are labeled according to the text; the luteins are labeled Lut1 and Lut2. Coordinates supplied courtesy of W. Kühlbrandt.

BR or RCs, wherein the various chromophores are surrounded by polypeptide and compose substantially less than 50% of the molecular mass contained within the membrane bilayer.

E. Other Membrane Proteins

At present, the structural data available for membrane proteins are limited, relative to water-soluble proteins. This lack of structural data reflects the current difficulty in obtaining well-diffracting crystals of membrane proteins. Much effort has gone into ameliorating this problem, and several new approaches to membrane protein crystallization are being investigated, including the use of "peptidetergents" (Schafmeister *et al.*, 1993) and novel fusion proteins (Prive *et al.*, 1994). The techniques of electron diffraction also continue to improve, and their ability to describe membrane proteins structurally at medium to high-resolution ensures that these methods will remain an important tool for such investigations. Several structural studies will offer more insights into membrane

proteins, such as the X-ray structure of photosystem I, described at 6 Å resolution (Krauss *et al.*, 1993). Electron crystallographic work on the acetylcholine receptor (Unwin, 1993) intriguingly suggests that the membrane-spanning regions of this protein may have mixed α-helical and β-sheet secondary structure. Studies on peripheral membrane proteins, including prostaglandin synthase (Picot *et al.*, 1994) and lipase–procolipase (Vantilbeurgh *et al.*, 1993), have provided structural information about this important class of membrane proteins. Undoubtedly, other studies are also in progress that will give new and important insights into the relatively uncharacterized realm of membrane protein structure.

F. General Structural Features of Membrane Proteins

Based on analyses of the available three-dimensional structures, the following general features of membrane proteins have been described (Rees *et al.*, 1989b, 1994; Yeates, 1993). Given the limited structural data available for membrane proteins, however, the reader should be keenly aware that these observations and deduced generalizations are based on a very limited sampling. Consequently, as much as the authors may hope that these views are correct, they may well turn out to need "some" modification as more detailed structural information on membrane proteins becomes available.

1. Membrane proteins with known three-dimensional structures exhibit a relatively simple up–down topology transversing the membrane, such that residues nearby in the sequence tend to be nearby in the structure. This behavior may reflect constraints associated with insertion of the folding polypeptide chain into the lipid bilayer (Engelman and Steitz, 1981). As suggested by the preliminary structural data for the acetylcholine receptor (Unwin, 1993), however, more complex tertiary folds almost certainly exist, and the details of these structures will be eagerly awaited.

2. Surface residues in the bilayer-spanning region of integral membrane proteins tend to be more apolar than the buried, interior residues. Although this is opposite to the hydrophobic organization characteristic of water-soluble proteins, the interior of membrane proteins (with the exception of torodial shaped proteins such as porin, which have aqueous-filled internal channels) is not polar. Rather, the average hydrophobicities of buried residues in both water-soluble and membrane proteins are nearly identical.

3. The packing volume of buried residues in the *Rb. sphaeroides* RC is very similar to that observed in water-soluble proteins, implying that

the same types of efficient packing interactions are seen in both classes of proteins. Furthermore, there is no significant difference in the accessible surface area of the *Rb. sphaeroides* RC and oligomeric, water-soluble proteins of comparable size.

Although the folding environments of water-soluble and integral membrane proteins differ significantly, the structural consequences of these different folding environments is surprisingly minimal. With the exception of surface residue polarity, membrane proteins and water-soluble proteins share strong similarities in general features such as hydrophobicity of buried residues, surface area, and interior packing efficiency. These observations are reminiscent of the solvent dependence of crystal morphology; while maintaining the same types of internal packing interactions, the nature of groups on a crystal surface can be altered, by changing the crystal morphology, to minimize the surface energy for interaction with a particular solvent (Rees and Wolfe, 1993). In the case of water-soluble and membrane proteins, the same type of efficient interior packing is maintained, while the surface polarity of a protein varies with the solvent environment. A striking example of this is found in a protein family with both hydrophobic and hydrophilic members (Baud *et al.*, 1993). An important challenge is to rationalize these similarities in view of the apparently different roles hydrophobic interactions should have in stabilizing the tertiary structure folds of these two classes of proteins.

III. Biological Membranes and the Fluid Mosaic Model

Any discussion of membrane protein structure and stability is incomplete without a discussion of the properties of the lipid bilayer. The composition of the lipid bilayer can exhibit extreme variations from organism to organism and from organelle to organelle (Table I). Variations in membrane composition constitute an important facet of the ability of an organism to adapt to the environment. This adaptability is necessary not only for maintaining the passive function of the bilayer as a semipermeable barrier, but also to maintain the proper function and stability of the membrane proteins contained within the lipid bilayer. To understand the role of the lipid bilayer in membrane protein function, it is necessary to have some knowledge of the structural and thermodynamic properties of membrane bilayers and the effects that can be caused by variations in lipid composition. Perhaps surprisingly, subtle changes in the membrane bilayer composition can have a dramatic effect on the myriad of possible phases that the membrane bilayer can adopt, as well

TABLE I
Selected Membranes and Corresponding Lipid Compositions[a]

Membrane	PE	PC	PG	PI	PS	PA	S	DPG	GD	SM
Nuclear	26	53	—	7.1	—	—	—	—	—	13
Mitochondrial (inner)	37	41	3	5	—	—	—	14	—	1.4
Mitochondrial (outer)	24	42	10	21	—	—	—	3	—	3.4
Chloroplast (thylakoid)	—	3	9	1	—	—	7	—	77	—
Erythrocytes (hen)	30.7	30.3	—	3.7	—	—	—	—	—	—
Erythrocytes (rat liver)	24.7	46.1	—	6.7	4.2	2	—	—	—	16.8
Golgi apparatus (rat liver)	17	45.3	12.3	6.3	8.7	—	—	—	—	4.2
Escherichia coli (inner)	74	—	19	—	—	—	—	3	—	—

[a]PE, Phosphatidylethanolamine; PC, phosphatidylcholine; PG, phosphatidylglycerol; PI, phosphatidylinositol; PS, phosphatidylserine; PA, phosphatidic acid; S, sulfolipid; DPG, diphosphatidylglycerol (cardiolipin); GD, galactosyldiglyceride; SM, sphingomyelin. Taken in part from Datta (1987) and Gennis (1989).

as the temperature at which these phase transitions occur (Quinn, 1981; Seddon, 1990).Two lipid phases of particular interest to biological membrane systems are the L_α and the H_{II} phases. The L_α, or liquid crystalline, phase, the fluid phase commonly observed for the lipid bilayer in biological systems, can be visualized by freeze–fracture experiments on whole cells. In the L_α phase, the fatty acid chains tend to be mobile and disordered. The H_{II}, or inverted hexagonal, phase, a lipid phase with a high radius of curvature at the head group–water interface, has been implicated in a number of cellular functions, including protein translocation and membrane fusion. Considerable effort has gone into understanding the thermodynamic forces that govern these two phases and the factors influencing their interconversion. The dominant properties that determine the phase of a lipid bilayer are the relative head group size and the length of the fatty acid acyl chain (Gruner, 1985). The head group size determines the spontaneous radius of curvature for the lipid bilayer, and the length of the acyl chain controls the hydrocarbon packing chain strain. Together, these two properties govern the phase-forming tendency of phospholipids, and will also influence how the phospholipids may pack against embedded membrane proteins.

The standard framework for describing the molecular details of biological membranes is the fluid mosaic model of Singer (Singer and Nicolson, 1972) that represents the membrane bilayer as a mosaic, composed of lipids interspersed with integral membrane proteins that span the lipid bilayer. Depending on the membrane system, lipids may constitute between 20 and 80% of the membrane mass. Both lipids and membrane proteins can diffuse laterally in the plane of the bilayer, in addition to

rotational motions around the membrane normal. The fluid mosaic model suggests an important role for the lipid in regulating membrane protein function, and also in stabilizing membrane protein structure. A role for the bilayer lipid composition in regulating the functioning of membrane proteins has been demonstrated in several studies. Experiments on rhodopsin have shown that the MI–MII transition in the rhodopsin photocycle is markedly effected by the presence of H_{II} forming phospholipids (Gibson and Brown, 1991; Mitchell *et al.*, 1992). Experiments with cytochrome c oxidase have demonstrated the important role of cardiolipin in the turnover cycle of this enzyme (Abramovitch *et al.*, 1990). Similar experiments with Ca^{2+}-ATPase have also demonstrated a functional role for H_{II} lipids (Navarro *et al.*, 1984). These experiments all demonstrate the significant relationship between the lipid bilayer composition and integral membrane protein function, and suggest that the regulation of membrane bilayer composition may be a method of regulating membrane protein function. These data also suggest that the lipid bilayer may play an important role in the stability or instability of membrane proteins (Section IV,C).

IV. Theoretical and Experimental Aspects of Protein Stability

A. *General Two-State Thermodynamic Model of Protein Stability*

Questions of protein stability are fundamentally thermodynamic in nature. Because the most extensive studies of protein stability have been conducted for water-soluble proteins, it is relevant to explore the thermodynamics of these systems in some detail to provide a framework for the corresponding discussion of membrane protein stability. For many water-soluble proteins, the thermodynamics of protein stability may be described by a two-state equilibrium model between the native (N) and denatured (D) forms of the protein: N $\leftrightharpoons$ D. For a two-state process with constant ΔC_p, the free energy of unfolding (ΔG_{ND}) for the N to D transition may be expressed as a function of temperature and pressure (Hawley, 1971):

$$\Delta G_{ND}(T,P) = \Delta H_m\left(\frac{T_m - T}{T_m}\right) - \Delta C_p\left\{T_m - T\left[1 - \ln\left(\frac{T}{T_m}\right)\right]\right\} + \frac{\Delta\beta}{2}(P - P_m)^2 + \Delta\alpha(P - P_m)(T - T_m) + \Delta V_m(P - P_m) \qquad (1)$$

where T_m and P_m are the transition and pressure for unfolding at a point where $\Delta G_{ND} = 0$; ΔH_m, $\Delta\alpha = (\partial\Delta V/\partial T)p$, $\Delta\beta = (\partial\Delta V/\partial P)_T$, and ΔV_m rep-

TABLE I
Selected Membranes and Corresponding Lipid Compositions[a]

Membrane	PE	PC	PG	PI	PS	PA	S	DPG	GD	SM
Nuclear	26	53	—	7.1	—	—	—	—	—	13
Mitochondrial (inner)	37	41	3	5	—	—	—	14	—	1.4
Mitochondrial (outer)	24	42	10	21	—	—	—	3	—	3.4
Chloroplast (thylakoid)	—	3	9	1	—	—	7	—	77	—
Erythrocytes (hen)	30.7	30.3	—	3.7	—	—	—	—	—	—
Erythrocytes (rat liver)	24.7	46.1	—	6.7	4.2	2	—	—	—	16.8
Golgi apparatus (rat liver)	17	45.3	12.3	6.3	8.7	—	—	—	—	4.2
Escherichia coli (inner)	74	—	19	—	—	—	—	3	—	—

[a]PE, Phosphatidylethanolamine; PC, phosphatidylcholine; PG, phosphatidylglycerol; PI, phosphatidylinositol; PS, phosphatidylserine; PA, phosphatidic acid; S, sulfolipid; DPG, diphosphatidylglycerol (cardiolipin); GD, galactosyldiglyceride; SM, sphingomyelin. Taken in part from Datta (1987) and Gennis (1989).

as the temperature at which these phase transitions occur (Quinn, 1981; Seddon, 1990).Two lipid phases of particular interest to biological membrane systems are the L_α and the H_{II} phases. The L_α, or liquid crystalline, phase, the fluid phase commonly observed for the lipid bilayer in biological systems, can be visualized by freeze–fracture experiments on whole cells. In the L_α phase, the fatty acid chains tend to be mobile and disordered. The H_{II}, or inverted hexagonal, phase, a lipid phase with a high radius of curvature at the head group–water interface, has been implicated in a number of cellular functions, including protein translocation and membrane fusion. Considerable effort has gone into understanding the thermodynamic forces that govern these two phases and the factors influencing their interconversion. The dominant properties that determine the phase of a lipid bilayer are the relative head group size and the length of the fatty acid acyl chain (Gruner, 1985). The head group size determines the spontaneous radius of curvature for the lipid bilayer, and the length of the acyl chain controls the hydrocarbon packing chain strain. Together, these two properties govern the phase-forming tendency of phospholipids, and will also influence how the phospholipids may pack against embedded membrane proteins.

The standard framework for describing the molecular details of biological membranes is the fluid mosaic model of Singer (Singer and Nicolson, 1972) that represents the membrane bilayer as a mosaic, composed of lipids interspersed with integral membrane proteins that span the lipid bilayer. Depending on the membrane system, lipids may constitute between 20 and 80% of the membrane mass. Both lipids and membrane proteins can diffuse laterally in the plane of the bilayer, in addition to

rotational motions around the membrane normal. The fluid mosaic model suggests an important role for the lipid in regulating membrane protein function, and also in stabilizing membrane protein structure. A role for the bilayer lipid composition in regulating the functioning of membrane proteins has been demonstrated in several studies. Experiments on rhodopsin have shown that the MI–MII transition in the rhodopsin photocycle is markedly effected by the presence of H_{II} forming phospholipids (Gibson and Brown, 1991; Mitchell *et al.*, 1992). Experiments with cytochrome c oxidase have demonstrated the important role of cardiolipin in the turnover cycle of this enzyme (Abramovitch *et al.*, 1990). Similar experiments with Ca^{2+}-ATPase have also demonstrated a functional role for H_{II} lipids (Navarro *et al.*, 1984). These experiments all demonstrate the significant relationship between the lipid bilayer composition and integral membrane protein function, and suggest that the regulation of membrane bilayer composition may be a method of regulating membrane protein function. These data also suggest that the lipid bilayer may play an important role in the stability or instability of membrane proteins (Section IV,C).

IV. Theoretical and Experimental Aspects of Protein Stability

A. *General Two-State Thermodynamic Model of Protein Stability*

Questions of protein stability are fundamentally thermodynamic in nature. Because the most extensive studies of protein stability have been conducted for water-soluble proteins, it is relevant to explore the thermodynamics of these systems in some detail to provide a framework for the corresponding discussion of membrane protein stability. For many water-soluble proteins, the thermodynamics of protein stability may be described by a two-state equilibrium model between the native (N) and denatured (D) forms of the protein: N $\leftrightharpoons$ D. For a two-state process with constant ΔC_p, the free energy of unfolding (ΔG_{ND}) for the N to D transition may be expressed as a function of temperature and pressure (Hawley, 1971):

$$\Delta G_{ND}(T,P) = \Delta H_m\left(\frac{T_m - T}{T_m}\right) - \Delta C_p\left\{T_m - T\left[1 - \ln\left(\frac{T}{T_m}\right)\right]\right\} + \frac{\Delta\beta}{2}(P - P_m)^2 + \Delta\alpha(P - P_m)(T - T_m) + \Delta V_m(P - P_m) \qquad (1)$$

where T_m and P_m are the transition and pressure for unfolding at a point where $\Delta G_{ND} = 0$; ΔH_m, $\Delta\alpha = (\partial\Delta V/\partial T)p$, $\Delta\beta = (\partial\Delta V/\partial P)_T$, and ΔV_m rep-

resent the enthalpy change, thermal expansivity factor, isothermal compressibility, and volume change for unfolding at (T_m, P_m), respectively. The entropy change at T_m is given by $\Delta S_m = \Delta H_m/T_m$. Provided ΔC_p, $\Delta\alpha$, and $\Delta\beta$ are independent of temperature and pressure, ΔG_{ND} is completely specified by the six parameters, T_m, ΔH_m, ΔC_p, $\Delta\alpha$, $\Delta\beta$, and ΔV_m. The dependence of ΔG_{ND} on T and P for a given set of solution conditions (pH, μ, etc.) defines a stability surface for a protein (Becktel and Schellman, 1987). Although pressure effects are often neglected, they are significant for the theoretical understanding of the thermodynamics of protein stability (Kauzmann, 1987). Additionally, pressure effects are relevant to more practical problems associated with marine barophilic organisms that grow under conditions of high hydrostatic pressure, and have possible applications to biotechnological processes.

In the physiological temperature range, to a good approximation, Eq. (1) may be expanded to second order in $(T - T_m)$ and $(P - P_m)$, yielding an expression for ΔG_{ND} with a quadratic dependence on T and P:

$$\Delta G_{ND}(T,P) = -\frac{\Delta C_p}{2T_m}(T - T_m)^2 - \frac{\Delta H_m}{T_m}(T - T_m) + \frac{\Delta\beta}{2}(P - P_m)^2 + \Delta\alpha\,(P - P_m)(T - T_m) + \Delta V_m(P - P_m) \qquad (2)$$

This quadratic form implies, at least mathematically if not always physically, that for a given pressure (or temperature), there will be two T values (or P values) where the protein undergoes denaturation. From Eq. (2), the temperature and pressure of greatest protein stability, T^* and P^*, occur at

$$T^* - T_m = -\frac{\Delta H_m \Delta\beta + T_m \Delta\alpha\, \Delta V_m}{\Delta C_p \Delta\beta + T_m(\Delta\alpha)^2} \qquad (3)$$

$$P^* - P_m = -\frac{\Delta C_p \Delta V_m - \Delta H_m \Delta\alpha}{\Delta C_p\Delta\beta + T_m(\Delta\alpha)^2} \qquad (4)$$

with the free energy of maximal stability given by:

$$\Delta G_{ND}(T^*, P^*) = \frac{\frac{\Delta H^2{}_m}{2T_m\Delta C_p} - \frac{\Delta V_m}{\Delta\beta}\left(\frac{\Delta V_m}{2} - \frac{\Delta H_m\Delta\alpha}{\Delta C_p}\right)}{\left(1 + \frac{T_m\Delta\alpha^2}{\Delta C_p\Delta\beta}\right)} \qquad (5)$$

or equivalently,

$$\Delta G_{ND}(T^*, P^*) = \frac{\frac{\Delta H^2{}_m}{2T_m\Delta C_p} + \Delta P_{max,T_m}\left(\frac{\Delta V_m}{2} + \Delta T_{max,P_m}\Delta\alpha\right)}{\left(1 + \frac{T_m\Delta\alpha^2}{\Delta C_p\Delta\beta}\right)} \quad (6)$$

where $T_m + \Delta T_{max.\,P_m} \equiv T_m - \Delta H_m/\Delta C_p$ is the temperature of maximal protein stability at $P = P_m$, and $P_m + \Delta P_{max,T_m} \equiv P_m - \Delta V_m/\Delta\beta$ is the pressure of maximal protein stability at $T = T_m$. In the absence of pressure effects, the maximal stability of a protein is given by

$$\Delta G_{ND}(T^*) \cong \frac{\Delta H^2{}_m}{2T_m\Delta C_p} \quad (7)$$

where $T^* = T_m - \Delta H_m/\Delta C_p$.

Formally, the maximum stability of a protein at T^* can be increased by some combination of increasing ΔH_m, decreasing T_m, and/or decreasing ΔC_p. If pressure effects are included, then maximal stability can be enhanced for increased values of ΔV, negative values of $\Delta\beta$ that approach 0, or smaller values of $\Delta\alpha$.

B. Water-Soluble Proteins and the Hydrophobic Effect

Although this review focuses on membrane proteins, given the paucity of experimental data on membrane protein stability and the relatively extensive experimental studies on the stability of water-soluble proteins, this latter group provides an appropriate starting point for developing a framework for understanding membrane proteins. From calorimetric studies of the stability of small, globular, water-soluble proteins, the following general observations have emerged [reviewed in Privalov (1979, 1990); Privalov and Gill (1988); and Murphy and Freire (1992)]:

1. The unfolding of proteins can often be characterized thermodynamically in terms of a transition between two states, N and D. Although intermediates between N and D can exist that may be significant for folding kinetics and pathways, their populations are often too low to contribute to the overall unfolding thermodynamics of these proteins. A notable exception to this generalization is the existence, for proteins such as lactalbumin, under some conditions of a relatively highly populated molten-globule intermediate between the N and D states [reviewed in Christensen and Pain, 1991].

2. The unfolding of water-soluble proteins is associated with a large, positive ΔC_p of unfolding. Thermodynamic studies of hydrophobic interactions demonstrate that the exposure of apolar groups is characterized by a large, positive ΔC_p. Accordingly, observation of a large, positive ΔC_p during protein denaturation is widely interpreted as reflecting the contribution of hydrophobic interactions to water-soluble protein stability. Consistent with this interpretation, the magnitude of ΔC_p has been shown to be proportional to the estimated exposure of nonpolar surface area during protein unfolding. More recent work has extended these initial observations to include a negative contribution to ΔC_p generated from the exposure of buried polar surface (peptide bonds, etc.) during protein unfolding (Murphy and Freire, 1992).

Due to the nonzero ΔC_p, the enthalpy of unfolding for a given protein measured at T_m, ΔH_m will change with variation in conditions (pH, denaturants, etc.) that alter the stability of the protein. In particular, because $\Delta C_p > 0$, ΔH_m will decrease with decreasing T_m. The slope of the dependence of ΔH_m on T_m provides a convenient mechanism for estimating ΔC_p for protein denaturation. Strikingly, when the temperature dependence of the specific enthalpy of unfolding (calories/gram) is examined for a range of water-soluble proteins, a nearly universal convergence toa value 13 cal/g at T = 110°C is observed (Privalov, 1979). Although the interpretation of this convergence value is still debated, it appears to reflect a characteristic energy associated with nonsolvation interactions such as packing and hydrogen bonding (Privalov, 1979; Fu and Freire, 1992). Additionally, this convergence temperature enthalpy value should provide a useful benchmark for comparison of the experimental unfolding enthalpies of both water-soluble and membrane proteins.

3. Energetically, the stabilizing and destabilizing interactions involved in protein folding are rather closely balanced, with a net difference of about 15 kcal/mol favoring protein folding under optimal conditions. Neglecting pressure effects for the moment, the free energy of maximal protein stability occurs at the temperature T^* and, from the derivation above, is approximated by Eq. (7). For a "typical" water-soluble protein such as lysozyme at pH 4, ΔH_m = 140 kcal/mol, T_m = 350 K, and ΔC_p = 1.6 kcal/mol/K, giving T^* = 263 K and $\Delta G_{ND}(T^*)$ = 17.5 kcal/mol (Privalov and Khechinashvili, 1974). Similar stabilizing energies have been observed for a variety of water-soluble, globular proteins, which leads to the somewhat surprising conclusion that, to a reasonable approximation, the stabilities of different proteins are independent of molecular size.

4. At low pressures, the volume change associated with protein denaturation is often positive ($\Delta V > 0$), which means that the volume of the

D state is greater than the N state. Under these conditions, increasing pressure will stabilize the N form of the protein. The D state is more compressible than N ($\Delta\beta < 0$), however, so that as the pressure increases, the volume difference between N and D, ΔV, approaches zero and eventually becomes negative. Consequently, in this regime, increasing pressure destabilizes N, ultimately leading to pressure denaturation. As noted by Kauzmann (1987), this behavior is quite different than expected from the solubility of low molecular weight, apolar compounds in water. For these systems, ΔV for transfer of apolar compounds to water is negative at low pressures and positive at higher pressures, which is just the opposite of that observed for protein denaturation. A satisfactory interpretation of this behavior has yet to be provided.

The pressure dependence of the stability of water-soluble proteins has been investigated in relatively few cases (Brandts *et al.*, 1970; Hawley, 1971; Zipp and Kauzmann, 1973; Heremans, 1982; Weber and Drickamer, 1983; Samarasinghe *et al.*, 1992; Royer *et al.*, 1993), despite the significance of these effects for understanding the contribution of the hydrophobic effect to protein stability. Hawley (1971) experimentally determined the relevant parameters in Eq. (1) for chymotrypsin at pH 2.07: T_m = 315 K, P_m = 1 atm = (1/41) cal/cm^3, ΔC_p = 3.8 kcal/mol/K, ΔH_m = 100.2 kcal/mol, $\Delta\beta = -1.24 \times 10^3$ cm^6/kcal/mol, $\Delta\alpha$ = 1.32 cm^3/mol/K, and ΔV_m = +41 cm^3/mol. Based on these values, the contribution of pressure-dependent effects to the maximal stability of this protein is small; at $T^* \cong$ 289K and P^* = 1.25 atm, $\Delta G^*(T^*, P^*)$ = 4.21 kcal/mol. Neglecting pressure-dependent effects, $\Delta G^*(T^*, 1\text{ atm})$ = 4.19 kcal/mol. Consequently, although pressure effects can significantly influence the stability of proteins, at least in this case, the pressure of maximal stability is shifted only slightly from 1 atm, so that the effect of pressure on the maximal stability of chymotrypsin at pH 2.07 is minimal.

5. Neglecting the pressure-dependent terms, and assuming that the measured ΔC_p for unfolding of water-soluble proteins reflects the exposure of apolar groups to water, the contribution of hydrophobic interactions, $\Delta G_{hyd.}$ to the free energy of protein unfolding is given by (Baldwin, 1986)

$$\Delta G_{hyd} = \Delta C_p(T - T_h) + \Delta C_p T \ln(T_s/T) \qquad (8)$$

where T_h and T_s are the temperatures at which the enthalpy and entropy changes associated with the hydrophobic effect vanish, respectively. Based on the thermodynamic properties of liquid hydrocarbons dissolved in water, Baldwin proposed that T_h and T_s equal 22.2°C and 112.8°C, respectively. Because ΔC_p is positive for protein unfolding,

ΔG_{hyd} from Eq. (8) is consequently found to be large and positive (i.e., stabilizing the native structure). The residual contributions to the observed thermodynamic parameters, from sources other than the hydrophobic interaction, were found to be largely temperature independent for lysozyme. According to Baldwin's analysis, ΔH_{res} = 52 kcal/mol lysozyme = ~3.7 cal/g and ΔS_{res} = 543 cal/mol lysozyme/deg = ~0.039 cal/g/deg.

How much, and even whether, hydrophobic interactions stabilize protein structures depends entirely on the assumptions used to assigned values for ΔC_p, T_h, and T_s that are inserted into Eq. (8), however. Privalov and Gill (1988; Murphy *et al.,* 1990) argue that the most appropriate value for T_h and T_s is ~110°C. With this parameter value, hydrophobic interactions are predicted to be destabilizing for all $T < 110$°C. This is a very different picture than traditionally envisioned for the origins of water-soluble protein stability. In some sense, these different interpretations amount to different choices of standard states that reflect the types of molecular interactions included in the definition of hydrophobic effects. What is clear, however, is that the contribution of hydrophobic interactions to protein stability decreases with decreasing temperature and that this can ultimately lead to the phenomenon of cold denaturation (Privalov, 1990).

C. Experimental Studies of Membrane Protein Stability

In contrast to the situation for water-soluble proteins, relatively few experimental studies have been reported on the thermodynamics of membrane protein stability. Calorimetric studies of membrane protein stability, which can provide definitive, model-independent values for various thermodynamic parameters of protein stability, are complicated by the often irreversible nature of this transition. Still, the available experimental studies do provide important, initial glimpses into the thermodynamics of membrane protein stability. As the preceding discussion has indicated, the goal of any thermodynamic characterization is to determine the stability curve, defined as $\Delta G(T)$. $\Delta G(T)$ may be calculated once the values of ΔC_p, ΔH_m, and ΔT_m have been determined at the transition temperature for unfolding. From the stability curve, it is possible to determine quantities that are important for comparisons to water-soluble proteins, such as the free energy of maximal stability [from $\Delta G(T^*)$; Eq. (7)], the contributions of hydrophobic interactions to protein stability (from the value of ΔC_p), and an estimate of the specific enthalpy of unfolding at 110°C, which for many water-soluble proteins has a common

value of 13 cal/g. The complete evaluation of these parameters is not available for any membrane protein system, but the available studies do at least permit these general issues to be addressed.

1. Bacteriorhodopsin

The most extensive calorimetric studies of membrane protein stability have been conducted for BR, which exists as a trimer in the purple membrane of *H. halobium*. Studies from both Sturtevant's (Jackson and Sturtevant, 1978) and Brouillette's (Brouillette *et al.*, 1987, 1989) groups indicate that at pH 7 in phosphate, BR unfolds at $T_m \sim 100°C$, with $\Delta H_m \sim 100$ kcal/mol. This corresponds to a specific enthalpy of ~4 cal/g (using a subunit molecular weight of 26,000), which is (perhaps coincidentally) close to Baldwin's (1986) estimate for the residual enthalpy of unfolding due to nonhydrophobic interactions (3.7 cal/g). Monomeric BR prepared in detergent micelles unfolds with $T_m \sim 74°C$ and $\Delta H_m \sim 100$ kcal/mol. Consequently, monomeric BR is less stable than trimeric BR in a phospholipid bilayer, which may reflect the importance of monomer–monomer interactions and/or may be a result of a detergent effects (see below). A study (Brouillette *et al.*, 1989) of the variation in ΔH_m with T_m (achieved by variation of the pH) suggests that the heat capacity for unfolding of trimeric BR in the purple membrane is ~1.2 kcal/mol/K or ~0.046 cal/g/K, which is lower (on a per gram basis) than for many water-soluble, globular proteins. For example, ΔC_p for denaturation of ribonuclease and myoglobin are 0.09 and 0.16 cal/g/K, respectively (Privalov and Khechinashvili, 1974). From $\Delta H_m = 100$ kcal/mol, $T_m = 373$ K, and $\Delta C_p = 1.2$ kcal/mol/K, the maximal stability of trimeric BR is estimated from Eq. (7) as $\Delta G(T^*) \sim 11$ kcal/mol at $T^* \sim 290$ K, which is within the range often observed for water-soluble proteins.

An important question in these studies concerns the extent of BR unfolding following thermal denaturation. This can be conveniently monitored by CD studies that are sensitive to the secondary structure content of a protein. In the case of BR, CD studies in the far-UV region indicate a reduction of ~27% in α helicity as the protein thermally denatures at pH 8.5 in 190 m*M* phosphate buffer (Brouillette *et al.*, 1987). Consequently, there is significant residual secondary structure in thermally unfolded BR, so that it would be incorrect to consider the D state as approximating a random coil. It has been suggested that the low specific enthalpy of BR unfolding, relative to water-soluble protein, may reflect the retention of structure after denaturation "due to the constraints imposed by the lipid bilayer" (Jackson and Sturtevant, 1978).

The contributions of the interhelical loops to the stability of BR have been probed by Engelman and co-workers (Popot *et al.*, 1987; Kahn

and Engelman, 1992). Using an *in vitro* regeneration system, BR was reconstituted from three fragments—two synthetic peptides corresponding to helices A and B, and a chymotryptic fragment containing the five helices C to G. After addition of retinal, spectroscopic and X-ray diffraction studies indicated that the reconstituted BR had properties virtually identical to those of wild-type BR. Consequently, the connecting loops between these helices are not essential for BR to adopt a native structure. Two significant implications of this work are that (1) helix–helix interactions are important for the folding of at least this membrane protein, and (2) entropic effects related to the approximate two-dimensional nature of membrane systems are not critical for membrane protein stability. Because the number of degrees of freedom that are available to a true, random-coil denatured membrane protein are significantly reduced relative to a three dimensionally denatured form of a water-soluble protein, it is possible that membrane proteins could be stabilized, in effect, by destabilization of the denatured form. The observation that proteolytic fragments of BR can reassemble to form the native protein suggests, however, that these entropic considerations are not dominant, because otherwise the various fragments would diffuse independently through the bilayer and not associate to form the native structure. In a subsequent analysis (Kahn *et al.*, 1992), calorimetric studies of regenerated BR demonstrated that proteolysis of one loop does somewhat destabilize BR, resulting in a decrease of T_m by 6°C and ΔH_m by 44 kcal/mol. Interestingly, removal of the retinal chromophore causes a more pronounced destabilization of BR, with observed changes in T_m and ΔH_m of −16°C and −77 kcal/mol, respectively.

Recently, it was reported that dehydrated multilayers of membrane-bound BR are stable up to 140°C (Shen *et al.*, 1993), at which point the protein denatures irreversibly. Although no information was obtained about the thermodynamics of BR stability under these conditions (i.e., to establish that BR is actually *thermodynamically* more stable under these conditions, as opposed to *kinetically* more stable), this is still a remarkable observation. The authors suggest that the increased thermostability of BR in stacked, dehydrated multilayers may be due to the imposition of steric constraints that prevent large-scale changes to the protein structure, such as those occurring on denaturation. There is some evidence that steric constraints may not be essential for increased protein stability, however, because protein suspensions in anhydrous solvents have shown dramatic increases in the apparent stability, relative to aqueous solutions (Volkin *et al.*, 1991). It should be noted, however, that solvent-free (dry) protein may be even more resistant to thermal unfolding compared to organic solvents (Toscano *et al.*, 1990). The transfer of a water-soluble

protein from an aqueous to nonaqueous environment can be accomplished with apparently few structural changes (Fitzpatrick *et al.*, 1993). The potential of nonaqueous environments to increase protein stability, such as those seen for BR in dehydrated multilayers, appears significant, and it is essential that more detailed thermodynamic analyses of protein stability under these conditions be obtained to understand the origins of this enhanced stability.

2. Erythrocyte Band 3

The principal erythrocyte anion transporter, or band 3, contains a 55-kDa transmembrane domain that can be separated from a 42-kDa cytoplasmic domain by proteolysis. The stability of the 55-kDa transmembrane domain has been studied following reconstitution into a series of different lipid environments by differential scanning calorimetry (Maneri and Low, 1988). In these different lipid environments, ΔH_m values for thermal denaturation were measured in a range from ~1 to 9 cal/g, with ΔC_p values of ~0 to 0.15 cal/g/K. If ΔH_m is plotted as a function of T_m, there is some tendency for the enthalpy of denaturation to increase with T_m (Fig. 8). The slope from a least-squares fit to this plot implies a

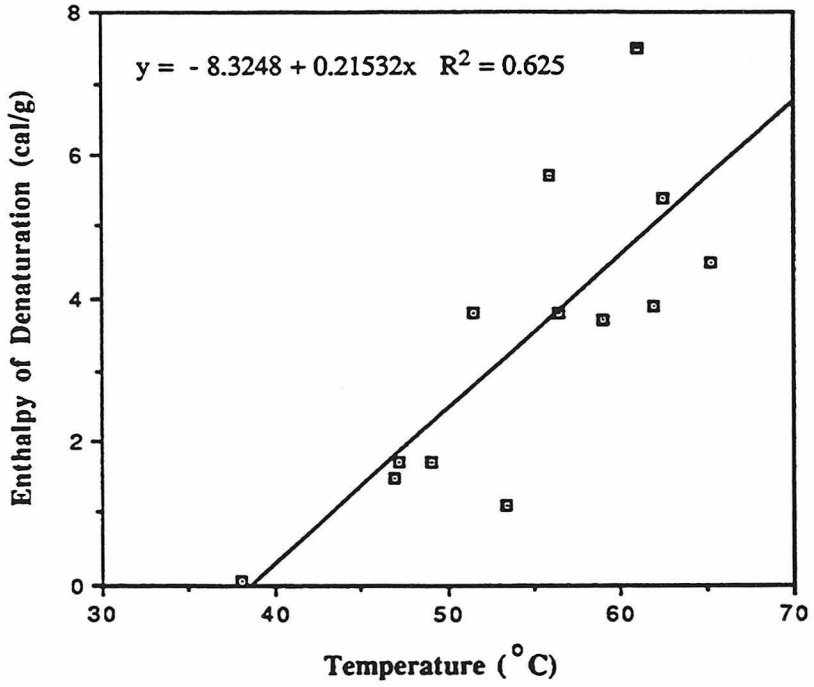

FIG. 8. Plot of the specific enthalpy of denaturation (ΔH_m) against the midpoint temperature for denaturation (T_m) for the membrane-bound domain of band 3 reconstituted in vesicles composed of different phospholipids. Data from Maneri and Low (1988).

ΔC_p of ~0.2 cal/g, and extrapolation of this line to 110°C yields a value for the specific enthalpy of unfolding of ~15 cal/g. These estimated values for both ΔC_p and the enthalpy of unfolding at 110°C are close to those expected for water-soluble proteins of comparable size (Privalov and Gill, 1988). Subsequent studies on band 3 in native membranes and in detergent micelles also found that the T_m and ΔH_m values obtained for thermal denaturation were "remarkably similar to those determined for concentrated solution of globular proteins," and further speculated that this reflects the presence of similar secondary structures (α helices) in both water-soluble and membrane proteins (Sami *et al.*, 1992).

3. Membrane-Associated Systems

Given the complexity of these systems, which contain a variety of different integral membrane proteins, it is difficult to extract quantitative thermodynamic parameters concerning the thermal denaturation of specific components. Nevertheless, some general observations have been reported that are relevant to the issue of membrane protein stability. Calorimetric studies of the erythrocyte ghost membrane system (Brandts *et al.*, 1986) revealed four structural transitions that occurred in the temperature range of 45–80°C. Of particular interest was the corresponding study of the temperature dependence of the circular dichroism spectrum for erythrocyte ghosts, which indicated that even at 90°C, ~50% of the α helicity measured at 30°C still remained. Consequently, both erythrocyte ghosts and BR retain considerable secondary structure in thermally denatured material. A scanning calorimetric study of photosystem II-containing membranes (Thompson *et al.*, 1986) observed five endothermal transitions in the 30–70°C temperature range. The enthalpy of denaturation for the entire complex, ΔH_m, was determined to be ~5–6 cal/g, which is within the range of values observed for denaturation of water-soluble proteins at these temperatures.

4. Glycophorin Dimer

Glycophorin A, a sialoglycoprotein found in erythrocyte membranes, forms homodimers mediated through interactions involving a single transmembrane-spanning α helix in each monomer. Although calorimetric or other types of thermodynamic characterizations have not been performed, the dimerization interactions are quite stable, persisting even in the presence of sodium dodecyl sulfate (Furthmayr and Marchesi, 1976). The glycophorin dimer can be disrupted, however, by addition of a synthetic peptide with the sequence of the transmembrane domain (Bormann *et al.*, 1989), which leads to complex formation between the

peptide and protein. Structural determinants of the helix–helix interactions responsible for dimerization have been explored by mutagenesis experiments (Lemmon *et al.*, 1992a,b), with analogous experiments recently reported for the transmembrane segment of phage M13 coat protein (Deber *et al.*, 1993). The helix–helix interface defined by these studies contains predominantly aliphatic side chains, with no highly polar groups. Consequently, noncovalent packing interactions between residues on the two helices appears to provide the principal driving force for dimerization. Furthermore, these packing effects appear to be sufficiently strong to generate a highly specific and stable dimer, even in the absence of other potentially stabilizing interactions such as connecting loops or polar (salt bridge) interactions. A calorimetric study of these membrane-localized helix–helix interactions would be quite informative for assessing the thermodynamic origins of the stability of this system.

5. Lipid and Detergent Influence on Membrane Protein Stability

The nature of the lipids and/or detergents that surround integral membrane proteins may have a profound influence on the structural stability of these proteins. The role of the membrane bilayer in membrane protein function was briefly discussed in Section III. A logical extension of these studies is the role of the membrane bilayer, or amphiphiles in general, in stabilizing or destabilizing membrane proteins. Only a few pioneering reports have investigated the role of the membrane bilayer lipids and detergents in membrane protein stability, and these are described below.

a. Lipid Studies. Early studies suggesting that the bilayer plays an important biological role in membrane protein stability were based on the observation that the thermostability of the Na^+, K^+-ATPase from brain membranes of various organisms, as measured by the rate of inactivation, was directly correlated with body temperature (Cossins *et al.*, 1987). These data implied that an increased body temperature corresponded to an increase in thermostability of the Na^+, K^+-ATPase. Although sequence identities of the Na^+,K^+-ATPase between the most diverse organisms in these experiments are greater than 85%, the remaining 15% differences could easily account for the increased thermostability at higher body temperature. More compelling support was provided by experiments performed with a single organism, the goldfish, acclimatized to different temperatures (Cossins *et al.*, 1987). In these studies, a significant increase was observed in the inactivation rate (74%) of 4°C acclimated goldfish Na^+,K^+-ATPase versus 25°C acclimated gold-

fish Na^+,K^+-ATPase. Although expression of two different Na^+,K^+-ATPases cannot be strictly ruled out, these data suggest that changes in the membrane bilayer composition, associated with growth at different temperatures, could be responsible for regulating the thermostability of the Na^+,K^+-ATPase.

Maneri and Low (1988) investigated the effect of variation in acyl chain length of phosphotidylcholine on the thermal stability of the erythrocyte anion transporter, band 3. This was the first calorimetric investigation of the thermodynamic role of the lipid bilayer in membrane protein stability. For a fixed head group type, the denaturation temperature of band 3 increased with increasing fatty acid chain length. Because the melting temperature of phospholipid bilayers increases with increasing fatty acid chain length, this indicates that the stability of the band 3 transporter increases with increasing stability of the bilayer. A more detailed description of this analysis is provided in Section IV,C,2.

b. Detergent Studies. A recent investigation of detergent effects on rhodopsin stability, although not rigorous, provides some interesting data on the thermostability of this protein and the effects of detergent (de Grip *et al.,* 1992). This study examined the role of 17 different detergents in stabilizing rhodopsin, as measured by the midpoint temperature associated with the loss of the native absorption spectrum for this protein. Although the data are limited, within a given class of detergents a lower critical micelle concentration (CMC) gives rise to a more stable protein. This result can most readily be explained by assuming that the free energy for micelle formation, ΔG°_{mic}, contributes to the stability of membrane proteins. ΔG°_{mic} for micelle formation can be expressed as (Gennis, 1989):

$$\Delta G^\circ_{mic} = RT \ln(X_{CMC})$$

where X_{CMC} is the mole fraction of the amphiphile at the critical micelle concentration. It must be stressed that for a rigorous calculation of ΔG°_{mic} the effects of counterions and activity coefficients should be included. Nonetheless, one can utilize this equation to calculate the differences in ΔG°_{mic}, $\Delta\Delta G^\circ_{mic}$, for several of the detergents utilized in the study, and to plot these data versus the corresponding ΔT for rhodopsin inactivation (Fig. 9). Although the general trend is clear, the observed correlation is far from ideal, however, which may reflect the simplified treatment of ΔG°_{mic} as well as the possibility of specific detergent protein interactions, which could be significant in cases such as the band 3 transporter in detergent micelles (Sami *et al.,* 1992).

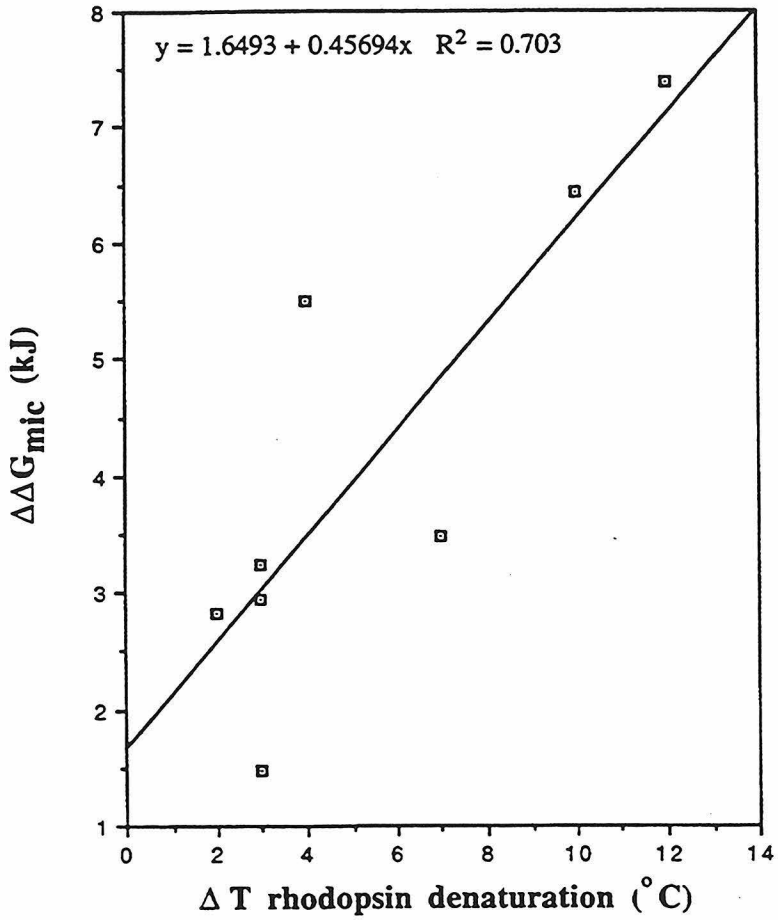

FIG. 9. Plot of $\Delta\Delta G_{mic}$ versus ΔT in the thermal denaturation of rhodopsin for a selected number of detergents. Data from de Grip *et al.* (1992).

6. *Pressure Effects on Membrane Protein Stability*

No studies of the pressure dependence of membrane protein stability were uncovered in preparing this review. It is anticipated that pressure effects could be quite interesting and complex, however, due to pressure effects on both the protein and the bilayer (Heremans, 1982). Lee (1983) has proposed that the compressibility of a protein will increase as the surface tension of the surrounding solvent decreases, because it then becomes easier to expand the solvent cavity in which the protein is embedded to accommodate volume fluctations. Consequently, pressure effects on protein stability could be more important for membrane proteins than for water-soluble proteins, because the surface tension of water, ~100 cal/Å^2, is much greater than the surface tension of hydrocarbons,

~30 cal/Å^2. Clearly, the significance of these effects needs to be addressed experimentally.

D. General Features of Membrane Protein Stability

Although the experimental evidence is limited, it appears that the thermodynamic parameters describing the stability of membrane proteins, especially T_m and ΔH_m, and to a lesser extent ΔC_p and $\Delta G(T)$, are within the range seen for more extensively characterized water-soluble proteins. A possible exception to this behavior may be provided by BR, where ΔH_m and ΔC_p appear to be somewhat lower than expected for water-soluble proteins unfolding at a T_m ~100°C, which may reflect a decreased contribution of hydrophobic interactions to BR stability (Baldwin, 1986) and/or the presence of residual structure in unfolded BR (Jackson and Sturtevant, 1978) (see below). Overall, however, membrane proteins do appear to have stabilities comparable to those of water-soluble proteins.

There is evidence from several systems that thermally denatured membrane proteins still retain extensive residual secondary structure. It may be that the denatured form of membrane proteins shares some similarities to the "molten globule" state of water-soluble proteins (Christensen and Pain, 1991), which contains extensive secondary structure but poorly defined tertiary interactions.

The stability of membrane proteins is sensitive to the nature of the lipid and/or detergent in the surrounding environment. In general, membrane protein stability increases with decreasing critical micelle concentration in a homologous series of detergents or lipids, although specific protein–lipid interactions can occur that counteract this tendency. In the case of BR, a significant increase in thermostability has been achieved by the preparation of anhydrous multilayers.

V. Energetic Basis of Membrane Protein Stability

Although membrane proteins and water-soluble proteins exist in very different types of solvent environments, there are striking similarities in both the stabilities and structural organizations of these two classes of proteins. This poses a serious dilemma, because hydrophobic interactions are believed to provide the dominant contribution to the stability of water-soluble proteins, and yet the contribution of hydrophobic interactions to the stability of integral membrane proteins should be greatly diminished in the nonaqueous environment of the lipid bilayer. Alterna-

tive factors to hydrophobic interactions that could contribute to the stability of membrane proteins are discussed below.

A. Packing Interactions

Studies on BR (Kahn and Engelman, 1992) and glycophorin (Lemmon *et al.*, 1992a,b) have shown that packing (van der Waals) interactions between helices are sufficient to promote stable tertiary structure interactions, without the need for connecting loops and highly polar interactions (Lemmon and Engelman, 1992; Popot, 1993). These principles have been recently used, for example, to develop an amino acid sequence motif that promotes specific dimerization of transmembrane α helices (Lemmon *et al.*, 1994). The efficient interior packing seen for both membrane proteins and water-soluble proteins should promote protein stability by maximizing the contributions of favorable van der Waals interaction energies. The sufficiency of packing interactions to drive molecular assembly has also been demonstrated in model systems, with the synthesis of molecules that dimerize in nonaqueous solvents in the absence of hydrophobic, hydrogen-bonding, and ion-pair interactions (Bryant *et al.*, 1990; Cram *et al.*, 1992).

B. Solvophobic Effects

Because it is energetically unfavorable to create a surface in a liquid, minimization of the surface energy of a liquid-immersed structure will tend to favor more compact objects (Israelachvili, 1992). Similarities in the surface areas between the RC and water-soluble proteins of similar size suggest that the surface energies of these proteins could be similar, despite the difference in surface tensions between hydrocarbon liquids ($\sim$30 cal/Å^2) and water ($\sim$100 cal/Å^2). This suggests that the greater energy required to create a surface in water, relative to nonpolar solvents, can be offset by the greater favorable interaction between the polar surface residues and water, relative to the weaker interactions possible between nonpolar surface residues and the hydrocarbon chains in the bilayer. As a consequence of these compensating effects, the net result could be comparable surface energies for the interaction of the relevant solvents with either water-soluble or membrane proteins, so that the work associated with placing a protein in a solvent could be, to first order, independent of the solvent (Rees *et al.*, 1994). By analogy to the term "hydrophobic," this more general type of effect is termed "solvophobic." Like hydrophobic effects, solvophobic effects will tend to minimize the exposed surface area and stabilize compactly folded structures.

C. *Increased Secondary Structure Stability*

The presence of nonaqueous solvents often stabilizes the formation of hydrogen-bonded, regular secondary structures, because competing hydrogen bonds to solvent molecules are either no longer possible, or not as favorable. Consequently, α helices (and presumably β sheets) are stabilized in a membrane environment, relative to an aqueous solution (Popot and Engelman, 1990). It seems plausible that the tertiary structure of a protein will be stabilized under conditions whereby the secondary structure is more stable, and this effect has been used to derive scales of amino acid secondary structure propensities (Blaber *et al.*, 1993; Kim and Berg, 1993). Consequently, this effect could contribute to the stability of membrane proteins through the enhancement of secondary structure stability. Experimental tests of this hypothesis that have been conducted with water-soluble proteins are consistent with a small, but not negligible, contribution of secondary structure stabilization to protein stability (Blaber *et al.*, 1993; Kim and Berg, 1993; Lin *et al.*, 1993; Pinker *et al.*, 1993).

D. *Entropic Effects*

As described above, the denatured state of some membrane proteins still retains residual secondary structure. The presence of residual order suggests that the denatured state may have conformational restrictions that reduce the entropic favorability of the unfolding process. As a consequence, it is possible that membrane proteins may be stabilized by a destabilization of the denatured state. In this regard, the N to D transition for membrane proteins may be more directly comparable to the N to "molten globule" transition observed for some water-soluble proteins, because the molten globule form contains significant secondary structure, but little ordered tertiary structure.

E. *Concluding Remarks*

An important lesson from the study of membrane proteins is that water is not absolutely indispensable for the ability of proteins to adopt stable three-dimensional structures; proteins can also stably exist in nonaqueous solvents, whether in the membrane bilayer or in nonbiological systems. By definition, then, hydrophobic interactions are not indispensable for protein stability, because proteins with stable tertiary structures occur in nonaqueous solvents. In this regard, the role of hydrophobic interactions in protein stability may be analogous to the role of disulfide

bridges; whereas some proteins cannot exist without disulfide bridges, they are certainly not required by every protein. As has been appreciated for some time (Singer, 1962), the continued study of proteins in membranes and other nonaqueous environments is fundamental to defining the contributions of all solvents, including water, to the origins of protein structure and stability.

Acknowledgments

We thank our colleagues/collaborators S.I. Chan, D.S. Eisenberg, and G. Feher for sharing their insights into membrane proteins; W. Kühlbrandt for providing LHCII coordinates; and NIH GM45162 for support.

References

Abramovitch, D. A., Marsh, D., and Powell, G. L. (1990). *Biochim. Biophys. Acta* **1020,** 34–42.

Allen, J. P., Feher, G., Yeates, T. O., Rees, D. C., Deisenhofer, J., Michel, H., and Huber, R. (1986). *Proc. Natl. Acad. Sci. U.S.A.* **83,** 8589–8593.

Allen, J. P., Feher, G., Yeates, T. O., Komiya, H., and Rees, D. C. (1987). *Proc. Natl. Acad. Sci. U.S.A.* **84,** 5730–5734.

Baldwin, R. L. (1986). *Proc. Natl. Acad. Sci. U.S.A.* **83,** 8069–8072.

Baud, F., Pebay-Peyroula, E., Cohen-Addad, C., Odani, S., and Lehmann, M. S. (1993). *J. Mol. Biol.* **231,** 877–887.

Becktel, W. J., and Schellman, J. A. (1987). *Biopolymers* **26,** 1859–1877.

Bernstein, F. C., Koetzle, T. F., Williams, G. J. B., Meyer, E. F., Brice, M. D., Rodgers, J. R., Kennard, O., Shimanouchi, T., and Tasumi, M. (1977). *J. Mol. Biol.* **112,** 535–542.

Blaber, M., Zhang, X.-J., and Matthews, B. W. (1993). *Science* **260,** 1637–1640.

Bormann, B.-J., Knowles, W. J., and Marchesi, V. T. (1989). *J. Biol. Chem.* **264,** 4033–4037.

Brandts, J. F., Oliveira, R. J., and Westort, C. (1970). *Biochemistry* **9,** 1038–1047.

Brandts, J. F., Erickson, L., Lysko, K., Schwartz, A. T., and Taverna, R. D. (1986). *Biochemistry* **16,** 3450–3454.

Brouillette, C. G., Muccio, D. D., and Finney, T. K. (1987). *Biochemistry* **26,** 7431–7438.

Brouillette, C. G., McMichens, R. B., Stern, L. J., and Khorana, H. G. (1989). *Proteins Struct. Funct. Genet.* **5,** 38–46.

Bryant, J. A., Knobler, C. B., and Cram, D. J. (1990). *J. Am. Chem. Soc.* **112,** 1254–1255.

Chang, C.-H., Tiede, D., Tang, J., Smith, U., and Norris, J. (1986). *FEBS Lett.* **205,** 82–86.

Chang, C.-H., El-Kabbani, O., Tiede, D., Norris, J., and Schiffer, M. (1991). *Biochemistry* **30,** 5352–5360.

Christensen, H., and Pain, R. H. (1991). *Eur. J. Biophys.* **19,** 221–229.

Cossins, A. R., Behan, M., Jones, G., and Bowler, K. (1987). *Biochem. Soc. Trans.* **15,** 77–81.

Cowan, S. W. (1993). *Curr. Opin. Struct. Biol.* **3,** 501–507.

Cowan, S. W., Schirmer, T., Rummel, G., Steiert, M., Ghosh, R., Pauptit, R. A., Jansonius, J. N., and Rosenbusch, J. P. (1992). *Nature (London)* **358,** 727–733.

Cram, D. J., Choi, H.-J., Bryant, J. A., and Knobler, C. B. (1992). *J. Am. Chem. Soc.* **114,** 7748–7765.

Datta, D. B. (1987). "A Comprehensive Introduction to Membrane Biochemistry." Floral Publishing, Madison, Wisconsin.

Deber, C. M., Khan, A. R., Li, Z., Joensson, C., Glibowicka, M., and Wang, J. (1993). *Proc. Natl. Acad. Sci. U.S.A.* **90,** 11648–11652.

de Grip, W. J., van Oostrum, J., and de Caluwe, G. L. J. (1992). *J. Crystal Growth* **122,** 375–384.

Deisenhofer, J., and Michel, H. (1989). *EMBO J.* **8,** 2149–2170.

Deisenhofer, J., Epp, O., Miki, K., Huber, R., and Michel, H. (1984). *J. Mol. Biol.* **180,** 385–398.

Deisenhofer, J., Epp, O., Miki, K., Huber, R., and Michel, H. (1985). *Nature (London)* **318,** 618–624.

Dill, K. A. (1990). *Biochemistry* **29,** 7133–7155.

Eisenberg, D. S., Weiss, R. M., and Terwilliger, T. C. (1984). *Proc. Natl. Acad. Sci. U.S.A.* **81,** 140–144.

Engelman, D. M. (1982). *Biophys. J.* **37,** 187–188.

Engelman, D. M., and Steitz, T. A. (1981). *Cell* **23,** 411–422.

Engelman, D. M., and Zaccai, G. (1980). *Proc. Natl. Acad. Sci. U.S.A.* **77,** 5894–5898.

Engelman, D. M., Henderson, R., McLachlan, A. D., and Wallace, B. A. (1980). *Proc. Natl. Acad. Sci. U.S.A.* **77,** 2023–2027.

Engelman, D. M., Steitz, T. A., and Goldman, A. (1986). *Annu. Rev. Biophys. Biophys. Chem.* **15,** 321–353.

Ermler, U., Fritzsch, G., Buchanan, S., and Michel, H. (1992). *In* "Research in Photosynthesis" (N. Murata, ed.), pp. 341–347. Kluwer, Dordrecht, Netherlands.

Fitzpatrick, P. A., Steinmetz, A. C. U., Ringe, D., and Klibanov, A. (1993). *Proc. Natl. Acad. Sci. U.S.A.* **90,** 8653–8657.

Fu, L., and Freire, E. (1992). *Proc. Natl. Acad. Sci. U.S.A.* **89,** 9335–9338.

Furthmayr, H., and Marchesi, V. T. (1976). *Biochemistry* **15,** 1137–1144.

Gennis, R. B. (1989). "Biomembranes—Molecular Structure and Function." Springer-Verlag, Berlin and New York.

Gibson, N. J., and Brown, M. F. (1991). *Photochem. Photobiol.* **54,** 985–992.

Gruner, S. M. (1985). *Proc. Natl. Acad. Sci. U.S.A.* **82,** 3665–3669.

Hawley, S. A. (1971). *Biochemistry* **10,** 2436–2442.

Henderson, R., and Unwin, P. N. T. (1975). *Nature (London)* **257,** 28–32.

Henderson, R., Baldwin, J. M., Ceska, T. A., Zemlin, R., Beckmann, E., and Downing, K. H. (1990). *J. Mol. Biol.* **213,** 899–929.

Heremans, K. (1982). *Annu. Rev. Biophys. Bioeng.* **11,** 1–21.

Israelachvili, J. N. (1992). "Intermolecular and Surface Forces," 2nd Ed. Academic Press, London.

Jackson, M. B., and Sturtevant, J. M. (1978). *Biochemistry* **17,** 911–915.

Kahn, T. W., and Engelman, D. M. (1992). *Biochemistry* **31,** 6144–6151.

Kahn, T. W., Sturtevant, J. M., and Engelman, D. (1992). *Biochemistry* **31,** 8829–8839.

Kauzmann, W. (1959). *Adv. Protein Chem.* **14,** 1–63.

Kauzmann, W. (1987). *Nature (London)* **325,** 763–764.

Kim, C. A., and Berg, J. M. (1993). *Nature (London)* **362,** 267–270.

Krauss, N., Hinrichs, W., Witt, I., Fromme, P., Pritzkow, W., Dauter, Z., Betzel, C., Wilson, K. S., Witt, H. T., and Saenger, W. (1993). *Nature (London)* **361,** 326–331.

Kühlbrandt, W., Wang, D. N., and Fujiyoshi, Y. (1994). *Nature (London)* **367,** 614–621.

Kyte, J., and Doolittle, R. F. (1982). *J. Mol. Biol.* **157,** 105–132.

Lee, B. (1983). *Proc. Natl. Acad. Sci. U.S.A.* **80,** 622–626.

Lemmon, M. A., and Engelman, D. M. (1992). *Curr. Opin. Struct. Biol.* **2,** 511–518.

Lemmon, M. A., Flanagan, J. M., Hunt, J. F., Adair, B. D., Bormann, B.-J., Dempsey, C. E., and Engelman, D. M. (1992a). *J. Biol. Chem.* **267,** 7683–7689.

Lemmon, M. A., Flanagan, J. M., Treutlein, H. R., Zhang, J., and Engelman, D. M. (1992b). *Biochemistry* **31,** 12719–12725.

Lemmon, M. A., Treutlein, H. R., Adams, P. D., Brünger, A. T., and Engelman, D. M. (1994). *Nature Struct. Biol.* **1,** 157–163.
Lin, L., Pinker, R. J., and Kallenbach, N. R. (1993). *Biochemistry* **32,** 12638–12643.
Llinás, M., DeMarco, A., and Lecomte, J. T. J. (1980). *Biochemistry* **19,** 1140–1145.
Maneri, L. R., and Low, P. S. (1988). *J. Biol. Chem.* **263,** 16170–16178.
Mitchell, D. C., Straume, M., and Litman, B. J. (1992). *Biochemistry* **31,** 662–670.
Murphy, K. P., and Freire, E. (1992). *Adv. Protein Chem.* **43,** 313–361.
Murphy, K. P., Privalov, P. L., and Gill, S. J. (1990). *Science* **560,** 559–561.
Navarro, J., Toivio-Kinnucan, M., and Racker, E. (1984). *Biochemistry* **23,** 130–135.
Paulsen, H., Finkenzeller, B., and Kuhlein, N. (1993). *Eur. J. Biochem.* **215,** 809–816.
Picot, D., Loll, P. J., and Garavito, R. M. (1994). *Nature (London)* **367,** 243–249.
Pinker, R. J., Lin, L., Rose, G. D., and Kallenbach, N. R. (1993). *Protein Sci.* **2,** 1099–1105.
Popot, J.-L. (1993). *Curr. Opin. Struct. Biol.* **3,** 532–540.
Popot, J.-L., and Engelman, D. M. (1990). *Biochemistry* **29,** 4031–4037.
Popot, J.-L., Gerchman, S.-E., and Engelman, D. M. (1987). *J. Mol. Biol.* **198,** 655–676.
Privalov, P. L. (1979). *Adv. Protein Chem.* **33,** 167–241.
Privalov, P. L. (1990). *Crit. Rev. Biochem. Mol. Biol.* **25,** 281–305.
Privalov, P. L., and Gill, S. J. (1988). *Adv. Protein Chem.* **39,** 191–234.
Privalov, P. L., and Khechinashvili, N. N. (1974). *J. Mol. Biol.* **86,** 665–684.
Privé, G. G., Verner, G. E., Weitzman, C., Zen, K. H., Eisenberg, D., and Kaback, R. H. (1994). *Acta Cryst. D.* **50,** 375–379.
Quinn, P. J. (1981). *Prog. Biophys. Molec. Biol.* **38,** 1–104.
Rees, D. C., and Wolfe, G. M. (1993). *Protein Sci.* **2,** 1882–1889.
Rees, D. C., DeAntonio, L., and Eisenberg, D. (1989a). *Science* **245,** 510–513.
Rees, D. C., Komiya, H., Yeates, T. O., Allen, J. P., and Feher, G. (1989b). *Annu. Rev. Biochem.* **58,** 607–633.
Rees, D. C., Chirino, A. J., Kim, K.-H., and Komiya, H. (1994). *In* "Membrane Protein Structure: Experimental Approaches" (S. White, ed.), pp. 3–26. Oxford, New York.
Rosenbusch, J. P. (1974). *J. Biol. Chem.* **249,** 8019–8029.
Royer, C. A., Hinck, A. P., Loh, S. N., Prehoda, K. E., Peng, X., Jonas, J., and Markley, J. (1993). *Biochemistry* **32,** 5222–5232.
Samarasinghe, S. D., Campbell, D. M., Jonas, A., and Jonas, J. (1992). *Biochemistry* **31,** 7773–7778.
Sami, M., Malik, S., and Watts, A. (1992). *Biochim. Biophys. Acta* **1105,** 148–154.
Schafmeister, C. E., Miercke, L. J. W., and Stroud, R. M. (1993). *Science* **262,** 734–738.
Schiffer, M., Chang, C. H., and Stevens, F. J. (1992). *Protein Eng.* **5,** 213–214.
Seddon, J. M. (1990). *Biochim. Biophys. Acta.* **1031,** 1–69.
Shen, Y., Safinya, C. R., Liang, K. S., Ruppert, A. F., and Rothschild, K. J. (1993). *Nature (London)* **355,** 48–50.
Singer, S. J. (1962). *Adv. Protein Chem.* **17,** 1–68.
Singer, S. J., and Nicolson, G. L. (1972). *Science* **175,** 720–731.
Tanford, C. (1980). "The Hydrophobic Effect." Wiley, New York.
Thompson, L. K., Sturtevant, J. M., and Brudvig, G. W. (1986). *Biochemistry* **25,** 6161–6169.
Toscano, G., Pirozzi, D., and Greco, G. (1990). *Biotechnol. Lett.* **12,** 821–824.
Unwin, N. (1993). *J. Mol. Biol.* **229,** 1101–1124.
Vantilbeurgh, H., Egloff, M. P., Martinze, C., Rugani, N., Verger, R., and Cambillau, C. (1993). *Nature (London)* **362,** 814–820.
Volkin, D. B., Staubli, A., Langer, R., and Klibanov, A. M. (1991). *Biotech. Bioengin.* **37,** 843–853.
Weber, G., and Drickamer, H. G. (1983). *Q. Rev. Biophys.* **16,** 89–112.

Weiss, M. S., Wacker, T., Weckesser, J., Welte, W., and Schultz, G. E. (1990). *FEBS Lett.* **267,** 268–272.

Weiss, M. S., Kreusch, A., Schiltz, E., Nestel, U., Welte, W., Weckesser, J., and Schulz, G. E. (1991). *FEBS Lett.* **280,** 379–382.

Yeates, T. O., Komiya, H., Rees, D. C., Allen, J. P., and Feher, G. (1987). *Proc. Natl. Acad. Sci. U.S.A.* **84,** 6438–6442.

Yeates, T. O. (1993). *In* "Thermodynamics of Membrane Receptors and Channels" (M. B. Jackson, ed.), pp. 1–25. CRC Press, Boca Raton, Florida.

Zipp, A., and Kauzmann, W. (1973). *Biochemistry* **12,** 4217–4228.

Chapter II

Transient Electron-Transfer Studies on the 2-Subunit Cytochrome c Oxidase from *Paracoccus Denitrificans*

Reprinted from the Journal of Physical Chemistry

Transient Electron-Transfer Studies on the Two-Subunit Cytochrome *c* Oxidase from *Paracoccus denitrificans*†

Michael H. B. Stowell,*,‡,§,⊥ Randy W. Larsen,§,⊕ Jay R. Winkler,∥ Douglas C. Rees,⊥ and Sunney I. Chan*,§

Arthur Amos Noyes Laboratory of Chemical Physics, Carl F. and Winfred H. Braun Laboratories, and The Beckman Institute, California Institute of Technology Pasadena, California 91125

Received: November 23, 1992

Intermolecular electron transfer between *c*-type cytochromes (equine cytochrome c_{550}, *P. denitrificans* c_{550}, and *P. denitrificans* detergent solubilized membrane-associated c_{552}) and the two-subunit cytochrome *c* oxidase from *P. denitrificans* has been studied using a photoinitiated uroporphyrin/NADH reduction system. In the presence of cytochrome *c* oxidase, the oxidation of transiently produced *soluble* ferrocytochrome c_{550}'s was biphasic with a fast phase k_{obs} between 80 and 90 s^{-1}. The simultaneous reduction of cytochrome *a* occurred with a k_{obs} of 50 s^{-1}, suggesting that cytochrome *a* is not the immediate electron acceptor for these soluble cytochromes. In contrast, the *membrane-associated* cytochrome c_{552} was not capable of transferring electrons to cytochrome *c* oxidase, either transiently or under steady-state conditions. It is concluded that the soluble and membrane-associated cytochrome *c*'s utilize separate electron-transfer pathways into *P. denitrificans* cytochrome *c* oxidase.

Cytochrome *c* oxidase (CcO) is the terminal enzyme in the respiratory chain of most aerobic organisms. This enzyme catalyses the four-electron reduction of molecular oxygen to H_2O and couples this thermodynamically favorable reaction to the vectorial translocation of protons across the membrane, i.e., proton pumping.[1] Four metal centers, cytochrome *a*, Cu_A, cytochrome a_3, and Cu_B, mediate the redox chemistry and coordinate the vectorial translocation of protons. Cytochrome a_3 and Cu_B compose a binuclear cluster that is the site of dioxygen reduction. The remaining redox active metal centers act as electron mediators between cytochrome *c* and the binuclear center. It has been demonstrated that the vectorial translocation of protons occurs during the third and fourth electron transfer, with an overall turnover stoichiometry of 0:0:2:2 for the proton-to-electron ratios.[2] While circumstantial evidence favors one of the two low potential centers, Cu_A or cytochrome *a*, as the site of linkage for proton pumping, the actual electron-transfer step linked to pumping has not been determined (for a recent review see ref 3).

To investigate the site of linkage in proton pumping, we have begun transient kinetic studies of cytochrome *c* mediated reduction of *Paracoccus denitrificans* CcO. *P. denitrificans* is perhaps the closest bacterial homologue to mammalian mitochondria that is known,[4] and the CcO from *P. denitrificans* is strikingly similar, both in sequence[5] and in physical properties,[6-8] to its mammalian counterpart. Two important differences, however, are that the mammalian CcO is composed of at least 12 subunits, whereas the *P. denitrificans* CcO contains only 3, and the mammalian CcO utilizes only a single water-soluble reductant, cytochrome *c*, whereas the CcO from *P. denitrificans* apparently utilizes two primary reductants. The first reductant is a soluble cytochrome c_{550} very similar to the mammalian cytochrome *c*[9,10] and is implicated in electron transport from various dehydrogenases to CcO when *P. denitrificans* is grown on C_1 carbon sources. The second is a membrane-associated cytochrome c_{552}[11] found in association with ubiquinol cytochrome *c* oxidoreductase and cytochrome *c* oxidase in a cytochrome $bc_1/c_{552}/aa_3$ supercomplex and is presumably involved in electron transport from the TCA cycle to CcO.[12] Because the cytochrome c_{552} is a membrane-associated protein whereas the cytochrome c_{550} is not, we reasoned that these two cytochromes may have different electron-transfer pathways into CcO.

In this paper, we report preliminary transient electron-transfer studies between several *c*-type cytochromes (equine cytochrome *c*, soluble *P. denitrificans* c_{550}, membrane-associated *P. denitrificans* c_{552}) and the two-subunit CcO from *P. denitrificans*. In experiments with soluble cytochrome *c*'s, the k_{obs} for ferrocytochrome *c* oxidation was approximately 2-fold greater than cytochrome *a* reduction and suggests that Cu_A is the primary electron acceptor for these soluble cytochrome *c*'s. Interestingly, while we were able to transiently reduce cytochrome c_{552}, we were unable to observe any electron transfer between this membrane-associated cytochrome *c* and CcO. We conclude from these data that the two cytochromes utilize separate electron-transfer routes into CcO and hypothesize that these two routes may be functionally distinct as well.

Materials and Methods

Materials. Uroporphyrin was obtained from Porphryin Products and was used without further purification. Horse heart cytochrome *c* (Type VI) and NADH were obtained from Sigma. All buffers were obtained from Calbiochem. All detergents used were obtained from Fluka and were stored at −20 °C under an argon atmosphere to minimize peroxide formation.

General. Protein assays were performed using the BCA method (Pierce). Heme concentrations were determined using the pyridine–hemochrome method, and the following extinction coefficients were used for the various cytochromes: *P. denitrificans* cytochrome *c* oxidase $\epsilon_{424-480(ox)} = 60.1\ mM^{-1}\ cm^{-1}$ and $\Delta\epsilon_{605(red-ox)} = 11.7\ mM^{-1}\ cm^{-1}$; equine c_{550}, $\epsilon_{550(red)} = 27.6\ mM^{-1}\ cm^{-1}$ and $\Delta\epsilon_{550(red-ox)} = 18.5\ mM^{-1}\ cm^{-1}$; *P. denitrificans* c_{550}, $\epsilon_{550(red)} = 26.8\ mM^{-1}\ cm^{-1}$ and $\Delta\epsilon_{550(red-ox)} = 17.5\ mM^{-1}\ cm^{-1}$; *P. denitrificans* c_{552}, $\epsilon_{551.5(red)} = 25\ mM^{-1}\ cm^{-1}$; *c*-type pyridine-hemochrome $\epsilon_{549(red)} = 21.1\ mM^{-1}\ cm^{-1}$.

* Authors to whom correspondence should be addressed.

† Contribution No. 8722 from the Division of Chemistry and Chemical Engineering, California Institute of Technology, Pasadena, CA. This work was supported by Grant GM22432 from the National Institute of General Medical Sciences, U.S.P.H.S. Portions described at the ASBMB/Biophysical Society Joint Meeting. *FASEB J.* 1992, *6*, A284.

‡ Recipient of a National Research Service Predoctoral Award and Albert L. Raymond Fellowship.

§ Arthur Amos Noyes Laboratory of Chemical Physics.

⊥ Carl F. and Winfred H. Braun Laboratories.

∥ The Beckman Institute.

⊕ Present address: Department of Chemistry, University of Hawaii, Honolulu, HI 96822.

0022-3654/93/2097-3054$04.00/0 © 1993 American Chemical Society

Growth of *P. denitrificans*. Small cultures of ATCC No. 13543 *P. denitrificans* were grown on succinate according to previous methods.[6] Large-scale growths were performed at the Caltech 300L fermenter facility using a fed-batch method. Cells were grown on 10 g/L each peptone, yeast extract, casaminoacids, dextrose; 5.6 g/L Na_2HPO_4; 3.8 g/L KH_2PO_4; 4 g/L $(NH_4)_2SO_4$; 1 g/L $MgSO_4 \cdot 7H_2O$; and 1 mL/L salt stock solution utilized for small culture growth. Cells were grown to a maximum optical density while maintaining an O_2 concentration greater than 70% of the initial concentration. Cells were harvested with a continuous flow centrifuge and frozen in liquid nitrogen as 200-g flat packs. Yields were typically 10–12 kg.

Purification of Cytochromes from *P. denitrificans*. The two-subunit CcO from *P. denitrificans* was prepared according to the method of Berry and Trumpower[12] with modifications similar to Steffens et al.[13] and was homogeneously pure by criteria of optical spectra, SDS-PAGE and IEF-PAGE. Activities were measured by following the oxidation of equine ferrocytochrome *c* spectrophotometrically at 550–540 nm in 100 mM HEPES, pH 7.4, 0.1% Brij-35. Turnover numbers were typically 20–25 s^{-1} under these conditions. Isolation of the soluble cytochrome c_{550} was carried out according to the procedure of Scholes et al.[9] with slight modifications. Cytochrome c_{552} fractions from the CcO purification were pooled and purified to homogeneity by anion-exchange chromatography using a Waters Protein Pack Q-Sepharose FPLC column in the presence of 0.5% TX100. Cytochromes were dialyzed against 10 mM HEPES, pH 7.4, and concentrated to ~500 μM using an Amicon 100-kD centricon microconcentrator for cytochrome *c* oxidase, 30-kD for cytochrome c_{552}, and 10-kD for cytochrome c_{550}, respectively. The concentrated cytochromes were aliquoted, snap frozen in liquid nitrogen, and stored at –78 °C until use.

Transient Absorption Experiments. Aliquots of purified cytochromes were thawed, prefiltered through a 0.2-μm cellulose acetate filter, placed in septum capped vials, and degassed for 30 min under a stream of argon at 4 °C. A septum-capped cuvette containing 1.5 mL of 100 mM HEPES, pH 7.4, 0.1% Brij-35, 20 μM uroporphyrin, 1 mM NADH, and a Teflon stirring flea was similarly degassed. Stock buffers were vacuum degassed and purged with argon prior to use. All samples were stored on ice prior to experimental measurements. The desired cytochrome and CcO were added to a degassed cuvette to final concentrations of 20 and 15 μM, respectively. Absorption transients were then recorded at appropriate wavelengths. Recorded transients are the average of 10 laser shots, unless otherwise stated, at repetition rates between 0.14 and 0.35 Hz with intermittent stirring.

Laser Instrumentation. The photoinitiated reduction of cytochromes was performed by excitation of uroporphyrin at 500 nm using a Lambda Physik FL 3002 dye laser (coumarin 480) pumped with a Lambda Physik LPX201i XeCl excimer laser. Shot selection was performed using a leading edge peak trigger directly linked to the digitizer. Excitation pulses were typically 2.0–3.0 mJ/pulse with a 20-ns pulse width. Single-wavelength transients were recorded using a 75-W xenon arc lamp probe source propagating colinearly with the excitation source and passing through a 160B Instruments SA double monochromator. The output from the monochromator was detected with a Hamamatsu R928 photomultiplier tube and amplified with a DSP 1402E programmable amplifier for kinetics out to 500 ms. Signals were digitized using a Tektronix R710 200-MHz 10-bit transient digitizer interfaced to a 386-based microcomputer.

Data Analysis. Transient signals were analyzed using an in-house nonlinear least-squares program or alternatively with LABCALC to obtain kinetic rates. Exponential fitting to the data was performed using the full 1024 data points recorded from the 10-bit digitizer and was linear for 4–5 half-lives. Data files for figures were compressed to 256 data points using 4-point averaging.

TABLE I: Observed Properties of *P. denitrificans* c-Type Cytochromes

	c_{550}	c_{552}
Soret[a]	415.0	415.5
β	521.5	522.0
α	550.0	551.5
molec mass (SDS),	17	27
molec mass (heme)[b]	15	22
heme[c]	*c* type	*c* type
heme/protein[d] (SDS)	0.90	0.81

[a] Absorbances are reported for the reduced cytochrome using equine cytochrome c_{550} as standard (549.5 nm). [b] Assumes one heme per cytochrome. [c] Determined as the pyridine–hemochrome complex. [d] Protein determination by BCA.

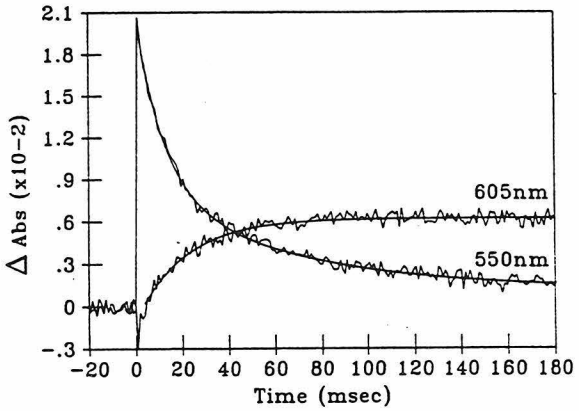

Figure 1. Transient electron transfer between 20 μM *P. denitrificans* cytochrome c_{550} and 15 μM *P. denitrificans* CcO monitored at 550 and 605 nm, with double- and single-exponential fits, respectively. Buffer contained 100 mM Hepes, pH 7.4, 0.1% Brij-35, 10 nM catalase, 20 μM uroporphyrin.

Results and Discussion

Properties of Isolated Cytochromes. Table I lists the spectral and physical properties of the *c*-type cytochromes isolated in this work. The properties of the soluble c_{550} are identical to those reported by Scholes et al.[9] The cytochrome c_{552} is reported to have a molecular mass of 22 kD[12] by SDS-PAGE, whereas we observe a 27-kD polypeptide. However, combined protein analysis and heme determination, assuming a single heme per cytochrome, resulted in a calculated molecular mass of 22 kD. Only the cytochrome c_{552} requires the presence of detergent in order to maintain solubility. Both cytochromes are rapidly reduced by dithionite, slowly reduced by ascorbate, and show negligible reduction by 100-fold excess NADH over a 2-h period at 23 °C.

Transient Reduction of c-Type Cytochromes. Both the c_{550} and the c_{552} cytochromes could be transiently reduced using the previously reported NADH/uroporphyrin photoinduced reduction system, with yields and time constants for reduction similar to those reported for equine cytochrome *c*.[14] As previously described, the yield of ferrocytochrome *c* from a single laser flash is ~1 μM, and pseudo-first-order conditions are therefore maintained.[14] Similar to earlier studies using bovine CcO, the uroporphyrin/NADH reduction system utilized in this study does not directly reduce *P. denitrificans* CcO despite the greater than 1 eV driving force achieved during photoexcitation.[14]

Transient Electron Transfer from Soluble c-Type Cytochromes to CcO. Figures 1 and 2 show the photoinitiated electron transfer from *P. denitrificans* cytochrome c_{550} and equine cytochrome c_{550} to CcO, respectively. Both the equine cytochrome *c* and the *P. denitrificans* cytochrome c_{550} readily donate electrons to CcO (15 μM) in a biphasic manner with similar k_{obs} of 97 ± 5 and 85 ± 3 s^{-1}, for the fast phase, respectively. The percent contribution of the slow phase to the overall transient varied

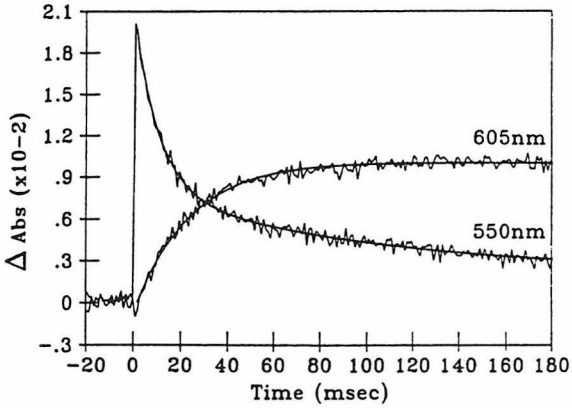

Figure 2. Transient electron transfer between 20 μM equine cytochrome c_{550} and 15 μM *P. denitrificans* CcO monitored at 550 and 605 nm, with double- and single-exponential fits, respectively. Buffer contained 100 mM Hepes, pH 7.4, 0.1% Brij-35, 10 nM catalase, 20 μM uroporphyrin.

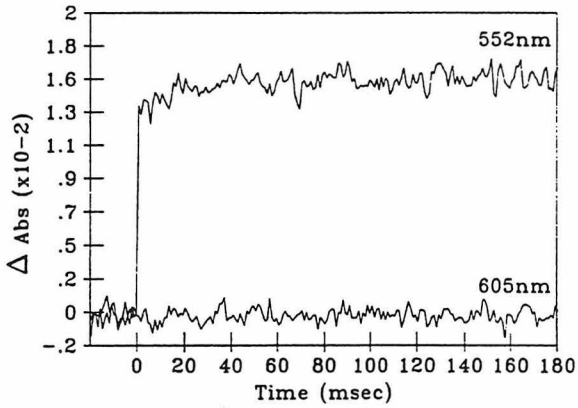

Figure 3. Transient electron transfer between 20 μM *P. denitrificans* cytochrome c_{552} and 15 μM *P. denitrificans* CcO monitored at 552 and 605 nm. Buffer contained 100 mM Hepes, pH 7.4, 0.1% Brij-35, 10 nM catalase, 20 μM uroporphyrin. Both traces are single transients.

slightly between different enzyme preparations and is attributed to an enzyme heterogeneity that presumably results in two populations of transiently bound cytochrome and was not investigated further.

In the above experiments, the reduction of cytochrome *a* occurs with first-order k_{obs} of 50 ± 2 and 48 ± 2 s^{-1} for the equine and *P. denitrificans* cytochrome *c*'s, respectively. Although we have not measured reduction of Cu_A directly, the 2-fold difference between the oxidation rate of the ferrocytochrome *c*'s and the reduction of cytochrome *a* suggests that the initial electron acceptor from these cytochromes is not cytochrome *a* but presumably Cu_A, which subsequently transfers the electron to cytochrome *a* at the observed rate of approximately 50 s^{-1}. This would be in agreement with previous studies which suggested that the initial electron acceptor from cytochrome *c* is Cu_A.[15-17] This interpretation requires, however, that the rate of electron equilibration between Cu_A and cytochrome *a* is significantly slower in *P. denitrificans* CcO than in the bovine CcO which has been reported to be between 6000 and 17 000 s^{-1}.[15,18]

The initial electron input rates observed for *P. denitrificans* CcO are 10-fold slower than those observed for the bovine CcO under similar[19] and identical[14] conditions. This result demonstrates a considerable difference between the bovine and *P. denitrificans* CcO's with regard to the initial electron-transfer complex. This difference could be due to marked differences in the redox potentials of the initial electron acceptors in the two enzymes, but recent results demonstrating the similarities in redox properties of the *P. denitrificans* CcO and the bovine enzyme[7,8] would seem to eliminate this possibility. Alternatively, such a difference could be due to distance changes in the cytochrome *c*/(Cu_A:cytochrome *a*) redox pair resulting in altered electron-transfer kinetics according to Marcus theory.[20] A third less likely, but certainly more intriguing, alternative is that the observed variation in electron-transfer rates is the manifestation of differences in the gating of the proton-pumping function of CcO.

The molar stoichiometry for ferrocytochrome *c* oxidation and cytochrome *a* reduction is approximately 1:1 for the equine cytochrome c_{550} and 1:0.5 for the *P. denitrificans* cytochrome c_{550}. These values are generally in agreement with those reported for bovine CcO, which range from 1:0.5[19] to 1:1[14] using bovine ferrocytochrome *c* and equine ferrocytochrome *c* as reductant, respectively. While these ratio differences have been attributed to enzyme heterogeneity, our ratios are obtainable with identical enzyme preparations and are therefore solely attributable to the nature of the cytochrome utilized. It is worth noting that ratios of 1:~0.5 are observed when utilizing the physiological cytochrome *c* and may reflect important redox interactions between the cytochrome *c* and CcO upon formation of the initial electron transfer complex. This interaction may cause a shift in the normal intramolecular electron-transfer route, resulting in electrons being transferred directly to the binuclear center and thus bypassing cytochrome *a*. This could account for the decreased stoichiometry observed for the physiological cytochrome c_{550}.

Transient Electron Transfer from Membrane-Associated c_{552} to CcO. Figure 3 shows the results from the attempted reduction of CcO by transiently produced ferrocytochrome c_{552}. No observable reduction of cytochrome *a* or oxidation of cytochrome c_{552} occurs during the time scale of these transient experiments. It is clear that under the conditions of these experiments, the cytochrome c_{552} and CcO cannot form a competent electron-transfer complex. This conclusion was further substantiated by steady-state experiments (data not shown) which demonstrated the detergent-solubilized ferrocytochrome c_{552} incapable of reducing CcO. It is important to note, however, that cytochrome c_{552} has been shown to reduce CcO in whole membrane preparations of *P. denitrificans*.[21] With this in mind, these results can be explained in several ways: (1) the cytochrome c_{552} is partially denatured during purification and is no longer a competent electron donor; (2) subunit III of CcO mediates or is required for the electron transfer from cytochrome c_{552} to either cytochrome *a* or Cu_A; or (3) the physiological electron-transfer route between the cytochrome c_{552} and CcO occurs via the hydrophobic regions of the two proteins, and formation of a competent electron-transfer complex is inhibited by bound detergent.

Because the cytochrome c_{552} maintains its reported physical properties during our purification and exhibits similar transient reduction properties as the soluble cytochromes studied, we regard the possibility that we have denatured this cytochrome to be unlikely. Although our preparation of CcO yields only the two-subunit enzyme, it is well established that all of the redox active metal centers are present in subunits I and II. Accordingly, the direct participation of subunit III in electron transfer seems an unlikely possibility. However, an indirect role in the formation of the cytochrome c_{552}/aa_3 electron-transfer complex may be played by subunit III. The last explanation appears to be the most tenable, but regardless of the exact nature of this electron-transfer inhibition, ignoring denaturation as a possibility, this result demonstrates a marked difference between the soluble *c*-type cytochromes and the membrane-associated cytochrome c_{552} in their ability to donate electrons to CcO. This result also suggests, but does not prove, that the physiological electron-transfer pathway from the membrane-associated cytochrome c_{552} to CcO may occur directly to cytochrome *a*, which has been previously located within the membrane-spanning region of CcO.[22-24]

Conclusions

We have directly observed for the first time electron transfer between soluble cytochrome *c*'s and *P. denitrificans* CcO. The rate of electron transfer is observed to be considerably slower than that for the mammalian enzyme under identical conditions and suggests that there are important differences between the bovine and *P. denitrificans* enzyme with regard to the primary electron-transfer complex. The 2-fold difference between the rate of ferrocytochrome *c* oxidation and cytochrome *a* reduction leads one to conclude that there is an intermediate electron acceptor, presumably Cu_A, between the soluble cytochrome *c*'s and cytochrome *a*. Perhaps the most striking observation is the absence of any electron-transfer activity between the solubilized membrane-associated cytochrome c_{552} and CcO. These results strongly support the contention that electron transfer from the soluble cytochrome c_{550} and the membrane-associated cytochrome c_{552} to CcO proceeds via two separate pathways. This is consistent with previous steady-state studies which showed that soluble cytochrome c_{550}'s can donate electrons to CcO in the presence of bound cytochrome c_{552}.[25] At present, it is unknown what role these postulated electron-transfer pathways play, but it is tempting to speculate that they may be differentially coupled to the proton-pumping function of CcO in *P. denitrificans*.

Acknowledgment. We thank Siegfried M. Musser and Dr. Theodore J. DiMagno for helpful discussions and critically reviewing this manuscript. We also thank Dr. Thomas Harrold and Larry Tudor for expert assistance in the growth of *P. denitrificans*.

References and Notes

(1) Wikstrom, M. K. F. *Nature* **1977**, *266*, 271–273.
(2) Wikstrom, M. K. F. *Nature* **1989**, *338*, 776–778.
(3) Chan, S. I.; Li, P. M. *Biochemistry* **1990**, *29*, 1–12.
(4) Yang, D. C.; Oyaisu, Y.; Oyaisu, H.; Olsen, G. J.; Woese, C. R. *Proc. Natl. Acad. Sci. U.S.A.* **1985**, *82*, 443–449.
(5) Raitio, M.; Jalli, T.; Saraste, M. *EMBO J.* **1987**, *6*, 2825–2833.
(6) Ludwig, B.; Schatz, G. *Proc. Natl. Acad. Sci. U.S.A.* **1980**, *77*, 196–200.
(7) Hendler, R. W.; Pardhasaradhi, K.; Reynafarje, B.; Ludwig, B. *Biophys. J.* **1991**, *60*, 415–423.
(8) Pardhasaradhi, K.; Ludwig, B.; Hendler, R. W. *Biophys. J.* **1991**, *60*, 408–414.
(9) Scholes, P. B.; Mclain, G.; Smith, L. *Biochemistry* **1971**, *10*, 2072–2076.
(10) Timkovich, R.; Dickerson, R. E. *J. Biol. Chem.* **1976**, *251*, 4033–4056.
(11) This cytochrome c_{552} is not to be confused with the inducible cytochrome c_{552}, also called c_{551i}, which is only expressed by *P. denitrificans* when grown on C_1 *carbon* sources.
(12) Berry, E. A.; Trumpower, B. L. *J. Biol. Chem.* **1985**, *260*, 2458–2467.
(13) Steffens, G. C. M.; Pascual, E.; Gerhard, B. *J. Chromatogr.* **1990**, *521*, 291–299.
(14) Larsen, R. W.; Winkler, J. R.; Chan, S. I. *J. Phys. Chem.* **1992**, *96*, 8023–8027.
(15) Hill, B. C. *J. Biol. Chem.* **1991**, *266*, 2219–2226.
(16) Pan, L.-P.; Hazzard, J. T.; Lin, J.; Tollin, G.; Chan, S. I. *J. Am. Chem. Soc.* **1991**, *113*, 5908–5910.
(17) Nilsson, T. *Proc. Natl. Acad. Sci. U.S.A.* **1992**, *89*, 6497–6501.
(18) Morgan, J. E.; Li, P. M.; Jang, D. J.; El-Sayed, M. A.; Chan, S. I. *Biochemistry* **1989**, *28*, 6975–6983.
(19) Hazzard, J. T.; Rong, S.; Tollin, G. *Biochemistry* **1991**, *30*, 213–222.
(20) Marcus, R. A.; Sutin, N. *Biochim. Biophys. Acta* **1985**, *811*, 265–322.
(21) Ericinska, M.; Davis, J. S.; Wilson, D. F. *Arch. Biochem. Biophys.* **1979**, *197*, 463–469.
(22) Shapleigh, J. P.; Hosler, J. P.; Tecklenburg, M. M. J.; Kim, Y.; Babcock, G. T.; Gennis, R. B.; Ferguson-Miller, S. *Proc. Natl. Acad. Sci. U.S.A.* **1992**, *89*, 4786–4790.
(23) Ohnishi, T.; LoBrutto, R.; Salerno, J. C.; Bruckner, R. C.; Frey, T. G. *J. Biol. Chem.* **1982**, *257*, 14821–14825.
(24) Blaise, J. K.; Pachence, J. M.; Tavormina, A.; Erecinska, M.; Dutton, P. L.; Stamatoff, J.; Eisenberger, P.; Brown, G. *Biochim. Biophys. Acta* **1982**, *679*, 188–197.
(25) Bolgiano, B.; Smith, L.; Davies, H. C. *Biochim. Biophys. Acta* **1988**, *933*, 341–350.

Chapter III

Light Induced Structural Changes in the Phtosynthetic Reaction Center: Implications on the Mechanism of Electron/Proton Transfer

Submitted to Science

Light Induced Structural Changes in the Photosynthetic Reaction Center: Implications on the Mechanism of Electron/Proton Transfer

M. H. B. Stowell[¥], T. M. McPhillips[¥], E. Abresch[†], G. Feher[†*], S. M. Soltis[ƒ], D. C. Rees[¥*]

[¥]Division of Chemistry and Chemical Engineering, California Institute of Technology
Pasadena, CA 91125

[ƒ]Stanford Synchrotron Research Laboratory, P.O. Box 4249, Bin 69
Stanford University, CA

[†]Department of Physics, 0319, University of California, San Diego
9500 Gilman Drive, La Jolla, CA 92093-0319

*to whom correspondence should be addressed

ABSTRACT

High resolution x-ray diffraction data of photosynthetic reaction center (RC) crystals from Rhodobacter sphaeroides in the dark and under illumination have been collected at cryogenic temperature and the structures refined at 2.2 Å and 2.6 Å respectively. In the charge separated state ($D^+Q_AQ_B^-$), Q_B^- is located approximately 5 Å from the charge neutral (DQ_AQ_B) Q_B position and has undergone a 180° propeller twist around the isoprene chain. A model based on the difference between the two structures is proposed to explain the observed kinetics of electron transfer from $Q_A^-Q_B$ to $Q_AQ_B^-$ and the relative binding affinities of the different ubiquinone species in the Q_B pocket. In addition, two distinct water channels (putative proton pathways) leading from the Q_B pocket to the surface of the RC were delineated, one of which, leads directly to the membrane surface.

The conversion of electromagnetic energy (light) into chemical energy occurs in a number of photosynthetic organisms ranging from bacteria to plants. The primary processes of photosynthesis are mediated by an integral membrane protein-pigment complex called the reaction center (RC) in which a sequence of photoinduced electron and proton-transfer reactions take place (reviewed in (1, 2)). Our knowledge of these processes was greatly enhanced through the determination of the three-dimensional structure of the RC from two purple photosynthetic bacteria: *Rps. viridis* (3, 4) and *Rb. sphaeroides* (5, 6, 7, 8, 9, 10, 11). In all previous structure determinations the primary reactants were in their neutral state, i.e., no electron transfer (charge separation) had taken place. Several independent experimental findings pointed towards a structural change accompanying charge separation (12, 13, 14, 15, 16, 17). A particularly drastic effect was reported by Kleinfeld et al. (18) who compared the rate of electron transfer in RCs that were frozen under illumination with those frozen in the dark. They observed an increase in the rate of the electron transfer from the primary ubiquinone Q_A^- to the secondary ubiquinone Q_B by several orders of magnitude when RCs were frozen under illumination, i.e., in the charge separated state, as compared to RCs frozen in the dark. To understand these observations, structural information about the charge separated state is required.

In this work we determined in detail the structural changes accompanying charge separation and use them as a basis for a model to explain changes in the kinetics of electron transfer observed upon freezing. The changes were obtained by comparing the structure of RCs in single crystals illuminated and cooled to cryogenic (~90K) temperatures (the light structure) with the structure of RCs cooled to cryogenic temperatures in the dark (the dark structure). In these experiments we used tetragonal crystals of *Rb. sphaeroides* R-26, which were first obtained by Allen (19). When cryogenically preserved, these crystals diffract to significantly higher resolution (1.9 Å in the dark state) than any previously reported RC crystals. Data collection and refinement to 2.2 Å resolution has enabled us to determine the position of a large number of water molecules and to delineate two separate

water (proton) "channels" leading from the aqueous phase to the Q_B pocket. One of these has been reported previously (11). The importance of the water molecules for proton transfer to reduced Q_B will be discussed.

Sample preparation, data collection and structure determination: RCs from *Rb. sphaeroides* were isolated and purified as described (20). Crystallization conditions were similar to those used by Allen (19). Crystals grew in 1-3 weeks to a thickness of 0.1-0.2 mm. The space group of the crystals was $P4_32_12$ having unit cell dimensions at cryogenic temperatures of a=b=140.1 Å, c=271.6 Å for the dark and a=b=140.1 Å, c=271.7 Å for the illuminated crystals. To increase the Q_B occupancy, crystals were soaked in a solution containing 1 mM ubiquinone-2 (21) for 2 days prior to data collection. Crystals were rapidly cooled in liquid nitrogen and transferred via cryo-transfer tongs (22) to a goniostat cooled with a stream of nitrogen to ~90K (23). Formation of the charge separated state $D^+Q_AQ_B^-$ (where D^+ is the primary donor, a bacteriochlorophyll dimer) was accomplished by illuminating a crystal with a filtered tungsten light source (bandpass 400 nm to 900nm) having a power density of 0.5 mW/cm^2 and placed directly above the liquid nitrogen bath. Samples were illuminated for ~100 ms prior to, and continuously during, immersion in liquid nitrogen. Following transfer of the sample to the goniostat, a constant illumination of 10 mW/cm2 was maintained. The occupancy of the Q_B site (24), as well as the completeness of the charge separation in the crystal, was determined using a microspectrophotometer on a control sample. Typical crystals showed >90% charge separation and a 70% Q_B occupancy. Dark adapted crystals were kept in dim light during manipulations and data collection. All crystals utilized were from the same batch, using the same crystallization conditions. Molecular replacement, phase improvement, and crystallographic refinement were performed with MERLOT(25), SOLOMON(26), and XPLOR(27), respectively. A summary of the X-ray diffraction results is shown in Table 1.

Structure of the RC in the DQ_AQ_B state (dark structure): The overall fold of the polypeptide chain follows, with only minor differences, the structure that has been

previously described (1, 5, 6, 7, 11). We shall focus, therefore, on the location of Q_B (and its surroundings) where we expect the largest changes to occur upon charge separation. The electron density map (Fig. 1) shows the position of the ubiquinone molecule in the Q_B binding site (Q_{B1}). It is located in a pocket with the O1 of Q_B 7.2 Å from the Nδ of His L190. The carbonyl oxygen O4 forms a single hydrogen bond with the amide backbone of Ile L224, in a manner similar to that in a recent report (11). The ubiquinone ring stacks directly upon the conserved Phe L216 in a parallel manner, (Fig 5B), suggesting that this interaction contributes to the binding affinity of the ubiquinone. Experimental evidence of this fact comes from an herbacide resistance mutant of *Rp. viridis* wherein Phe L216 is replaced with serine, resulting in an RC with reduced affinity (60 μM versus 4.5 μM for wild type) for ubiquinone (28). The atomic displacement factor of Q_B is greater than that of Q_A (43 $Å^2$ vs. 29 $Å^2$) indicative of a slightly more disordered structure or a lowered occupancy at the Q_B site as compared to the Q_A site, which is fully occupied. The electron density between the bound ubiquinone and His L190 and Glu L212 is at present somewhat problematic. It can be modeled either by three water molecules, or by a partially occupied ubiquinone at a second binding site (Q_{B2}) or a combination of both. A partially occupied ubiquinone site is most likely, and would be consistent with the model discussed below.

The positions of ubiquione in the Q_B pocket of dark adapted crystals reported by various groups differ significantly from each other as illustrated in Fig. 2. In these structures, we believe that the position of ubiquinone in the Q_B pocket is prone to error due to the lower occupancy at the Q_B pocket and the lower resolution of these structure determinations. The differences may also be due to the variability in sample preparations, specifically in regards to the detergent, which has been shown to influence the binding of ubiquinone to the Q_B pocket (29, 30). It is also conceivable that the reducing electrons created by the X-ray irraditaion during data collection could ultimately reduce ubiquinone in the Q_B pocket. This could explain why the position of Q_B in several of the structures are closer to that observed in the charge separated state discussed below.

As mentioned, the higher resolution data obtained in this work enabled us to determine the location of many water molecules. Figure 3 shows two distinct water channels, P1 and P2, that lead to the Q_B pocket to the surface of the protein. P1 is essentially identical to the water chain reported earlier (11). Details of these paths and their relevance will be discussed below.

Structure of the RC in the $D^+Q_AQ_B^-$ state (light structure): The overall fold of the polypeptide is approximately the same as that of the DQ_AQ_B (dark) structure. The O4 carbonyl of the Q_B semiquinone hydrogen bonds to His L190 and the O1 carbonyl hydrogen bonds to the backbone amide nitrogen of Ile L224 (Fig. 4). This binding site is similar to the partially occupied Q_{B2} site postulated for the dark structure. The refined atomic displacement parameters for Q_B^- are similar to those of Q_A, indicative of a nearly fully occupied ubiquinone at this site. In addtion to the L224 amide nitrogen, Ser L223 and the backbone amide of L225 are both ~3.1 Å from the O1 carbonyl of the ubiquinone and may form a second set of hydrogen bonds (albeit longer) to the ubisemiquinone anion. The presence of these three hydrogen bonds to the O1 carbonyl of the ubisemiquinone at the Q_{B2} site, especially the longer interactions with Ser L223 and L225 amide, are consistant with ENDOR studies on native and Ser-Ala L223 mutant RCs (31).

The most striking observation in the light adapted structure is a 4.5 Å (center to center distance) movement of the ubisemiquinone towards the cytoplasm with an accompanying 180° propeller twist about the isoprene tail (Fig. 5). There are fewer well ordered water molecules along the P1 and P2 pathways in comparison to the DQ_AQ_B structure. Particularly striking is the observation that Glu H173, located along the P2 water channel, is highly disordered compared to either Glu H173 in the dark structure or to the surrounding residues in the light structure. This suggests movement of water (protons) within the P1 and P2 channels that is concomitant with formation of the $D^+Q_A^-Q_B$ or the $D^+Q_AQ_B^-$ state.

Model of the electron transfer mechanism from $Q_A^-Q_B$ to $Q_AQ_B^-$ based on the dark and light structures of RCs. We need to explain the observation that at low temperatures (~90°K) the electron transfer from $Q_A^-Q_B$ to $Q_AQ_B^-$ is completely blocked in RCs cooled in the dark, whereas the electron transfer proceeds readily when RCs are frozen under illumination (18). The differences between the light and dark structures of the RCs offer a straightforward and simple explanation of these observations. We postulate a model in which the ubiquinone can assume two positions; in one, electron transfer from Q_A^- is inhibited, and in the other it is not. In the dark adapted RCs the positions Q_{B1} shown in Fig. 1 is thermodynamically favored. In this position the distance between the carbonyl oxygen O1 of Q_B and Nδ of His L190 is 7.2 Å. It is, therefore, disconnected from the most direct pathway for electron transfer from Q_A^- and hence, electron transfer from $Q_A^-Q_B$ to $Q_AQ_B^-$ is inhibited. However, a fraction of RCs exist in an activated state Q_{B2} corresponding to a quinone position that is ~5 Å removed from Q_{B1}. In this position the ubiquinone is hydrogen bonded to His L190 and electron transfer from Q_A^- can readily proceed. This position corresponds to the residual patch of electron density of the dark structure shown in Fig. 1. We propose that the movement of the quinone from Q_{B1} to the Q_{B2} position is a neccassary prerequisite for electron transfer from $Q_A^-Q_B$ to $Q_AQ_B^-$. The observed activation energy (32, 33) represents the barrier between these two states. The main contribution to the activation energy is probably the breaking of the hydrogen bond from O1 to the backbone amide of Ile L224 (see Figs. 1 and 5) and the energy associated with the 180° propeller twist. The above model is also consistent with the observation that the measured electron transfer rate from $Q_A^-Q_B$ to $Q_AQ_B^-$ is independent of the redox potential (i.e., driving force) of different ubiquinones substituted in the Q_A site (34), demonstrating that the rate limiting step is not electron transfer.

In the light adapted structure of the RC, the ubiquinone forms a hydrogen bond with His L190 thereby favoring the Q_{B2} site as shown in Figs. 4 and 5. In this position, electron transfer can readily take place as experimentally observed. It is interesting to note that the

ground state (dark) x-ray crystal structure that has been universally reported is not the kinetically active structure for electron transfer. In the above discussion we have neglected contributions from possible light induced structural changes upon forming $D^+Q_A^-Q_B$ (35) to the electron transfer from $D^+Q_A^-Q_B$ to $D^+Q_AQ_B^-$. Those are at present being investigated.

The protonation of Q_B and the release of Q_BH_2 from the RC: Following the one-electron reduction of Q_B, discussed in the previous section, a second electron is transferred to Q_B^-. The doubly reduced ubiquinone is protonated to form the ubiquinol (Q_BH_2) which leaves the RC (36) initiating the formation of the proton gradient across the plasma membrane that drives ATP synthesis (reviewed in (37)). Thus, the protonation of Q_B and the release of quinol are two fundamentally important processes. The main question associated with the protonation concerns the mechanism by which protons are transferred from the outside, aqueous phase, to the Q_B site which is buried inside the RC, reviewed in (38). The generally accepted view is that protons move along a chain of proton donor and acceptor groups. These groups could be either side-chains of protonatable amino acids or water molecules. Several of the amino acids in the chain have been identified in *Rb. sphaeroides* by site directed mutagenesis (39, 40, 41, 42, 43, 44). The role of the water molecules has been less well established. In one of the RC structures from *Rb. sphaeroides* , the position of several water molecules had been determined (11); the presence of water molecules were also inferred by a computational approach (45).

The higher resolution of this work made it possible to determine the positions of a large number of water molecules giving rise to two water channels (proton paths) indicated as P1 and P2 in Fig. 3. A detailed presentation of the two pathways is shown in Fig. 6A and 6B. Pathway P1 (Fig. 6A) proceeds from the Q_B site via Glu L212 through the H subunit to the cytoplasm over an approximately 23 Å distance. This pathway is approximately normal to the membrane surface and is similar to the one previously described (11). The second pathway, P2, which had been previously proposed (38) has now been identified (Fig. 6B). It leads from Ser L223 to Asp L213 via the interface between the H and M subunits,

parallel to the membrane surface at approximately the depth of the non-heme iron. This pathway traverses a number of residues that have been identified by mutational studies to be involved in proton uptake by Q_B. These include Ser L223 (39), Asp L213 (40, 41), and Glu H173 (42, 43). It is interesting to note that the terminus of this pathway is near the surface of the negatively charged membrane (46, 47) where the proton concentration is expected to be substantially greater than that in bulk water (48, 49, 50, 51, 52).

Concerning the release of quinol and its replacement by ubiquinone, the binding affinities of the three species Q_BH_2, Q_B^- and Q_B must meet certain criteria for proper function. The affinity for Q_B^- must be greater than that for Q_BH_2 and Q_B to prevent the loss of the Q_B^- intermediate and to avoid potentially detrimental release of the ubisemiquinone radical anion. The affinity of the RC for Q_B should be greater than for Q_BH_2 to thermodynamically favor the replacement of the quinol with ubiquinone. This insures the presence of an electron acceptor for continuing ubiquinone reduction. Indeed, the observed binding affinities correspond to these expectations (25, 36, 53, 54), i.e., the affinities decrease in the order

$$Q_B^- > Q_B > Q_BH_2$$

These results are readily explained by the current structures. As discussed in the section on the structure of light RCs, both carbonyl oxygens of Q_B^- form multiple close (<2.9 Å) hydrogen bonds (Figs. 4 and 5), whereas in the dark adapted structure, only one of the hydrogen bonds to Q_B (NH of Ile L224) is present (Figs. 1 and 5). For ubiquinol, both carbonyl oxygens are protonated, resulting in a weak binding. The release of ubiquinol may be further facilitated by the uptake of water in either P1 or P2 channels.

In summary, we have shown how the structures of dark and light adapated RCs can explain the observed kinetics of electron transfer from $Q_A^-Q_B$ to $Q_AQ_B^-$ as well as the protonation pathway to the Q_B pocket and the relative binding affinities of the different ubiquinone species in the Q_B binding pocket.

Table 1. Data Collection and Refinement Statistics

	DQ_AQ_B state (dark)	$D^+Q_AQ_B^-$ state (light)
Data collection		
Resolution range [Å]	30.0 - 2.2	30.0 - 2.6
Observations (unique)	335,463 (114,087)	203,621 (74,104)
Average I/sig (last shell)	19.5 (3.1)	14.3 (2.6)
R_{sym} (last shell) [%]	5.6 (14.6)	8.5 (16.0)
Completeness [%]	86	88
Redundancy	2.9	3.1
Refinement		
Resolution [Å]	10-2.2	10-2.6
Reflections	112,234	71,316
R_{cryst} [%]	22.2	21.5
R_{free} [%]	27.6	29.9

Data were collected at beamline 7-1 at the Stanford Synchrotron Radiation Laboratory using a 30 cm MAR Research imaging plate system. Data were processed with the DENZO/HKL (55) package and merged and scaled using rotavata/agrovata of the CCP4 program suite (56). Molecular replacement was performed using the program MERLOT (25). The molecular replacement solution without ubiquinones was used to calculated the A and B Hendrickson-Lattman coefficients (57) in the PHASES (58) program using Sim's weighting. These starting phase probabilities were utilized in a series of solvent flattening and twofold averaging cycles as implemented in the program SOLOMON (26). Inspection of the SOLOMON electron density maps were of excellent overall quality and allowed straightforward rebuilding of the starting model with the programs TOM/FRODO and O (59, 60). Iterative cycles of model building, XPLOR refinement (27) without NCS twofold restrictions and inspection of 2Fo-Fc and Fo-Fc electron density maps lead to the final models presented. The final models contain two RCs, 4 ubiquinones, 8 bacteriochlorophylls, 4 bacteriopheophytins, 2 irons, 2 LDAO molecules for a total of 17937 protein atoms. The dark adapted structure contains 411 waters and the light adapted structure contains 60 waters. Residual electron density that has not yet been modeled in the current structures is indicative of a number detergent and lipid molecules surrounding the RCs as well a large number of unmodelled waters. Further model building and refinement

incorporating these species is in progress. Molecular representations were prepared with the program SETOR (61).

REFERENCES AND NOTES

1. G. Feher, J. P. Allen, M. Y. Okamura, D. C. Rees, *Nature* **339**, 111-116 (1989).
2. M. Blaber, X.-j. Zhang, B. W. Matthews, *Science* **260**, 1637-1640 (1993).
3. J. Deisenhofer, O. Epp, K. Miki, R. Huber, H. Michel, *J. Mol. Biol.* **180**, 385-398 (1984).
4. C. R. D. Lancaster, H. Michel, *Reaction Centers of Photosynthetic Bacteria*. M. E. Michel-Beyerle, Ed. (Springer-Verlag, Berlin, 1995).
5. J. P. Allen, et al., *Proc. Nat. Acad. Sci. USA* **83**, 8589-8593 (1986).
6. J. P. Allen, G. Feher, T. O. Yeates, H. Komiya, D. C. Rees, *Proc. Natl. Acad. Sci. USA* **84**, 5730-5734 (1987).
7. J. P. Allen, G. Feher, T. O. Yeates, H. Komiya, D. C. Rees, *Proc. Natl. Acad. Sci. USA* **85**, 8487-8491 (1988).
8. C. H. Chang, et al., *FEBS Lett.* **205**, 82-86 (1986).
9. O. E. Kabbani, C. H. Chang, J. Tiede, J. Norris, M. Schiffer, *Biochemistry* **30**, 5352-5360 (1986).
10. B. Arnoux, J. F. Gaucher, A. Ducruix, F. Reishhusson, *Acta Cryst. D* **51**, 368-379 (1995).
11. U. Ermler, G. Frtizsch, S. Buchanan, H. Michel, in *Research in Photosynthesis* N. Murata, Ed. (Kluwer Academic Publishers, Amsterdam, 1992) pp. 341-347.
12. P. P. Noks, E. P. Lukashev, A. A. Komonekko, P. S. Benedikto, A. B. Rubin, *Mol. Biol. (Moscow)* **11**, 1909 (1977).
13. H. Arata, W. W. Parson, *Biochim. Biophys. Acta* **638**, 201 (1981).
14. N. W. Woodbury, W. W. Parson, *Biochim. Biophys. Acta* **767**, 345 (1984).
15. C. Kirmaier, D. Holten, W. W. Parson, *Biochim. Biophys. Acta* **810**, 33 (1985).

16. P. Parot, J. Thiery, W. Vermeglio, . J. Breton, W. Vermeglio, Eds., The Photosynthetic Bacterial Reaction Centers (Plenum Press, New York, 1988).

17. E. Nabedryk, et al., *FEBS Lett.* **266**, 59 (1990).

18. D. Kleinfeld, M. Y. Okamura, G. Feher, *Biochemistry* **23**, 5780-5786 (1984).

19. J. P. Allen, *Proteins* **20**, 283-286 (1994).

20. J. A. Isaacson, F. Lendzian, E. C. Abresch, W. Lubitz, G. Feher, *Biophys. J.* **69**, 311-322 (1995).

21. M. H. B. Stowell, G. Y. Wang, D. C. Rees, S. I. Chan, *in preparation* (1996).

22. H. Hope, *SSRL 22nd annual users meeting, Workshop on Techniques in Macromolecular Crystallography* (1995).

23. H. D. Bellamy, R. P. Phizackerley, S. M. Soltis, H. Hope, *Journal of Applied Crystallography* **27**, 967-960 (1994).

24. M. Y. Okamura, R. J. Debus, D. Kleinfeld, G. Feher, . B. L. Trumpower, Ed., Function of Quinones in Energy Conserving Systems (Academic Press, New York, 1982), vol. Chapter V.

25. P. M. D. Fitzgerald, *J. Appl. Cryst.* **21**, 273-278 (1988).

26. J. P. Abrahams, A. Leslie, *Acta Crystalogr.* **D52**, 30-42 (1996).

27. A. T. Brünger, J. Kuriyan, M. Karplus, *Science* **235**, 458-460 (1987).

28. I. Sinning, H. Michel, P. Mathis, A. W. Rutherford, *Biochemistry* **28**, 5544-5553 (1989).

29. M. Y. Okamura, R. A. Isaacson, G. Feher, *Proc. Nat. Acad. Sci. USA* **72**, 3491-3495 (1975).

30. C. A. Wraight, R. R. Stein, . Y. Inoue, et al., Eds., The Oxygen Evolving System of Photosynthesis (Academic press, London and New York, 1983).

31. M. L. Paddock, E. Abresch, R. A. Isaacson, G. Feher, M. Y. Okamura, *Biophysical Journal* **in press** (1997).

32. D. Kleinfled, M. Y. Okamura, G. Feher, *Biochim. Biophys. Acta* **766**, 126-140 (1984).

33. L. J. Mancino, D. P. Dean, R. E. Blankenship, *Biochim. Biophys. Acta* **764**, 46-54 (1984).

34. A. Labahn, J. M. Bruce, M. Y. Okamura, G. Feher, *Chemical Physics* **197**, 355-366 (1995).

35. P. Brzezinski, M. Y. Okamura, G. Feher, . J. Breton, A. Vermeglio, Eds., The photosynthetic bacterial reaction center II (Plenum Press, New York, 1992).

36. P. H. McPherson, M. Y. Okamura, G. Feher, *Biochim. Biophys. Acta* **1016**, 289-292 (1990).

37. W. A. Cramer, D. B. Knaff, , Energy Transduction in Biological Membranes (Springer-Verlag, New York, 1990).

38. M. Y. Okamura, G. Feher, *Ann. Rev. Biochem* **61**, 861-896 (1992).

39. M. L. Paddock, P. H. McPherson, G. Feher, M. Y. Okamura, *Proc. Nat. Acad. Sci. USA* **87**, 6803-6807 (1990).

40. E. Takahashi, C. A. Wraight, *Biochim. Biophys. Acta* **1020**, 107-111 (1990).

41. Paddock-ML, et al., *Biochemistry* **33**, 734-745 (1994).

42. S. H. Rongey, A. L. Juth, M. L. Paddock, G. Feher, M. Y. Okamura, *Biophys. J.* **68**, A247 (1995).

43. Takahashi-E, Wraight-CA, *Proc. Nat. Acad. Sci. USA* **93**, 2640-2645 (1996).

44. S. H. Rongey, M. L. Paddock, G. Feher, M. Y. Okamura, *Proc. Natl. Acad. Sci. USA* **90**, 1325-1329 (1993).

45. P. Beroza, D. R. Fredkin, M. Y. Okamura, G. Feher, . J. Breton, A. Vermeglio, Eds., The photosynthetic bacterial reaction center II (Plenum Press, New York, 1992).

46. D. B. Datta, *A Comprehensive Introduction to Membrane Biochemistry* (Floral Publishing, Madison, WI, 1987).

47. J. Barber, *Biochim. Biophys. Acta* **594**, 253-308 (1980).

48. A. P. Winiski, A. C. McLaughlin, R. V. McDaniel, M. Eisenberg, S. McLaughlin, *Biochemistry* **23**, 8206-8214 (1986).

49. S. C. Hartsel, D. S. Cafiso, *Biochemistry* **25** (1986).

50. S. McLaughlin, *Current Topics in Membranes and Transport* **9**, 71-144 (1977).

51. W. L. C. Vaz, A. Nicksch, F. Jahnig, *Eur. J. Biochem* **83**, 299-305 (1978).

52. S. McLaughlin, *Experimental tests of the assumptions inherent in the Gouy-Chapman-Stern theory of the aqueous diffuse double layer*. G. Spach, Ed., Physical Chemistry of Transmembrane Ion Motions (elsevier, amsterdam, 1983).

53. C. A. Wraight, *Isr. J. Chem* **21**, 348-354 (1981).

54. B. A. Diner, C. C. Schenck, C. DeVitry, *Biochim. Biophys. Acta* **776**, 9-20 (1984).

55. Z. Otwinowski, . L. Saywer, L. Issacs, S. Bailey, Eds., Data Collection and Processing (SERC Daresbury Laboratory, Daresbury, 1993).

56. S. Bailey, *Acta Crystallogr* **D50**, 760-763 (1994).

57. W. A. hendrickson, E. A. Lattman, *Acta Crystallogr* **B26**, 136-140 (1970).

58. W. Furey, S. Swaminathan, C. Carter, B. Sweet, Eds., Method. Enzym (Academic Press, Orlando, 1996), vol. in press.

59. T. A. Jones, *Methods Enzymol.* **115**, 157-171 (1985).

60. T. A. Jones, J. Y. Zhou, S. W. Cowan, M. Kjeldgaard, *Acta Crystallogr.* **A47**, 110-119 (1991).

61. S. V. Evans, *J. Mol. Graphics* **11**, 134-138 (1993).

62. W. Kabsch, *Acta Cryst.* **A32**, 922-923 (1976).

63. We gratefully acknowledge insightful comments and discussions with M.Y. Okamura, M.L. Paddock, H.L. Axelrod, and M.S. Graige. This work was supported by grants from the National Institutes of Health (NIH GM13191, NIH GM45162)

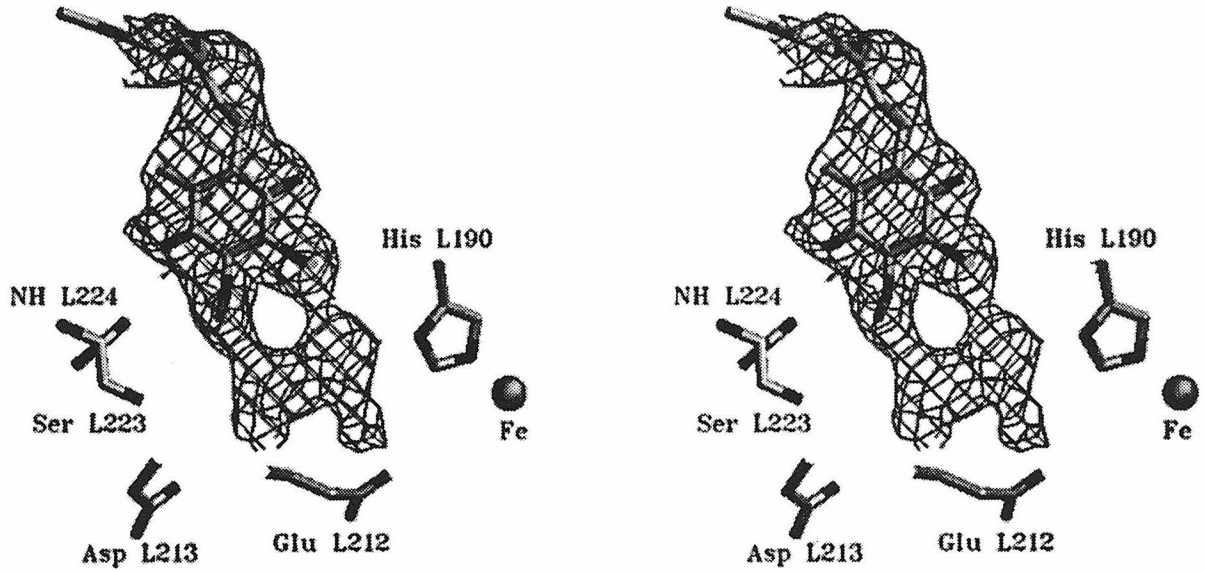

Fig. 1. Stereoview of the final $2F_O$-F_C omit refined electron density at the Q_B binding pocket in the DQ_AQ_B (dark) state; contoured at 1 σ. The ubiquinone is bound in the position referred to as the QB1 site. The electron density between the QB1 site and Glu L212 and His L190 is postulated to be due to partial occupancy of ubiquinone at the second site QB2. Compare with the structure of the $D^+Q_AQ_B^-$ (light) state in Fig 4.

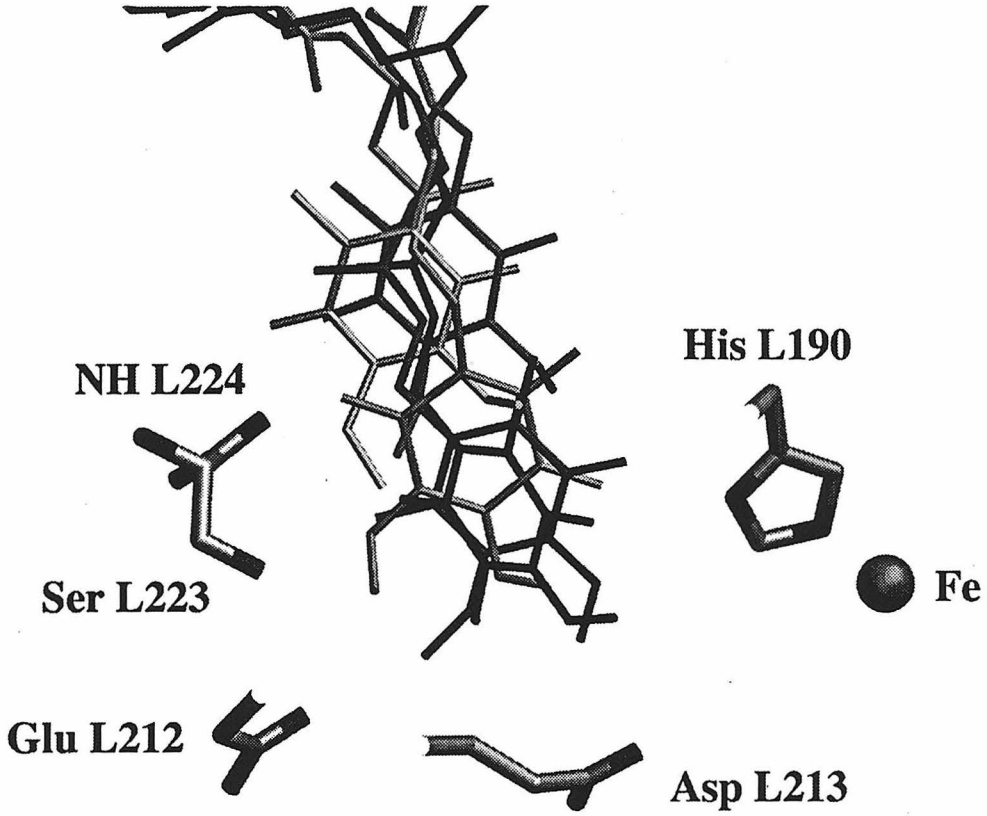

Fig. 2. Superposition of previously reported positions of ubiquinone in the Q_B binding pocket. PDB entries and color code: 1PCR(11), yellow; 2RCR (8), blue; 1YST (10), cyan; 4RCR (5, 6, 7), red; Present model of the dark structure: magenta. Superpostions was performed using the method of Kabsch (59) .

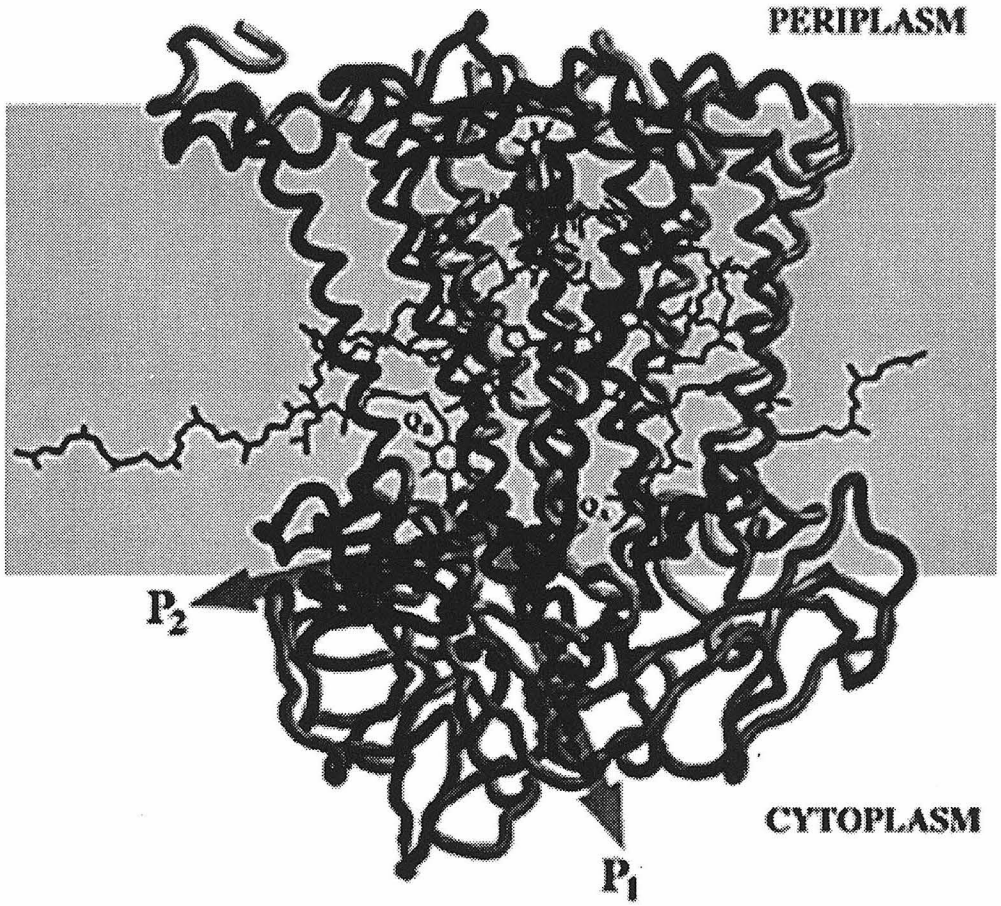

Fig. 3. Positions of the two water channels P1 and P2 leading from the Q_B pocket to the surface of the protein on the cytoplasmic side (dark structure). H-subunit: green, L-subunit: yellow, M-subunit: blue, oxygens of water: red, quinones and cofactors: purple. The approximate location of the membrane is indicated by the shaded region. For details of the P1 and P2 pathways, see Figs. 6A and 6B.

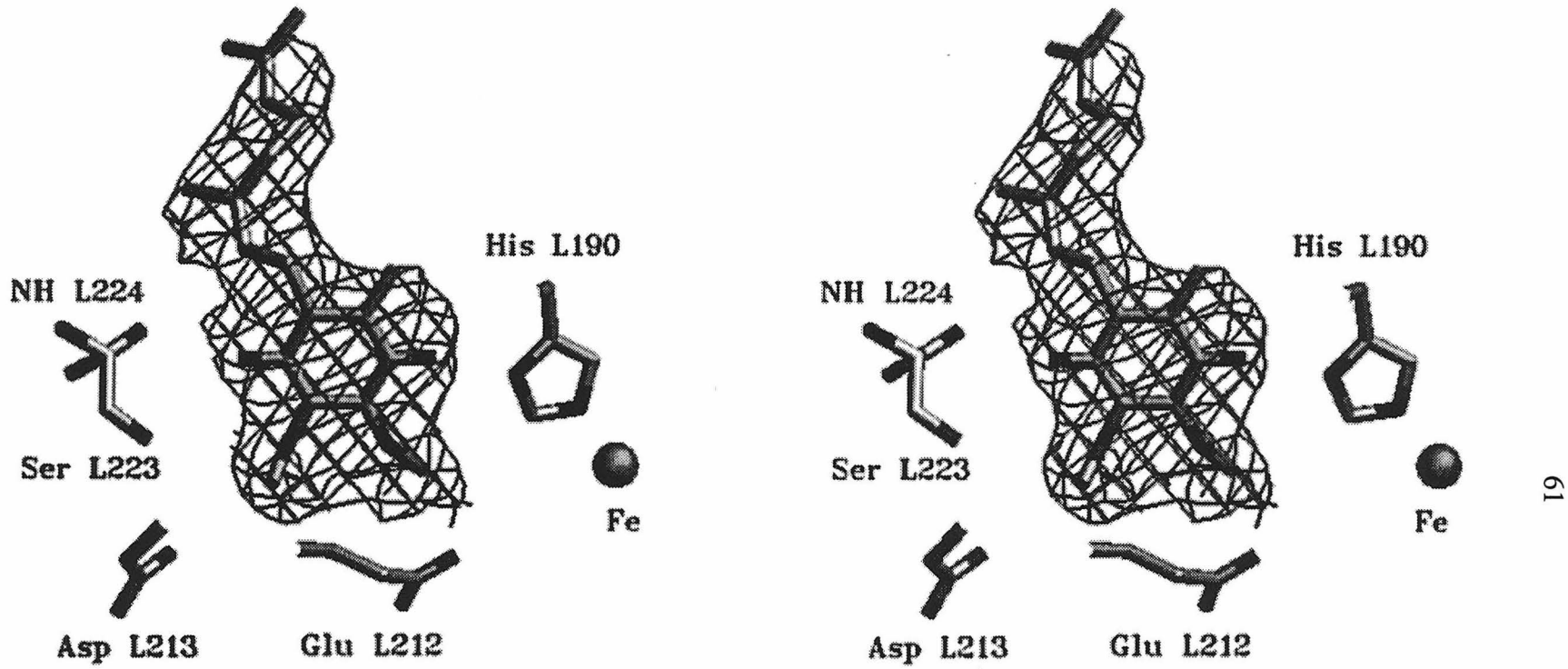

Fig. 4. Stereoview of the final $2F_O$-F_C omit refined electron density at the Q_B binding pocket in the $D^+Q_AQ_B^-$ (light) state; contoured at 1 σ. The ubiquinone is now in a position referred to as the Q_{B2} site, which is ~5.0 Å removed from the Q_{B1} site shown in Fig. 1. In addition the ubiquinone has undergone a 180° propeller twist with respect to the QB1 site observed in the dark structure.

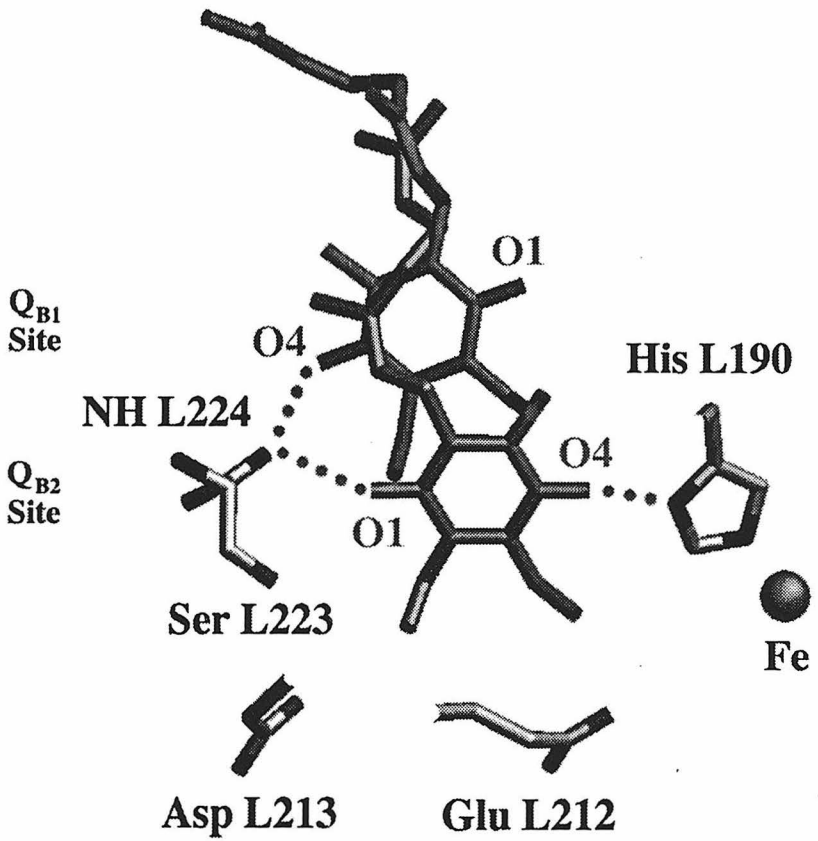

Fig. 5. Comparison of the dark (DQ_AQ_B) and the light ($D^+Q_AQ_B^-$) structures in the Q_B binding pocket. Dark structure: magenta, light structure: cyan. Hydrogen bonds are shown by dotted lines. This distance between the O1 carbonyl of the ubiquinone in the light structure and Ser L223 is 3.2 Å. In the light structure the ubiquinone has moved ~5.0 Å and undergone a 180° propeller twist.

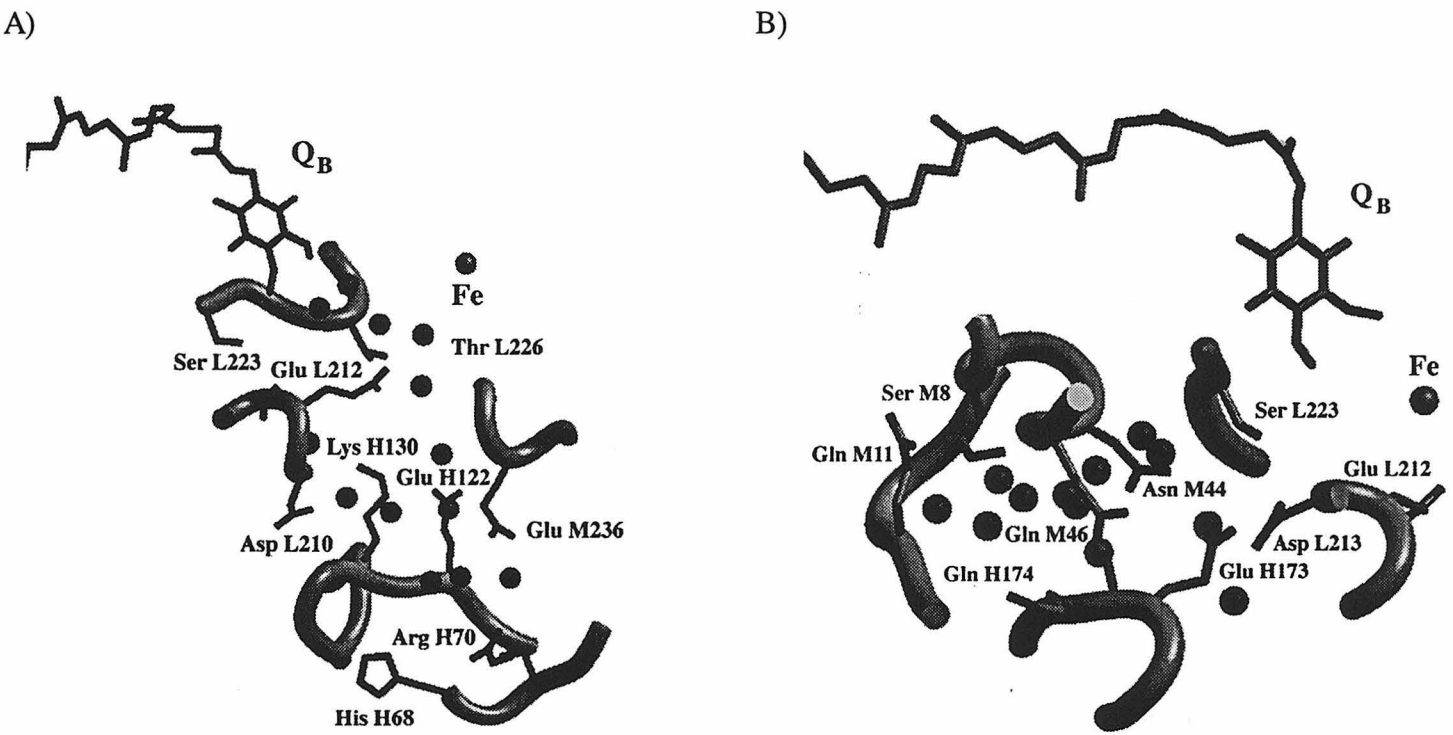

Fig 6. Details of the two water channels P1 (A) and P2 (B). Oxygens of water are shown in red. Positions of ubiquinone and iron are indicated. Cytoplasmic side of the RC is at the bottom.

Chapter IV

MEMBFAC: A Factorial Screening Method for Crystallizing Membrane Proteins. Crystallization and Diffraction Analysis of Complex II from *Paracoccus Denitrificans*

Submitted to the Journal of Molecular Biology

MEMBFAC: A Factorial Screening Method for Crystallizing Membrane Proteins. Crystallization and Diffraction Analysis of Complex II from *Paracoccus denitrificans*.

Michael H.B. Stowell[1,2,*], S. I. Chan[2], and D.C. Rees[1,*]

Carl F. and Winifred H. Braun Laboratories[1]

Arthur Amos Noyes Laboratory of Chemical Physics[2]

Department of Chemistry and Chemical Engineering

California Institute of Technology, Pasadena

California, 91125 USA

* Corresponding authors

Abstract. A factorial screening method is presented that is founded upon an in situ detergent exchange principle. The principle of in situ detergent exchange is based upon experimental and theoretical aspects of membrane protein stability. The method has been applied the crystallization of succinate:quinone oxidoreductase or complex II from *Paracoccus denitrificans*. The results suggest that this approach shows promise as a useful starting point for membrane protein crystallization, and perhaps more importantly, may lead to better diffracting crystals of membrane proteins.

Keywords: membrane protein; crystallization; factorial method; detergent exchange; complex II; succinate:quinone oxidoreductase.

Introduction

The crystallization of membrane proteins for x-ray crystallographic work is well recognized as a difficult and frustrating endeavor. The fact that only a few integral membrane protein structures have been determined by x-ray crystallography (1, 2, 3, 4, 5, 6, 7, 8), while thousands of soluble proteins have similarly been characterized (9), is a testimony to the difficulty of membrane protein crystallization. The principles and methods of crystallizing membrane proteins have been reviewed (10, 11, 12, 13). Such methods include the use of small amphiphiles to minimize the detergent micelle size, optimizing the approach to the detergent consulate boundary, and maximizing the soluble surface area of the protein. However, at present there appears to be no single principle which is universally applicable to the few membrane proteins that have been crystallized. Furthermore, while a number of membrane proteins have been crystallized, it is quite common that such crystals diffract to poor resolution, typically worse than 6 Å. In trying to understand these observations, we developed a factorial screening method which relies upon an in situ detergent exchange principle. The basis for this principle derives primarily from the general observation that membrane proteins are most stable in low critical micelle concentration (CMC) detergents and least stable in high CMC detergents. We feel that a potential obstacle to obtaining well diffracting crystals of membrane proteins lies in the incompatibility of detergents which are optimal for crystallization, and detergents which are optimal for stabilization. It is hoped that the simplicity of the in situ detergent exchange principle, together with the sparse matrix screening method described here, will encourage others to persue the crystallization of membrane proteins.

Experimental and Theoretical Basis for In Situ Detergent Exchange

The thermodynamic stability of proteins is a widely discussed topic and yet relatively little attention has been given to the specific problem of membrane protein stability (14, 15). The stability of proteins is very dependent upon the solution environment and, in the case of membrane proteins, the membrane. A handful of experiments have investigated the membrane's role in membrane protein stability. The thermostability of the Na^+K^+ ATPase was studied in a variety of organisms inhabiting different climatic regions (16). It was observed that the membrane bound stability of the Na^+K^+ ATPase correlated with the average body temperature of the organism. More compelling in this study was the observation that 4°C acclimated goldfish have a much less thermostable Na^+K^+ ATPase than 25°C acclimated goldfish. Since the composition of membranes are known to vary considerably with growth temperature, the change in stability of the Na^+K^+ ATPase most likely arises from the change in membrane composition. Quantitative evidence for this phenomenon comes from work of Maneri and Low who studied the thermostability of the erythrocyte anion transporter, Band 3 (17). These workers found that the thermostability of Band 3 increased with increasing fatty acid chain length. Because the gel to liquid crystal melting temperature of bilayer increases with acyl chain length, these studies directly demonstrate that the stability of the membrane protein is directly linked to the properties of the membrane.

An important question for membrane protein crystallization concerns the thermodynamic contribution of the detergent to membrane protein stability and how this might affect crystallization. In general, little information is available on the effects of detergent on membrane protein stability. However, an investigation by DeGrip et al. (18) provides some interesting and enlightening information on the effects of detergent on the thermostability of membrane proteins. This study examined the influence of 17 different detergents on rhodopsin stability, as measured by the midpoint temperature associated with the loss of the native absorption spectrum. Although the data are limited, within a given class of detergents, a lower CMC results in a more stable protein sample. As previously

noted, this is most readily explained by assuming that the free energy of micelle formation, ΔG_{mic}, contributes to the stability of the membrane protein. Figure 1 shows the correlation between the Tm of rhodopsin and the difference in ΔG_{mic}, $\Delta\Delta G_{mic}$, for a number of detergents. These data demonstrate the important role that the detergent and/or lipid plays in the thermodynamic stability of membrane proteins.

The preceeding considerations motivated the formulation of an in situ detergent exchange principle for membrane protein crystallization. As discussed, the detergent plays a critical role in the crystallization of membrane proteins. Reaching a crystalline state requires the formation of appropriate protein-protein interactions, as well as appropriate detergent-protein and detergent-detergent interactions. Crystallization of membrane proteins therefore requires the formation of a detergent-protein complex that optimizes all three types of interactions. Importantly, maximizing the protein-protein interactions requires minimizing the size of the micellar torus that surrounds the membranous portion of the protein. As shown in figure 2 the micelle size of detergents are inversely correlated with the CMC. Accordingly, detergents with high CMC's have been preferred for crystallization because they would in principle allow for maximum protein-protein interactions, and it has been recommended that the low CMC detergents used during purification be removed and exchanged for detergents with a high CMC, prior to crystallization trials. Although this may be possible for some membrane proteins, the majority of membrane proteins are likely to be unstable in high CMC detergents, for the reasons discussed above. Accordingly, the detergent exchange normally recommended, may in fact result in a destabilized or even denatured protein. To circumvent this problem, we propose that detergent exchange be carried out during the crystallization process. In this fashion, a range of micelle sizes can be sampled during the crystallization trials and the problem of destabilization and or denaturation by detergent exchange can be circumvented, or at least minimized. To illustrate this method, a simplified thermodynamic profile of an in situ detergent exchange experiment is shown in Fig 3. A membrane protein purified in a low CMC detergent is

allowed to equilibrate with a high CMC detergent under crystallization conditions. In a typical experiments, the concentration of the high CMC detergent would be a factor of 5-10 times that of the purification detergent. During equilibration, the micelle surrounding the protein will move from the large size of the isolation detergent to the small size of the crystallization detergent. As a result of the exchange the free energy of the system will favor either denatured protein, or crystallization, with one state being entropically favored and the other being enthalpically favored. If all goes well, conditions that favor formation of crystals will be achieved at some point during the equilibration. Optimization of this process can be achieved by varying both the starting detergent concentration of the protein sample as well as the starting concentration of the equilibration detergent.

Results

The INFAC program (19) was utilized to determined the 48 solutions listed in Table 1. These 48 solutions. along with the addition of a number of detergents, were utilized to screen for appropriate conditions for complex II crystallization. The crystallization of complex II occurred in 1-2 weeks and resulted in very small diamond shaped crystals with largest dimensions of 5-10μm under several conditions (#3 and #9). Optimization of both the final detergent concentration in the purified protein and in the crystallization, resulted in the formation of larger crystals (300-500μm) shown in figure 4, that were suitable for x-ray diffraction work. Confirmation that the crystals contained complex II was obtained by washing several crystals in synthetic mother liquor and dissolving them in an aqueous buffer. This solution gave the characteristic UV/VIS absorption spectra for purified complex II and SDS-PAGE analysis of this material showed the correct polypeptide composition for complex II (data not shown). The diffraction quality of these crystals was measured on beam line 7-1 at the Stanford Synchrotron Radiation Laboratory. Figure 5 shows a diffraction image resulting from a 10 second exposure with 1.0 degree oscillation

for a crystal mounted at room temperature. The red + indicates a resolution of 2.9 angstroms. A complete data set to 3.5 angstroms has been collected, and the space group has been assigned to R32,with unit cell dimensions of a=b=173.0 Å and c=373.0 Å in the hexagonal setting. Assuming a single complex II molecule of 120 kD per asymmetric unit, a Matthew's coefficient of 4.18 which is calculated that is typical for membrane protein crystals. Two molecules per asymmetric unit would give an unacceptably small Matthew's coefficient of 2.09. Self rotation functions have not yielded any indication of possible noncrystallographic symmetry, which further supports the assignment of a single complex II molecule per asymmetric unit. We are currently screening heavy atom compounds for structure determination by multiple isomorphous replacement methods.

Discussion

The development of a factorial screening method that employs an situ detergent exchange principle has been presented. The method was motivated from general observations about membrane protein stability and in particular the instability of the protein utilized in this study, complex II from *Paracoccus denitrificans*. The method has been succesfully applied to the crystallization of complex II from *P. denitrificans* (presented here), fumarate reductase from *E. coli*, the photosynthetic reaction center from *Rb. sphaeroides* and implementation on a number of other proteins is currently in progress.

Although the precise thermodynamic reasons for the destabilization of membrane proteins in high CMC detergents is not known, stability is correlated with the ΔG of micelle formation ,as shown in figure 2. Theoretical models for lipid-protein interactions in membranes suggest that energetic strain is introduced into the bilayer by the "hydrophobic mismatch" between the bilayer thickness and an integral membrane protein. Hydrophobic mismatch gives rise to an interfacial free energy term that is minimized when the lipid (or detergent) chain lengths ideally match the hydrophobic region of the protein. As the

interfacial free energy increases, either the protein or the lipid can undergo compressions or extensions in response. An important question concerns the possible manipulation of this effect for the benefit of membrane protein crystallization. At the present time, little is known about the energetics of the intramembraneous regions of membrane proteins and a more rigorous treatment of these effects is clearly necessary to fully understand the phenomenon and to help guide efforts in crystallization. Nonetheless, the importance of maintaining a stable protein detergent complex for crystallization is clear, and we feel that the use of in situ detergent exchange for membrane protein crystallization is an important factor to be considered and utilized.

Materials and Methods

All detergents were purchased from either Boehrenger-Manheim or Anatrace. Buffers were purchased from Calbiochem. PEG's were purchased from Fluka. Precipitant solutions were made from premade stock solutions and the pH was not readjusted. The 48 precipitant solutions were determined using the program INFAC (19), with slight modifications. Crystal trials were performed using the sitting drop technique in Linbro trays. To each of the 48 crystallization solutions, a screening detergent was added to a final concentration of 0.5 to 1.0 % final concentration. Precipitant wells were 600 µL in volume and each experiment consisted of layering 2 µL of protein solution on top of 2 µL of well solution. Wells were sealed with a cover slip using standard vacuum grease and allowed to stand for 1-2 weeks before inspection.

Complex II from *Paracoccus denitrificans* (ATCC13543) was purified using a method similar to Pennoyer et al (20) and activity assays and enzyme concentrations were as described except that ubiquinone-1 was used in the activity assays. Maximal turnover rates for purified complex II were typically 300-350 s^{-1}. The purified enzyme had a molar ratio of FAD to b-heme and ubiquinone of 1:1.0±0.3:0.9±0.3. The final detergent

concentration in the enzyme prepartation was determined using a colorametric assay recently developed (21). SDS-PAGE analysis was performed according to the method of Laemmli (22). Optical spectra were recorded on an HP8453 UV/VIS spectrophotometer.

Table I.

1.	0.1 M NaAcetate	pH 4.6	12% MPD	0.1 M NaCl	
2.	0.1 M NaAcetate	pH 4.6	12% PEG 4000	0.1 M ZnCl	
3.	0.1 M NaAcetate	pH 4.6	10% PEG 4000	0.2 M NH4SO4	
4.	0.1 M NaAcetate	pH 4.6	12% Isopropanol	0.1 M NaCl	
5.	0.1 M NaAcetate	pH 4.6	12% PEG 4000		
6.	0.1 M NaAcetate	pH 4.6	1.0 M ANH4SO4		
7.	0.1 M NaAcetate	pH 4.6	1.0 M MgSO4		
8.	0.1 M NaAcetate	pH 4.6	18% PEG 400	0.1 M MgCl	
9.	0.1 M NaAcetate	pH 4.6	1.0 M NH4PO4	0.1 M LiSO4	
10.	0.1 M NaAcetate	pH 4.6	12% PEG 6000	0.1 M NaCl	
11.	0.1 M NaAcetate	pH 4.6	12% PEG 6000	0.1 M MgCl	
12.	0.1 M NaCitrate	pH 5.6	18% PEG 400	0.1 M NaCl	
13.	0.1 M NaCitrate	pH 5.6	12% PEG 4000	0.1 M LiSO4	
14.	0.1 M NaCitrate	pH 5.6	10% Isopropanol	0.1 M NaCitrate	
15.	0.1 M NaCitrate	pH 5.6	12% MPD	0.1 M NaCl	
16.	0.1 M NaCitrate	pH 5.6	1.0 M MgSO4		
17.	0.1 M NaCitrate	pH 5.6	12% PEG 4000	0.1 M NaCl	
18.	0.1 M NaCitrate	pH 5.6	12% PEG 6000	0.1 M LiSO4	
19.	0.1 M NaCitrate	pH 5.6	4% MPD	0.1 M MgCl	
20.	0.1 M NaCitrate	pH 5.6		0.1 M NaCl	
21.	0.1 M NaCitrate	pH 5.6	4% PEG 400	0.1 M LiSO4	
22.	0.1 M ADA	pH 6.5	1.0 M NH4SO4		
23.	0.1 M ADA	pH 6.5	12% PEG 4000	2% Isopropanol	0.1M LiSO4
24.	0.1 M ADA	pH 6.5	1.0M (NH4)2PO4		
25.	0.1 M ADA	pH 6.5	12% PEG 6000	0.1M MgCl	
26.	0.1 M ADA	pH 6.5	12% MPD		
27.	0.1 M ADA	pH 6.5	1.0 M MgSO4	0.1 M LiSO4	
28.	0.1 M ADA	pH 6.5	4% PEG 400	0.3 M LiSO4	
29.	0.1 M HEPES	pH 7.5	1.0 M NaKPO4	0.1 M NH4SO4	
30.	0.1 M HEPES	pH 7.5	10% PEG 4000	0.1 M NaCl	
31.	0.1 M HEPES	pH 7.5	18% PEG 400	0.1 M MgCl	
32.	0.1 M HEPES	pH 7.5	1.0 M NaK Tartrate		
33.	0.1 M HEPES	pH 7.5	18% PEG 400	0.1 M NH4SO4	
34.	0.1 M HEPES	pH 7.5	10% PEG 4000	0.1 M NH4SO4	
35.	0.1 M HEPES	pH 7.5	12% MPD	0.1 M NaCitrate	
36.	0.1 M HEPES	pH 7.5	1.0 M NaCitrate		
37.	0.1 M HEPES	pH 7.5	4% PEG 400	0.6 M MgSO4	
38.	0.1 M HEPES	pH 7.5	4% MPD	0.6 M MgSO4	
39.	0.1 M HEPES	pH 7.5	0.1 M NaK Tartrate	0.1 M LiSO4	
40.	0.1 M Tris-HCl	pH 8.5	12% MPD	0.1 M LiSO4	
41.	0.1 M Tris-HCl	pH 8.5	1.0 M NaKPO4	0.1 NH4PO4	
42.	0.1 M Tris-HCl	pH 8.5	0.1 M NaAcetate		
43.	0.1 M Tris-HCl	pH 8.5	0.1 M NaCl		
44.	0.1 M Tris-HCl	pH 8.5	12% PEG 6000	0.1 NH4PO4	
45.	0.1 M Tris-HCl	pH 8.5	0.4 M MgSO4	0.1 M KNa Tartrate	
46.	0.1 M Tris-HCl	pH 8.5	0.2 M LiSO4		
47.	0.1 M Tris-HCl	pH 8.5	0.5 M NH4SO4		
48.	0.1 M Tris-HCl	pH 8.5	5% PEG 400	0.1 M NaCitrate	

PEG, polyethylene glycol; ADA, N-(2-acetamido)-iminodiacetic acid; HEPES, N-2-hydroxyethyl piperazine-N-2-ethanesulfonic acid ; Tris, tris-(hydroxymethyl)aminomethane.

Acknowledgments

We thank Michael C. Weiner, Gil G. Prive, and Siegfried M. Musser for insightful discussions. This work was supported by NIH grants to D. C. R. and S. I. C. The SSRL beam line 7-1 facility is supported by the DOE Office of Basic Energy Sciences and the NIH Biomedical Technology Program, Division of Research Resources.

REFERENCES AND NOTES

1. J. P. Allen, et al., *Proc. Nat. Acad. Sci. USA* **83**, 8589-8593 (1986).
2. J. Deisenhofer, O. Epp, K. Miki, R. Huber, H. Michel, *Nature* **318**, 618-624 (1985).
3. M. S. Weiss, et al., *FEBS Lett.* **280**, 379-382 (1991).
4. S. W. Cowan, et al., *Nature* **358**, 727-733 (1992).
5. T. Tsukihara, et al., *Science* **272**, 1136-1144 (1996).
6. S. Iwata, C. Ostermeier, B. Ludwig, Michel-H., *Nature* **376**, 660-669 (1996).
7. D. Picot, P. J. Loll, R. M. Garavito, *Nature* **367**, 243-249 (1994).
8. G. McDermott, et al., *Nature* **374**, 517-521 (1995).
9. PDB, .
10. H. Michel, *Trends Biochem. Sci.* **8**, 56-59 (1983).
11. W. Kühlbrandt, *Q. Rev. Biophys.* **21**, 429-477 (1988).
12. R. M. Garavito, D. Picot, *Methods* **1**, 57-69 (1990).
13. R. M. Garavito, D. Picot, P. J. Loll, *Journal of Bioenergetics and Biomembranes* **28**, 1996 (1996).
14. M. H. B. Stowell, D. C. Rees, *Advances in Proteins Science* **46**, 279-311 (1995).
15. T. Haltia, E. Freire, *Biochimica et Biophysica Acta* **1228**, 1-27 (1995).
16. A. R. Cossins, M. Behan, G. Jones, K. Bowler, *Bioch. Soc. Trans.* **15**, 77-81 (1987).
17. L. R. Maneri, P. S. Low, *J. Biol. Chem.* **263**, 16170-16178 (1988).
18. W. J. de Grip, J. van Oostrum, G. L. J. de Caluwe, *Journal of Crystal Growth* **122**, 375-384 (1992).
19. J. r. Carter, W. C, C. W. Carter, *J. Biol. Chem.* **254**, 12219-12223 (1979).

20. J. D. Pennoyer, T. Ohnishi, B. L. Trumpower, *Biochimica et Biophysica Acta.* **935**, 195-207 (1988).

21. M. H. B. Stowell, K. Zhu, Chan, S. I., D. C. Rees, in preparation.

22. U. K. Laemmli, *Nature* **227**, 680-685 (1970).

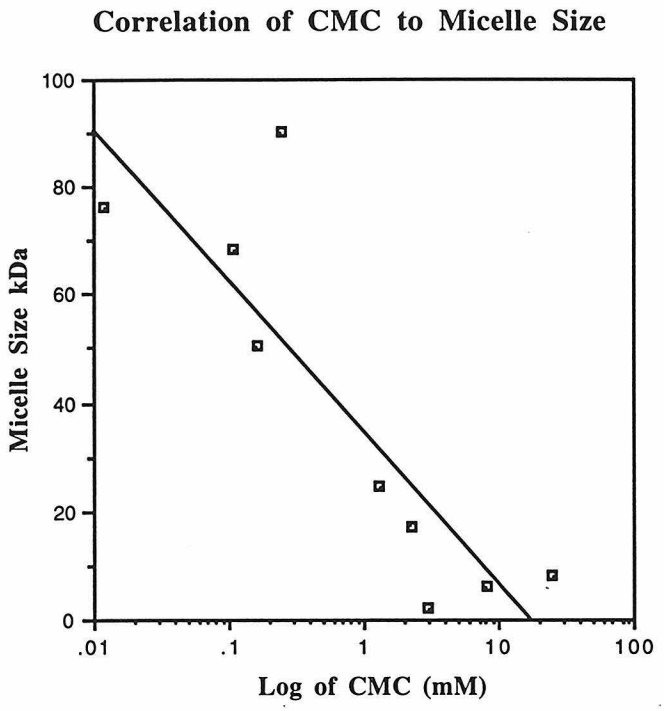

Fig 1. Correlation of detergent micelle size and CMC for a variety of comercially available detergents.

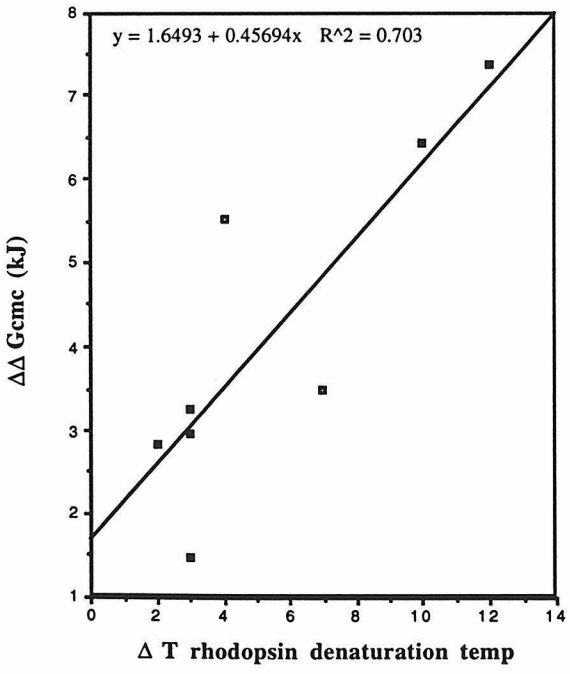

Fig. 2. Plot of ΔΔG of micelle formation versus Tm for rhodopsin in a variety of detergents, data from DeGripp et al.

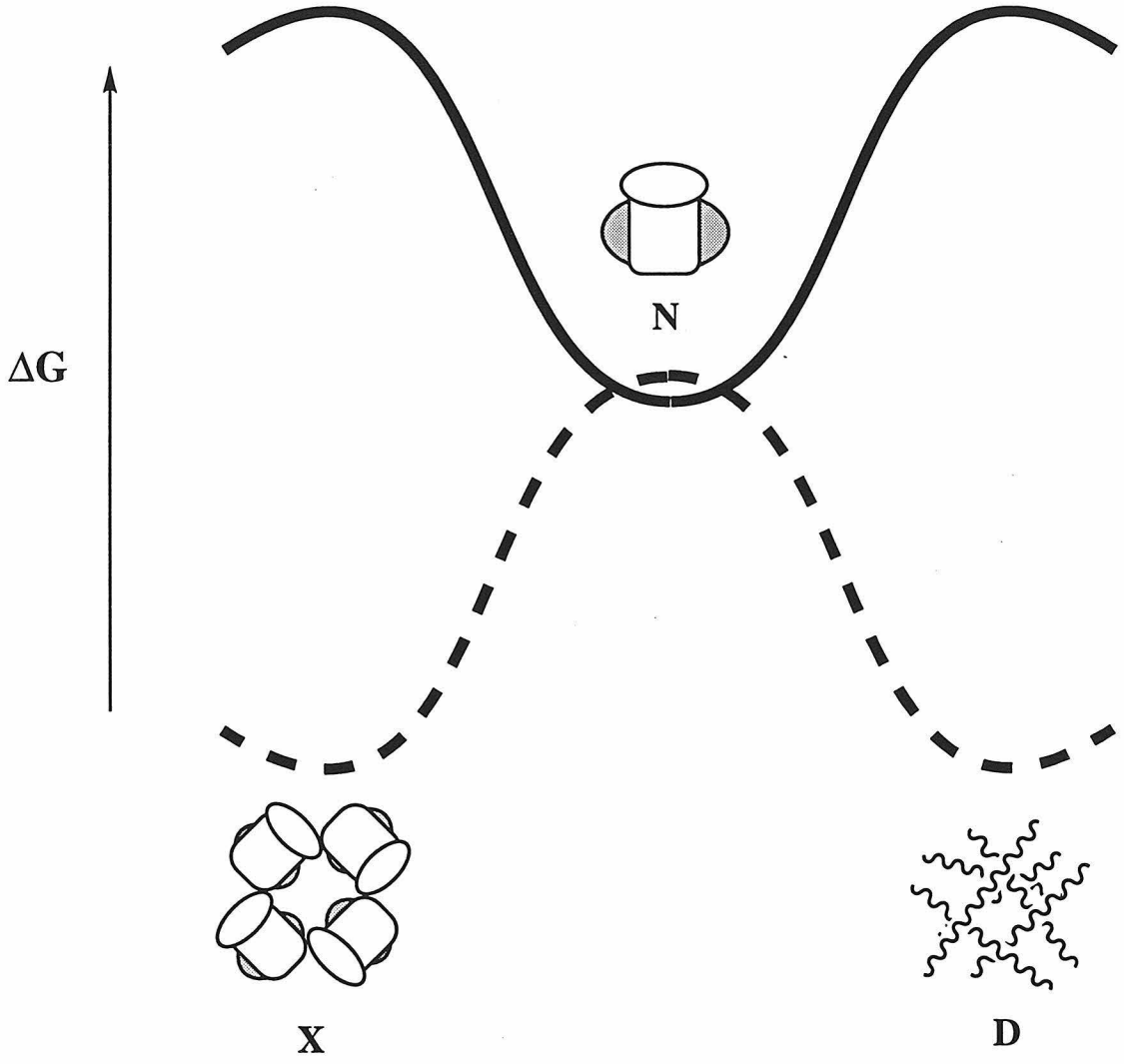

Fig. 3. Simplified thermodynamic surface for a crystallization experiment performed during in situ detergent exchange. State X is the crystalline state, D is the denatured state and N is the native as isolated state.

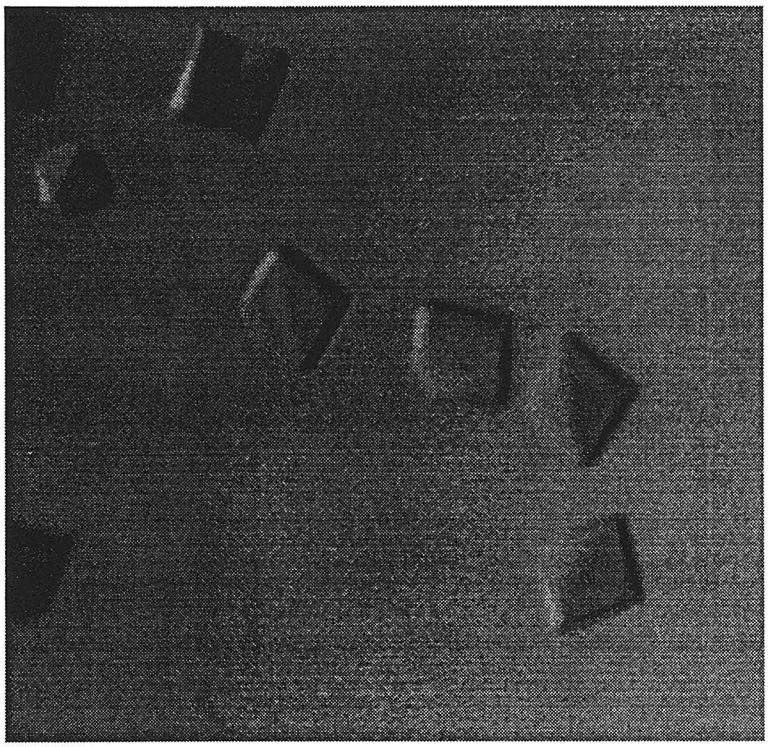

Fig. 4. Photograph of complex II crystals obtained using in situ detergent exchange with Membfac.

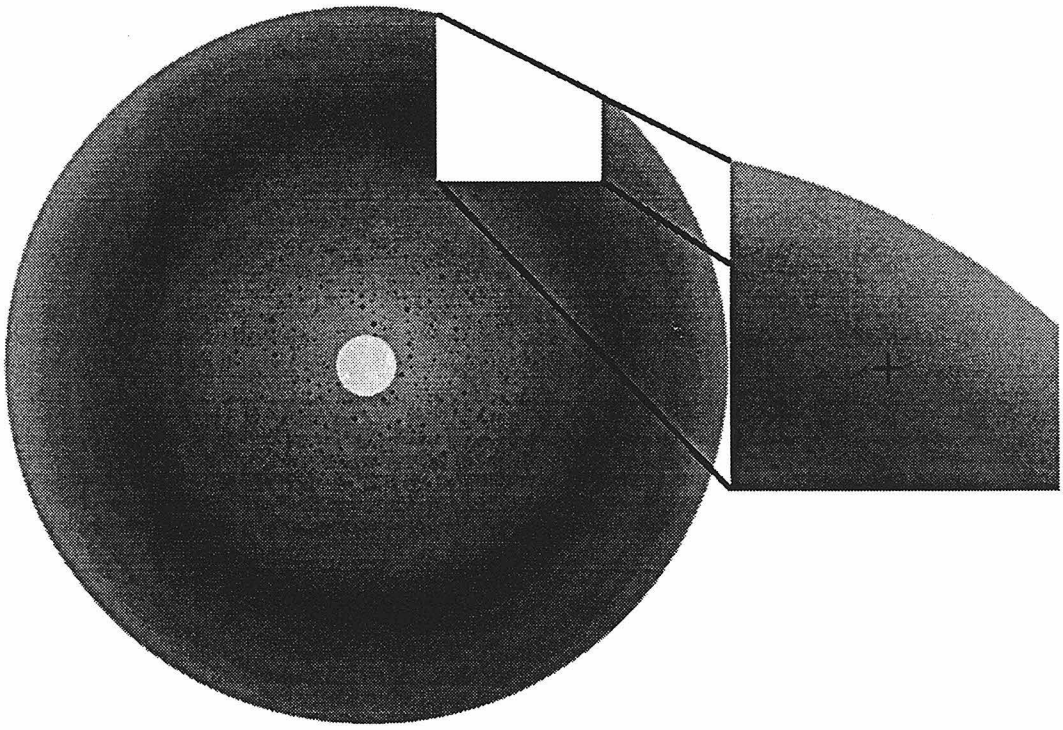

Fig. 5. Photograph of diffraction image from the crystals shown in Fig 4. The red + mark indicates a resolution of 2.9 angstroms. See text for details.

Chapter V

Design, Synthesis, and Photochemical Properties of a Photoreleasable Ubiquinol-2: A Novel Compound for Studying Rapid Electron-Transfer Kinetics in Ubiquinol Oxidases

Submitted to Journal of the American Chemical Society

Design, Synthesis, and Photochemical Properties of a Photoreleasable Ubiquinol-2: A Novel Compound for Studying Rapid Electron-Transfer Kinetics in Ubiquinol Oxidases

Michael H. B. Stowell,[1a,b,*] Guanyang Wang,[1a] Michael W. Day, [1c] and Sunney I. Chan[1a]

Contribution from the Arthur Amos Noyes Laboratory of Chemical Physics, the Beckman Institute, and the Carl F. and Winifred H. Braun Laboratories, Division of Chemistry and Chemical Engineering, California Institute of Technology, Pasadena, CA 91125

Abstract. The design and multistep convergent synthesis of the novel photoactive ubiquinol-benzoin adduct **1a,b** has been accomplished. Optical spectra of the steady state photolysis reactions showed a smooth conversion from **1a,b** to 5,7-dimethoxy-2-phenylbenzofuran (**2**) and ubiquinol-2 (**3**) with an isobestic point at 258 nm. HPLC analysis of the photoproducts was also consistent with the clean formation of the desired ubiquinol-2 (**3**), and the expected 5,7-dimethoxy-2-phenylbenzofuran (**2**). Transient photolysis at 355 nm was consistent with a rapid photolysis rate that exceeded the instrument response time ($>10^6$ s^{-1}). Accordingly, the study of rapid electron transfer events in ubiquinol oxidizing enzymes is now feasible. Furthermore, the synthetic methods developed herein will be of general application for the facile synthesis of a variety of phtoreleasable substrates for studying rapid kinetic events in enzymatic reactions.

Introduction

The study of rapid electron transfer events in redox active enzymes is critical to understanding the detailed enzymatic mechanism of these proteins. An example is cytochrome *c* oxidase where the methods for rapid photoreduction of cytochrome *c* have facilitated the investigation of the electron transfer processes in this enzyme[1,2] . While such methods are well suited for single electron donating or accepting proteins such as cytochrome *c* , a number of redox active enzymes are ubiquinol oxidizing enzymes and are not amenable to these methods because they require a rapid two electron reduction of ubiquinone to form ubiquinol. A novel approach to this problem was the use of the photosynthetic reaction center (PRC) to produce ubiquinol from ubiquinone and to study the rapid kinetic events in the b_6f complex[3] . Unfortunately, the rate for ubiquinol release from the PRC is slow in comparison to typical ubiquinol oxidation rates for enzymes such as the bc_1 or b_6f complex. Consequently, a more rapid method is required for producing ubiquinol on a sufficiently fast time scale to make kinetic resolution possible. Towards this end, we have developed a method that can rapidly produce ubiquinol through the use of "caged" compounds. Caged compounds were originally utilized as protecting groups in organic synthesis and have the convenient property that they can be removed photochemically. In a classic paper, Woodward described the synthesis and photocleavage properties of a series of substituted nitrobenzyl protecting groups.[4] Subsequently, a variety of nitrobenzyl protecting groups have played important roles in synthetic strategies, as well as being exploited for use in such diverse fields as semiconductor lithography [5] and as "caged" compounds in the study of rapid enzymatic processes.[6,7]

Scheme I

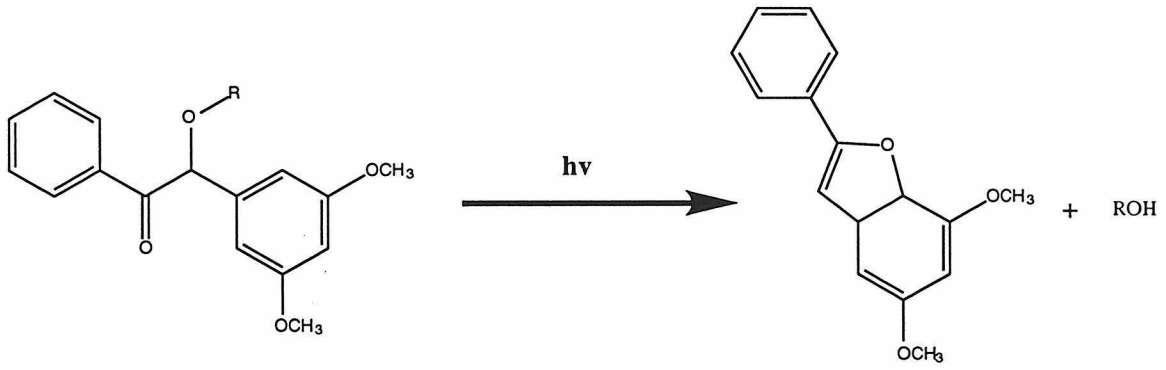

1 **13**

Recently, a recurring interest in 3',5'-dimethoxy benzoin (DMB) compounds has been generated as these compounds posses remarkable photolysis properties. Such compounds have been reported to photolyze with rates exceeding 10^{10} s^{-1} and quantum yields of 0.67, to give 5,7-dimethoxy-2-phenylbenzofuran (**13**) and the caged substrate **ROH**, Scheme I. Herein we report the design, synthesis and photochemical properties of a "caged" ubiquinol-2 (**1a,b**), based upon the photoactive 3',5'-dimethoxy benzoin. We also report the remarkable photocleavage properties of this "caged" ubiquinol and demonstrate the production of ubiquinol-2 with rates exceeding 10^6 s^{-1}. Accordingly, with this newly available caged ubiquinol-2, rapid electron transfer studies on ubiquinol oxidizing enzymes are now feasable which will lead to a greater understanding of this important class of enzymes.

Results and Discussion

In designing a system for rapidly producing ubiquinol by flash photolysis several factors were considered. First, to insure kinetic resolution, the photolysis rate must exceed the enzymatic turnover rate by several orders of magnitude. Secondly, the quantum yield of photolysis should be large enough to produce readily measurable signals for kinetic studies by transient absorption. Lastly, the photolysis should minimize secondary radicals or other reactive species that could inhibit or damage the protein sample. For these reasons, the use

of the DMB compounds, originally described by Sheehan and coworkers [Sheehan, 1971 #1031] , seemed ideal. These compounds exhibit very rapid photolysis rates (> 10^{10} s^{-1}, for the acetates), have a high quantum efficiency of 0.64, and in addition, the benzofuran photolysis product is stable and unreactive. A simple retrosynthetic scheme leads to ubiquinone-2 (**2**) and the readily available dithiane (**3**).

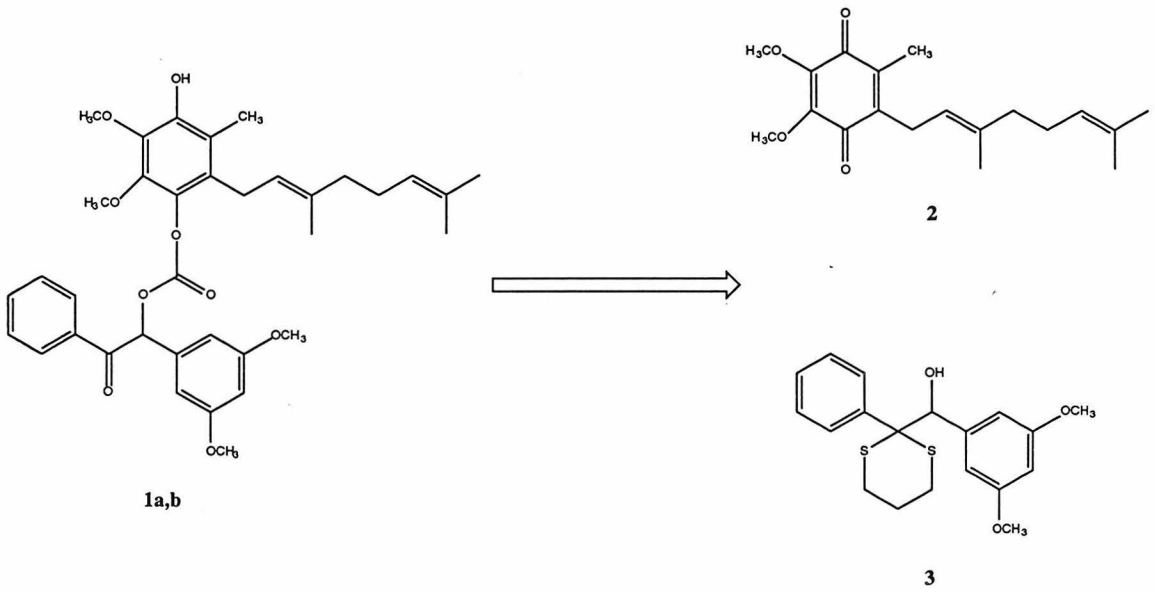

Synthesis of a DMB coupling reagent. The crtitical step in this scheme is the formation of the carbonate linkage between the ubiquinol and the dithiane **3**. Several methods were investigated for the formation of an activated carbonate dithiane. These included the use of phosgene, di- and tri-phosgene, carbonyl diimidazole, as well as the triflate salt of dimethyl carbonyl diimidazole. These methods were persued but ultimately were deemed inefficient for our purposes due to the formation of a dehydration product (**4**) in substantial, to near quantitative, yield, scheme I.

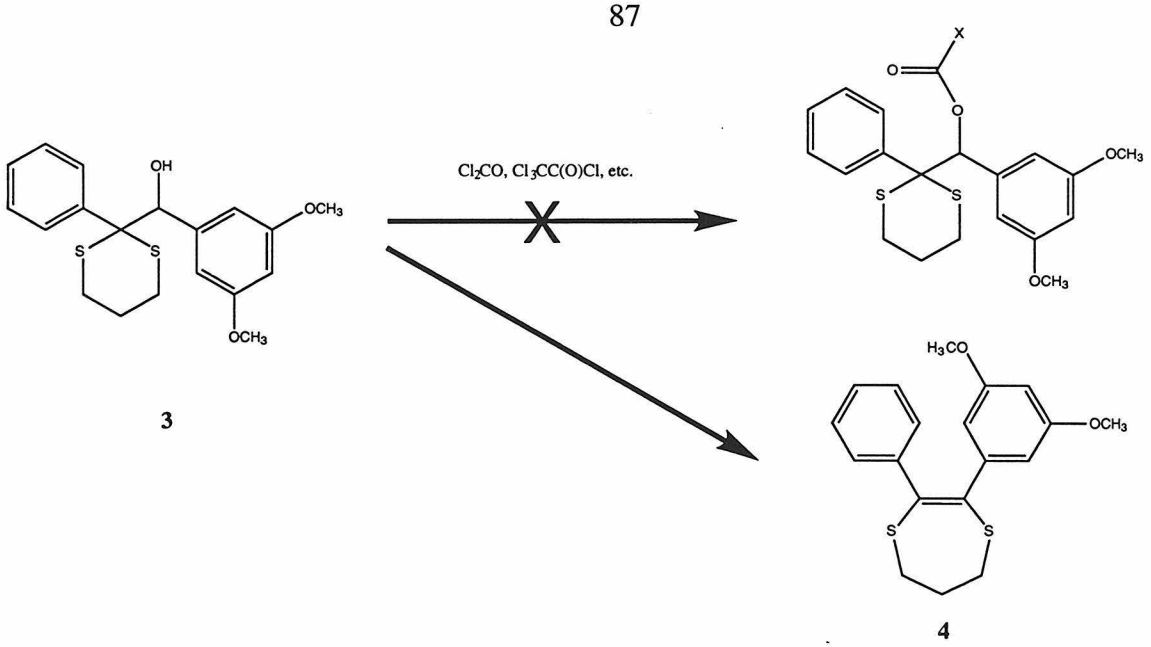

3 4

We then attempted to form the mixed carbonate of 2-nitrophenol and dithiane **3**. The 2-nitrophenol carbonate was chosen because it has been reported that such carbonates are highly reactive in the presence of DMAP and we anticipated that the coupling of a hindered 2,6 substuted aromatic system would be difficult. Reaction of dithiane **3** with 2-nitrophenyl-chlorocarbonate in methylene chloride and excess pyridine readily produced the desired mixed carbonate **5** in good yield and without formation the previsouly observed dehydration product **4**.

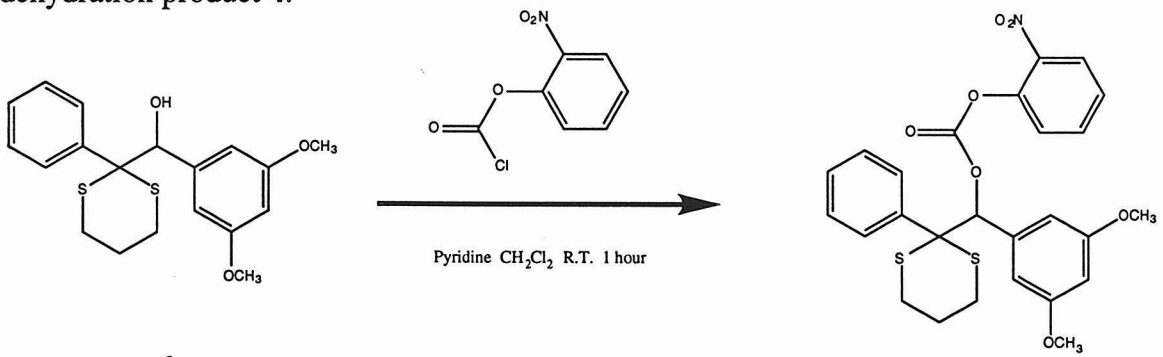

3 5

With a readilly available coupling compound in hand, we then attempted to establish if the coupling between compound **5** and a sterically hindered phenol would be possible. Accordingly, we reacted compound **5** with 2,6-dimethoxyphenol in the presence of DMAP at room temperature.

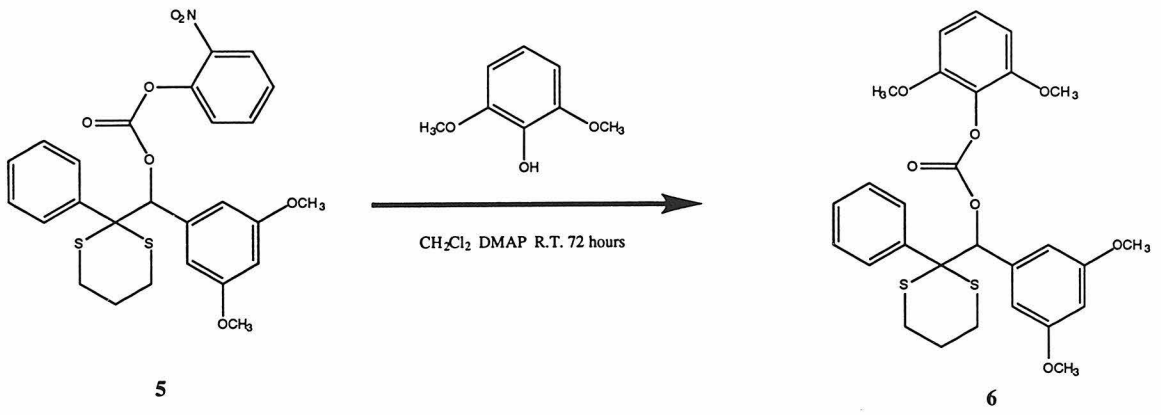

5 6

We were delighted to observe the nearly quantitative formation of the the desired compound **6**. This compound readily crystallized and was subjected to X-ray diffraction analysis in order to firmly establish that the desired synthetic tranformations had proceded as expected. Figure 1 diplays the 50% thermal elipsoid ORTEP drawing of X-ray crystal structure of compound **6**, and confirms the correctness of the synthetic methods to this point. It is worth noting that the ease of preparation and the observed coupling effeciency of compound 5 should make it a versatile reagent in a variety of synthetic methods were orthogonal protecting groups are required.

Synthesis of the ubiquinol-2 substrate. The next synthetic target was the ubiquinone-2 molecule. The methods utilized were similar to those described earlier utilized a Diels-Alder tranformation of quinone to the tricyclodione (**7**). Alkylation and subsequent retro-Diels-Alder reaction of the alkylated tricyclodione (**8**) afforded the desired ubiquinone-2 in an overall yield of 73%.

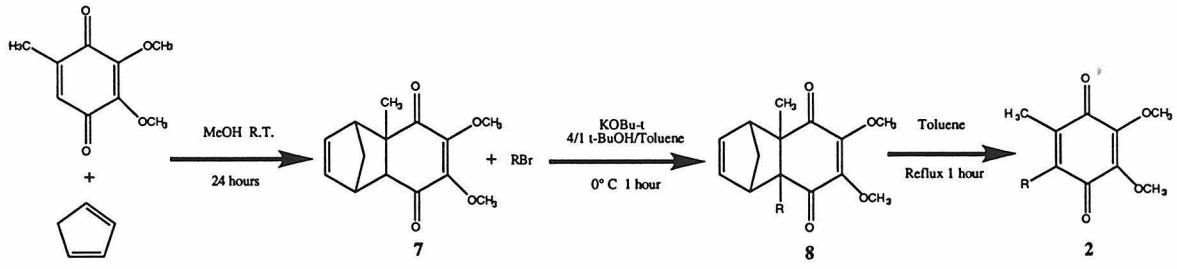

7 8 2

Because of the bifunctional nature of the ubiquinol-2 we chose to selectivly silyate a single phenolic oxygen using triethylsilyl chloride. Treatment of ubiquinone-2 with sodium dithioinite in aqueous methanol and extraction with hexane gave ubiquinol-2 in greater than 99% yield. Silyation of the ubiquinol-2 with triethylsilyl chloride in dry acetonitrile with pyridine catalyst afforded the monosilyl ubiquinol-2 (**9**) in 61% yield.

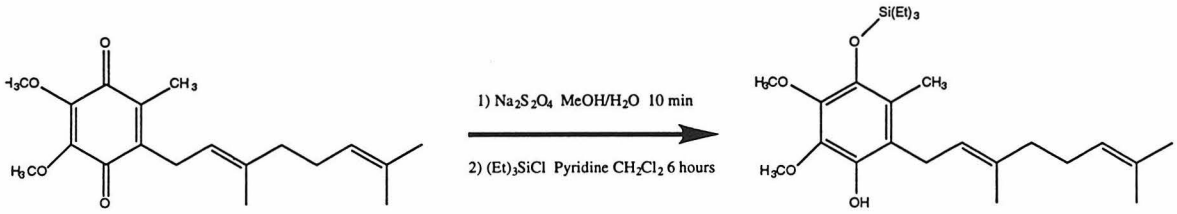

2 **9**

Assembly of the caged ubiquinol-2. The mono-silyl ubiquinol-2 was subsequently coupled to the o-nitrophenyl carbonate ester of 3',5'-dimethoxy-phenyl-(phenyl-dithiane) using DMAP in methylene chloride. Formation of the o-nitrophenyl carbonate ester of 3',5'-dimethoxy-phenyl-(phenyl-dithiane) was accomplished using and o-nitrophenyl-chloroformate in pyridine.

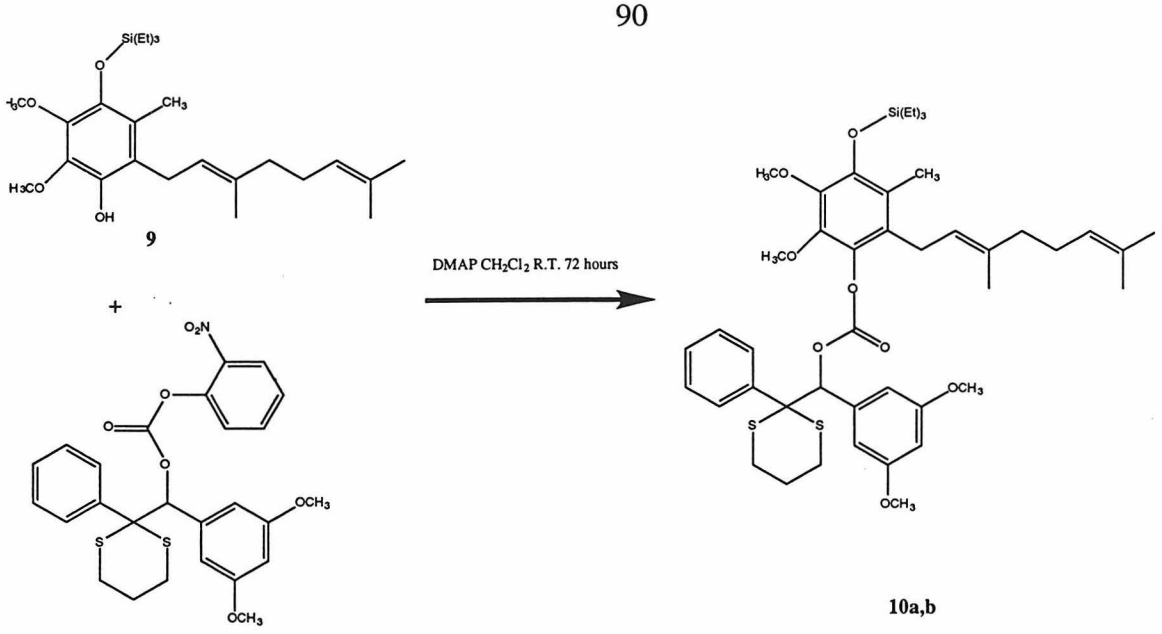

Activation and deprotection was accomplished in one step by first treatment with bisTFAiodobenzene in THF water, followed by silyldeprotection by HF:pyridine in acetonitrile. The resultant product was purified by reverse phase HPLC to yield the desired "caged" ubiquinol-2 (**1a,b**) as a clear colorless waxy solid.

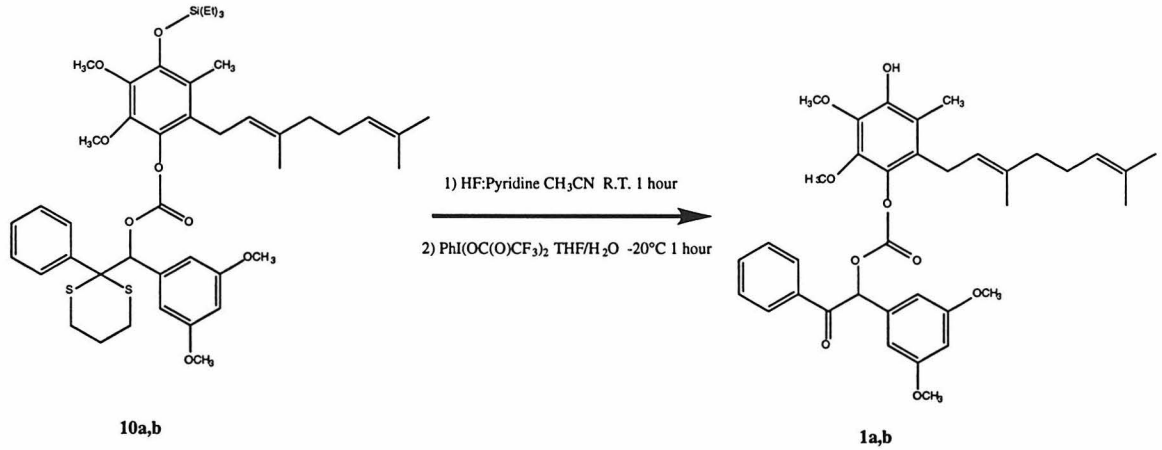

Photolysis of the assembled caged ubiquinol-2. Three experimental criteria were utilized to determine the usefulness of compound 1a,b for rapid kinetic studies. First was the faciel steady state photolysis in the presence of 355 nm light. Figure

2, shows the steady state phtolysis of compound 1a,b. Over the course of the photolysis experiment a clean transition for the starting material to products is observed. The increase in absorbance at 300 nm is due to the formation of BF (**13**). The isobestic point at 258 nm indicates that the photolysis occurs as a single transition from the starting material to products. Concomitant with the spectral changes observed is the formation of the desired ubiquinol-2 (**14**) and the expected of BF (**13**). Figure 3 shows an HPLC trace of a number of standards as well as the starting compound **1a,b**. As can be seen, ubiquinol-2, ubiquinone-2 (**2**) and BF (**13**) are the sole products. The presence of ubiquinone-2 is most likely due to a small amount of oxidation that occurs during handling of the sample during HPLC analysis. It shoudl be noted that the extinction coeffecient for ubiquinol-2 is an order of magnitude less than that of ubiquinone-2 at the detection wavelength of 284 nm so that the ratio of ubiquinol-2 to ubiquinone-2 is much greater that 10:1 for the HPLC trace shown in figure 3. Figure 4, show a difference chromatogram between the starting material and the photolysis product. It is evident from this data that the photolysis occurs in an exceptionally smooth manner without the production of any side products. The formation of ubiquinol-2 was further confirmed by allowing a phtolyzed sample to air oxidize. HPLC analysis of this sample revealed that virtually all the ubiquiol-2 had undergone oxidation to ubiquinone-2. Figure 4 shows the results of this experiment. In order to determine the rate of photolysis, transient absorption experimentes were performed to determine thrate of formation of the BF product (data not shown). These studies demonstarted that the BF photoproduct is formed within the dead time of the instrument. This would put a lower bound limit on the photolysis rate of 10^6 s^{-1}.

Experimental Section

General. Anhydrous THF was prepared by refluxing over sodium metal and benzophenone. Anhydrous acetonitrile, methylene chloride and pyridine were purchased

from Aldrich. All other solvents were of reagent grade. Geranyl bromide and 2-3-dimethoxy-5-methyl-benzoquinone were from Fluka. O-nitrophenyl chloroformate was purchased from Carbolabs, Inc. DMAP was purchased from ACROS. NMR spectra were recorded on Bruker AM500 spectrophotometer or a GE QE300 spectrometer operating at nominal frequencies of 500 and 300 MHz for ^1H respectively. High resolution mass spectra were recorded on a Fisons VG mass spectrometer operating in FAB mode. Routine GC/MS data were recorded on a HP 5890A/5970 GC/MS equipped with a 12 meter silicon gum capillary column. TLC plates were visualized with either UV light or iodine.

Steady state photolyis of 1. A 10 μM solution of **1** in methanol was prepared in a 1 cm pathlength quartz cuvette equipped with a septum. The sample was purged with oxygen free argon and irradiated with an Oriel 66011 Hg vapor lamp operating at 450 W and filtered through a 355 nm band pass filter. The sample was removed and the optical absorbance recorded at 5 min time intervals using an HP 8452 diode array spectrophotometer. HPLC analysis was performed using a Waters 625LC system equipped with a Delta-Pak C18 reverse phase.

Transient photolysis of 1. A 10 μM solution of **1** in methanol was prepared in a 1 cm pathlength quartz cuvette equipped with a septum. The sample was purged with oxygen free argon and irradiated at 355 nm using a 10 ns pulse from a Nd:YAG laser. Absorbance spectra were then recorded after successive laser shots.

Synthesis of 4,5-dimethoxy-2-methyltricyclo[6.2.1.0^{2,7}]undeca-4,9-diene-3,6-dione (7). A 25 mL flask was charged with a stir bar, 5 mL of dry methanol, and 500 mg (3mM) of 2,3-dimethoxy-5-methyl-1,4-benzoquinone. To this solution is added 3 mL of freshly distilled cyclopentadiene. The reaction is allowed to stir overnight during which time the dark reddish orange color of the 2,3-dimethoxy-5-methyl-1,4-benzoquinone fades to the pale yellow color of the product. Solvent and excess cyclopentadiene are removed in vacuo to give a pale yellow oil. Yield 0.75g, (>99%). HRMS (FAB) *m/z* (MH^+) calcd 249.11267, obsd 249.11283. ^1H NMR ($CDCl_3$, TMS)

σ 6.15 (m, 1H), 6.00 (m, 1H), 3.94 (s, 3H), 3.92 (s, 3H), 3.41 (bs, 1H), 3.07 (bs, 1H), 2.82 (d, 1H) 1.66 (d, 1H), 1.53 (d, 1H), 1.47 (s, 3H); HRMS (FAB) *m/z* (MH^+) calcd 249.11267, obsd 249.11283.

Synthesis of 2-[3,7-dimethyl-(2E)-2,6-octadienyl]-4,5-dimethoxy-7-methyltricyclo[6.2.1.0^{2,7}]undeca-4,9-diene-3,6-dione (8). A flame dried flask is charged with geranyl bromide (1.44 g, 6.6 mmol), **7** (1.5 g, 6 mmol), a stir bar, and 40 mL of dry 1/3 toluene/*t*-butanol. This solution is cooled to 0°C using an ice bath, and 10 ml of 1M potassium t-butoxide in t-butanol is added via canula with rapid stirring. The solution immediately turns a dark brown color and the reaction is allowed to stir for 1 hr at 0°C. The reaction mixture is then poured into 50 mL of saturated $NH_4^+Cl^-$ and extracted with 2x100 mL of dry diethyl ether. The organic layers are combined, filtered through a plug of $MgSO_4$ and solvent removed in vacuo. The resultant dark brown oil is purified by flash column chromatography using 4/1 hexane ethyl acetate to yield 1.68 grams (73%) of **8**. ^1H NMR ($CDCl_3$, TMS) σ 6.05 (bs, 2H), 5.07 (m, 2H), 3.90 (s, 3H), 3.88 (s, 3H), 3.05 (d, 2H), 3.75 (dd, 1H), 2.42 (dd, 1H), 2.00 (m, 4H), 1.65 (s, 3H), 1.57 (s, 3H), 1.58 (s, 3H), 1.49 (s, 3H), 1.78 (d, 1H), 1.45 (d, 1H); HRMS (FAB) (MH+)*m/z* calcd 384.230060, obsd 384.228649.

Synthesis of 2-[3,7-dimethyl-(2E)-2,6-octadienyl]-5,6-dimethoxy-3-methylbenzo-1,4-quinone (ubiquinone-2) (2). A stirred solution of **8** (1.68 g) dissolved in 20 mL of toluene was refluxed for 60 min, during this time the solution turned from a pale yellow to a reddish orange. Solvent was removed in vacuo and the resultant oil purified by flash column chromatography using 4/1 hexane/EtOAc. Yield 1.4 g (>99%). ^1H NMR ($CDCl_3$, TMS) σ 5.03 (t,1H), 4.93 (t, 1H), 4.00 (s, 3H), 3.98 (s, 3H), 3.18 (d, 2H), 2.01 (s, 3H), 1.99 (m, 4H), 1.73 (s, 3H), 1.65 (s, 3H), 1.58 (s, 3H); HRMS (FAB) *m/z* (MH^+) calcd 319.19876, obsd 319.199838.

Synthesis of 4-(triethylsiloxy)-2-[3,7-dimethyl-(2E)-2,6-octadienyl]-5,6-dimethoxy-3-methylphenol and 4-(triethylsiloxy)-3-[3,7-dimethyl-(2E)-

2,6-octadienyl]-5,6-dimethoxy-2-methylphenol (9a and 9b). A round bottom flask equipped with stir bar is charged with **2** (0.63g, 2.0 mmol) and 10 mL of 10/1 methanol/water. With vigorous stirring, sodium dithionite (0.38 g, 2.2 mmol) was added. The reddish orange color of the ubiquinone-2 quickly dissipates signaling the formation of the ubiquinol. The resultant slurry is extracted with 100mL of hexane and filtered into a dry round bottom flask through a small plug of $MgSO_4$. Solvent is removed in vacuo and the nearly colorless oil is redissolved in dry acetonitrile and the flask purged with dry nitrogen. The flask is charged with a stirring bar and dry pyridine (0.16 g, 2.2 mmol). Chlorotriethylsilane (0.33 g, 2.2 mmol) was added dropwise using a syringe pump over a 6 hour period. The reaction was monitored by GC/MS. Solvent and excess TESCl were removed in vacuo when the disilyl product began to accumulate. The resultant oil is purified by flash chromatography using 9/1 hexane/EtOAc to give a clear colorless oil. Yield 0.4 g (61%). ^{1}H NMR ($CDCl_3$, TMS) for **9a** σ 5.43 (s, 1H), 5.19 (m, 2H), 3.89 (s, 3H), 3.76 (s, 3H), 3.28 (d, 2H), 2.09 (s, 3H), 2.00 (m, 4H), 1.72 (s, 3H), 1.65 (s, 3H), 1.56 (s, 3H), 0.95 (t, 9H), 0.73 (q, 6H). ^{1}H NMR ($CDCl_3$, TMS) for **9b** σ 5.41 (s, 1H), 5.06 (m, 2H), 3.89 (s, 3H), 3.76 (s, 3H), 3.31 (d, 2H), 2.09 (s, 3H), 2.00 (m, 4H), 1.75 (s, 3H), 1.65 (s, 3H), 1.56 (s, 3H), 0.96 (t, 9H), 0.73 (q, 6H); HRMS (FAB) *m/z* (MH^+) calcd 435.29304, obsd 435.29323 for a mixture of **9a** and **9b**.

Synthesis of (±)-3,5-dimethoxyphenyl-2-phenyl-1,3-dith-2-ylmethanol (3). A flame dried flask was charged with a stir bar, 100 mL of dry THF, and 2-phenyl-1,3-dithiane (3.9 g, 20 mmol). This solution is cooled to 0°C and 22 mmol of *n*-butyl lithium was added dropwise via syringe (11 mL of a 2.0 M solution in hexane). Formation of the dithiane anion is indicated by the presence of a pale olive green color. Upon completion of the addition the reaction is allowed to stir for 30 min and then 3,5-dimethoxy benzaldehyde dissolved in dry THF is added via syringe (3.3 g, 20 mmol, 2x10 mL THF). The reaction is allowed to stir for 1 hour at 0°C and then poured into 100 mL of 0.1 M HCl and extracted with diethyl ether. The organic phase was filtered through a plug

of $MgSO_4$ and solvent removed in vacuo to yield a colorless oil which was further purified by flash chromatography using 4/1 hexane/EtOAc. Yield: 7.1 g (98.6%). ^1H NMR (300 MHz, $CDCl_3$) σ 7.73 (dd, 2H), 7.31 (m, 3H), 6.30 (t, 1H), 5.99 (d, 2H), 4.94 (d, 1H), 3.00 (d, 1H), 3.57 (s, 6H), 2.74-2.65 (bm, 4H), 1.94-1.90 (bm, 2H); HRMS (FAB) *m/z* (MH^+) calcd 363.1122, obsd 363.1513.

Synthesis of (±)-2-nitrophenoxy-3,5-dimethoxyphenyl(2-phenyl-1,3-dithi-2-yl)methoxymethanone (5). A flame dried flask equipped with stirring bar and septum was charged with **3** (8.16 g, 24.4 mmol), 150 mL of dry methylene chloride, and 2-nitro-phenyl chloroformate at room temperature under dry nitrogen. To this solution was added 2.2 eq of dry pyridine via syringe. The solution was allowed to stir for 1 hour at room temperature and then solvent was removed in vacuo. The resultant residue was washed with dry ether and the ether extract was filtered through a plug of $MgSO_4$. Solvent was removed in vacuo to yield a thick oil which when dried under high vacuum produced a pale yellow solid. Yield 9.96 g (77%). ^1H NMR (300 MHz, $CDCl_3$) σ 8.11 (dd, 1H), 7.74 (m, 2H), 7.66 (t, 1H), 7.42 (t, 1H), 7.32 (m, 4H), 6.36 (t, 1H), 6.03 (s, 1H), 6.01 (d, 2H), 3.59 (s, 6H), 2.75 (m, 4H), 1.96 (m, 2H); HRMS (FAB) *m/z* (MH^+) cacld 527.107246, obsd 527.106851.

Synthesis of (±)-2,6-dimethoxyphenoxy-3,5-dimethoxyphenyl(2-phenyl-1,3-dithi-2-yl)methoxymethanone (6). A flame dried flask equipped with stir bar and septum was charged with **5** (0.53g, 1mmol), 2,6-dimethoxyphenol (0.15g, 1mmol), DMAP (0.13g, 1 mmol), and 10 mL of methylene chloride under dry nitrogen. The reaction was allowed to stir at room temperature for 72 hours and then poured into 10 mL of 0.1 M HCl and extracted with 2x10 mL of methylene chloride. The organic phases were combined and filtered through a plug $MgSO_4$ and solvent removed in vacuo to yield a crystalline solid. Recrystallization from ethyl acetate gave large rectangular rods. Yield Xg (99%). ^1H NMR (300 MHz, $CDCl_3$) σ 7.68 (dd, 2H), 7.28 (m, 3H), 7.12 (t, 1H), 6.59 (d, 2H), 6.33 (t, 1H), 6.03 (s, 1H), 6.01 (d, 2H), 3.75 (s,6H), 3.58 (s, 6H), 2.85-2.55

(bm, 4H), 2.05-1.85 (bm, 2H); HRMS (FAB) *m/z* (MH^+) Unit cell, a=9.201, b=28.599, c=10.664, alpha=90.0, beta=104.05, gamma=90.0. Space group P2(1)/c. Reflections 10078, R_{cryst} 0.042.

Synthesis of (±)-4-(triethylsiloxy)-2-[3,7-dimethyl-(2E)-2,6-octadienyl]-5,6-dimethoxy-3-methylphenoxy-3,5-dimethoxyphenyl(2-phenyl-1,3-dithi-2-yl)methoxymethanone and 4-(triethylsiloxy)-3-[3,7-dimethyl-(2E)-2,6-octadienyl]-5,6-dimethoxy-2-methylphenoxy-3,5-dimethoxyphenyl(2-phenyl-1,3-dithi-2-yl)methoxymethanone (10a and 10b). A flame dried flask equipped with stir bar and septum was charged 5 and 6 (1.73g, 4 mmol), 8 (2.2 g, 4.2mmol), DMAP (0.5 g, 4.1mmol), 50 mL of dry methylene chloride under dry nitrogen. The reaction was allowed to stir for 72 hours and then poured into 25 mL of 0.1 M HCl and extracted with 2x50 mL of methylene chloride. The organic phases were combined and filtered through a plug of $MgSO_4$ and solvent removed in vacuo. The resultant oil was purified by flash chromatography using 5/1 hexane/EtOAc. Yield 1.8 g (55 %). Rf = 0.5 (5/1 hexane/EtOAc); ^1H NMR ($CDCl_3$, TMS) σ 7.78-7.65 (m, 2H), 7.35-7.25 (m, 3H), 6.35 (t, 1H), 6.05 (d, 2H) 5.9 (s, 1H), 5.10-4.86 (bm, 2H), 3.72 (s, 3H), 3.68 (s, 3H), 3.59 (s, 6H), 3.38-3.10 (bm, 2H), 2.85-2.60 (bm, 4H), 2.18-1.84 (bm, 9H), 1.64 (m, 3H), 1.54 (m, 6H), 0.96 (m, 9H), 0.76 (m, 6H); HRMS (FAB) *m/z* (MH^+) calcd 823.375702, obsd 823.373367.

Synthesis of (±)-3,5-dimethoxyphenyl(2-phenyl-1,3-dithi-2-yl)methoxy-2-[3,7-dimethyl-2(E)-2,6-octadienyl]4-hydroxy-5,6-dimethoxy-3-methylphenoxymethanone and (±)-3,5-dimethoxyphenyl(2-phenyl-1,3-dithi-2-yl)methoxy-3-[3,7-dimethyl-2(E)-2,6-octadienyl]4-hydroxy-5,6-dimethoxy-2-methylphenoxymethanone (12a and 12b). ^1H NMR ($CDCl_3$, TMS) σ 7.78-7.65 (m, 2H), 7.35-7.25 (m, 3H), 6.35 (t, 1H), 6.05 (d, 2H) 5.9 (s, 1H), 5.10-4.86 (bm, 2H), 3.72 (s, 3H), 3.68 (s, 3H), 3.59 (s, 6H), 3.38-

3.10 (bm, 2H), 2.85-2.60 (bm, 4H), 2.18-1.84 (bm, 9H), 1.64 (m, 3H), 1.54 (m, 6H); HRMS (FAB) *m/z* (M^+) calcd. 708.279063, obsd 708.274750.

Synthesis of (±)-3,5-dimethoxyphenyl-2-{2-[3,7-dimethyl-2(E)-2,6-octadienyl]-4-hydroxy-5,6-dimethoxy-3-methylphenoxycarbonylox}-1-phenyl-1-ethanone and (±)-3,5-dimethoxyphenyl-3-{2-[3,7-dimethyl-2(E)-2,6-octadienyl]-4-hydroxy-5,6-dimethoxy-2-methylphenoxycarbonylox}-1-phenyl-1-ethanone (1a and 1b). A flask equipped with a stir bar was charged with **12a** and **12b** (x g, X mmol) and 10 mL of 10/1 THF/water. This solution was cooled to -20°C with an ethylene glycol dry ice batch. To this solution was added bis(triflouroacetoxy)iodobenzene (X g, X mmol dissolved in 1 mL THF) dropwise. After completion of the addition the solution was stirred for 30 min and then allowed to warm to room temperature. ^1H NMR ($CDCl_3$, TMS) σ 7.78-7.65 (m, 2H), 7.35-7.25 (m, 3H), 6.35 (t, 1H), 6.05 (d, 2H) 5.9 (s, 1H), 5.10-4.86 (bm, 2H), 3.72 (s, 3H), 3.68 (s, 3H), 3.59 (s, 6H), 3.38-3.10 (bm, 2H), 2.18-1.84 (bm, 7H), 1.64 (m, 3H), 1.54 (m, 6H); HRMS *m/z* (MH^+) calcd 619.290708, obsd. 619.290763

REFERENCES AND NOTES

---

1. R.W. Larsen, J.R. Winkler, S. I. Chan, J. Phys. Chem., **96**, 8023-8027 (1992).
2. L.-P Pan, J.T. Hazzard, J. Lin, G. Tollin, S.I. Chan, J. Amer. Chem. Soc., **113**, 5908-5910 (1991).
3. R.C. Prince, K. Matsuura, E. Hurt, G. Hauska, P.L. Dutton, J. Biol. Chem., **257**, 3379-3381 (1982).
4. A. Patchornik, B. Amit, R.B. Woodward, J. Amer. Chem. Soc., **92**, 6333 (1970).
5. G.J. Sabomgi, Chemical Triggering; Plenum: New York (1987).
6. A.M. Gurney, H.A. Lester, Physiol. Rev., **67**, 583 (1987).
7. J. A. McCray, D. R.Trentham, Annu. Rev. Biophys. Chem., **18,** 239 (1989).
8. A. Ruttiman,P. Lorenz, Helv. Chim. Acta., **73**, 790 (1990).

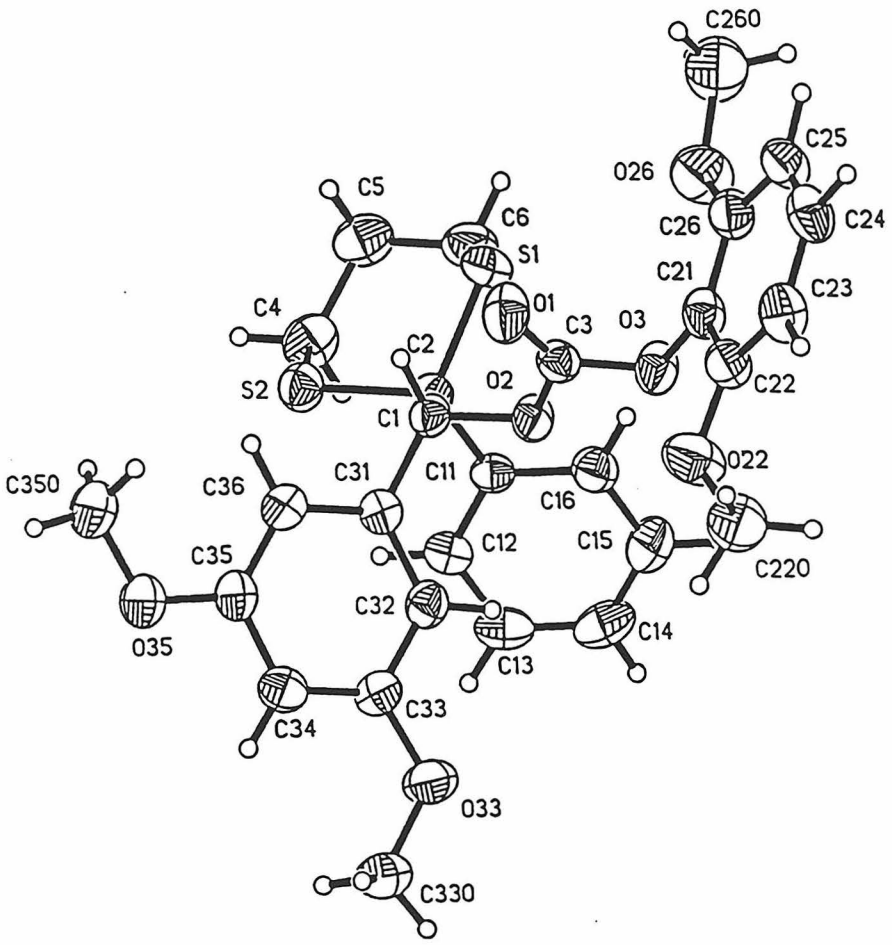

Fig. 1. ORTEP representation of compound **6**. 50% thermal ellipsoids are drawn.

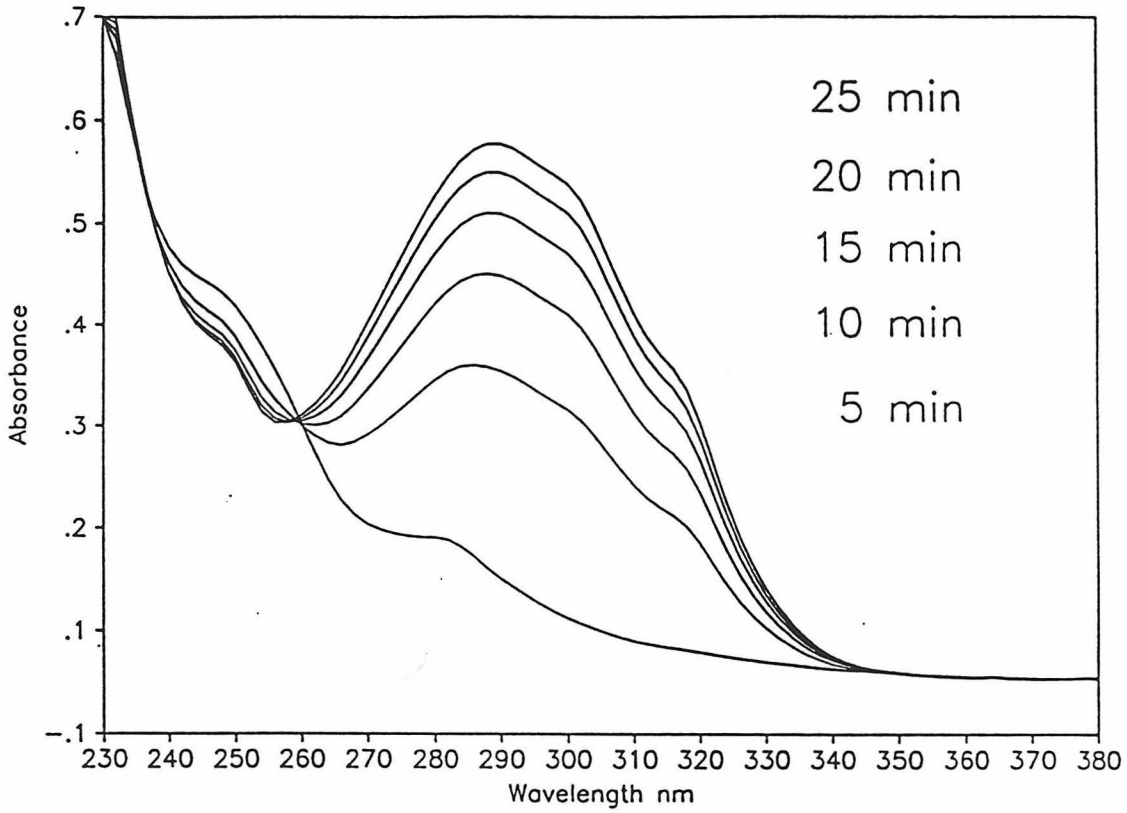

Fig. 2. Steady state photolysis of compound **1** in methanol as followed by UV/VIS absorption. See methods for details.

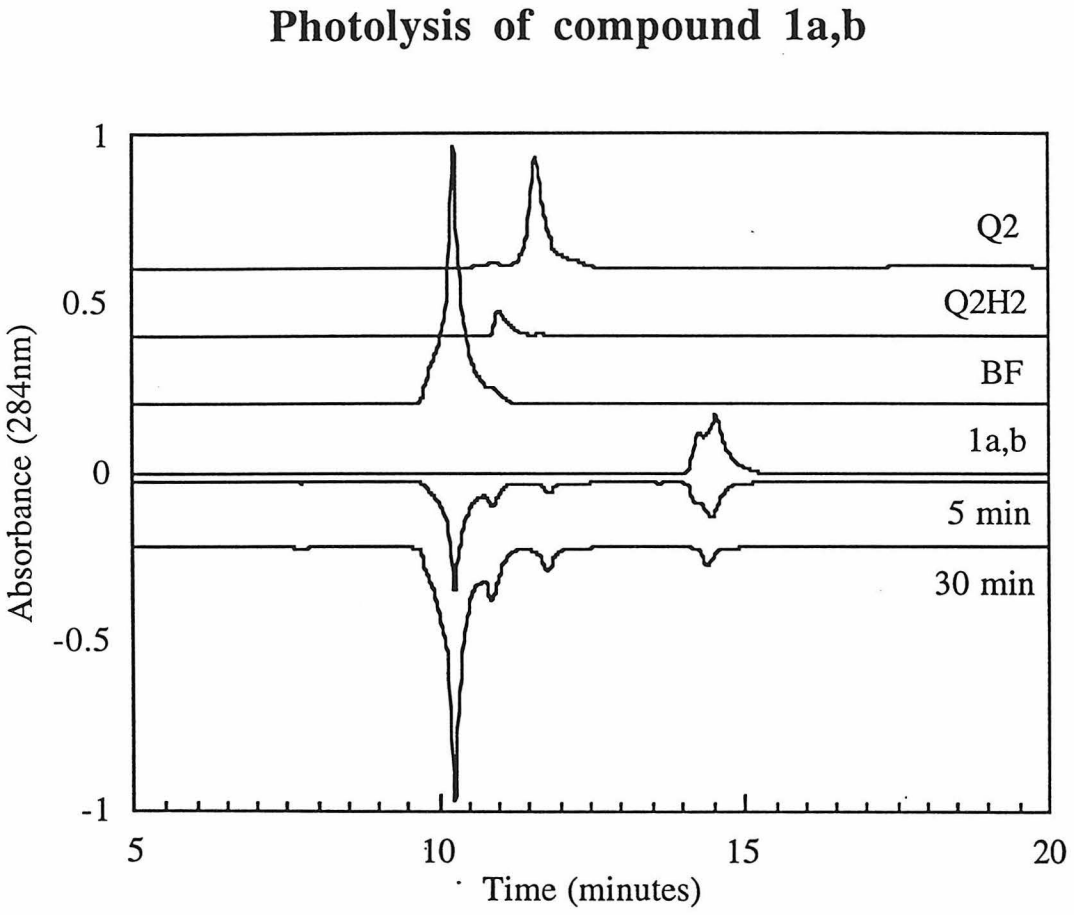

Fig 3. HPLC analysis of the photoproducts from the steady state photolysis of compound **1a,b**. See methods for details. Standards are labeled and the phoproduct samples are inverted. Q2, ubiquinone-2; Q2H2, ubiquinol-2; BF, 5,7-dimethoxy-2-phenylbenzofuran.

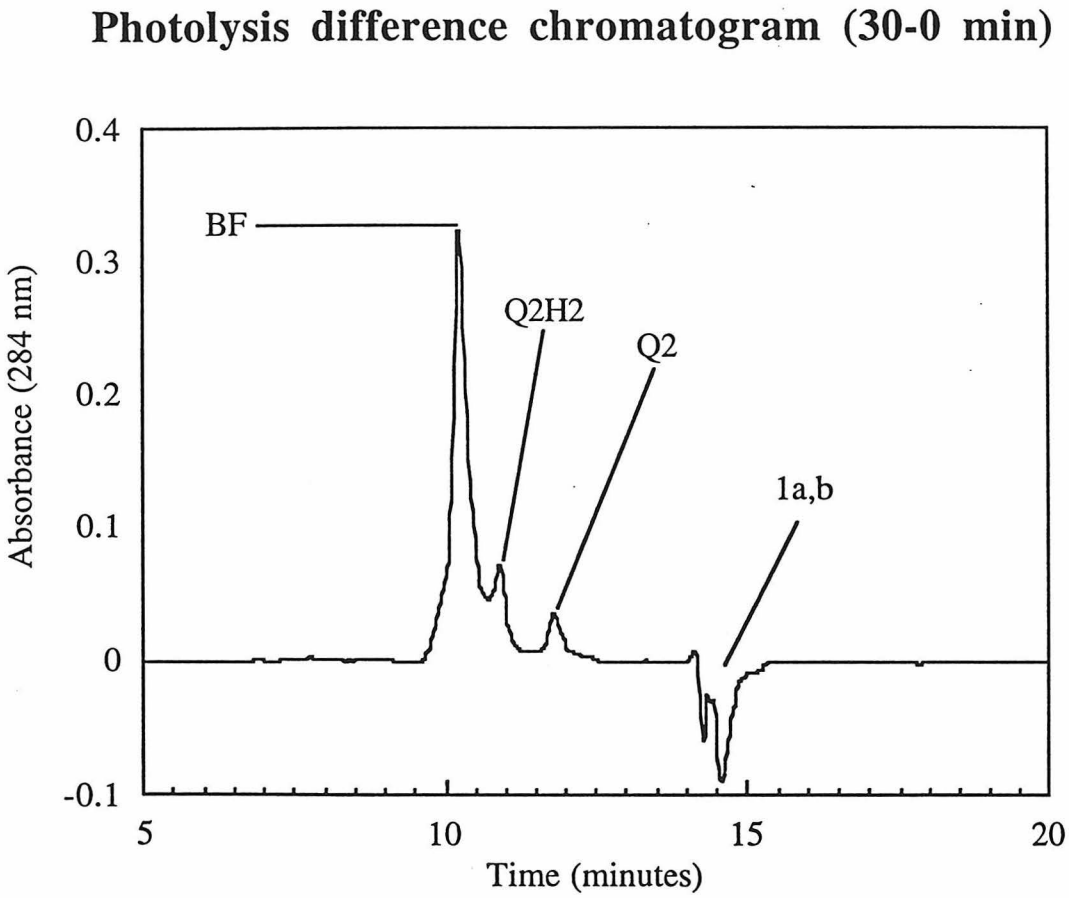

Fig 4. HPLC difference chromatogram of the 30 min photolysis products minus the starting material **1a,b**.

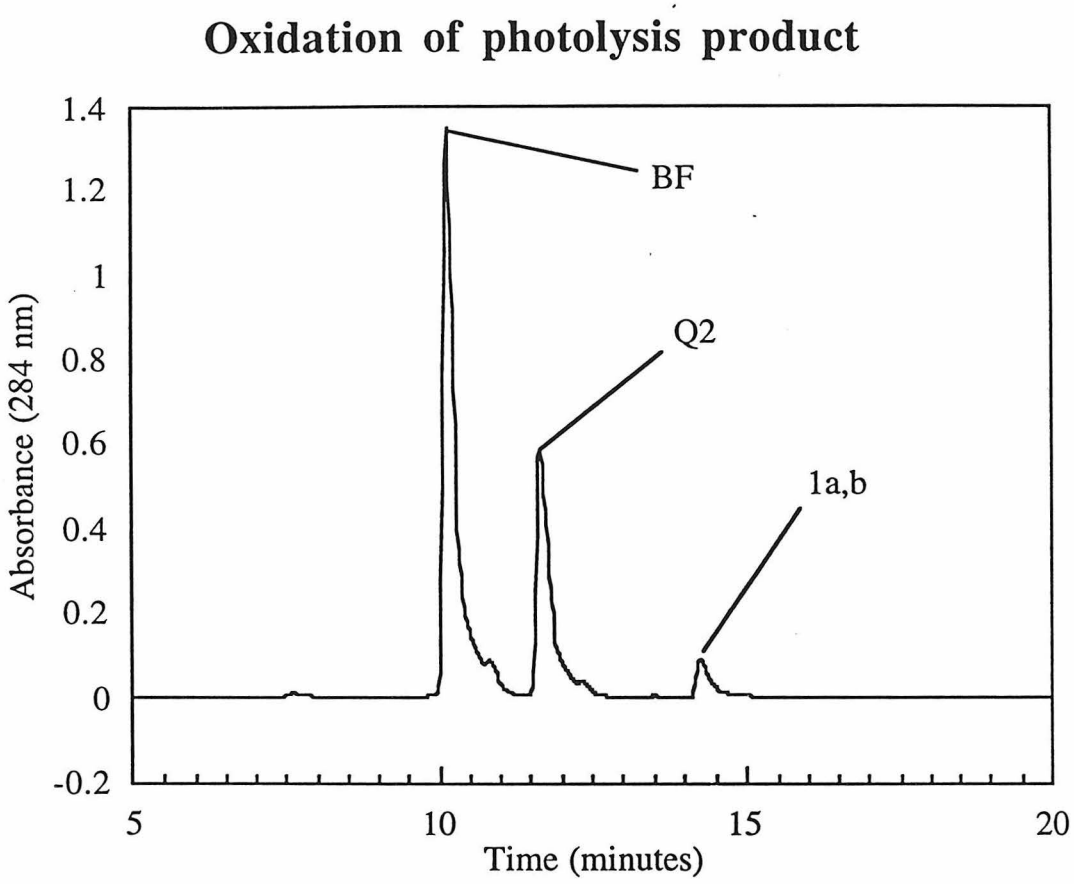

Fig 5. HPLC analysis of the photoproducts formed in figure 3, following air oxidation.

Section II

Chapter VI

Efficient Synthesis of Photolabile Alkoxy Benzoin Protecting Groups

Reprinted from Tetrahedron Letters

Efficient Synthesis Of Photolabile Alkoxy Benzoin Protecting Groups

Michael H.B. Stowell*[¥£], Ronald S. Rock*[¥], D.C. Rees[£] and Sunney I. Chan[¥]
[¥]Arthur Amos Noyes and [£]Carl F. and Winifred H. Braun Laboratories
California Institute of Technology
Pasadena, CA 91125

Abstract: *An effective implementation of the Corey-Seebach dithiane addition for the synthesis of photolabile alkoxy benzoin adducts is reported. The method allows for the facile synthesis of photolabile 3',5'-dimethoxybenzoin protected compounds in near quantitative yield and is general in that it can be used for the synthesis of both symmetrical and unsymmetrical benzoins. Importantly, the dithiane intermediate reported is a versatile starting material for the synthesis of many photolabile compounds and should serve as a useful protecting group in complex synthetic schemes requiring multiple orthogonal protecting groups.*

The use of protecting groups in organic synthesis has been invaluable in allowing the complete synthesis of numerous complex organic molecules.[1] A number of protecting groups in organic synthesis have the convenient property that they can be removed photochemically. In an early paper, Woodward described the synthesis and photocleavage properties of a series of substituted nitrobenzyl protecting groups.[2] Subsequently, such protecting groups have played important roles in synthetic strategies, as well as being exploited for use in such diverse fields as semiconductor lithography[3] and the study of rapid enzymatic processes.[4,5]

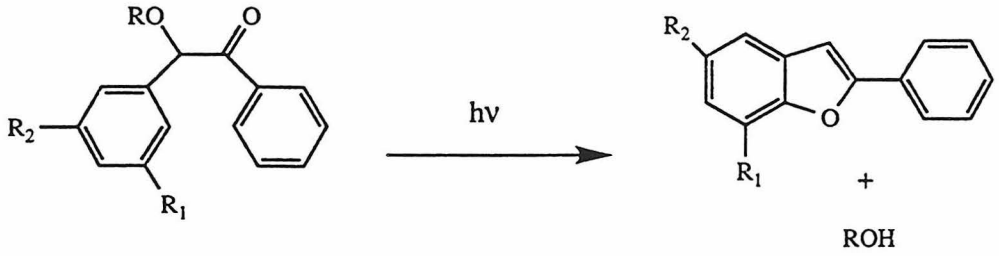

Eq. 1

One class of protecting groups that have seen less use are the substituted benzoins **1a-e**, initially reported by Sheehan et al.[6] Of particular interest are the substituted alkoxybenzoins which have quite remarkable photocleavage properties. An example is the 3',5'-dimethoxybenzoin (3',5'-DMB) protecting group which undergoes a photoinitiated cyclization and cleavage, Eq. 1, with a rate constant estimated to be greater than 10^{10} sec^{-1} and a quantum efficiency of 0.64, where R is acetyl. Such a protecting group is of

considerable interest, not only in synthesis, but also for the study of rapid enzyme kinetics and several recent papers have described the use of the 3',5'-DMB as a protecting group in oligonucleotide synthesis,[7] and for 'caged' substrates.[8,9,10] Advantages of the 3',5'-DMB versus substituted nitrobenzyl protecting groups are the rapid release rate, high quantum yield, and the easily detectable, nonreactive, benzofuran photoproduct.

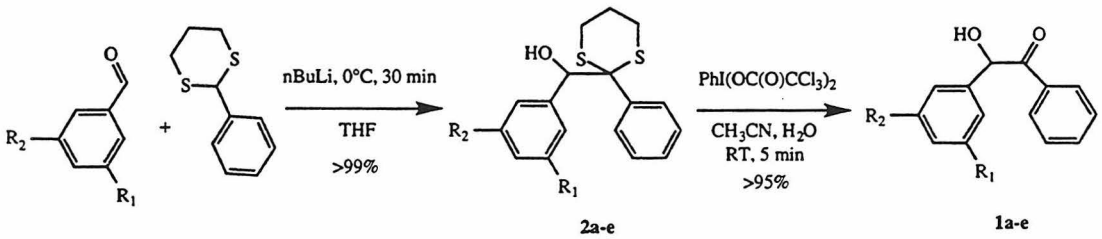

Scheme 1

While the 3',5'-DMB protecting group has many advantages, there are two distinct disadvantages to using such a protecting group. First, while considerable effort has gone into the synthesis of acyloins,[11] many of these methods have proven to be inefficient for a number of targeted acyloins, in particular 3',5'-DMB. Secondly, due to the remarkable photocleavage properties of the 3',5'-DMB protecting group, photolysis occurs in standard laboratory light and samples must be keep in complete darkness, thus making subsequent synthetic transformations cumbersome. Herein we describe the effective implementation of the Corey-Seebach dithiane addition for the synthesis of benzoins (**scheme 1**) via the dithiane protected adduct **2**. As examples, we targeted several benzoins whose synthesis has been reported to give poor or no yield via traditional methods (**2c** and **2d** from ref. 11). We further report that the dithiane adduct **2a** serves as a very convenient synthon for the introduction of the 3',5' DMB photocleavable protecting group. In such a manner, complex protected molecules can be synthesized that remain photochemically stable until the desired conversion of the dithiane moiety to the parent ketone is accomplished. As an example, we synthesized O-acetyl-3'-carbamylmethoxybenzoin (**1e**) in 6 steps, (**scheme 2**) from starting 3-hydroxy benzaldehyde, via the intermediate 3'-TBDMSO-dithiane protected benzoin (**2e**) with an overall isolated yield of 60%.

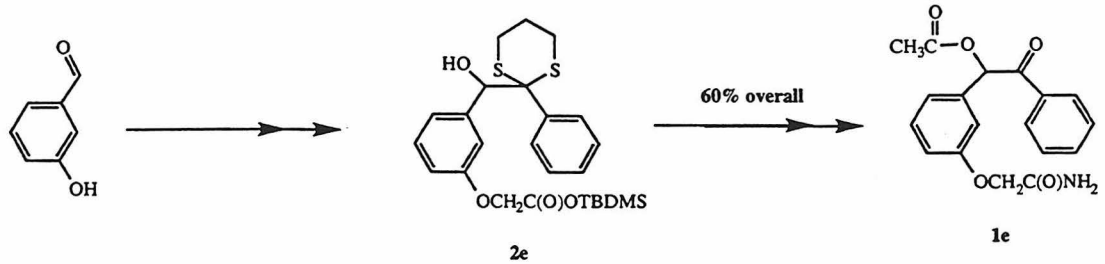

Scheme 2

In pursuing the synthesis of 3',5' DMB a number of synthetic methods (A-I of Table, see note 17) were attempted.[5,11,12] These methods, while effective, gave poor to moderate yields of the desired benzoin, Table, and were deemed inefficient for our purposes. The final method involves the addition of the 2-phenyl-1,3-dithiane lithium anion (PDLA) to 3,5-dimethoxybenzaldehyde in THF according to the procedures described by Corey and Seebach[13] (Method I). Previous investigators had reported that a similar method gave poor yields of the desired benzoin.[14] In our hands, however, the PDLA readily reacted with the aldehyde to give a quantitative yield of the dithiane adduct **2**. Subsequent deprotection (**scheme 1**) using a variety of standard methods[15] smoothly converts the dithiane adduct to the desired benzoin in near quantitative yields. To demonstrate the utility of this method we have synthesized benzoins **1b-1e** via the dithiane adduct in excellent yields (**Table**).

Table. Synthesis of Benzoins

Benzoin	Method[a]	% Yield Dithiane[b]	%Yield Benzoin	Lit. %Yield (ref 6,8,9,10,11)
3',5' Dimethoxy (**1a**)	A-H (see text)	----	0-55	0-61
same	I (this work)	**>99**	**96**	----
4'-Methoxy (**1b**)	I	**97**	**99**	----
same	A	----	----	50-74
2'-Ethoxy (**1c**)	I	**>99**	**97**	
same	A	----	----	14
2'-Methyl (**1d**)	I	**>99**	**95**	
same	A	----	----	15
3'-TBDMSO (**1e**)	I	**93**	**98**[c]	

a) Cf. text and note 16 b) Determined from GC/MS analysis using an HP4100 GCMS equipped with a 10 meter silicon gum column c) Yield determined for the O-acetyl-3'-carbamylmethoxybenzoin, see text.

In conclusion, we have demonstrated that the Corey and Seebach dithiane addition is a simple and efficient method for the preparation of both symmetrical and unsymmetrical substituted benzoins. Since most aldehydes can be converted to dithiane adducts using standard methods, it is expected that virtually any set of benzaldehydes may be coupled in this manner to afford the desired benzoin. Furthermore, the stable and nonphotolabile dithiane adducts serve as convenient intermediates in the synthesis of complex molecules incorporating the alkoxy benzoin protecting group (**scheme 2**), which would otherwise be difficult and cumbersome to prepare. The full details of this method and further examples of its utility will be reported elsewhere.[17,18]

Acknowledgments: We thank Prof. E. M. Carreira for helpful discussions and critical reading of this manuscript. This work was supported by NIH grant GM 22432 from the National Institute of General Medical Sciences, U.S. Public Health Service. Contribution number 9139.

References and Notes

1. Greene, T. W. Protective Groups in Organic Synthesis, John Wiley and Sons, Inc: New York.**1991**.
2. Patchornik, A.; Amit, B.; Woodward, R.B. *J. Am .Chem. Soc.* **1970**, *92*, 6333.
3. Sabomgi, G. J. *Chemical Triggering*, Plenum: **1987**.
4. Gurney, A. M.; Lester, H. A. *Physiol. Rev.* **1987**, *67*, 583.
5. McCray, J. A.; Trentham, D. R. *Annu. Rev. Biophys. Chem.* **1989**, *18*, 239.
6. Sheehan, J. C.; Wilson, R.M.; Oxford, A.W. *J.Am. Chem. Soc.* **1971**, *93*, 7222.
7. Pirrung, M. C.; Bradley, J-C. *J. Org. Chem.* **1995**, *60*, 1116.
8. Baldwin, J. E.; McConnaughie, A. W.; Moloney, M. G.; Pratt, A. J.; Shim, S. B. *Tetrahedron*, **1990**, *46*, 6879.
9. Corrie, J. E. T.; Trentham, D. R. *J. Chem. Soc. Perkin. Trans. 1*, **1992**, 2409.
10. Pirrung, M. C.; Shuey, S. W. *J. Org. Chem.* **1994**, *59*, 3890.
11. Harrison, I. T.; Harrison, S. Compendium of Organic Synthetic Methods, Vol II; John Wiley and Sons, Inc: New York, **1974**; pp 302-307. Hegedus, L.S.; Wade, Jr., L.G.; Compendium of Organic Synthetic Methods, Vol III John Wiley and Sons, Inc: New York, **1977**; pp 366-369. Wade, Jr., L.G.; Compendium of Organic Synthetic Methods, Vol II; John Wiley and Sons, Inc: New York, **1980**; pp 375-379.
12. Krepski, L.R.; Heilmann, S.M.; Rasmussen, J.K. *Tetrahedron Letters*, **1983**, *24*, 38 4075.
13. Corey, E. J.; Seebach, D. *Angew. Chem. Int. Ed. Engl.* **1965**, *4*, 1075.
14. Lee, R. A., *U.S. Pat.*, **1984**, 4-469-774.
15. Ibid. ref. 1, pages 203-205.
16. **Method A**: A standard benzoin condensation between 3,5-dimethoxybenzaldehyde and benzaldehyde was unsuccessful in accord with previously reported results, ref 11. **Method B**: Benzoin condensation using phenylmagnesium bromide and the cyanohydrin of the desired aldehyde, yields 12-27%. **Method C**: Synthesis via the corresponding 3',5'-dimethoxydesoxybenzoin was also attempted using a variety of methods. Oxidation with iodosobenzoic acid and hydrolysis of the corresponding epoxide afforded a mixture of diastereomers in 30-50% yield. **Method D**: 3',5'-dimethoxydesoxybenzoin was treated with one equivalent of I_2 in the presence of light, TMSCl, AcOH, or DMAP gave no reaction **Method E**: 3',5'-dimethoxy-desoxybenzoin was treated with 1 equivalent of Br_2 in DCM, a quantitative yield of the ring brominated product was formed. **Method F**: 3',5'-dimethoxydesoxybenzoin was treated with 1.1 equivalents of thionyl chloride at room temp in CCl4. A high yield of the ring halogenated product was isolated. **Method G**: Similar to the method of Krepski et al. (ref. 12) except that the O-TMS cyanohydrin of 3,5-dimethoxybenzaldehyde was generated by treatment of the benzaldehyde with 1.1 equivalents of KCN and TMSCl in CH_3CN at room temperature, yields 34-40%. **Method H**: Procedure was identical to that described by Krepski et al. reference 13, yields 42-55%. **Method I**: A solution of 2-phenyl-1,3-dithiane (390mg, 2mM) in 20mL of dry THF was cooled to 0 C ° and 1.01 equivalents of nBuLi was added dropwise via syringe with rapid stirring. This solution was allowed to stir for 30 min and then 1.0 equivalents of the desired benzaldehyde, dissolved in 1ml dry THF, was added dropwise. The solution was allowed to warm to room temperature and stir for 1 hr. The reaction is quenched by the addition of aqueous NH_4Cl, THF solvent is removed in vacuo and the resultant slurry extracted with dichloromethane. The DCM was washed with 2x20mL of water and solvent removed in vacuo to yield a pale yellow oil. The obtained oils typically crystallize upon standing and are greater than 99% pure based on GC/MS, H^1 NMR and TLC. As such, they can be used for further synthetic transformations without purification .
17. Stowell, M. H. B. et al. manuscript in preparation.
18. Rock, R. S. and Chan, S. I. *J. Org. Chem.* submitted.

(*Received in USA* 7 *September* 1995; *revised* 7 *November* 1995; *accepted* 10 *November* 1995)

Chapter VII

Nitrobenzene "Caged" Compounds as Irreversible Photoreductants: A Rational Approach to Studying Photoinduced Intermolecular Electron-Transfer Reactions in Proteins

Reprinted from the Journal of Physical Chemistry

Nitrobenzene "Caged" Compounds as Irreversible Photoreductants: A Rational Approach to Studying Photoinduced Intermolecular Electron-Transfer Reactions in Proteins[†]

Theodore J. DiMagno, Michael H. B. Stowell, and Sunney I. Chan*

Arthur Amos Noyes Laboratory of Chemical Physics, 127-72, California Institute of Technology, Pasadena, California 91125

Received: June 8, 1995[⊗]

Nitrobenzene "caged" compounds are well-known for their use in delivering biologically active substrates to a reaction mixture after photoexcitation. We have discovered that they also behave as photoreductants from the triplet state after photoexcitation. To explore the properties of these newly discovered photoreductants, a series of substituted nitrobenzene derivatives have been synthesized. These nitrobenzene derivatives exhibit many desirable characteristics suitable for the physiological photoreduction of different proteins, and examples are shown for the photoreduction of cytochrome *c* and other heme proteins. The observed rate constant for photoreduction of cytochrome *c*, k_{obs}, ranges from 300 to 36 000 s^{-1} for the various nitrobenzene derivatives. pH and ionic strength experiments are consistent with a bimolecular reaction wherein the photoreductant and the protein form an electrostatic complex prior to electron transfer. A kinetic model for this bimolecular reaction is described and simulations of the experimental data for the photoreductant 4,5-dimethoxy-2-nitrophenylacetic acid (DMNPAA) yield an inherent unimolecular electron-transfer rate constant (k_{et}) of 14 600 s^{-1} for the photoreduction of cytochrome *c* at pH 6.6.

Introduction

Over the past 10 years, photoactivatable "caged" probes have been used to control the spatial and temporal release of biologically active substrates in molecular biophysics. The caging group is designed to detach from the biological substrate after illumination with UV radiation (<360 nm) to generate a burst of substrate in the millisecond to microsecond time scale. This temporal release of substrate has allowed the kinetic measurements in a wide variety of applications such as the following: photoinitiated nucleotide release to study skinned muscle fibers,[1-3] erythrocyte ghosts,[4] sarcoplasmic reticulum vesicles,[5] skeletal muscle fibers,[6] and G-proteins;[7,8] photoinitiated calcium release[9] or calcium scavengers;[10] photoinitiated neurotransmitter release to initiate or block neurotransmitter action;[11-13] or photoinitiated amino acid release to study such processes as the functional circuitry in the brain.[14]

Recently, we have discovered that these photoactivatable "caged" probes are facile in their photoreduction of proteins as well. These derivatives function as photoreductants because of the large redox driving force of the nitrobenzene moiety when they are photoactivated into the triplet state (>2 V[15]). Because of the intramolecular rearrangement process that these nitrobenzene derivatives undergo upon photolysis (process which releases the substrate from the cage), these compounds behave as irreversible electron-transfer donors. In addition, these photoreductants can be synthetically modified to rationally design the absorption profile of these electron donors to minimize the overlapping absorption transitions with the protein of interest. The synthetic manipulation of the nitrobenzene derivatives also allows control of the charged groups on the photoreductant to optimize maximum binding between the donor and protein; in this manner, the observed electron transfer rate can be controlled and maximized.

A number of different methods have been developed for the rapid reduction of proteins necessary for studying electron-transfer events. Pulse radiolysis was one of the first techniques used for determining the kinetic behavior of one electron reductions of a variety of different proteins.[16-20] This technique uses the hydrated electron (e_{aq}^-) or weaker reductants such as the CO_2^- or 1-methylnicotinamide[21] radical to reduce the redox center. Another popular method is to use a reductant which donates an electron through a bimolecular process after being photoexcited by a laser. Several photoreductants have been used with success so far. These include porphyrins,[22,23] flavins,[24,25] ruthenium complexes,[26,27] and NADH.[28] A related method exploits ruthenium-labeled proteins[29,30] which can be photoexcited to initiate intramolecular first-order electron transfer to an electron acceptor within the protein.

Although all of the above photoexcitation methods have been successful, they all have certain disadvantages for studying enzymatic reactions. One major disadvantage is that the electron-transfer back reaction rate is on the same order as the forward electron transfer rate to the protein. Consequently, the net yield of photoreduced protein is often negligible. This has been overcome, for the most part, by adding sacrificial quenchers to rapidly rereduce the photoreductant in order to prevent the back-electron-transfer reaction from occurring. However, this solution creates added complications by having a radical quencher species as well as newly created radicals present in solution. In some cases, the radical species that are formed and the manner in which they react with the protein are unclear or unknown. Oftentimes, a more serious problem is that the photoreductants and quenchers used in the photoreduction process have absorption and emission bands from both the ground and excited states throughout the visible absorption region. This introduces a spectroscopic complexity that makes it necessary to deconvolute the observed transient signals from the real electron-transfer process of interest. The large signals from the electron donor and quencher in combination with the usually poor yield of the directly reduced protein can make deconvolution difficult. This particular situation is what prompted us to investigate the nitrobenzene photoreductants described in this study.

In this paper, we describe the properties of a series of substituted nitrobenzene derivatives (Figure 1) designed to act as photoreductants. As an example of the utility of these new

[†] Contribution No. 9014 from the Division of Chemistry and Chemical Engineering, California Institute of Technology.

* To whom correspondence should be addressed.

[⊗] Abstract published in *Advance ACS Abstracts*, August 1, 1995.

0022-3654/95/2099-13038$09.00/0 © 1995 American Chemical Society

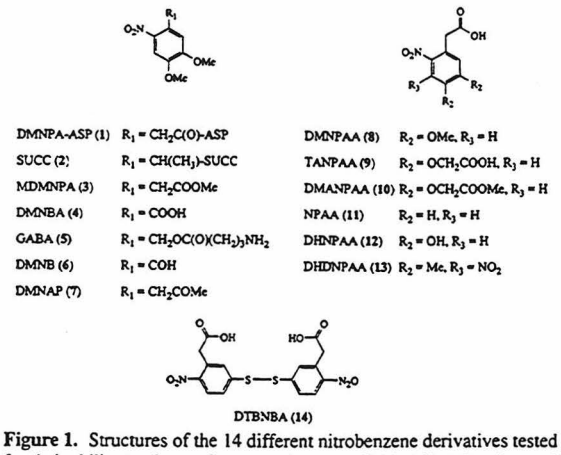

Figure 1. Structures of the 14 different nitrobenzene derivatives tested for their ability to photoreduce cytochrome *c*. Table 1 lists the observed electron transfer rate constants for the photoreduction of cytochrome *c*.

SCHEME 1

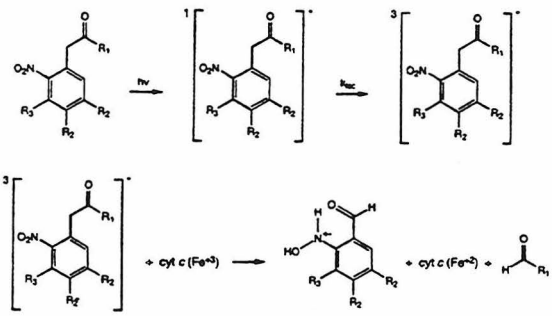

nitrobenzene derivatives, the photoreduction of cytochrome *c* and other heme proteins (indicated in Scheme 1) was investigated. We feel that this series of nitrobenzene derivatives exhibits many of the desired characteristics for a suitable photoreductant for protein systems. First, the photoreductant undergoes internal quenching via irreversible photochemistry following electron transfer to the protein so that no back electron transfer is observed. Second, the absorption profile of the photoreductant and photoproducts has no absorption or emission bands with wavelengths >430 nm that will overlap and interfere with the prosthetic groups of the protein. In addition, the absorption profile can be partially tuned by synthetically modifying the various substituents on the parent nitrobenzene (R1, R2, and R3 in Scheme 1) to avoid spectral overlaps among the various species in solution. Third, the nitrobenzene derivatives do not reduce other species in the solutions used for these experiments. Fourth, because of the large yield of reduced protein and the excellent signal-to-noise ratio, the nitrobenzene photoreductants allow enzymatic processes to be studies in the single turnover mode, thus allowing the physiological process to be studied. In the single-turnover mode, photoreductants that rely on multiple-shot signal averaging to obtain a high signal-to-noise ratio cannot be used because a distribution of enzyme intermediates become populated and a heterogeneous mixture results.

To illustrate, we report here the effects of pH, ionic strength, and the various substituents on the rate of electron transfer from the nitrobenzene photoreductants to cytochrome *c*. In a future paper, we will describe the use of these nitrobenzene photoreductants to examine the intermolecular electron transfer between cytochrome *c* and its physiological electron-acceptor cytochrome *c* oxidase under various conditions of activation of the oxidase.

TABLE 1: Single-Exponential Fit for the Photoreduction of Cytochrome c by the Nitrobenzene Photoreductants[a]

photoreductant	R1	R2	R3	k_{obs} (s^{-1})
DMNPA-ASP	$CH_2C(O)$-Asp	OMe	H	12100
SUCC	$CH(CH_3)$-Succ	OMe	H	10300
DMNPAA	CH_2COOH	OMe	H	8900
DANPATA	CH_2COOH	OCH_2COOH	H	7200
MDMNPA	CH_2COOMe	OMe	H	6300
DMANPAA	CH_2COOH	OCH_2COOMe	H	5900
DMNBA	COOH	OMe	H	5500
DTBNBA[b]	COOH	S-	H	5300
GABA	$CH_2OC(O)(CH_2)_3NH_2$	OMe	H	5300
DMNB	COH	OMe	H	5200
DMNAP	CH_2COMe	OMe	H	3300
NPAA	CH_2COOH	H	H	300
DHNPAA	CH_2COOH	OH	H	
DHDNPAA	CH_2COOH	OH	NO_2	

[a] Substituents R1, R2, and R3 as positioned in Figure 1. Experimental conditions were 100 mM ADA buffer, pH 6.6, 15 μM cyt c, and 100 μM photoreductant. Photoexcitation was initiated with a Nd:YAG laser fired at a repetition rate of 1 Hz with 1.5 mJ/pulse. [b] Dimer linked through disulfide bond between two monomers at R2 position as shown in Figure 1.

TABLE 2: Electron-Transfer Rates from DMNPAA to Several Heme Proteins[a]

protein	k_{obs} (s^{-1})	pI
cytochrome *c*	8900	10.4
hemoglobin	730	7.7
myoglobin	390	6.8
peroxidase	91	7.2

[a] Experimental conditions the same as described in Table 1 except that hemoglobin, myoglobin, and peroxidase were all at 20 μM. The fits listed in Table 2 were obtained by fitting the data to a single exponential. However, a biexponential fit gave much better results for hemoglobin, myoglobin, and peroxidase (see Figure 8 for biexponential fits).

In general, the binding properties of these nitrobenzene electron donors with any protein acceptor may be altered by appropriate substituents on the parent nitrobenzene framework, thus maximizing the intermolecular electron transfer to the physiological electron donor in these protein complexes. For the cytochrome *c*/cytochrome *c* oxidase complex, K_M and V_{max} are unaffected by the presence of these nitrobenzene photoreductants.

Results

Table 1 shows the results for the single exponential fit, k_{obs}, for the photoreduction of cytochrome *c* via the 14 different nitrobenzene derivatives in order of decreasing rates. Figure 2 shows a typical kinetic trace for the photoreduction of cytochrome *c* by DMNPAA at 550 nm. The fastest electron transfer to cytochrome *c* in 100 mM *N*-2-acetamidoiminodiacetic acid (ADA) buffer was k_{obs} = 12 100 s^{-1} ($\tau \approx 90$ μs) for the DMNPA-ASP derivative, and the slowest electron input was k_{obs} = 300 s^{-1} for the NPAA derivative under identical experimental conditions. The two dihydroxy derivatives (DHNPAA and DHDNPAA) showed no electron transfer to cytochrome *c*. However, this is most likely caused by either the lack of photoexcitation of these two derivatives due to the small cross-sectional area at 355 nm (the absorption maxima have shifted to ≈420 nm in these photoreductants) or the possible altered photophysics that these dihydroxy derivatives may exhibit.

The amount of cytochrome *c* reduced by the nitrobenzene photoreductant per laser flash is dependent on the photoreductant concentration and laser power. The yield of reduced cytochrome *c* increases with increasing donor concentration and there is a linear dependence of the yield on the *observed* reduction rate (Figure 3). In order to extract the rate constant for the electron transfer to cytochrome *c* for the second order bimolecular process, a study of rate versus cytochrome *c* concentration was

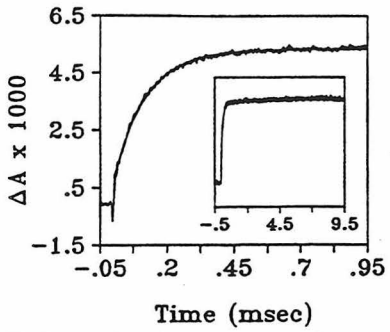

Figure 2. Typical transient absorption kinetics for the reduction of cytochrome *c* at 550 nm from the photoreductant DMNPAA. The experimental conditions were 15 μM cytochrome *c* and 100 μM DMNPAA in 100 mM ADA buffer, pH 6.6. DMNPAA was excited at 1 Hz with a Nd:YAG laser at 355 nm (1.5 mJ/pulse at the sample), and approximately 0.3 μM of cytochrome *c* was reduced per laser flash (2%). The kinetic curve is the average of two laser shots, and the single-exponential fit gave k_{obs} = 8900 s^{-1}. The inset shows the cytochrome *c* kinetics at 550 nm over a longer time scale to show that no back electron transfer to the nitrobenzene photoreductant occurs.

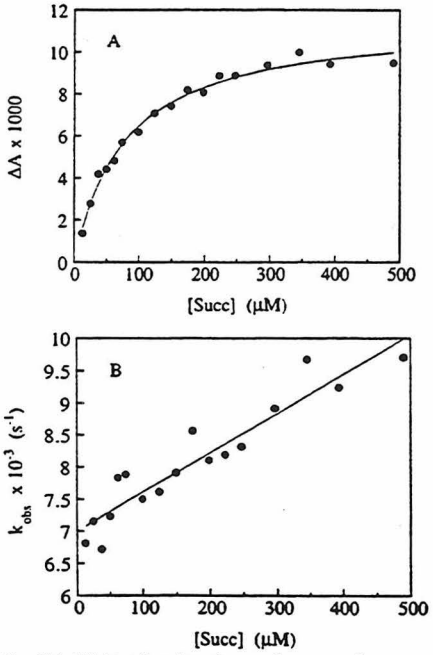

Figure 3. (A) Yield of reduced cytochrome *c* increases with a hyperbolic dependence (solid line) as the concentration of the photoreductant SUCC increases. Each point is the average of five laser shots, and ΔA was determined from the constant obtained with a single-exponential fit of the transient kinetic data. The experimental conditions were the same as given in Figure 2 except that the SUCC was used instead of DMNPAA as the photoreductant. (B) Single-exponential fit (k_{obs}) for the formation of reduced cytochrome *c* at 550 nm increases linearly (solid line) as the concentration of the photoreductant SUCC increases. The exponential fit was obtained from the same data that was used in (A).

performed (Figure 4). Over the range of concentrations of cytochrome *c* that were used in the transient absorption measurements, the rates increase linearly and did not saturate as would be expected for typical bimolecular kinetics. Therefore, only approximate limits could be placed on the electron-transfer rate constant using this analysis (see discussion for a complete analysis of the electron-transfer rate constant, k_{et}).

Laser Power Dependence. The observed electron-transfer rate to cytochrome *c* and the yield of reduced cytochrome *c*

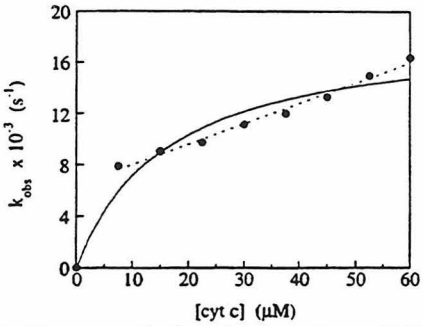

Figure 4. Electron transfer from the photoreductant DMNPAA to cytochrome *c* measured as a function of cytochrome *c* concentration from 7.5 to 60 μM. The data were fit to both a hyperbolic dependence (solid line) and a linear dependence (dashed line). Since the linear fit was much better than the expected hyperbolic dependence for the bimolecular process, the electron-transfer rate constant could not be reliable determined from these data. The experimental conditions were the same as given in Figure 2.

were measured as a function of the laser power (0.2−4.0 mJ/pulse). The observed electron-transfer rate remained constant over all pulse energies used, and the yield of reduced cytochrome *c* increased linearly with increasing laser power (data not shown). These results indicate that the electron transfer is a one-photon, single-electron-transfer event. Further evidence for a single-electron-transfer event was obtained by photoexciting a 1:3 mixture of DMNPAA:cytochrome *c* and obtaining only 1 equiv of reduced cytochrome *c* after exhaustive excitation at 355 nm (data not shown).

pH and Ionic Strength Dependence on Electron Transfer. The dependence of the electron transfer as a function of pH was probed with DMNPAA as the photoreductant. Two trends were observed for this reaction. First, the yield of reduced cytochrome *c* increased as the pH increased. Figure 5A shows the steady-state reduced minus oxidized difference spectra of the sample after 50 laser shots, and Figure 5B shows the transient spectrum obtained from the same sample, while Figure 6A shows the change in absorption at two wavelengths from the reduced minus oxidized difference spectra in Figure 5A. Second, the observed rate of electron transfer to cytochrome *c* decreased as the pH increased (Figure 6B).

The two trends observed for the ionic strength dependence were similar to those observed for the pH dependence. The ionic strength was changed by varying either the ADA buffer concentration as shown in Figure 7A or the NaCl concentration as shown in Figure 7B. The variation in the ADA buffer concentration for the triacid photoreductant DANPATA showed an increase in the yield of reduced cytochrome *c* (both transient and steady-state yields) and a decrease in the observed electron-transfer rate as the ionic strength was increased. When the ionic strength was increased with NaCl, the observed rate of electron transfer also decreased, but to a much smaller extent than the ADA ionic strength dependence. This smaller decrease was due to the higher initial ionic strength in the NaCl dependence from the ADA buffer itself (50 mM). When comparing the NaCl dependence starting at 50 mM with the ADA dependence, then the magnitude of the rate decrease is roughly the same for both methods of changing the ionic strength (Figure 7A). However, when the ionic strength was increased with NaCl, the yield of reduced cytochrome *c* decreased, in contrast to the ADA dependence. A decrease in yield is expected as the ionic strength is increased because the binding affinity of the photoreductant DANPATA to cytochrome *c* decreases with increasing ionic strength. The results from the ADA ionic strength dependence seem anomalous in this light, but the

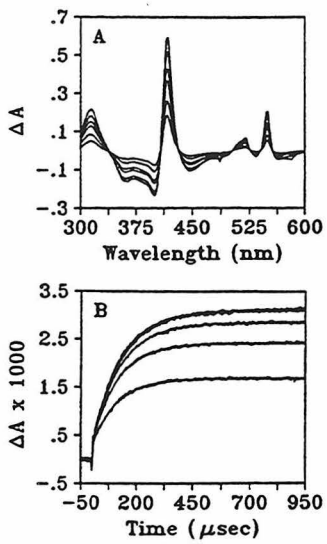

Figure 5. (A) Reduced minus oxidized difference spectra for cytochrome *c* as a function of pH obtained by photoreduction with DMNPAA after 50 laser shots. The yield of reduced cytochrome *c* increase as the pH increased from pH 6.0 (smallest signal at 550 and 418 nm), pH 6.4, pH 6.8, pH 7.2, pH 7.6, to pH 8.0 (largest signal at 550 and 418 nm). (B) Transient kinetics for the reduction of cytochrome *c* at 550 nm as a function of pH. The range of pH values was the same as given in (A). The smallest transient signal in (B) was at pH 6.0, and the signal increased with increasing pH. The transient signals for pH 7.2, pH 7.6, and pH 8.0 all have essentially the same magnitude, but their k_{obs} obtained from a single-exponential fit decrease slightly. k_{obs} = 9100 s^{-1} (pH 6.0), k_{obs} = 8800 s^{-1} (pH 6.4), k_{obs} = 8100 s^{-1} (pH 6.8), k_{obs} = 8000 s^{-1} (pH 7.2), k_{obs} = 7600 s^{-1} (pH 7.6), and k_{obs} = 7700 s^{-1} (pH 8.0). The experimental conditions were the same as given in Figure 2.

observations here are most likely related to the enhanced electron-transfer yield observed for ADA over other buffers such as phosphate, TRIS·HCl, and HEPES and do not represent an ionic strength dependence. This enhanced reduced cytochrome *c* yield is thought to be from the ability of ADA to complex free metals in solution which quench the excited state of the photoreductant.[31] In support of this hypothesis, the photoreduction of cytochrome *c* by DMNPAA was effectively quenched by the addition of metal ions (Cu^+, Fe^{2+}, Zn^{2+}) into the reaction mixture (data not shown). This would explain the observed increase in the reduced cytochrome *c* yield as the ADA concentration is increased and the variable yield of reduced cytochrome *c* observed in HEPES buffer.

Electron Transfer to Other Heme Proteins. DMNPAA is also an effective electron donor for other proteins. Myoglobin, hemoglobin, and peroxidase were all photoreduced by DMNPAA under both aerobic and anaerobic conditions. Under aerobic conditions, the observed electron-transfer rate constant was often difficult to extract because the reoxidation by dioxygen was on the same time scale as the photoreduction and the errors in the deconvolution process became large. Under anaerobic conditions, however, no reoxidation was detected and the observed electron-transfer rate was measured to be k_{obs} = 390 s^{-1} for myoglobin (20 μM), k_{obs} = 730 s^{-1} for hemoglobin (20 μM), and k_{obs} = 91 s^{-1} for peroxidase (20 μM) under identical experimental conditions (Figure 8). The fast phase of the photoreduction observed for all three species (τ < 1 μs) is due to the direct photoexcitation of these heme proteins as previously observed by Gu et al.[32] and is observed in the absence of the DMNPAA photoreductant.

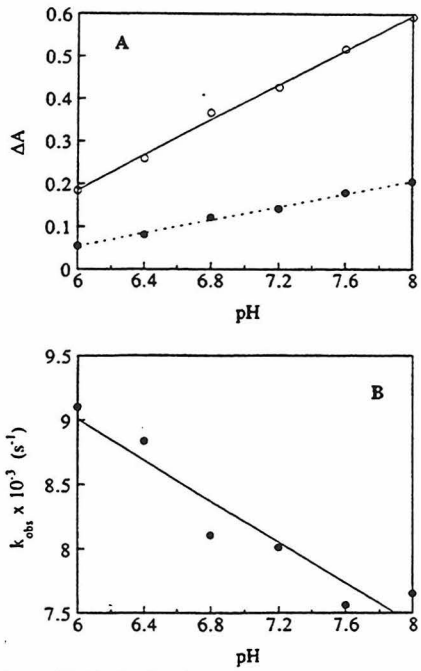

Figure 6. (A) Yield of reduced cytochrome *c* increases linearly as a function of increasing pH at both 418 nm (○) and 550 nm (●). The data points are extracted from the steady-state reduced minus oxidized difference spectra for cytochrome *c* shown in Figure 5A. (B) Observed rate of reduction of cytochrome *c* as a function of pH. The data are the single-exponential fits to the transient decay curves shown in Figure 5B.

Discussion

Ideally a photoreductant should have several characteristics. First, the radical cation photoproduct produced must exhibit a slow or nonexisting back-electron-transfer reaction from the protein. This would increase the overall yield of reduction of the protein and make it unnecessary to add quenchers to the solution, which in turn would simplify the interpretation of the results. Second, the photoreductant and its final photoproduct should not have absorption or emission bands in the visible region which overlap with the protein prosthetic group being reduced and studied. Third, and a generally ignored property, the photoreductant should not reduce any other components of the system. Fourth, the photoreductant should not interfere with the binding of substrate(s) or other physiological processes involving the protein.

The nitrobenzene derivatives work well in their newly discovered use as photoreductants for several reasons. First, the photoreductant and its products are optically transparent throughout the visible region (λ > 430 nm) and thus do not interfere with the measurements of the heme chromophores. This precludes the need for deconvolution of complicated kinetics arising from several different species. Only the protein signal is observed in the visible region, and the data analysis is accordingly straightforward.

Second, no appreciable back electron transfer is observed over the time scale of the electron-transfer reactions to the protein. Figure 2 shows that the photoreduced cytochrome *c* does not decay over a 10 ms time scale in the presence of a 10-fold excess of DMNPAA (same results for the other donors). The back electron transfer does not occur because the photolytically oxidized DMNPAA is presumed to undergo an intramolecular rearrangement reaction to form the nitroxide species[33] (Scheme 1), which can disproportionate to form the stable ground-state

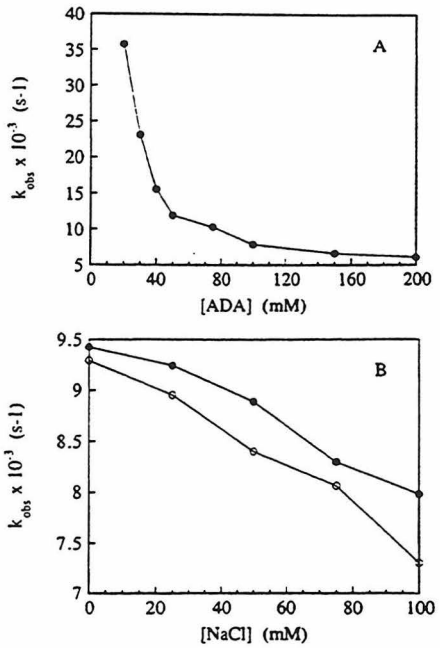

Figure 7. (A) Effect of the ionic strength ([ADA] dependence) on the electron transfer to cytochrome *c* from the photoreductant DANPATA. At [ADA] <20 mM, the transient signal-to-noise decreases too much to be reliably fit. Experimental conditions were 15 μM cytochrome *c*, 100 μM DANPATA, pH 6.6, and the [ADA] given for each point. (B) Effect of the ionic strength ([NaCl] dependence) on the electron transfer to cytochrome *c* from the photoreductant DANPATA at pH 6.4 (●) and 7.8 (○). The experiment conditions were 15 μM cytochrome *c*, 100 μM DANPATA, 50 mM ADA (to provide adequate signal-to-noise), and pH 6.4 (●) or pH 7.8 (○). The approximate linear dependence obtained in (B) is similar to the approximate linear region observed in (A) when the ADA concentration was above 50 mM.

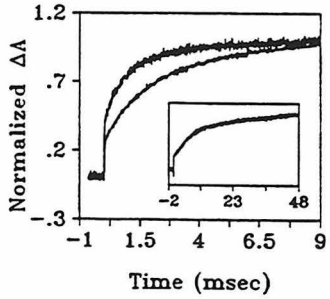

Figure 8. Transient absorption of the Soret band at 426 nm for the photoreduction of hemoglobin (upper kinetic trace), myoglobin (lower kinetic trace), and peroxidase (inset, expanded time scale) using DMNPAA as the photoreductant. The data shown here were fit to a biexponential decay (see Table 2 for a single-exponential fit). The two observed rate constants were $k^f_{obs} = 1500\ s^{-1}$ (62%) and $k^s_{obs} = 290\ s^{-1}$ (38%) for hemoglobin, $k^f_{obs} = 910\ s^{-1}$ (38%) and $k^s_{obs} = 210\ s^{-1}$ (62%) for myoglobin, and $k^f_{obs} = 160\ s^{-1}$ (27%) and $k^s_{obs} = 3.5\ s^{-1}$ (73%) for peroxidase, where k^f_{obs} and k^s_{obs} are the fast and slow components, respectively. The weighted average of the two exponentials approximates the single exponential value listed in Table 2. The experimental conditions were 20 μM protein (hemoglobin, myoglobin, or peroxidase), 100 μM DMNPAA, and 100 mM ADA at pH 6.6.

hydroxylamine- and nitrosobenzoic acid products. The nitroxide intermediate has been observed at 77 K by electron spin resonance (data not shown), the hydroxylamine photoproduct isolated, and its identity confirmed by GCMS. However, the rate of disproportionation of the nitroxide species has not been determined. Because these nitrobenzene photoreductants undergo this intramolecular rearrangement, no external quenchers are necessary to quench the radical cation donor species. This simplifies the experiment by reducing the number of chemical species in solution which can interact and interfere with electron transfer to the protein, an advantage that the other photoreducing systems do not have.

SCHEME 2

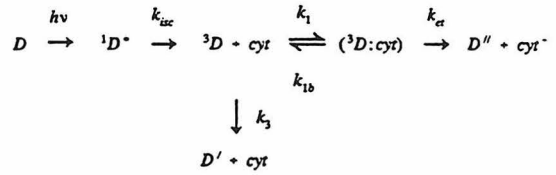

An important advantage of the nitrobenzene photoreductants is that they can be readily synthesized as well as modified with various substituents. This enables the absorption profile of the photoreductant to be shifted to either higher or lower energy to avoid overlapping absorption bands with the protein under study. Furthermore, the easy addition of charged substituents also makes it possible to engineer a specific photoreductant that can bind tightly to a desired protein of interest or even to be covalently bound to the amino acids of the protein with well-known coupling reactions. These derivatives could then be designed to function as unimolecular electron donors in the same manner that ruthenium-labeled cytochrome *c* derivatives have been used.[29,30] This flexibility may make these donors appropriate for many proteins other than the few examples examined in this introductory work.

Reaction Mechanism and Electron-Transfer Kinetics. Only the observed electron-transfer rate has been discussed for this bimolecular electron-transfer process. Even though k_{obs} for the photoreduction of cytochrome *c* is relatively slow ($\sim 10^4\ s^{-1}$) at the physiological ionic strength (100 mM) for the cytochrome *c*/cytochrome *c* oxidase redox partners, this does not mean that the inherent electron transfer between the nitrobenzene donor and cytochrome *c* is slow. Rather this indicates that the bimolecular process under the observed experimental conditions is slow. What is most important is the inherent electron-transfer rate, k_{et}, because this is the limit on how fast electron transfer can occur under optimal conditions.

A simplified reaction mechanism which includes all known chemical reactions for the photoreduction of cytochrome *c* is shown in Scheme 2, where D is the nitrobenzene donor; $^1D^*$ is the photoexcited singlet state of the donor; ^3D is the photoexcited triplet state of the donor, i.e., the species that initiates the electron-transfer chemistry; (^3D:cyt) is the bound complex; and D′ and D″ are the nitrobenzene product derivatives after the intramolecular photochemical rearrangement process or the intermolecular electron-transfer process, respectively. The kinetic pathway designated by k_3 describes the intramolecular photoinitiated rearrangement process that occurs in the absence of cytochrome *c* without electron transfer.[33] In the absence of this process, the reduction of cytochrome *c* can proceed no faster than the rate of formation of the complex ^3D:cyt.

The rate law for the kinetic mechanism described in Scheme 2 can be formulated in terms of the rate of formation of reduced cytochrome *c* (eq 1). The concentration of the bound DMNPAA:cytochrome *c* complex, [^3D:cyt], can be related to the concentration of its photoexcited precursor ^3D by the differential equation:

$$d[cyt^-]/dt = k_{et}[^3D:cyt] \quad (1)$$

$$d[^3D:cyt]/dt = k_1[^3D][cyt] - (k_{1b} + k_{et})[^3D:cyt] \quad (2a)$$

where the concentration of ^3D will evolve with time according to the differential equation

$$d[^3D]/dt = k_{1b}[^3D{:}cyt] - k_1[^3D][cyt] - k_3[^3D] \quad (2b)$$

To obtain the concentration of the bound DMNPAA:cytochrome *c* complex, the coupled differential equations in eq 2 must be solved, with the following initial conditions for ^3D, namely, $[^3D]_0$ is proportional to the initial concentration of the photoreductant, $[D]_0$, the laser power, as well as the duration of laser excitation of the sample. Substituting the result for $[^3D{:}cyt]$ back into eq 1 and integrating over time yield the following integrated rate expression for Scheme 2:

$$[cyt^-(t)] = \left[\frac{\Delta A_{550} k_{et} k_1 \cdot cyt_0 [^3D]_0}{[(k_{1b} + k_{et})(k_1 \cdot cyt_0 + k_3) - k_{1b} k_1 \cdot cyt_0] 2\Phi}\right] \times$$

$$[(\psi - \Phi)\exp(\{\psi + \Phi\}t) - (\psi + \Phi)\exp(\{\psi - \Phi\}t) + 2\Phi) \quad (3)$$

where

$$\Phi = {}^1/_2\sqrt{(k_{1b}+k_{et})^2 + 2k_{1b}k_1 \cdot cyt_0 - 2k_1 \cdot cyt_0 \cdot k_{et} - 2k_3 k_{1b} - 2k_3 k_{et} + (k_1 \cdot cyt_0 + k_3)^2}$$

$$\psi = -{}^1/_2(k_{1b} + k_{et} + k_1 \cdot cyt_0 + k_3)$$

and ΔA_{550} is the molar absorption coefficient for reduced minus oxidized cytochrome *c*.

In an attempt to determine the individual rate constants k_1, k_{1b}, k_3, and k_{et}, the observed electron transfer to cytochrome *c* was measured as a function of cytochrome *c* concentration from 3 to 60 μM. A global fitting for one exclusive set of rate constants to all eight experimentally obtained transient kinetic traces at different cytochrome *c* concentrations to the kinetic model described by eq 3 was attempted using a Levenberg-Marquardt least-squares fitting routine. However, no convergent global solution was obtained. This indicated that either the kinetic model proposed in Scheme 2 was incorrect (other processes unaccounted for in Scheme 2) or that the solution to the kinetic model (eq 3) was too complex to be solved (the fitting routine could not escape a local minima from the various initial guesses) for the limited cytochrome *c* concentrations attainable in these experiments. Because the photochemistry of the nitrobenzene derivatives is not fully understood at this time, it is quite possible that other processes exist which further complicate the kinetic model given in Scheme 2. We have, for example, neglected any effects of cytochrome *c* concentration on the quantum yield of production of the triplet donor. Additional processes such as a bimolecular and unimolecular quenching of the complexed intermediate have been added to the kinetic mechanism (Scheme 3) where k_{bm} and k_{um} represent

SCHEME 3

$$[^3D{:}cyt] + cyt \xrightarrow{k_{bm}} [D{:}cyt] + cyt$$

$$[^3D{:}cyt] \xrightarrow{k_{um}} [D{:}cyt]$$

the bimolecular and unimolecular rate constants, respectively. The new coupled set of differential equations which include these additional steps in the kinetic mechanism were solved as described above. The resulting kinetic expressions were again used in the global fitting of the eight experimental kinetic decay curves. However, no global fit was found when either one or both of these additional processes were included in the kinetic scheme. Introduction of further reaction pathways into the kinetic model seemed unwarranted given our current understanding of the nitrobenzene photochemistry.

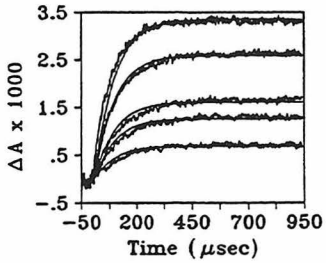

Figure 9. Concentration dependence of the transient absorption photoreduction of cytochrome *c* at 550 nm by DMNPAA. The five transient kinetic traces shown are for increasing concentrations of cytochrome *c*: 3 μM (lower trace), 6 μM, 7.5 μM, 15 μM, and 30 μM (upper trace). The transient kinetic traces for 45 and 60 μM cytochrome *c* are not shown for clarity since the transient signals are smaller than for 30 μM. The fit to each kinetic trace is from eq 3 using the parameters from the average rate constants given in Table 3. The experimental conditions were the same as in Figure 2 and the transients are an average of five laser shots.

TABLE 3: Average Least-Squares Fit to Eq 3 for the Cytochrome *c* Dependent Kinetic Traces

parameter	average fit	standard deviation
k_1	$3.27 \times 10^7\ s^{-1}\ M^{-1}$	2.05×10^6
k_{1b}	$1.04 \times 10^5\ s^{-1}$	4.23×10^3
k_3	$1.11 \times 10^4\ s^{-1}$	2.86×10^3
k_{et}	$1.46 \times 10^4\ s^{-1}$	1.44×10^3
$^3D_0$	3.63×10^{-5} M	4.39×10^{-6}

When each of the eight experimental kinetic decay curves at different cytochrome *c* concentrations were fit independently to eq 3, two consistent solutions were obtained. Each solution had similar rate constants for all eight experimentally measured kinetic traces. However, one set of rate constants was not evaluated further since k_1 was at the diffusion limit and did not seem feasible for the observed chemistry. The second set is given in Table 3. The fit and standard deviation listed in Table 3 for each rate constant is the average from all eight independent fits over the varied cytochrome *c* concentrations. Figure 9 shows the fit to the experimental kinetic decay curves using the average rate constants given in Table 3. The only factor in eq 3 which is not constant for all fits to the experimental kinetic curves is the amplitude of the photoexcited DMNPAA, $[^3D]_0$. Attempts were made to correct the yield of photoexcited DMNPAA because of the increased number of photons absorbed by the increasing cytochrome *c* concentration. However, models using the molar absorption coefficients for cytochrome *c* and DMNPAA at 355 nm were unsuccessful in correcting the discrepancy in the yield of $[^3D]_0$ found in the kinetic fitting routine. These results seem to indicate a competitive process between cytochrome *c* or some other quenching species for the photoexcited DMNPAA electron donor. This competitive side reaction has not been identified, although the most obvious candidate is quenching of the excited singlet state by cytochrome *c* via processes other than intersystem crossing. Another possibility is variable quenching of the excited state (singlet or triplet) by exogenous metals in solution as described previously. Despite the small discrepancy in the calculated excited DMNPAA concentration for the various concentrations of cytochrome

c, the kinetic model provides a satisfactory simulation of the cytochrome c photoreduction and the experimentally determined binding constants ($K_D > 1000\ \mu M$), and we obtain a value of $1.46 \times 10^4\ s^{-1}$ for the unimolecular electron-transfer rate constant (k_{et}) when DMNPAA is employed as the photoreductant.

Unimolecular Limit of the Reaction Kinetics. The solution to the kinetic model (Scheme 2) results in two exponential terms for the bimolecular reaction (eq 3). However, when the rate constants determined from the simulation for DMNPAA (Table 3) are inserted into eq 3, the two exponential components are different in both their amplitude and decay rate. The first exponential, $[\exp(\Psi + \Phi)t]$, has roughly a 90% amplitude and $\sim 100\ \mu s$ time constant while the second exponential, $[\exp(\Psi - \Phi)t]$, has roughly a 10% amplitude and $\sim 10\ \mu s$ time constant. The sum of these two exponentials is essentially a single $\sim 100\ \mu s$ exponential decay except at very short times. Even then, the deviations are sufficiently small that they cannot be detected within experimental error. Therefore, under the experimental conditions used in this work, a single-exponential fit satisfactory approximates the kinetic model and corresponds to the fits listed in Table 1 for the observed rate constants.

Effect of Electrostatic Interactions on Electron Transfer. The one major drawback with these donors thus far is that the observed electron-transfer rate is relatively slow under the high ionic strength conditions used to study the electron input into cytochrome c ($k_{obs} \approx 10\ 000\ s^{-1}$). For hemoglobin, myoglobin, and peroxidase, the observed electron-transfer rate is even slower for the same experimental conditions and concentration of substrates (Table 2). One possible explanation for these observed rates is the electrostatic interaction between the DMNPAA donor and the protein acceptor. Under the pH conditions in which the electron-transfer rates were measured (pH 6.6), DMNPAA is deprotonated and has a negative charge from the carboxyl group. The isoelectric point (pI) for the four proteins studied here are: pI = 10.4 for cytochrome c, pI = 7.7 for myoglobin, pI = 6.8 for hemoglobin, and pI = 7.2 for peroxidase. This means that DMNPAA would have the greatest electrostatic interaction with cytochrome c, then myoglobin, peroxidase, and hemoglobin the weakest binding. The observed electron-transfer rates approximately follow this ordering except that hemoglobin and peroxidase are reversed in regard to their electron-transfer rates. If this trend turns out to be correct, then these donors can be easily modified synthetically to have more positive or negative charges as substituents to complement the charge on the protein of interest and increase the electrostatic interaction and ultimately the electron-transfer rates.

Another factor that affects the electron transfer from the nitrobenzene derivatives to the various proteins is the accessibility of the heme crevice to the electron donors. Even though the isoelectric point for *Paracoccus denitrificans* cytochrome 550 (pI = 3.5) is much lower than for horse cytochrome c (pI = 10.4), the observed electron-transfer rate from DMNPAA under identical concentrations is the same within experimental error (data not shown). This apparent discrepancy is easily explained by noting that the heme crevice for both horse cytochrome c and *Paracoccus denitrificans* cytochrome 550 is highly positively charged[34] due to the presence of several lysine residues in this region of the protein. Therefore, the charge in the heme crevice and the binding affinity for the photoreductant is the same for both cytochromes even though the overall isoelectric point of the two proteins varies substantially. The positively charged domain surrounding the heme is therefore the major contributor influencing the intermolecular electron transfer because it dominates the electrostatic interaction between the donor and acceptor.

Although the data (Table 1) do not show an exact correlation between the observed electron-transfer rate and charge on the donor, the trend is certainly clear. The negatively charged donors exhibit the fastest observed rates, and the neutral and the positively charged donors are slower. This correlation is remarkably good considering that the charged group is not the only substituent varying among the various donors examined, and the other substituents may also have some effect on the electron-transfer and binding processes. Through the manipulation of the side chains and charged groups on these electron donors, these nitrobenzene derivatives could be used to make "designer" electron donors to a wide variety of proteins.

pH and Ionic Strength Dependence on Electron Transfer. The pH dependence and the ionic strength dependence results can be rationalized in terms of the same electrostatic model mentioned above. As the pH increases, the electron donor is essentially unaffected since the pK_a of the acid is lower than the lowest pH used in these experiments. However, the increasing pH causes the effective positive charge on cytochrome c to decrease, thus decreasing the electrostatic interaction between the donor and protein and causing the observed electron-transfer rate to decrease with increasing pH. Following similar reasoning, when the ionic strength decreases, there is enhanced binding between the electron donor and the protein. In the limit of a bound donor:protein complex, the electron-transfer rate would approach its fastest possible rate. Under these conditions, the process becomes unimolecular with $k_{obs} = k_{et}$, and the kinetics are not limited by the collision rate. Under high ionic strengths, the reaction should be second order with a slower observed electron-transfer rate.

The data for the ionic strength dependence are consistent with the above model. DMNPAA has a single acid functionality and does not form a tight complex with cytochrome c ($K_D > 1000\ \mu M$ at 5 mM ADA) and would be expected to have little ionic strength dependence in agreement with the small changes observed in the experimental data. The triacid DANPATA, on the other hand, has three negative carboxyl groups which should bind much tighter to the positively charged cytochrome c ($K_D = 70 \pm 5\ \mu M$ at 5 mM ADA). Accordingly, as the ionic strength decreases, the observed electron-transfer rate increases significantly from $k_{obs} = 6100\ s^{-1}$ at 200 mM ADA to $k_{obs} = 36\ 000\ s^{-1}$ at 20 mM ADA (Figure 7). In addition to the large increase in the observed rate with decreasing ionic strength, a smaller overall ΔA signal is observed. This could be interpreted as the DANPATA donor having several tight binding sites on cytochrome c with only one which is an electron-transfer-competent site. So even though the number of DANPATA donors which are tightly bound increases, the protein is capable of accepting only one electron, thus the overall ΔA observed decreases. The remaining bound photoexcited donors presumably become deactivated via radiative or rearrangement processes. It should be noted, however, that those donors which are in the electron-transfer-competent site should exhibit a dramatically increased observed electron-transfer rate, probably approaching the unimolecular electron-transfer rate constant k_{et}. Another possible explanation for the decreased yield is the effect of the ADA buffer on the electron-transfer yield as mentioned before. The yield of reduced cytochrome c is consistently greater in ADA buffer than in phosphate, HEPES, or Tris·HCl, although equivalent yields have been observed on occasion for these alternative buffers. Thus the decrease in the yield of reduced cytochrome c may be due to the decrease in yield caused by the lower ADA concentration used for the ionic strength dependence and not from multiple tight-binding sites.

Even with this caveat, the results confirming the increased electron-transfer rates as the donor:acceptor complex becomes more tightly bound remains true.

General Utility for Studying Enzymatic Reactions. The principal motivation for this work was to develop a photoreductant which would enable us to study the electron transfer between cytochrome *c* and cytochrome *c* oxidase during the turnover of dioxygen to water under physiological conditions. Recent work by Millett and co-workers[29] and Nilsson[35] have found that the electron input from cytochrome *c* to Cu_A in cytochrome *c* oxidase is greater than 10^5 s^{-1}. This electron input rate is faster than the observed photoreduction of cytochrome *c* by these new nitrobenzene photoreductants reported in this work and suggest that the nitrobenzene photoreductants could not be used to study this enzymatic reaction. However, this is not the case. The experiments by Millett and co-workers[29] and Nilsson[35] were studied under low ionic strengths where cytochrome *c* and cytochrome *c* oxidase form a tight 1:1 electrostatic complex. The electron-transfer mechanism may be different and slower for the physiological process, as shown by the much slower input rates into heme *a* under physiological ionic strengths.[24,36,37]

Even if the electron input rate was greater than 10^5 s^{-1} under physiological conditions, the nitrobenzene photoreductants could be modified to increase the electron-transfer rate to cytochrome *c*. One method would be to put on more negative charges to increase the electrostatic complexation between the nitrobenzene photoreductant and cytochrome *c* at physiological ionic strength. Our results reported here have shown that the electrostatic binding between the nitrobenzene photoreductant and cytochrome *c* increases as more negative charges are placed on the nitrobenzene framework (DANPATA triacid) and the observed electron-transfer rate increases to 36 000 s^{-1} when the tighter complex forms. Increasing the number of negative charges on the photoreductant would increase the binding constant and ultimately increase the electron-transfer rate constant, where the limiting rate would be determined by the inherent intramolecular electron-transfer rate constant, k_{et}.

A second method would be to covalently link the nitrobenzene photoreductant to cytochrome *c* by well-known coupling reactions to form an intramolecular photoreductant similar to the Ru–cytochrome *c* derivatives used by Millett and co-workers.[29] Then the limiting effect for the photoreduction of cytochrome *c* would not be the bimolecular collision rate as observed for this work at high ionic strength. The unimolecular electron transfer could be substantially greater than the bimolecular rate for the electron transfer from cytochrome *c* to cytochrome *c* oxidase at physiological ionic strength (no tight 1:1 electrostatic complex is formed). Then the electron-transfer rate between these new nitrobenzene photoreductants and cytochrome *c* would not be limiting in studying the physiological electron transfer between cytochrome *c* and cytochrome *c* oxidase. These photoreductants could also be used with other enzymatic systems using a similar methodology.

Conclusions

Substituted nitrobenzene derivatives, which were previously used as protecting groups in organic chemistry and for the photoinitiated release of substrates, have been successfully adapted as effective photoreductants for proteins as shown with cytochrome *c* and other heme proteins. In addition, they can be synthetically modified to function as photoreductants for other proteins as well. We have shown that the photoreductant can be engineered by increasing the number of negatively charged substituents on the nitrobenzene framework (DMNPAA to DANPATA) to increase the electrostatic interaction and increase the observed electron-transfer rate from ~9000 s^{-1} to 36 000 s^{-1} for the photoreduction of cytochrome *c*. The general utility of these nitrobenzene photoreductants is being extended by using them to initiate intermolecular electron transfer between two physiological redox proteins.

Experimental Section

Transient Absorption Spectroscopy. Stock solutions of the photoreductants were 10 mM in H_2O/methanol and stored at −80 °C until needed. Typical transient absorption samples contained 980 μL of 100 mM ADA buffer at pH 6.6, 10 μL of 10 mM photoreductant (100 μM), and 10 μL of 1.5 mM cytochrome *c* (15 μM) in a 1 cm quartz cuvette with a micro stir bar. Cytochrome *c* was photoreduced by exciting the photoreductant at 355 nm with the third harmonic from a Spectra Physics DCR-12 Nd:YAG laser. The excitation pulse typically had a 10–20 ns pulse width (fwhm) and an output power of 1.5 mJ/pulse at the sample. The Nd:YAG flash lamp was fired at a 10 Hz repetition rate but the Q-switch was externally triggered at 1 Hz to achieve a 1 Hz laser pulse repetition rate. The probe source for the transient absorption spectra was a 75 W xenon arc lamp which passed through a 530 nm Schott glass long-pass filter before the sample and the transmitted light was passed through a second 530 nm Schott glass long-pass filter before going through an Instruments SA 1690B double monochromator set at 550 nm and detected with a photomultiplier tube. The transient signal was amplified with a Keithly 427 current amplifier and digitized using a Tektronix R710 200 MHz transient digitizer interfaced to a microcomputer.

Materials. Horse heart cytochrome *c* (Sigma), horse heart myoglobin (Sigma), horseradish peroxidase (Sigma), human hemoglobin (Sigma), and *N*-2-acetamidoiminodiacetic acid (ADA, Calbiochem) were used without further purification.The photoreductants 2-nitrophenylacetic acid (NPAA), 4,5-dimethoxy-2-nitrobenzaldehdye (DMNB), 4,5-dimethoxy-2-nitrobenzoic acid (DMNBA), and 5,5′-dithiobis(2-nitrobenzoic acid) (DTB-NBA) were purchased from Aldrich and used without further purification. γ-Aminobutyric acid, 4,5-dimethoxy-2-nitrobenzyl ester, hydrochloride (GABA) was purchased from Molecular Probes and used without further purification.

Synthesis. Tetrahydrofuran was refluxed over sodium metal/benzophenone and freshly distilled prior to use. All other solvents were of reagent grade or better and used without further purification. Proton NMR data were collected on a Bruker AM 500 or a GE QE 300 using a deuterium lock. IR spectra were taken on a Perkin-Elmer 1600 FTIR. GCMS was performed on a Hewlett-Packard 5890A gas chromatograph equipped with a 12 m silicon gum capillary column coupled to a 5970 Series mass-sensitive detector. Absorption spectroscopy was performed on a Hewlett-Packard 8452A diode array spectrophotometer.

4,5-Dimethoxy-2-nitrophenylacetic Aspartamide (DMNPA-ASP, 1). 4,5-Dimethoxy-2-nitrophenylacetic acid (0.18 g, 0.77 mmol) was dissolved in 5 mL of CH_2Cl_2 and 3 mL of DMF and cooled to 0 °C in an ice bath. Dicyclocarbodiimide (0.16 g, 0.77 mmol) was added dropwise and stirred for 90 min. Aspartic acid (0.12 g, 0.94 mmol) in 1 mL of DMF was added to this solution at 0 °C, then the reaction mixture was allowed to warm to room temperature and stirred for 24 h. The resultant precipitate was filtered, the filtrate was quenched with 20 mL of H_2O, extracted with ethyl acetate (3 × 40 mL), and dried with $MgSO_4$, and solvent was removed in vacuo. The resultant solid was recrystallized from ethyl acetate to yield a light yellow powder. Absorption spectrum (water) λ_{max} ($\epsilon_M \times 10^{-3}$ M^{-1} cm^{-1}) 349 nm (6.3); ^1H NMR (acetone-d_6, 300 MHz) δ 7.65 (s, 1 H), 6.97 (s, 1 H), 4.13 (s, 2 H), 3.88 (s, 6 H), 2.79 (m, 1 H), 1.76 (m, 1 H), 1.31 (m, 1 H).

1-(4,5-Dimethoxy-2-nitrophenyl)ethyl-1-succinic Acid (SUCC, 2). Succinic acid (0.944 g, 8.0 mmol) was added to 20 mL of DMF, and the resultant heterogeneous mixture was stirred at room temperature. 1-(4,5-Dimethoxy-2-nitrophenyl)-1-diazaethane (25 mg, 0.2 mmol, prepared according to the procedure described by Molecular Probes) dissolved in chloroform was added dropwise to the heterogeneous solution. The dark orange color of the diaza solution slowly faded during the addition, and the solution was stirred for 4 h at room temperature. The resulting pale yellow solution was lyophilized, and the resulting solid was dissolved in 25 mL of 5:1 $CHCl_3$:THF and washed with water (4 × 10 mL). The organic layer was collected, and the solvent removed in vacuo to yield a yellow oil. This oil was purified by preparative TLC using 10:1 $CHCl_3$:THF (R_f 0.4). The product was extracted from the silica with THF, and the solvent removed in vacuo. Concentrated NH_4OH (3 drops), water (5 mL), and $CHCl_3$ (5 mL) were added to the product. The aqueous layer was washed with $CHCl_3$ (2 × 5 mL) and lyophilized to yield 0.0212 g of a pale yellow powder. Absorption spectrum (water) λ_{max} ($\epsilon_M \times 10^{-3}$ M^{-1} cm^{-1}) 347 nm (5.7), 310 nm (sh); ^1H NMR (methanol-d_4, 300 MHz) δ 7.57 (s, 1 H), 7.15 (s, 1 H), 6.34 (q, 1 H, $J = 6.3$ Hz), 3.97 (s, 3 H), 3.87 (s, 3 H), 2.60 (m, 2 H), 2.47 (m, 2 H), 1.59 (d, 3 H, $J = 6.3$ Hz).

Methyl-4,5-dimethoxy-2-nitrophenylacetate (MDMNPA, 3). 4,5-Dimethoxy-2-nitrophenylacetic acid (2.67 g, 11.1 mmol) was suspended in 150 mL of methanol. $SOCl_2$ (1.5 mL, 20.6 mmol) was added dropwise and stirred overnight at room temperature. The precipitated ester was vacuum filtered and washed with cold methanol to yield 1.68 g of a light yellow powder (60%); mp 108−109 °C; IR 1723.1 cm^{-1}; MS calculated for $C_{11}H_{13}NO_6$ 210, *m/e* found 210; absorption spectrum (water) λ_{max} ($\epsilon_M \times 10^{-3}$ M^{-1} cm^{-1}) 348 nm (6.6), 310 nm (sh); ^1H NMR ($CDCl_3$, TMS, 500 MHz) δ 7.79 (s, 1 H), 6.79 (s, 1 H), 4.05 (s, 2 H), 4.00 (s, 3 H), 3.98 (s, 3 H), 3.75 (s, 3 H).

4,5-Dimethoxy-2-nitroacetophenone (DMNAP, 7). 3,4-dimethoxyacetopheneone (14.98 g, 83.2 mmol) was added over 1 h to 90 mL of concentrated HNO_3 and stirred for an additional 1 h, maintaining the temperature between 18 and 22 °C. The solution was poured into 1200 mL of H_2O and chilled in an ice bath. The precipitated crystals were collected by vacuum filtration and recrystallized from H_2O and then ethanol to yield 10.97 g (59%) of yellow needles; mp 131−132 °C; MS calculated for $C_{11}H_{13}NO_5$ 239, *m/e* found 239; absorption spectrum (water) λ_{max} ($\epsilon_M \times 10^{-3}$ M^{-1} cm^{-1}) 349 nm (5.6), 309 nm (sh); ^1H NMR ($CDCl_3$, TMS, 500 MHz) δ 7.61 (s, 1 H), 6.78 (s, 1 H), 3.99 (s, 6 H), 2.50 (s, 3 H).

4,5-Dimethoxy-2-nitrophenylacetic Acid (DMNPAA, 8). 3,4-Dimethoxy-2-phenylacetic acid (5.12 g, 26.1 mmol) was dissolved in 50 mL of glacial acetic acid at 0 °C in an ice bath. Concentrated HNO_3 (67%, 30 mL) was added dropwise with stirring and then allowed to react for 2 h at 0 °C. The solution was poured into 1 L of saturated NaCl solution, and the product immediately precipitated from solution and was vacuum filtered and washed with cold H_2O to yield 5.34 g of yellow powder (85%). MS calculated for $C_{10}H_{11}NO_6$, *m/e* 241, found 241; absorption spectrum (water): λ_{max} ($\epsilon_M \times 10^{-3}$ M^{-1} cm^{-1}) 350 nm (5.4), 310 nm (sh); ^1H NMR (acetone-d_6, 300 MHz) δ 10.89 (s, 1 H), 7.75 (s, 1 H), 7.15 (s, 1 H), 4.08 (s, 2 H), 3.99 (s, 3 H), 3.97 (s, 3 H).

4,5-Dimethylalkyl-2-phenylalkyl Acetate (DMAPA, 9a). 3,4-Dihydroxyphenylacetic acid (2.19 g, 12.03 mmol) was dissolved in 75 mL of DMF. K_2CO_3 (4.99 g, 36.08 mmol) was added to the solution, then 3.42 mL (36.08 mmol) of bromo acetate (Aldrich) was added dropwise, and the reaction mixture stirred at room temperature for 24 h. The reaction was quenched with 100 mL of H_2O and extracted with ethyl acetate (3 × 100 mL). The combined organic layers were dried with $MgSO_4$, and solvent was removed in vacuo at room temperature. The product was purified by flash silica chromatography (diethyl ether) to yield 2.96 g (61%) of clear oil. MS calculated for $C_{17}H_{20}O_{10}$ 384, *m/e* found 384; ^1H NMR ($CDCl_3$, 300 MHz) δ 6.78 (m, 3 H), 4.63 (s, 2 H), 4.61 (s, 2 H), 4.52 (s, 2 H), 3.68 (s, 3 H), 3.67 (s, 3 H), 3.63 (s, 3 H), 3.55 (s, 2 H).

4,5-Dimethylalkyl-2-nitrophenylalkyl Acetate (DMANPA, 9b). 4,5-Dimethylalkyl-2-phenylalkyl acetate (0.38 g, 1.0 mmol) was dissolved in 15 mL of glacial acetic acid and 8 mL of concentrated HNO_3 was added dropwise with stirring at room temperature. After 8 h, 50 mL of H_2O was added, and the reaction mixture extracted with diethyl ether (3 × 30 mL). The combined organic layers were dried with $MgSO_4$, and solvent was removed in vacuo at room temperature. The product was purified by flash silica chromatography (diethyl ether) to yield 0.33 g (79%) of the light yellow oil. MS calculated for $C_{17}H_{19}NO_{12}$, *m/e* 429, found 429; ^1H NMR (acetone-d_6, 300 MHz) δ 7.72 (s, 1 H), 6.80 (s, 1 H), 4.84 (s, 2 H), 4.79 (s, 2 H), 4.66 (s, 2 H), 4.08 (s, 2 H), 3.82 (s, 3 H), 3.81 (s, 3 H), 3.76 (s, 3 H).

4,5-Dialkyl-2-nitrophenylacetic Triacid (DANPATA, 9). 4,5-Dimethylalkyl-2-phenylalkyl acetate (1.17 g, 3.0 mmol) was dissolved in 15 mL of glacial acetic acid and 15 mL of concentrated HNO_3 was added dropwise at room temperature with stirring. After 48 h, 50 mL of H_2O was added and the reaction mixture extracted with ethyl acetate (3 × 75 mL). The combined organic layers were dried with $MgSO_4$, and solvent was removed in vacuo at room temperature. The product was recrystallized twice from ethyl acetate to yield 0.65 g of light yellow powder (55%). Absorption spectrum (water): λ_{max} ($\epsilon_M \times 10^{-3}$ M^{-1} cm^{-1}) 346 nm (5.7), 308 nm (sh); ^1H NMR (acetone-d_6, 300 MHz) δ 7.80 (s, 1 H), 7.21 (s, 1 H), 4.96 (s, 2 H), 4.94 (s, 2 H), 4.65 (s, 2 H), 4.13 (s, 2 H).

4,5-Dimethylalkyl-2-nitrophenylacetic Acid (DMANPAA, 10). NaOH (1 N, 5 mL) was added to 4,5-dimethylalkyl-2-nitrophenylalkyl acetate (0.30 g, 0.7 mmol) and stirred for 8 h at room temperature. H_2O (10 mL) was added, and the reaction mixture extracted with ethyl acetate (3 × 25 mL). The combined organic layers were dried with $MgSO_4$, and solvent was removed in vacuo at room temperature. The product was purified by flash silica chromatography (2:3, hexanes:acetone) to yield a white powder. Absorption spectrum (water): λ_{max} ($\epsilon_M \times 10^{-3}$ M^{-1} cm^{-1}) 335 nm (3.8), 298 nm (sh); ^1H NMR (acetone-d_6, 300 MHz) δ 7.61 (s, 1 H), 6.80 (s, 1 H), 4.81 (s, 2 H), 4.77 (s, 2 H), 4.12 (s, 2 H), 3.87 (s, 6 H).

4,5-Dihydroxy-2-nitrophenylacetic Acid (DHNPAA, 12) and 3,4-Dihydroxy-1,6-dinitrophenylacetic Acid (DHDNPAA, 13). H_2O (15 mL) was added to 3,4-dihydroxyphenylacetic acid (0.50 g, 2.97 mmol) and sodium nitrite (0.68 g, 9.92 mmol) and stirred at room temperature. Concentrated H_2SO_4 (1 mL) was added dropwise and stirred for 1 h and then reaction extracted with ethyl acetate (3 × 75 mL). The combined organic layers were dried over $MgSO_4$, and solvent was removed in vacuo. The products were purified by flash silica chromatography (1:1 ethyl acetate:diethyl ether) to yield 0.26 g (41%) 4,5-dihydroxy-2-nitrophenylacetic acid (R_f 0.6; absorption spectrum (water) λ_{max} ($\epsilon_M \times 10^{-3}$ M^{-1} cm^{-1}) 383 nm (4.4); ^1H NMR (acetone-d_6, 300 MHz) δ 7.64 (s, 1 H), 6.86 (s, 1 H), 3.87 (s, 2 H)) and 0.22 g (29%) of 3,4-dihydroxy-1,6-dinitrophenylacetic acid (R_f 0.2; absorption spectrum (water) λ_{max} ($\epsilon_M \times 10^{-3}$ M^{-1} cm^{-1}) 427 nm (5.6); ^1H NMR (acetone-d_6, 300 MHz) δ 7.09 (s, 1 H), 3.85 (s, 2 H)).

Acknowledgment. We would like to thank Dr. Jay Winkler for his assistance with the nanosecond transient absorption apparatus in the Beckman Institute Laser Resource Center. This

work was supported by grant GM22432 from the National Institute of General Medical Sciences, U. S. Public Health Service. TJD is the recipient of a National Research Service Award from the National Institute of General Medical Sciences (GM15647).

References and Notes

(1) Somlyo, A. P.; Somlyo, A. V. *Annu. Rev. Physiol.* **1992**, *52*, 857–874.
(2) Homsher, E.; Millar, N. C. *Annu. Rev. Physiol.* **1992**, *52*, 875–896.
(3) Thirlwell, H.; Corrie, J. E. T.; Reid, G. P.; Trentham, D. R.; Ferenczi, M. A. *Biophys. J.* **1994**, *67*, 2436–2447.
(4) Kaplan, J. H.; Forbush, B. III; Hoffman, J. F. *Biochemistry* **1978**, *17*, 1929–1935.
(5) Buchet, R.; Jona, I.; Martonasi, A. *Biochim. Biophys. Acta* **1992**, *1104*, 207–214.
(6) Tanner, J. W.; Thomas, D. D.; Goldman, Y. E. *J. Mol. Biol.* **1992**, *223*, 185–203.
(7) Kozlowski, R. Z.; Twist, V. W.; Brown, A. M.; Powell, T. *Am. J. Physiol.* **1991**, *261*, H1665–H1670.
(8) Dolphin, A. C.; Wootton, J. F.; Scott, R. H.; Trentham, D. R. *Pflügers Arch.* **1988**, *411*, 628–636.
(9) Ellisdavies, G. C. R.; Kaplan, J. H. *Proc. Natl. Acad. Sci. U.S.A.* **1994**, *91*, 187–191.
(10) Adams, S. R.; Kao, J. P. Y.; Tsien, R. Y. *J. Am. Chem. Soc.* **1989**, *111*, 7957–7968.
(11) Corrie, J. E. T.; Trentham, D. R. *Bioorganic Photochemistry*; Morrison, H., Ed.; Wiley Press: New York, 1993, Vol. 2, pp 243–305.
(12) Hess, B. P. *Biochemistry* **1993**, *32*, 989–1000.
(13) Wieboldt, R.; Ramesh, D.; Carpenter, B. K.; Hess, B. P. *Biochemistry* **1994**, *33*, 1526–1533.
(14) Wieboldt, R.; Gee, K.; Niu, L.; Ramesh, D.; Carpenter, B. K.; Hess, B. P. *Proc. Natl. Acad. Sci. U.S.A.* **1994**, *91*, 8752–8756.
(15) Snyder, R.; Trotter, W.; Testa, A. C. *J. Lumin.* **1985**, *33*, 327–332.
(16) Kobayashi, K.; Hayashi, K. *Fast Methods in Physical Biochemistry and Cell Biology*; Sha'afi, R., Fernandez, R., Eds.; Elsevier North-Holland Biomedical Press: Amsterdam, 1983, pp 87–111.
(17) Van Buuren, K. J. H.; Van Gelder, B. F.; Wilting, J.; Braams, R. *Biochim. Biophys. Acta* **1974**, *333*, 421–429.
(18) Pecht, I.; Faraggi, M. *Nature* **1971**, *233*, 116–118.
(19) O'Neil, P.; Fielden, E. M.; Finazzi-Argo, A.; Aviglicino, L. *Biochem. J.* **1983**, *209*, 167–174.
(20) Anderson, R. F.; Hille, R.; Massey, V. *J. Biol. Chem.* **1986**, *261*, 15870–15876.
(21) Kobayashi, K.; Une, H.; Hayashi, K. *J. Biol. Chem.* **1989**, *264*, 7976–7980.
(22) Cho, K. C.; Che, C. M.; Ng, K. M.; Choy, C. L. *J. Am. Chem. Soc.* **1986**, *108*, 2814–2818.
(23) Zhou, J. S.; Granada, E. S. V.; Leontis, N. B.; Rodgers, M. A. J. *J. Am. Chem. Soc.* **1990**, *112*, 5074–5080.
(24) Hazzard, J. T.; Rong, S.-Y.; Tollin, G. *Biochemistry* **1991**, *30*, 213–221.
(25) Tollin, G.; Hurley, J. K.; Hazzard, J. T.; Meyer, T. E. *Biophys. Chem.* **1993**, *48*, 259–279.
(26) Brunschwig, B. S.; Delaive, P. J.; English, A. M.; Goldberg, M.; Mayo, S. L.; Sutin, N.; Gray, H. B. *Inorg. Chem.* **1985**, *24*, 3743–3749.
(27) Wishart, J. F.; Vaneldik, R.; Sun, J.; Su, C.; Isied, S. S. *Inorg. Chem.* **1992**, *31*, 3986–3989.
(28) Orii, Y. *Biochemistry* **1993**, *32*, 11910–11914.
(29) Pan, L. P.; Hibdon, S.; Liu, R.-Q.; Durham, B.; Millett, F. *Biochemistry* **1993**, *32*, 8492–8498.
(30) Wuttke, D. S.; Bjerrum, M. J.; Chang, I. J.; Winkler, J. R.; Gray, H. B. *Biochim. Biophys. Acta* **1992**, *1101*, 168–170.
(31) Czarnik, A. W. *Acc. Chem. Res.* **1994**, *27*, 302–308.
(32) Gu, Y. G.; Li, P. S.; Sage, J. T.; Champion, P. M. *J. Am. Chem. Soc.* **1993**, *115*, 4993–5004.
(33) Walker, J W.; Reid, G. P.; McCray, J. A.; Trentham, D. R. *J. Am. Chem. Soc.* **1988**, *110*, 7170–7177.
(34) Timkovich, R.; Dickerson, R. E. *J. Biol. Chem.* **1976**, *251*, 4033–4046.
(35) Nilsson, T. *Proc. Natl. Acad. Sci. U.S.A.* **1992**, *89*, 6497–6501.
(36) Larson, R. W.; Winkler, J. R.; Chan, S. I. *J. Phys. Chem.* **1992**, *96*, 8023–8027.
(37) Pan, L.-P.; Hazzard, J. T.; Lin, J.; Tollin, G.; Chan, S. I. *J. Am. Chem. Soc.* **1991**, *113*, 5908–5910.

JP9516304

Chapter VIII

A Leucine-Rich Repeat Variant With a Novel Repetative Protein Structural Motif

In press in Nature Structural Biology

A Leucine-Rich Repeat Variant With a Novel Repetitive Protein Structural Motif

John W. Peters, Michael H. B. Stowell and Douglas C. Rees*

Department of Chemistry and Chemical Engineering, 147-75CH

California Institute of Technology

Pasadena, California 91125 USA

*to whom correspondence should be addressed

telephone (818)-395-8393

fax (818)-584-6785

e-mail rees@citray.caltech.edu

Summary

The structure of the leucine-rich repeat variant protein reveals a novel fold consisting of alternating α and 3_{10} helices arranged in a right-handed superhelix that follows an N-terminal 4Fe:4S cluster containing domain.

Sir: Leucine-rich repeat (LRR) proteins are classified on the basis of their distinctive primary sequences, which consist of multiple tandem repeats of 24-29 residues rich in conserved leucines and other aliphatic residues (reviewed in [1, 2]). Members of this class include hormone receptors, cell adhesion molecules, bacterial virulence factors, DNA repair enzymes, as well as many other proteins of unknown function. The x-ray crystal structure of one of these proteins, the porcine ribonuclease inhibitor, demonstrates that the protein folds into 15 domains containing 28-29 residues each, with an overall fold generated by an extended right-handed superhelix of alternating α-helices and β-strands[3]. We have identified a variant of the LRR class of proteins which is thought to be expressed in the microorganism *Azotobacter vinelandii* under nitrogen fixing conditions[4]. In contrast to the structure of the ribonuclease inhibitor, the structure of the leucine-rich repeat variant (LRV) protein reveals a novel fold consisting of alternating α and 3_{10} helices arranged in a right-handed superhelix, with the complete absence of any β-sheet structure.

The gene encoding the LRV protein is located at the 3' terminus of an operon that contains the genes coding for the Fe-protein and the MoFe-protein of nitrogenase and was previously[4] referred to as open-reading frame 2. The deduced primary amino acid sequence of this gene product (Genbank accession number M20568) suggests a two domain structure for LRV, composed of a smaller domain containing a cluster of 4 Cys residues and a larger domain with 8 tandem repeats of 24 amino acids each (Fig. 1). Preliminary biochemical studies have indicated that the protein contains a single 4Fe:4S cluster that is highly sensitive to oxygen and not reversibly redox active (M.K. Johnson and D.R. Dean, unpublished results). Comparison of the deduced amino-acid sequence of the LRV consensus repeat unit to an overall consensus sequence of LRR proteins [1, 2] indicates that LRV exhibits strong sequence similarities to members of the LRR class of proteins. There is an important difference between the consensus sequence for LRR

proteins and LRV, however; the highly conserved 'xLxL' pattern corresponding to the β-sheet region of LRR proteins (where x indicates less well conserved amino acids), occurs as 'LxxL' in LRV. Since the sequences corresponding to the α-helical region of the LRR are relatively well conserved in LRV, this suggests that LRV might differ principally from the LRR fold in the β-sheet region.

The structure of LRV was solved by multiple isomorphous replacement and native anomalous scattering (MIRAS) together with solvent flattening. The structure, including residues 9-241 of 244 total residues, has been refined to 2.6 Å resolution to a present crystallographic R-factor of 0.204 and a free R-value of 0.272. The polypeptide fold of LRV resembles a comma (Fig. 2a), with overall dimensions of approximately 15 x 25 x 80 Å. The head of the comma corresponds to the 4Fe:4S cluster-containing domain, while the repeating units generate the tail. Significantly, in contrast to the alternating α-helix and β-strand repeating units of the ribonuclease inhibitor (RI), the repeating units of LRV consist of alternating α-helices and 3_{10} helices (Fig 2a). The α-helices line the inner curvature of the protein, unlike RI where α-helices are found to flank the outer circumference. The outer circumference of LRV is composed of 3_{10} helices that can be readily contrasted to the α-helices in electron density maps (Fig 2b). Despite several differences in the primary amino acid sequences of the individual repeat units (Fig. 1), the units are virtually superimposable with an overall r. m. s. deviation of 0.3 Å for equivalent α-carbons when five repeats are superimposed onto one (Fig 2c).

The α-helices of each repeating domain average 10 residues in length[5], and are arranged in nearly parallel fashion with respect to each other, with calculated crossing angles[5] averaging -3.9° (range -12° to +7°). In a similar manner, the 3_{10} helices (average length 6 residues) are nearly parallel, with calculated crossing angles averaging 0.6° (range -35° to +25°). Each α-helix is related to its nearest 3_{10} helices by an average crossing angle

of -136.5° angle (range -117° to -151°). The spacing between equivalent Cα positions on neighboring α-helices averages 9.0 ± 0.6Å, while the spacing between adjacent 3_{10} helices averages 11.4 ± 1.0 Å. The rotation angle required to superimpose adjacent repeating units[6] is close to 15° about an axis nearly parallel to the axes of the α-helices, so that ~24 units are required to form a complete turn. Together with the α-helix spacings of ~9.0Å, the average radius of curvature of the α-helices is ~34Å. For comparison, adjacent helices in RI [3] are related by a 17° rotation and are spaced by ~9.3Å, yielding a somewhat tighter radius of curvature for the helices in RI of ~32Å, relative to LRV. Unlike RI, where adjacent units are very nearly related by a pure rotation operation, the relationship between repeating units in LRV includes a 1.3Å screw translation along the rotation axis[7]. The total translation after one complete turn (24 units) is approximately 32Å, which is close to the length of one α-helix-3_{10} helix unit. Consequently, extrapolation to indefinitely long chains of LRV repeating units suggests that they will fold to form a cylinder with closed walls and a channel radius of ~34Å.

The repeating units of LRV are linked by a ladder of hydrogen bond and salt bridge interactions formed between conserved Asp and Arg residues (Fig. 3a). The Asp sidechain at position 22 forms a salt bridge to the Arg sidechain at position 4 of the neighboring unit (residue numbers refer to the position within the repeating unit (Fig. 1)). The ladder continues through a hydrogen bond from Nε of the Arg to the mainchain carbonyl oxygen of the Asp at position 22 in the same repeating unit. These interactions form a network that spans nearly the entire molecule. This conserved Asp is located at the same position as the conserved Asn in the LRR protein consensus sequence (Fig. 1) that is found in the RI structure to also participate in a sidechain hydrogen bond network that links together the repeating units. Structural requirements for the conservation of Arg, Glu and Asp at positions 10, 14 and 24 of the LRV repeat are not evident, and it is possible that these residues may play a role in interacting with other molecules.

As in the case of LRR proteins, the conserved Leu and other aliphatic residues of LRV form the hydrophobic core of the protein (Fig. 3b). A key difference, however, is the spacing of these residues in the sequence which may explain in part the observed differences in topology. The consensus sequence of LRR proteins indicates that Leu are preferred at positions 17 and 19. The LRV consensus repeat sequence, however, has Leu residues at positions 16 and 19 (Fig. 1). In both LRR and LRV proteins, these particular Leu contribute to the hydrophobic core of the protein (Fig. 3b). The spacing of two residues between leucines in LRV apparently stabilizes formation of 3_{10} helices to provide a hydrophobic interface to pack against the protein core, in contrast to LRR proteins, where the one residue spacing between leucines permits packing of a β-strand against the protein core.

A significant number of LRR proteins contain clusters of Cys residues flanking the LRR domains. Although these Cys clusters appear to be a property of adhesive proteins and receptors, their function is not known[1]. The consensus sequence derived for the amino terminal Cys clusters of LRRs can be described[1] as CxC[~20x]C[~20x]C, where x is any residue. This consensus is different from that observed in the amino-terminal Cys cluster of LRV, which has the spacing CxxC[11x]C[5x]C (Fig. 1). The four cysteines in LRV coordinate an oxygen sensitive 4Fe:4S cluster (Fig. 3c). Space filling models of LRV indicate that the 4Fe:4S cluster of LRV is exposed to the solvent, which may contribute to its apparent oxygen sensitivity. This accessibility suggests that the cluster could possibly act as a biosensor of oxygen and/or iron, as observed in regulatory proteins such as the bacterial FNR transcription factor and the mammalian iron-responsive-element-binding protein (reviewed in [8]).

A striking aspect of the LRV protein is the proportion and length of 3_{10} helix present in the structure; there are 7 helices containing 5-9 residues each, for an overall occurrence of 20%. For comparison, Barlow and Thornton[9] observed that 3.4% of all residues in a general survey of proteins were found in 3_{10} helices, with an average length of 3.3 residues. As in this earlier study, the 3_{10} helices in LRV deviate somewhat from an ideal 3_{10} helix, with an average of 3.2 residues per turn and a pitch of 5.8Å (as compared to the ideal values of 3.0 residues per turn and a pitch of 6.0Å). The average mainchain ϕ,ψ values (-60°, -29°) for the 3_{10} helices in LRV are close to those observed (-57°,-30°) in the structures of 3_{10} helical peptides studied by small molecule crystallography[10]. Stabilization of 3_{10} helices in LRV must certainly reflect the underlying pattern of residue polarity in the amino acid sequence. As clearly indicated by the α-helical conformation adopted by the corresponding sequence in the terminal repeating unit of LRV (Fig. 1), however, other factors, such as side-chain packing, must also influence the secondary structure of these sequences. This sensitivity of the stability of 3_{10}-helices in LRV to environmental conditions is consistent with the proposal that switching from 3_{10} to α-helices may occur along the folding pathway of helical peptides and sequences[11 12].

Methods

Azotobacter vinelandii nitrogen fixation specific LRV protein was expressed heterologously in *E. coli* using a T7 expression system, and purified by anion exchange and gel filtration chromatography of the soluble fraction of the cell lysate under anaerobic conditions described in [13]. LRV was crystallized in space group $P3_121$ (a=b=69.8Å, c=159.8Å, with one molecule in the asymmetric unit for a solvent fraction of 0.7) using the microcapillary batch diffusion method under anaerobic conditions [14]. The precipitant solution contained 2.0 M ammonium sulfate and 1 mM sodium dithionite, buffered with Tris-HCl pH 8.5. The Native-1 and Au derivative data sets were collected on an RAXIS image plate detector

with CuKα (1.54 Å) radiation from a RIGAKU rotating anode x-ray generator. Native -2 and Xe [15] derivative data sets were collected on the MAR imaging plate detector at beam-line 7-1 of the Stanford Synchrotron Radiation Laboratory (λ = 1.08Å). Data sets were processed with DENZO [16] and scaled with either SCALEPACK [16] or ROTAVATA/AGROVATA [17]. All data sets were collected from single crystals, with the exception of Native-2 that consisted of merged data from three crystals. The position of the 4Fe:4S cluster was determined from native anomalous Patterson maps. Derivative sites were located in isomorphous difference Fouriers maps using the phases calculated from the cluster. Initial MIRAS phases were refined and calculated to 4Å resolution with MLPHARE [18] and PHASES [19]. The phasing powers calculated with PHASES for the native anomalous, gold and xenon data sets were 1.7, 1.9 and 1.2, respectively to 4Å resolution, with an overall figure of merit of 0.39. Phases were refined and extended to 3.5Å resolution with the density modification algorithm of SOLOMON [20], using a solvent fraction of 0.6. Following model building with the program O [21], the structure was refined with X-PLOR[22] using the protein parameters of Engh and Huber [23]. The model was improved by iterative cycles of rebuilding, refinement and phase combination (with the program SIGMAA[24]). The refined model contains 1896 protein atoms, no solvent molecules and has been refined to R_{cryst} and R_{free} of 0.204 and 0.272, respectively for the 12544 reflections with $F > 2\sigma(F)$ for data between 8-2.6Å resolution (92% complete). The rms deviations in bond length and bond angles are 0.016 and 2.0°, respectively, and 87% of the residues occur in the most favored regions of the Ramachandran plot, as calculated in PROCHECK [25]. The coordinates will be deposited in the Brookhaven Data Bank and in the interim can be obtained from peters@citray.caltech.edu. The program PROMOTIF was used for secondary structure assignments [5]; α-helices were identified as including residues 41-50, 64-71, 88-95, 112-121, 136-145, 160-169, 184-193, 208-217, 220-225 and 231-238, while 3_{10} residues were identified as including residues 52-58, 76-82, 101-105, 125-

130, 148-153, 172-177, and 196-204. All structural figures were produced using the programs MOLSCRIPT [26] and RASTER3D [27, 28].

REFERENCES AND NOTES

1. Kobe, B. & Deisenhofer, J. *Trends Biochem. Sci.* **19**, 415-421 (1994).
2. Kobe, B. & Deisenhofer, J. *Curr. Opin. Struct. Biol.* **5**, 409-416 (1995).
3. Kobe, B. & Deisenhofer, J. *Nature* **366**, 751-756 (1993).
4. Jacobson, M.R., *et al. J. Bact.* **171**, 1017-1027 (1989).
5. Hutchinson, E.G. & Thornton, J.M. *Prot. Sci.* **5**, 212-220 (1996).
6. Kabsch, W. *Acta crystallogr.* **A32**, 922-923 (1976).
7. Cox, J.M. *J. Mol. Biol.* **28**, 151-156. (1967).
8. Rouault, T.A. & Klausner, R.D. *Trends Biochem. Sci.* **21**, 174-177 (1996).
9. Barlow, D.J. & Thornton, J.M. *J. Mol. Biol.* **201**, 601-619 (1988).
10. Toniolo, C. & Benedetti, E. *Trends Biochem. Sci.* **16**, 350-353 (1991).
11. Millhauser, G.L. *Biochem.* **34**, 3873-3877 (1995).
12. Miick, S.M., Martinez, G.V., Fiori, W.R., Todd, A.P. & Millhauser, G.L. *Nature* **359**, 653-655 (1992).
13. Peters, J.W., Fisher, K. & Dean, D.R. *J. Biol. Chem.* **269**, 28076-28083 (1994).
14. Georgiadis, M.M., *et al. Science* **257**, 1653-1659 (1992).
15. Stowell, M.H.B. *J. Appl. Cryst.* **in press** (1996).
16. Otwinowski, Z. in *Data Collection and Processing* (eds. Sawyer, L., Issacs, N. & Bailey, S.) 56-62 (SERC Daresbury Laboratory, UK, 1993).
17. Bailey, S. *Acta crystallogr.* **D50**, 760-763 (1994).
18. Otwinowski, Z. in *Isomorphous Replacement and Anomalous Scattering* (eds. Wolf, W., Evans, P. & Leslie, A.) 80-86 (SERC Daresbury Laboratory, UK, 1991).
19. Furey, W. & Swaminathan, S. in *Meth. Enzym.* (eds. Carter, C. & Sweet, R.) in press (Academic Press, Orlando, 1996).
20. Abrahams, J.P. & Leslie, A. *Acta crystallogr.* **D52**, 30-42 (1996).

21. Jones, T.A., Zhou, J.Y., Cowan, S.W. & Kjeldgaard, M. *Acta crystallogr.* **A47**, 110-119 (1991).

22. Brünger, A.T., Kuriyan, J. & Karplus, M. *Science* **235**, 458-460 (1987).

23. Engh, R.A. & Huber, R. *Acta crystallogr.* **A47**, 392-400 (1991).

24. Read, R.J. *Acta crystallogr.* **A42**, 140-149 (1986).

25. Laskowski, R.A., McArthur, M.W., Moss, D.S. & Thornton, J.M. *J. Appl. Crystallogr.* **26**, 283-291 (1993).

26. Kraulis, P.J. *J. Appl. Crystallogr.* **24**, 946-950 (1991).

27. Bacon, D. & Anderson, W.F. *J. Mol. Graphics* **6**, 219-220 (1988).

28. Merritt, E.A. & Murphy, M.E.P. *Acta crystallogr.* **D50**, 869-873 (1994).

Acknowledgments. We thank D. Dean and L. Zheng for the LRV expression plasmid and suggestions on its purification, and the structural biology group at the Stanford Synchrotron Radiation Laboratory (SSRL) for assistance during data collection. This work was supported by a grant from NIH to D. C. R. and an NIH postdoctoral fellowship to J.W.P. The rotation camera facility at SSRL is supported by the DOE Office of Basic Energy Sciences and the NIH Biomedical Research Technology Program, Division of Research Resources.

Table I. Data Collection Statistics and Structure Determination

	Native-1	Native-2	Au	Xe
Resolution (Å)	3.5	2.6	3.5	3.5
Observations	28171	63817	20826	15401
Unique Reflections	6151	13656	5982	5266
Completeness (%)	99	94	98	88
R_{merge} (%)	10.3	7.7	12.4	10.0
R_{iso} (%)			10.3	10.0

$R_{merge} = \sum_{hkl}(\sum_i(|I_{hkl,i} - \langle I_{hkl}\rangle|))/\sum_{hkl,i}\langle I_{hkl}\rangle$, where $I_{hkl,i}$ is the intensity of an individual measurement of the reflection with indices hkl and $\langle I_{hkl}\rangle$ is the mean intensity of that reflection.

R_{iso} - mean fractional isomorphous difference = $(\sum_{hkl}(||F_{hkl,P}| - |F_{hkl,PH}||))/\sum_{hkl}|F_{hkl,P}|)$ where $F_{hkl,P}$ is the structure factor of a reflection from the native data set 1 and $F_{hkl,PH}$ is the structure factor of the corresponding reflection from the derivative data set.

4Fe:4S Cluster Domain

```
 1  M A D D R G D I T P T G D C R V C S F R
21  M S L L L T G R C T P G D A C V A V E S
```

Repeat Domain

```
      1           5           10          15          20
41      G R Q I D R F F R N N P H L A V Q Y L A D P F
64  W E R R A I A V R Y S P V E A L T P L I R D S D
88  E V V R R A V A Y R L P R E Q L S A L M F D E D
112 R E V R I A V A D R L P L E Q L E Q M A A D R D
136 Y L V R A Y V V Q R I P P G R L F R F M R D E D
160 R Q V R K L V A K R L P E E S L G L M T Q D P E
184 P E V R R I V A S R L R G D D L L E L L H D P D
208 W T V R L A A V E H A S L E A L R E L D - E P E
231 P E V R L A I A G R L G I A
```

```
        -      α Helix      - L1 -  3₁₀ Helix  - L2
LRV     X X V R X X V A X R L X X E X L X X L X X D X D
        1           5           10          15          20
LRR     X X L X X X I F X X L X X L X X L X L X X N X I
              α Helix                  β strand
```

Figure 1. The amino-acid sequence of the *A. vinelandii* LRV, indicating the division into 4Fe:4S cluster and repeating unit domains. Cysteine residues coordinating the 4Fe:4S cluster are colored green. Aliphatics residues forming the hydrophobic core of LRV are indicated in dark yellow, while Asp and Arg residues generating a ladder are designated by red and blue, respectively. Secondary structure assignments [5] are detailed in Table 1. Underneath the sequence is a comparison of a consensus sequence for LRR proteins [3] and the corresponding region of LRV. In both LRV and LRR proteins, "conserved" leucines may be replaced by other aliphatic residues. Residues that are not well conserved in the consensus sequences are represented by X. Secondary structures of the repeating units are indicated adjacent to the corresponding sequence. The 3_{10} helical region of the last repeating unit actually adopts an α-helical conformation. L1 and L2 denote loop regions between the α- and 3_{10}-helices; residues in the L2 region are typically found in a type I turn conformation [5]. For this comparison, the amino- and carboxy-halves of the LRR consensus sequence are switched from the convention commonly used [3].

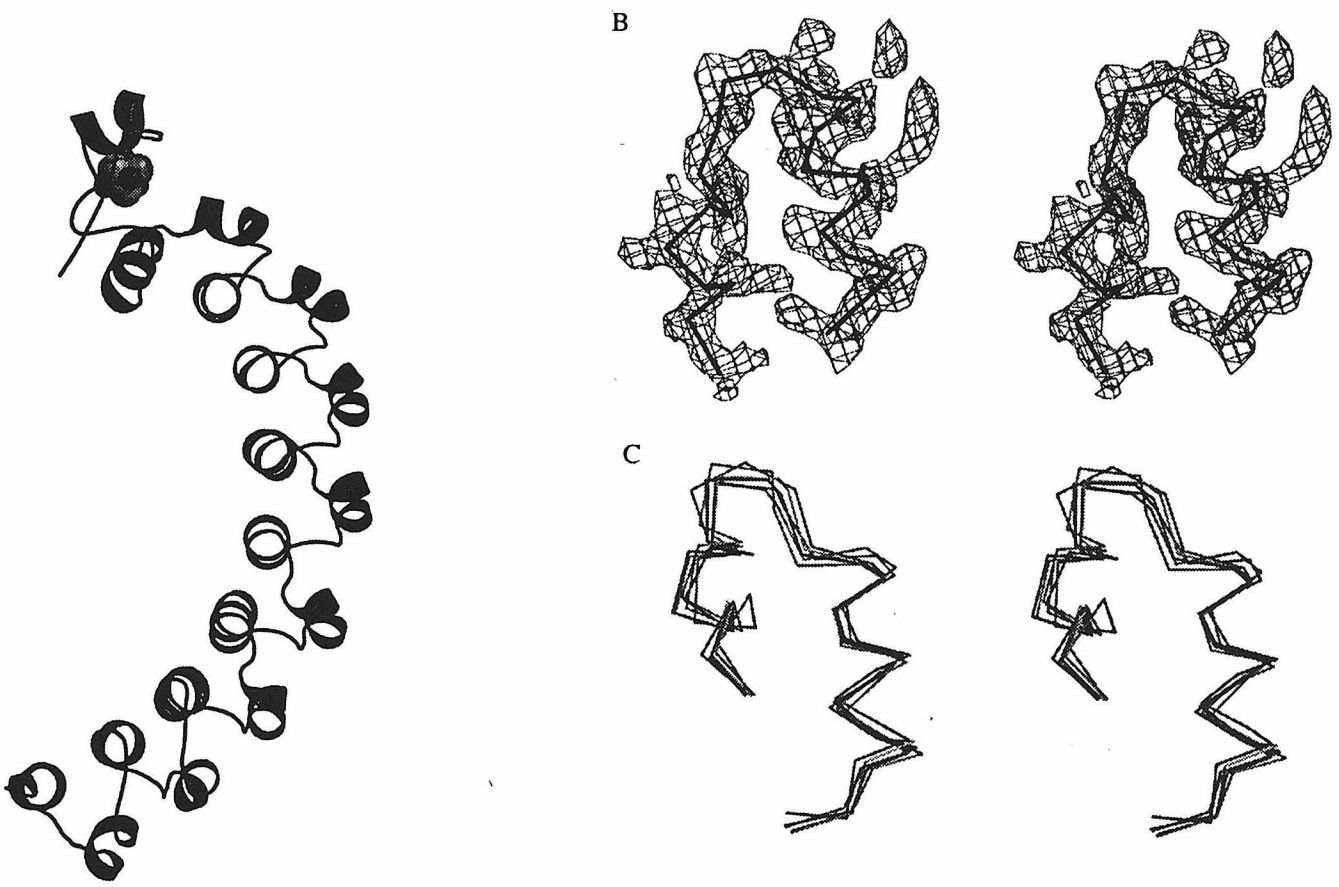

Figure 2. (a) Ribbons representation of LRV with α-helices and 3_{10} helices shown in red and blue, respectively. The N-terminal 4Fe:4S cluster is included as a space filling model. (b) Stereoview of a 2Fo-Fc electron density map contoured at 2 sigma, with superimposed α and 3_{10} helices from residues 173 to 194. (c) Stereoview of the superposition of the main-chain atoms of six LRV repeat units.

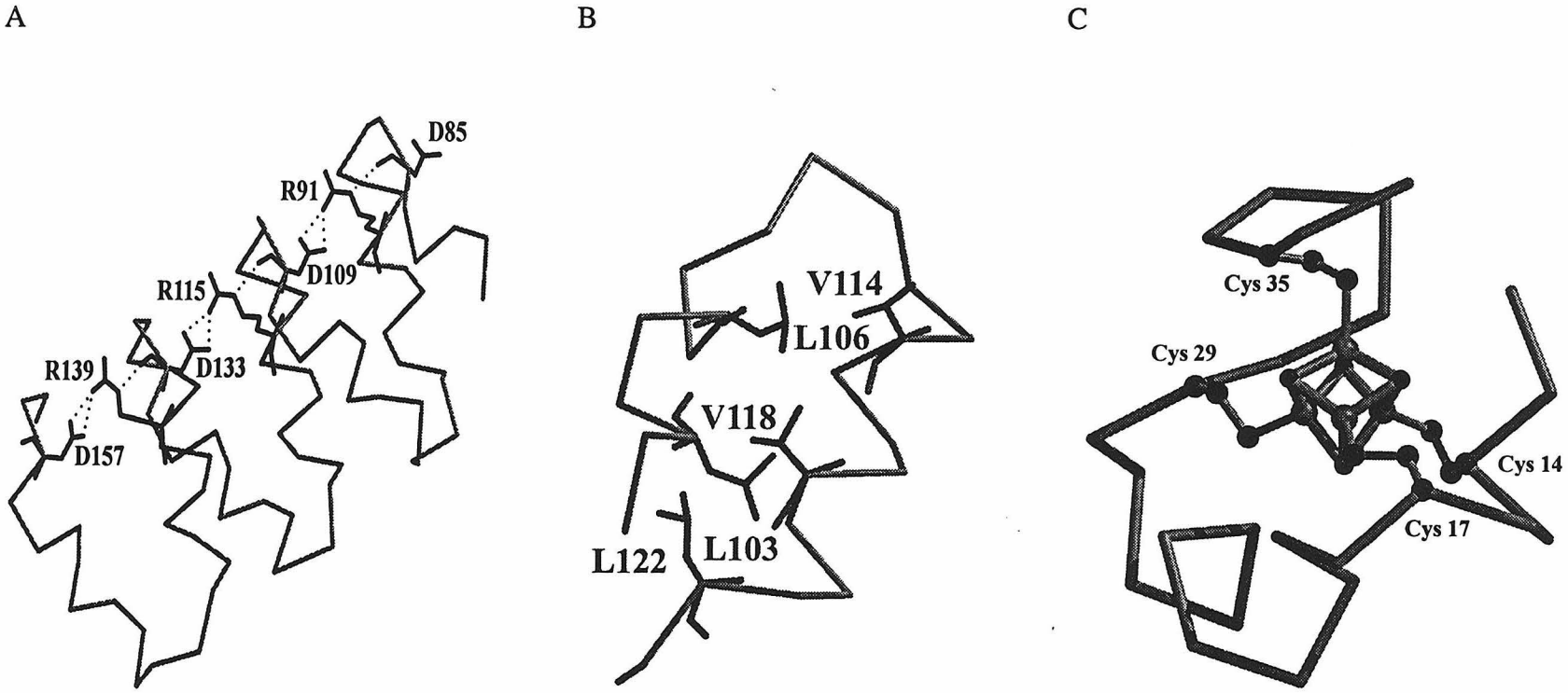

Figure 3. (a) Details of the interactions in the Asp-Arg ladder that links repeating units of LRV. The main chain is colored green, while the Asp and Arg residues in the ladder are indicated by single letter code and shaded red and blue, respectively. (b) A single repeat unit of LRV with the conserved aliphatic residues of the hydrophobic core shown in brown. (c) Polypeptide fold of the N-terminal domain of LRV, with the 4Fe:4S cluster and coordinating cysteine residues indicated.

Chapter IX

Successful Flash-Cooling of Xenon Derivatized Myoglobin Crystals

In press in the Journal of Applied Crystallography

Successful Flash-Cooling of Xenon Derivatized Myoglobin Crystals

S. Michael Soltis[1*], Michael H. B. Stowell[2*], Michael C. Wiener[3], George N. Phillips, Jr.,[4] and D. C. Rees[2]

[1]Stanford Synchrotron Radiation Laboratory, SLAC, P. O. Box 4349, Bin 69, Stanford University CA 94309

[2]Division of Chemistry and Chemical Engineering, Mail Stop 147-75CH California Institute of Technology, Pasadena CA 91125

[3]Department of Biochemistry and Biophysics, University of California San Francisco, San Francisco CA 94143

[4]Department of Biochemistry and Cell Biology and the W. M. Keck Center for Computational Biology, Rice University, Houston TX 77251

Abstract

We have demonstrated for the first time a method for preparing cryo-cooled xenon-derivatized protein crystals. The method is based upon the hypothesis and subsequent observation that the diffusion of a xenon atom from a tight binding site following depressurization occurs on the time scale of minutes. We have observed significant changes in diffraction intensities from myoglobin crystals, for up to 5 minutes following depressurization from 10 atm of xenon. In accord with this observation, a xenon derivatized myoglobin crystal was cryo-cooled at ~95 K within 20 seconds of complete depressurization. A crystallographic data set was then collected to 2.0 Å resolution and isomorphous and anomalous difference Patterson maps revealed the presence of a well-ordered xenon site with an occupancy of approximately 0.5. Phasing statistics for this site were of good quality and demonstrate the practicality of this method. The ability to cryo-cool xenon-derivatized crystals will make this heavy atom substitution method even more useful for SIR and MIR phasing of macromolecules.

Introduction

It is now well established that xenon binds to numerous proteins (see Table I). We have observed an approximate 50% success rate where useful phasing statistics have been obtained [1]. Similar statistics were recently reported by Prange, Schlitz and Fourme [2]. There are a number of advantages for using xenon as a heavy atom derivative; the derivative crystals can be extremely isomorphic with the native crystals, xenon binds to sites that are unique to most conventional heavy atom sites and the number of binding sites can sometimes be controlled by simply changing the pressure.

The preparation of xenon derivatives or the incubation of macromolecular crystals with gases, to study ligand binding, has prompted the development of suitable cells for

such purposes [1,3-7]. There are disadvantages of using a pressure cell for x-ray diffraction experiments, however. A major disadvantage is the inability to cryo-cool [8] the sample which has been shown to help prevent radiation damage due to the intense x-ray beam. Another disadvantage of a pressure cell is the increase in background in the x-ray diffraction pattern as well as the attenuation of the x-ray beam by the pressurized gas. In addition, whenever glass or quartz capillary tubes are pressurized, there exists an explosion hazard. Accordingly, it is desirable to develop methods which will allow the pressurization and cryo-cooling of gas pressurized samples. Cryo-cooling affords significant reduction in radiation damage to the crystal, less background in the x-ray diffraction pattern, and provides a simple mounting technique for samples. In addition, the formation of xenon hydrates [7] may be avoided. Herein, we describe experiments to demonstrate the feasibility of preparing cryo-cooled xenon-derivatized protein crystals. We chose to begin our studies with myoglobin since it has a well-characterized xenon binding site [3,4,9,10]. We monitored the intensity changes in the diffraction pattern from a myoglobin crystal during pressurization and depressurization with xenon gas at room temperature. The results indicate that xenon diffuses from the crystal after 5 minutes following depressurization to atmospheric pressure. These results prompted us to cryo-cool a sample immediately following depressurization, in hopes of trapping xenon in the binding site.

Xenon Binding/Release Studies

x-ray diffraction data were recorded from a hexagonal (P6) crystal of spermwhale myoglobin mutant (Asp122 to Asn) [11] mounted in a pressure cell [1] using a MAR Imaging Plate Scanner System on beam line 7-1 at the Stanford Synchrotron Radiation Laboratory (SSRL). The same one degree rotation was recorded for each image. The x-ray exposure time was 10 seconds (time resolution) and the time for detector read-out, erasure and phi-axis reset was approximately 110 sec (sampling rate). Data were collected

before, during and after pressurization with 10 atm of xenon gas at room temperature. Data reduction was carried out using the HKL Package [12] and 2,282 intensities for fully recorded reflections were output unmerged using SCALEPACK. Figure 1a shows the change in intensity for six reflections. The time at which the cell was pressurized and vented are indicated in the Fig. After the initial change in intensity following the pressurization step, we observed gradual changes of relatively small magnitude over a period of ~1 hour. In addition, following the depressurization step, the rate of change of the individual intensities varied. These observations may be a result of the differing binding rates for three additional xenon binding sites in myoglobin [4,10], although these sites have lower occupancy. Also, there were reflections that did not return to their original intensity after depressurization. This may be an indication of residual xenon or that partial dehydration has occurred. The changes in intensity of 60 reflections for which the intensity increased after pressurization have been averaged and are plotted in Fig. 1b and expanded in Fig. 1c. We made no attempt to measure the initial binding time, but we can say that xenon binding is nearly complete after 10 minutes (see Figure 1c) in accord with a previous report [7]. Xenon diffusion from the crystal is nearly complete after 5 min.

Pressure/Cryo Device

Fig. 2a shows a schematic of a prototype pressure cell for quickly cryo-cooling samples after depressurization. Fig. 2b shows an exploded view of the pressure cell. Corresponding numbers (in parentheses) are shown in the figures and in the text. The steel base (1) is composed of a hollow shaft which houses the sample; a standard stainless steel Swagelok fitting is used for connection of a gas delivery tube. The sample is mounted on a loop which is fixed to the mounting pin with cement. The pressure cell uses an o-ring seal (2) against the bottom of the cap (4). A magnetic steel mounting pin (3) rests in the base. Manipulation of the mounting pin is performed with magnetic tongs (5).

The pressure cell is simple and safe to use. A piece of filter paper, saturated with mother liquor, or a small vial containing mother liquor, can be placed in the cell to prevent crystal dehydration. The crystal is mounted on a loop affixed to the steel mounting pin using standard cryo-mounting techniques. The mounting pin is inserted into the base using magnetic tongs. The long thread on the base prevents the cap from being propelled should the cell be opened while it is pressurized. When the cell is depressurized, the cap can be swiftly removed, allowing the pin to be quickly transferred directly into liquid nitrogen, thereby flash-cooling the sample. The shortest time between depressurization and cryo-cooling that can be achieved using this device is approximately 7 sec. Once the sample has been cooled in liquid nitrogen, it can be transferred to an x-ray camera equipped with a nitrogen gas cold stream using transfer cryo-tongs [13].

Cryo-Cooling of Xenon Derivatized Myoglobin

A myoglobin crystal mounted on a nylon loop was dipped in succession into three fresh drops of cryo-protectant solution for ~2 sec each. The cryo-protectant solution was made by the addition of 250 mg sucrose and 8 mg sodium dithionite to 1 ml of 70%-saturated ammonium sulfate with 50 mM Tris-HCL pH 9.0. A drop of cryo-protectant solution was added to a pressure cell [14] to prevent the crystal and loop from drying out and the sample was pressurized with 10 atm of xenon gas for 10 minutes at room temperature. The pressure was then released and the myoglobin crystal was cryo-cooled down to a temperature of ~95 K directly in a cryo-nitrogen gas stream [15] on beam line 7-1 at SSRL. The time over which the pressure was released was about 10 seconds and the time between complete depressurization and cryo-cooling was approximately 20 seconds. A complete data set to 2.0 Å resolution was collected in just under 1.5 hr and was processed using the HKL package [12]. In addition, a native data set was collected at

cryogenic temperature; data collection statistics for both data sets can be found in Table II. Scaling statistics gave no indication that xenon was escaping from the crystal during data collection as would be expected from the relatively high melting point of xenon, 137 K, compared to the temperature of data collection, ~95 K.

Data analysis was carried out with the CCP4 package [16]. The xenon site was located by difference Patterson analysis. The strongest peak in the Harker section of an isomorphous difference Patterson synthesis computed with data in the resolution range 10 to 2.0 Å was 16 times the standard deviation of the map (Fig. 3). The position and occupancy of the xenon atom were refined using VECREF and phases were calculated using the program MLPHARE (Table III). Our cryo-cooled xenon derivative proved to be of good quality with an overall figure of merit of 0.32 to 2.0 Å. It should be noted that Vitali et al. [10] have demonstrated that phases from a single xenon atom in myoglobin are sufficient to produce an interpretable electron density map for the structure of myoglobin.

We have observed that xenon binds in less than 10 minutes in the case of myoglobin. This observation is similar to that of porcine pancreatic elastase [7]. We concur with Schlitz, Prange and Fourme [7] that xenon binding appears to take place on a time scale of minutes rather than hours. From the calculated occupancy of the xenon site in myoglobin, we can estimate the half-life for the xenon off-rate to be on the order of 20 seconds. Thus, the pressure-cryo device described above should be useful for producing reasonably occupied xenon sites for biomolecules displaying similar off-rates.

One disadvantage of cryo-cooling is that the native and derivative data can not be obtained from the same crystal. This may pose a problem for crystal systems that produce nonisomorphic crystals upon flash-cooling. For those particular cases, room temperature data may suffice. On the other hand, cryogenic temperature may be required to obtain

useful data and thus techniques will have to be developed for those systems whereby nonisomorphism between crystals is minimized.

Conclusions

We have successfully prepared a cryo-cooled xenon derivative of myoglobin. This method of derivative preparation avoids the increase in background and x-ray absorption from the pressurized gas as well as the hazard of pressurizing glass capillaries. This method should be of general use for proteins where release rates of xenon are on the time scale of minutes, which is similar to or slower than that of myoglobin. Other proteins, where the off-rate of xenon is substantially faster than that observed for myoglobin, will undoubtedly require methods that allow for the flash cooling of crystals directly under xenon pressure. Such a method is currently under development in our laboratories.

Acknowledgments

The work was supported in part by NIH GM45062 of the NSF to DCR and by the DOE, Office of Basic Energy Sciences and the Office of Health and Environmental Research, and by the NIH, Biomedical Research Technology Program, National Center for Research Resources for support of the rotation camera facilities at SSRL. We wish to thank R. P. Phizackerley and Henry D. Bellamy for helpful discussions.

Table I. Protein crystal derivatization using xenon gas. Reproduced in part from ref. [1].

Protein	MW (kD)	Xe (atm)	Patterson	Difference Fourier	# of Sites	Unique Site
BPI	50	10		Yes	4	Yes
CAM	23	4-10	Noniso			
CHIP	28	4-10	No			
C554	25	10	Poor		3	
DMSOR	85	10	Yes		1	Yes
HHB	67	3			1	
HLC	25	12			1	Yes
IMPDH	58	4-10	Noniso			
LYS	14	8	Poor		4	
MBA	18	3		Yes	2	
MB	18	3		Yes	1	
MB	18	7		Yes	4	
MB	18	7	Yes		4	
ORF2	30	12	Yes	Yes	1	No
PPE	26	8	Yes		1	
RXR-a	30	20	Yes		2	Yes
SC	27	12		Yes	1	
SOD	16	10		Yes	1	Yes
STCN	12	10		Yes	1	Yes

Abbreviations: BPI (Human bactericidal permeability-increasing protein), CAM (Carbonic anhydrase, *Methanosarcina thermophila*), CHIP (Human erythrocyte aquaporin), C554 (Cytochrome c554, *Nitrosomonas europaea*), DMSOR (Dimethyl sulfoxide reductase, *Rhodobacter spheroides*), HHB (Horse hemoglobin), HLC (Collagenase, *Hypoderma lineatum*), IMPDH (Inosine monophosphate dehydrogenase, *Tritrichomonas-fetus*), ORF2 (Nitrogen fixation specific open reading frame 2, *Azotabacter vinelandii*), PPE (Porcine pancreatic elastase), RXR-a (Human retinoid-X receptor alpha), STCN (Stelacyanin, cucumber), MB (Sperm whale myoglobin), MBA (Alkaline sperm whale myoglobin), SC (Subtilisin Carlsberg, *Bacillus licheniformis*), SOD (Superoxide dismutase, *Saccharomyces cerivisiea*).

REFERENCES AND NOTES

1. M.H.B. Stowell, et al. *J. Appl. Cryst.,* **29**, 608 (1996).
2. T. Prange, M. Schiltz, R. Fourme, International Union of Crystallography Meeting, Abstract (1996).
3. B.P. Schoenborn, H.C. Watson, J.C. Kendrew, *Nature* **207**, 28-30 (1965).
4. R.F. Tilton, I.D. Kuntz, G.A. Petsko, *Biochemistry* **23**, 2849-2857 (1984).
5. R.F. Tilton, *J. Appl. Cryst.* **21**, 4-9 (1988).
6. K.S. Kroeger, C.E. Kundrot, *J. Appl. Cryst.* **27**, 609-612 (1994).
7. M. Schiltz, T. Prange, R. Fourme, *J. Appl. Cryst.* **27**, 950-960 (1994).
8. H. Hope, *Acta. Cryst.* **B44**, 22-26 (1988).
9. B.P. Schoenborn, *J. Mol. Biol.* **45**, 297-303 (1969).
10. J. Vitali, A.H. Robbins, S.C. Almo, R.F. Tilton, *J. Appl. Cryst.* **24**, 931-935 (1991).
11. G.N. Jr. Phillips, R.M. Arduini, B.A. Springer, S.G. Sligar, *Proteins-Structure, Function, and Genetics* **7**, 358-365 (1990).
12. Z. Otwinowski, W. Minor, W. (1993). HKL macromolecular crystallographic data reduction package (DENZO, SCALEPACK and XDISPLAYF).
13. H. Hope, SSRL 22nd Annual Users Meeting, Workshop on Techniques in Macromolecular Crystallography: Cryo-cooling and Data Reduction/Analysis (1995).
14. In our initial trials, we used a smaller prototype of the pressure cell described in the text.
15. H. Bellamy, R.P. Phizackerley, S.M. Soltis, H. Hope, *J. Appl. Cryst.* **27**, 967-970 (1994).
16. Collaborative Computing Project No. 4, SERC Daresbury Laboratory, CCP4 suite of crystallographic programs (1979).

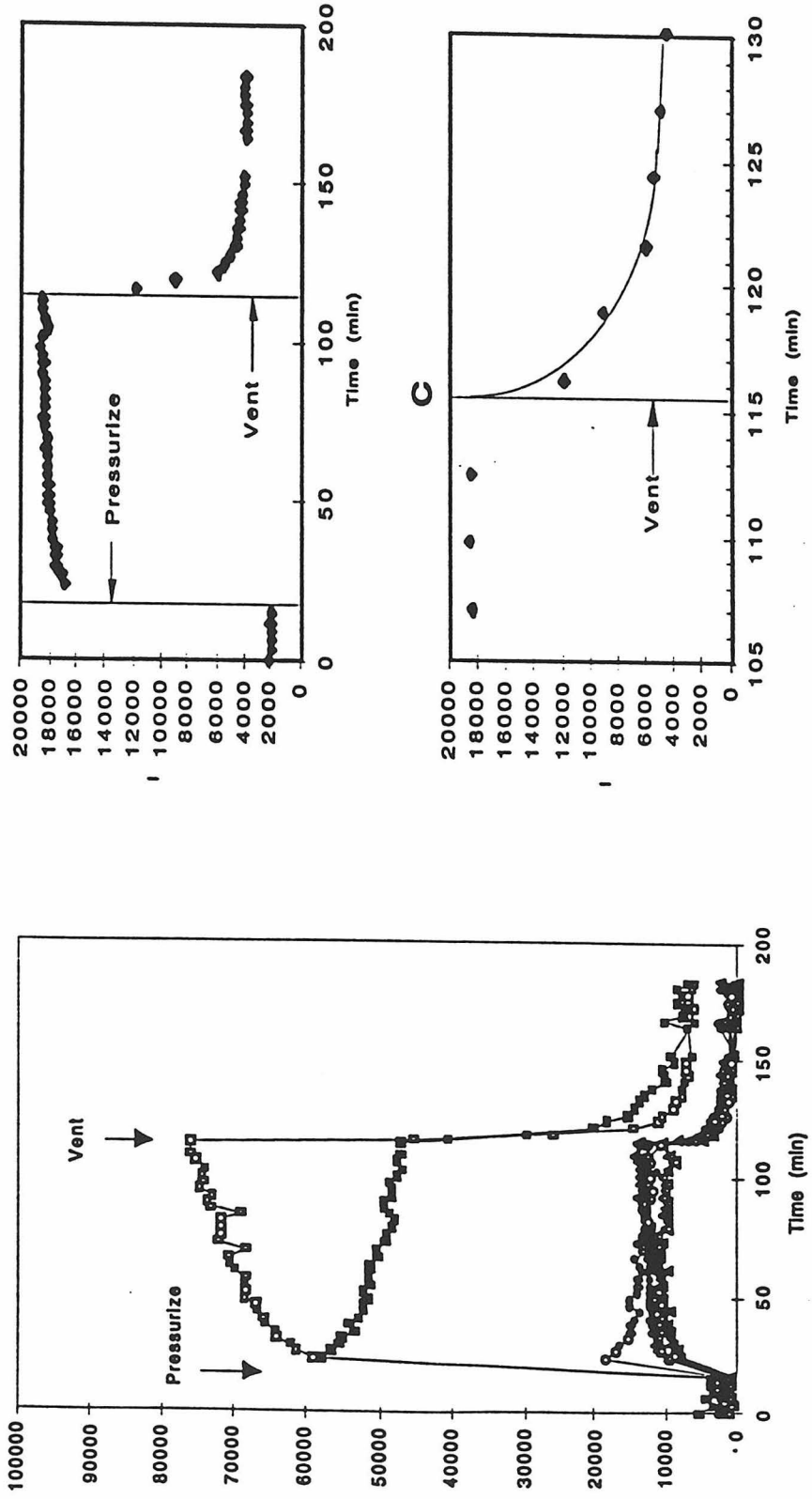

Figure 1. (A) Intensity changes as a function of time for 6 individual reflections. The times at which the cell was pressurized and vented are indicated in the Fig. (B) Average Intensity for 60 reflections that increased in intensity during xenon pressurization. (C) Enlarged view of the xenon depressurization step in (B).

A)

B)

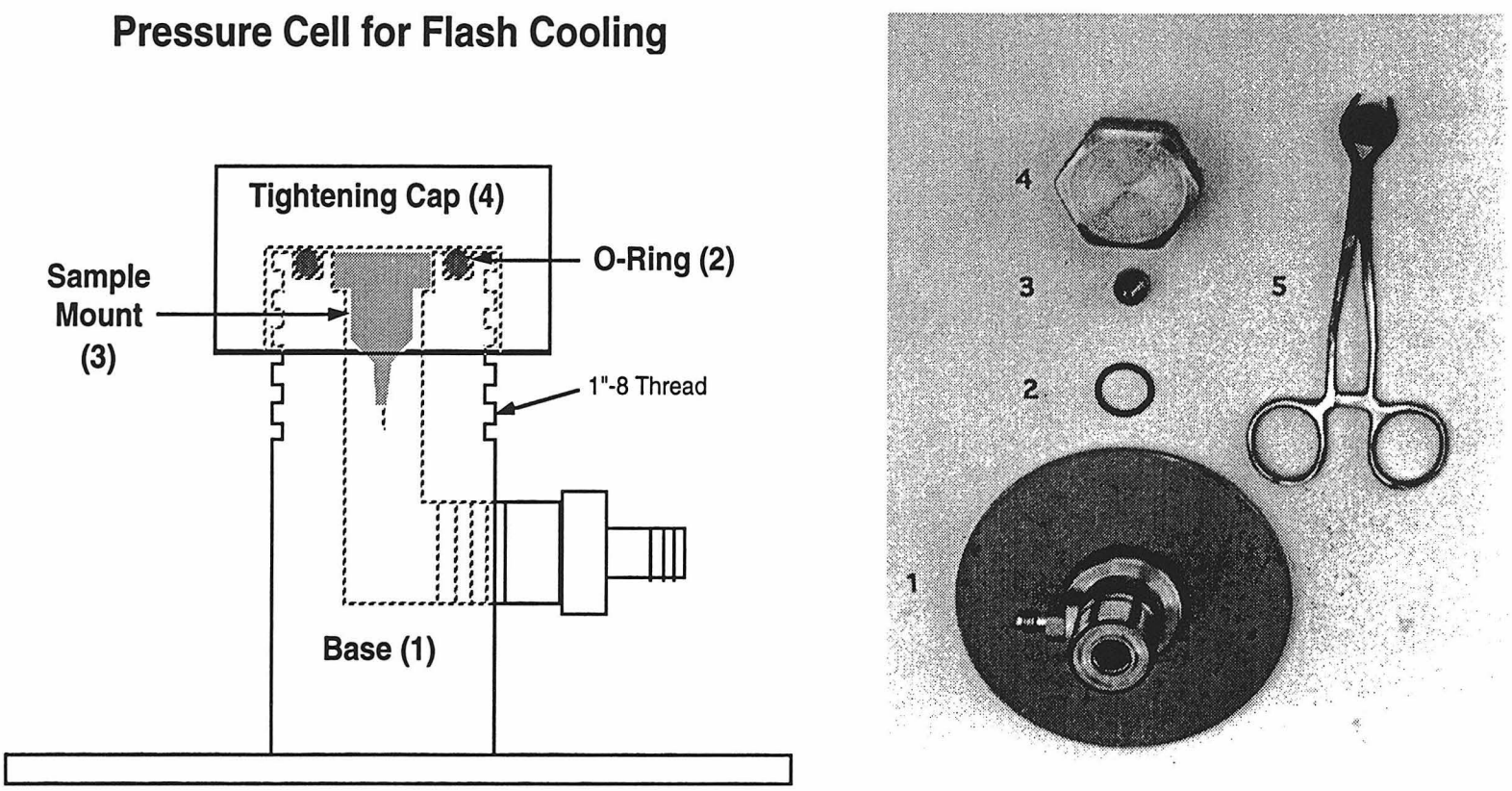

Figure 2. Schematic (A) and exploded (B) view of a pressure cell for quick cryo-cooling of protein samples.

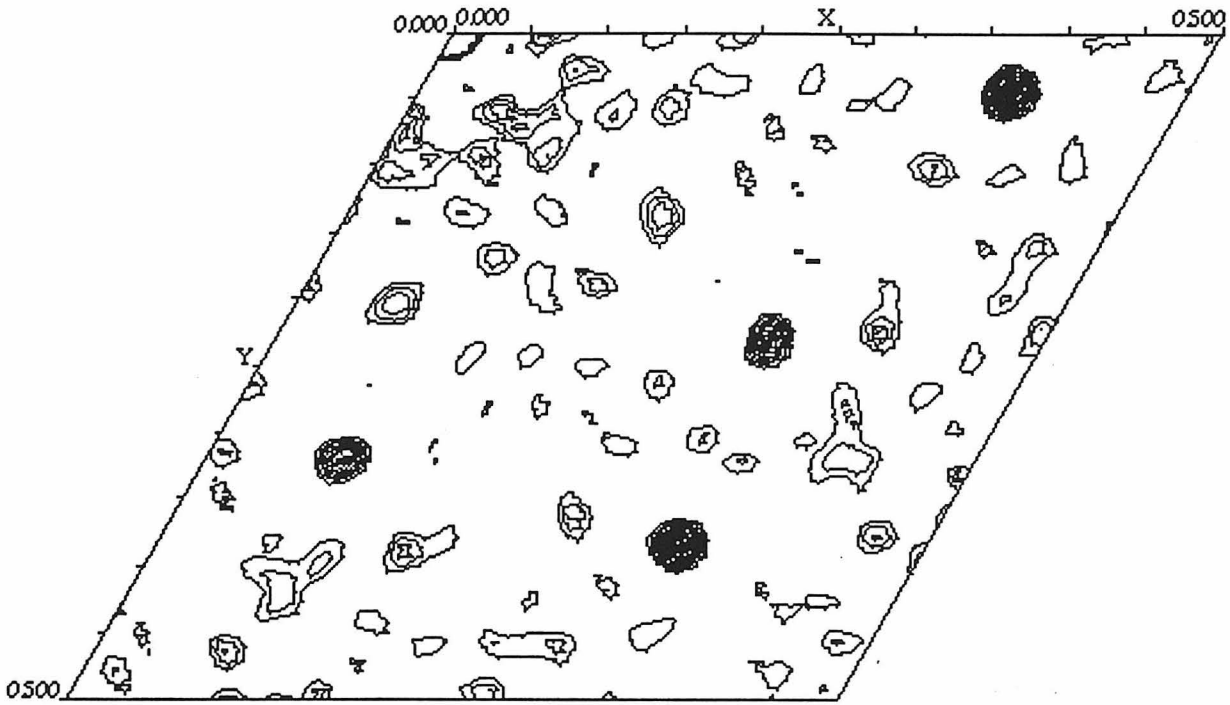

Figure 3. Asymmetric unit of the cryo-cooled xenon isomorphous difference Patterson for P6 myoglobin, w = 0 Harker section. The map is contoured at 1.0 σ intervals, starting at 1 σ. Created using the XtalView 2.0 software package (D. McRee, 1995).

Chapter X

Comparison of Ubiquinol and Cytochrome c Terminal Oxidases: An Alternative View

Reprinted from FEBS Letters

Minireview

Comparison of ubiquinol and cytochrome *c* terminal oxidases

An alternative view

Siegfried M. Musser, Michael H. B. Stowell and Sunney I. Chan

Arthur Amos Noyes Laboratory of Chemical Physics, 127–72, California Institute of Technology, Pasadena, CA 91125, USA

Received 11 May 1993; revised version received 7 June 1993

There have been numerous instances in the recent literature where the properties of ubiquinol and cytochrome *c* terminal oxidases are compared. Here we specifically examine the cytochrome bo_3-type ubiquinol oxidase from *Escherichia coli* and the cytochrome aa_3-type cytochrome *c* oxidases. A second redox-active copper site (Cu_A) is present only in the cytochrome *c* oxidases and the physiological electron donors for the two enzymes are different (ubiquinol-8 vs. ferrocytochrome *c*). In our opinion, these differences are significant and most likely indicate that distinct turnover mechanisms are operative in the two enzymes.

Ubiquinol oxidase; Cytochrome oxidase; Electron transfer; Proton pumping

1. INTRODUCTION

In a recent review [2], it was postulated that a variety of ubiquinol and cytochrome *c* oxidases form a superfamily of heme-copper oxidases. Following the example of this review, we classify the cytochrome bo_3 (*Escherichia coli*), cytochrome ba_3 (*Acetobacter aceti*) and cytochrome aa_3 (*Bacillus subtilis* and *Sulfolobus acidocaldarius*) complexes in the family of ubiquinol oxidases and the cytochrome aa_3 (mitochondrial version and similar bacterial enzymes), cytochrome ba_3 (*Thermus thermophilus*), and cytochrome caa_3 (*T. thermophilus*, *Bacillus cereus*, *Bacillus stearothermophilus*, thermophilic bacillus PS3, and *B. subtilis*) complexes in the family of cytochrome *c* oxidases (Table I). All of these oxidases appear to have a similar heme–copper dioxygen activating center. The major difference between the two families is obviously the different substrates (quinol vs. ferrocytochrome *c*) but it also appears that most, if not all, of the quinol oxidases are missing the Cu_A site found in the cytochrome *c* oxidases. Since the *E. coli* cytochrome bo_3 complex and the aa_3-type cytochrome *c* oxidase complexes are the best characterized enzymes in their respective families, we center on these two enzymes in the discussion which follows. However, it is not fair to compare the bacterial *E. coli* cytochrome bo_3 complex with the mammalian aa_3-type oxidases as the latter oxidases are significantly more evolved containing at least 13 polypeptides [3]. Thus, in the comparisons which follow, the aa_3-type cytochrome *c* oxidase from bacterial sources is emphasized, though data from more complex organisms are included where appropriate.

Correspondence address: S.I. Chan, Arthur Amos Noyes Laboratory of Chemical Physics, 127–72, California Institute of Technology, Pasadena, CA 91125, USA. Fax: (1) (818) 568 8824.

Contribution No. 8798 from the Division of Chemistry and Chemical Engineering, California Institute of Technology.

In order to maintain clarity in our comparison of terminal oxidases, we have followed the lead of Puustinen and Wikström [1] in the nomenclature of heme structures. Isolated heme structures are indicated by upper-case letters (hemes A, B, C, O), whereas when the corresponding hemes are within their natural proteinaceous surroundings, the term cytochrome is applied and italic lower-case letters are used (cytochromes *a*, *b*, *c*, *o*). A further distinction is sometimes necessary when the heme macrocycle itself of a particular cytochrome is under discussion. So whereas the term cytochrome encompasses the heme and immediate surrounding protein matrix thus identifying a general region of the protein (for example, 'reduction potential of cytochrome *a*'), the term heme and italic lower-case letters (hemes *a*, *b*, *c*, *o*) is used when the heme macrocycle is being referred to (for example, 'the ligation of heme *a*'). In addition, the low-spin heme which is unreactive towards extraneous ligands is denoted without subscript, yet following the classical terminology of the mitochondrial cytochrome *c* oxidase complex, the O_2-binding heme is denoted with the subscript 3 (hemes a_3 and o_3).

2. BIOPHYSICAL CHARACTERISTICS

There are several recent reviews comparing the bo_3- and aa_3-type oxidase complexes [4–6]. For completeness, we summarize the main conclusions. The *E. coli* cytochrome bo_3 ubiquinol oxidase complex and cytochrome aa_3-type cytochrome *c* oxidase complexes catalyze the four electron reduction of dioxygen to water by utilizing electrons from ubiquinol-8 and ferrocytochrome *c*, respectively. In addition, these proteins cou-

ple part of the free energy of dioxygen reduction to the endergonic vectorial translocation of protons across the membrane in which they reside (Fig. 1). Other similarities between the two terminal oxidases include: (1) subunit sequence similarity [7]; (2) the presence of one low-spin (six-coordinate) and one high-spin (five-coordinate) heme [8,9]; (3) exchange coupling between the high-spin heme and a copper ion (binuclear site) in their resting states; and (4) heme-heme interaction and alignment of these hemes with respect to the membrane bilayer normal [4,10,11]. Nevertheless, there are notable differences between the two proteins including: (1) one heme B and one heme O (bo_3) versus two heme A's (aa_3); (2) one (bo_3) versus two (aa_3) redox active copper ions (the cytochrome bo_3 complex lacks the unusual $g = 2$ EPR signal found in the cytochrome aa_3 complex, which is attributed to the Cu_A site); and (3) the different substrates, i.e. ubiquinol-8 (bo_3) versus ferrocytochrome c (aa_3) [4,12,13]. We now discuss these similarities and differences in greater depth.

3. SEQUENCE SIMILARITIES

The purified cytochrome bo_3 complex contains stoichiometric amounts of four, possibly five, polypeptides [14] which are encoded by the *cyo*ABCDE operon. The *cyo*B gene product corresponds to subunit I (COI) of the aa_3-type oxidases and is by far the most homologous subunit. In fact, for this subunit, there exists 37% sequence identity between the cytochrome bo_3 and the *Paracoccus denitrificans* cytochrome aa_3 complexes [7] (40% identity with the subunit I sequence of the bovine heart cytochrome c oxidase complex [2]). Site-directed mutagenesis studies have shown that the histidines ligating the redox centers in subunit I (the two hemes and Cu_B) are conserved in the two terminal oxidases [15–17]. In addition, the amino acid sequence around the ligands of the binuclear site is highly conserved [18,19]. In conjunction with the biophysical studies noted above, these sequence similarities suggest that subunit I of the two oxidases are likely to be structurally similar. This structural similarity indicates that the dioxygen chemistry of the two enzymes is likely to be very similar if not identical. Thus, one may think of the 'catalytic core' (i.e. subunit I and its associated redox centers) as a highly conserved motif for dioxygen activation and reduction. However, note that recent data reveal different proton transfer characteristics during dioxygen reduction for the two enzymes [20].

The homology between the other subunits of the two enzyme complexes is not nearly so high as that for the respective subunit I sequences. Subunit II (the *cyo*A gene product) of the cytochrome bo_3 complex lacks the four putative ligands for Cu_A in cytochrome aa_3 complexes (two cysteines and two histidines all four of which are invariant in the known cytochrome aa_3 complex sequences) but otherwise has a similar hydropathy profile. Not surprisingly, conserved residues which have been implicated in the binding of cytochrome c to the aa_3-type oxidases (Asp-158, Glu-198; bovine numbering) are absent in the subunit II sequence of the cytochrome bo_3 complex. Sequence identity between subunit II of the *P. denitrificans* cytochrome aa_3 and cytochrome bo_3 complexes is only 10%. The *cyo*C gene product (subunit III) shows slightly greater sequence identity with COIII (23%) yet two putative transmembrane helices found at the N-terminus of COIII are missing in subunit III of the cytochrome bo_3 complex. The coun-

Table I

Comparison of ubiquinol and cytochrome c terminal oxidases

Type	Number of subunits	Number of coppers	Cu_A present[a]	Species	Reference(s)
Ubiquinol oxidases					
bo_3[b]	4–5	1	no	*Escherichia coli*	7,14,42
ba_3	4	1	no	*Acetobacter aceti*	43
aa_3	4	1	no	*Bacillus subtilis*	44,45
aa_3	1–3	2–3	no	*Sulfolobus acidocaldarius*	46,47,48,49
Cytochrome c oxidases					
aa_3[c]	3–13	2–3	yes		
ba_3	4[d]	2	yes	*Thermus thermophilus*	50
caa_3	2–4	2–3	yes	*T. thermophilus*	51,52
				Bacillus cereus	53
				Bacillus stearothermophilis	54
				Thermophilic bacillus PS3[e]	55,56
				B. subtilis	57

[a] The presence or absence of a Cu_A site has not been definitely confirmed in all cases. A best guess is made based on the present literature.
[b] This enzyme is expressed as a cytochrome oo_3 complex with little difference in activity in various overexpressing strains [42].
[c] The aa_3-type cytochrome c oxidase has been isolated from many organisms, from bacteria to mammals. See ref. 58 for a review.
[d] The cytochrome ba_3 complex was originally reported to contain one subunit but other investigators report four subunits [59].
[e] The PS3 enzyme is expressed as a cytochrome cao_3 complex with a 2-fold higher V_{max} under air-limited conditions [60].

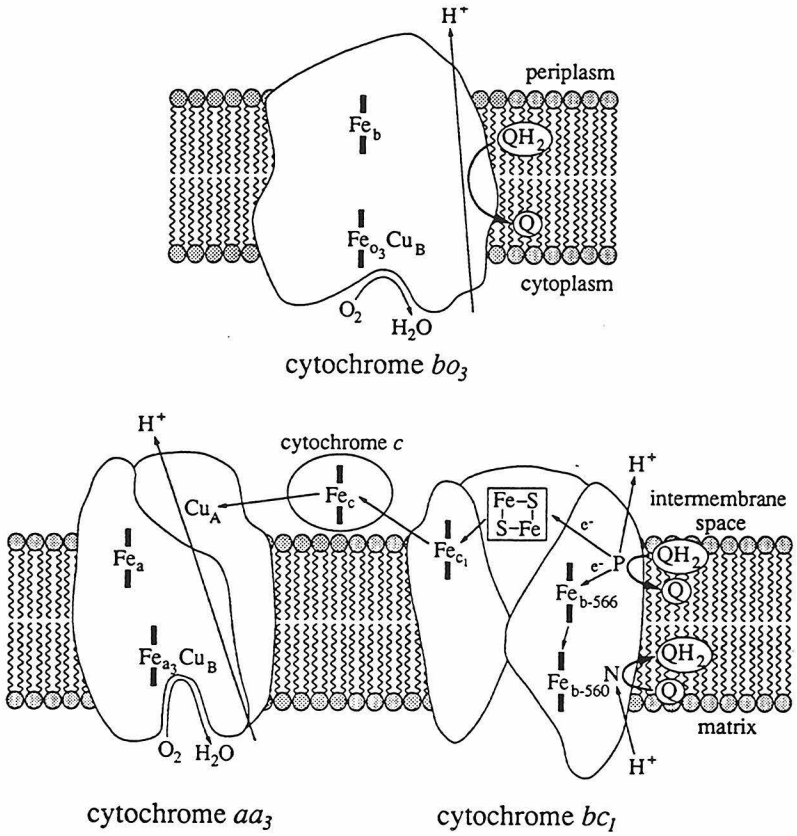

Fig. 1. Schematics of the electron transfer and proton translocation functions of the cytochrome bo_3, cytochrome aa_3 and cytochrome bc_1 complexes. Ubiquinol oxidation occurs at center P (P) of the cytochrome bc_1 complex and ubiquinone reduction occurs at center N (N).

terparts of *cyo*D and *cyo*E are found in the operons of bacterial aa_3-type oxidases but the homology is minimal [7,21]. In bacteria, COIV (corresponding to the gene product of *cyo*D) has been identified chemically only for the aa_3-type oxidase complex of PS3 [22,23]. A polypeptide analog of the *cyo*E gene product has not been found in purified cytochrome aa_3 complexes from bacteria.

4. THE UNDERLYING QUESTION

The reduced homology between the *cyo*ACDE gene products and the polypeptide counterparts of the aa_3-type oxidases relative to the extensive similarities between the largest polypeptides of the respective enzyme complexes leads us to the basic premise which we wish to address in this discussion: Do the structural differences in the remaining subunits serve merely to accommodate the different electron donors, or do they additionally reflect altered electron transfer mechanisms which result in unique physiological capabilities with respect to control of both electron transfer pathways and electron transfer mechanisms? Further, is the linkage between the various electron transfer events and the proton translocation capabilities of the respective enzymes, as well as the control of this linkage, affected by the structural differences of the two oxidases? In order to answer these questions, we first attempt to assess the magnitude of the difference in structure required to accommodate the two different electron donors for the bo_3- and aa_3-type oxidases.

5. THE SUBSTRATE BINDING SITES

The physiological substrate for the aa_3-type oxidases is the redox protein ferrocytochrome *c* (MW ~ 12 kDa), a water-soluble one-electron donor whereas that for the bo_3-type oxidases is the organic cofactor ubiquinol-8 (MW < 1 kDa), a very hydrophobic two-electron donor. The difference in size between the two substrates indicates that the binding domain for these electron donors on their respective proteins is expected to be much different with regards to size and shape. Thus, the binding domain for ferrocytochrome *c* is envisioned to be a negatively charged surface patch on the oxidase

complex [24] whereas ubiquinol-8 is expected to bind in a small hydrophobic pocket within the protein matrix. These structural differences, while significant, can be easily accommodated by appropriate sequence changes.

According to transient electron transfer studies, the primary electron input site in the aa_3-type oxidases is the Cu_A site [25–27]. This redox site is thought to be in the cytoplasmic domain of the enzyme complex [28]. Additionally, it is noteworthy, that Cu_A is the only redox site found in subunit II [29] and cytochrome *c* binding residues have been localized on this subunit [30–32]. Thus, Cu_A appears appropriately situated to act as an intermediary acceptor of electrons from aqueous ferrocytochrome *c*, subsequently donating electrons to the hemes and Cu_B in the more hydrophobic recesses of the enzyme in the membrane. In contrast, ubiquinol-8 is expected to be localized in the hydrophobic interior of the membrane bilayer. Thus, the binding domain for ubiquinol-8 is expected to be in a different three-dimensional location on the enzyme complex relative to the binding domain for ferrocytochrome *c*. This analysis implies that Cu_A may serve merely to funnel the electron into the 'catalytic core.' Since ubiquinol-8 can approach closer to the hemes and Cu_B in subunit I, the intermediary electron acceptor, Cu_A, becomes unnecessary. There is an alternative viewpoint, however, which we will discuss later.

6. ELECTRON TRANSFER PATHWAYS

Perhaps the most significant difference between the ferrocytochrome *c* and ubiquinol-8 substrates is that the former is a one-electron donor and the latter is a two-electron donor. This difference is relevant to the present analysis because it likely indicates different electron transfer mechanisms which in turn may reflect disparities in functional capabilities of the respective enzymes. The electron transfer between ferrocytochrome *c* and the aa_3-type oxidases is an outer-sphere process which merely requires that the two redox proteins approach within a given distance and in the correct orientation (i.e. the binding may be fleeting). On the other hand, one expects ubiquinol-8 to bind fairly strongly to the bo_3-type oxidases. More accurately, the ubisemiquinone-8 species must have a high affinity for the enzyme complex. The reason is, of course, that the semiquinone intermediate is a highly reactive species that must be stabilized by the enzyme complex in order to prevent non-productive electron transfer. We note that there is no precedent in biology for concerted two-electron transfer between an *unbound* quinol and a redox protein. It is possible for concerted two-electron transfer to proceed from a *bound* ubiquinol, however. For example, concerted inner-sphere electron transfer to the binuclear center is possible. Since the binuclear center is the site of dioxygen reduction, we consider it unlikely to be able to accommodate a bulky ubiquinol molecule in addition to the dioxygen intermediates. Thus, a situation in which electron transfer proceeds first to cytochrome *b* followed by subsequent electron transfer to the binuclear center appears more likely. Note that in this latter scenario, the oxidation of ubiquinol-8 cannot be concerted since ferricytochrome *b* is a one-electron acceptor. One might postulate two rapid one-electron transfers through cytochrome *b*, yet an evalution of the reduction potentials of ubiquinone and the cytochrome bo_3 complex indicates that this is probably not a feasible model.

Whereas the midpoint potentials of the four redox centers in the aa_3-type oxidases are all between ~ 250 and ~ 400 mV, the corresponding potentials for the cytochrome bo_3 complex are distributed over a much wider range. There is some disagreement in the literature, but recent data indicate that the room temperature midpoint potentials for cytochrome *b*, cytochrome o_3 and Cu_B are about 60, 220 and 400 mV, respectively [33,34]. The most obvious explanation for the requirement of the lower redox potential cytochromes *b* and o_3, especially the former, relative to cytochromes *a* and a_3, respectively, is the different redox potentials of the electron donors to the protein complexes. Ubiquinone has been estimated to have a midpoint reduction potential of about 60 mV in the inner mitochondrial membrane [35] while cytochrome *c* has a midpoint potential of about 250 mV [36]. Thus, cytochrome *b* appears to be well suited to be the primary electron acceptor from ubiquinol. One should remember, however, that the 60 mV midpoint reduction potential for ubiquinone is an average potential of the ubiquinone/ubisemiquinone and ubisemiquinone/ubiquinol couples. The former couple has the lower midpoint potential and the absolute difference between these couples is at least 80 mV [37] but could be as much as ~ 400 mV [38] depending on the protonation state of the ubisemiquinone intermediate. Thus, it is unlikely that cytochrome *b* can accept the first electron from ubiquinol (midpoint reduction potential for ubisemiquinone → ubiquinol is ≥ ~ 100 mV). On the other hand, the two electrons from ubiquinol may reduce the cytochrome bo_3 complex via a split electron transfer pathway (reminiscent of the Q cycle in the cytochrome bc_1 complex), the first electron going to the binuclear site and the second going to cytochrome *b* (Fig. 2). Note that in this scenario, the midpoint potentials of the donor and acceptor are more closely matched, as in the cytochrome bc_1 complex [38], promoting efficient electron transfer.

7. PROTON TRANSLOCATION MECHANISMS

In light of the above discussion, it is clear that some of the electron transfer mechanisms in the bo_3-type oxidases are necessarily different from those in the aa_3-type oxidases. The pertinent question to ask at this juncture, then, is whether these alternative mechanisms affect the

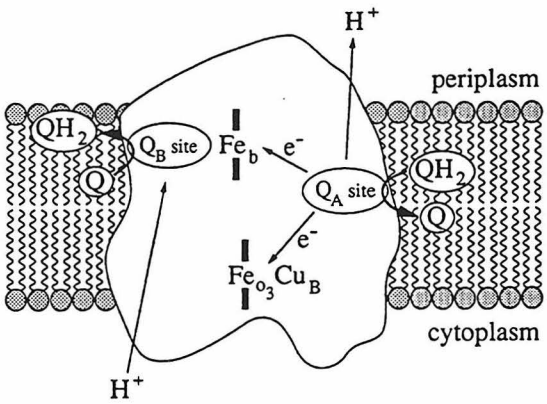

Fig. 2. Schematic of a possible Q-loop mechanism in the cytochrome bo_3 complex. The Q_A site is like center P in the cytochrome bc_1 complex and the Q_B site is like center N. See text for details.

functional capabilities of the enzyme in any significant way. For example, both enzyme complexes have been shown to catalyze the active transport of protons across the membrane in which they reside. Is the coupling mechanism between dioxygen reduction and proton translocation similar or different for the two enzymes, and if different, how so? For the translocation process to be identical, one would expect the binuclear center or cytochrome *a/b* to be the site of redox linkage. It is our opinion that the binuclear site is not the site of redox linkage, since the dioxygen chemistry occurs at the binuclear center, and the electron transfer between heme a_3/o_3 and Cu_B is likely very fast ruling out efficient coupling between electron transfer and the conformational changes that accompany the proton pump [39]. This leaves the low-spin heme as the site of redox linkage if the enzymes have similar proton translocation mechanisms. On the other hand, the two oxidases could have radically different proton translocation mechanisms. We note that the different proton transfer characteristics seen during dioxygen reduction for the two enzymes [20] support a scenario which invokes alternative translocation mechanisms. For example, the Cu_A site could somehow be involved in proton translocation in the aa_3-type oxidases, and a redox loop mechanism involving two ubiquinone/ubiquinol binding sites similar to that proposed for the cytochrome bc_1 complex could be operative in the bo_3-type oxidases (Fig. 2). Note that the cytochrome bo_3 complex combines the electron transfer processes of both the cytochrome bc_1 and aa_3 complexes (Fig. 1). Thus, to us, it is an attractive notion that the bo_3-type oxidases combine features from both the bc_1-(ubiquinone/ubiquinol redox loop) and aa_3-type oxidases (dioxygen chemistry). In this respect, the cytochrome bo_3 complex is similar to the cytochrome bc_1/cytochrome *c*/cytochrome aa_3 supercomplexes isolated from *P. denitrificans* [40] and PS3 [41] the latter complexes being the more evolved enzymes. Note that a redox loop mechanism necessarily requires two ubiquinone/ubiquinol binding sites (a testable proposal). Finally, we emphasize that these arguments may also apply to other less well characterized enzymes which lack a Cu_A site and exhibit quinol oxidase activity such as the cytochrome aa_3 ubiquinol oxidases from *B. subtilis* and *S. acidocaldarius* and the cytochrome ba_3 ubiquinol oxidase (originally termed cytochrome a_1) from *A. aceti* (Table I).

8. CONCLUSIONS

This discussion reveals that while the bo_3- and aa_3-type terminal oxidases are similar in some respects, other processes may in fact be quite different. Thus, it would be imprudent to assume, based on a few similarities, that the proteins are similar in all respects or that the differences are minor; such a view might lead us astray or inhibit us from designing appropriate experiments to decipher the function of these enzymes. While it is useful to point out similarities between proteins, we note that it is often the study of differences that yields greater insight. We hope that the issues brought up in this discussion serve to stimulate investigations directed at understanding the function of these exciting terminal oxidases.

Acknowledgements: This work was supported by Grant GM22432 from the National Institute of General Medical Sciences, U. S. Public Health Service (SIC). SMM and MHBS are recipients of National Research Service Predoctoral Awards and MHBS is a recipient of an Albert L. Raymond Fellowship.

REFERENCES

[1] Puustinen, A. and Wikström, M. (1991) Proc. Natl. Acad. Sci. USA 88, 6122–6126.
[2] Gennis, R.B. (1991) Biochem. Biophys. Acta 1058, 21–24.
[3] Kadenbach, B., Stroh, A., Hüther, F.-J., Reimann, A. and Steverding, D. (1991) J. Bioenerg. Biomembr. 23, 321–334.
[4] Ingledew, W.J. and Bacon, M. (1991) Biochem. Soc. Trans. 19, 613–616.
[5] Saraste, M., Holm, L., Lemieux, L., Lübben, M. and van der Oost, J. (1991) Biochem. Soc. Trans. 19, 608–612.
[6] Brown, S., Moody, A.J., Mitchell, R. and Rich, P.R. (1993) FEBS Lett. 316, 216–223.
[7] Chepuri, V., Lemieux, L., Au, D.C.-T. and Gennis, R.B. (1990) J. Biol. Chem. 265, 11185–11192.
[8] Uno, T., Nishimura, Y., Tsuboi, M., Kita, K. and Anraku, Y. (1985) J. Biol. Chem. 260, 6755–6760.
[9] Hata, A., Kirino, Y., Matsuura, K., Itoh, S., Hiyama, T., Konishi, K., Kita, K. and Anraku, Y. (1985) Biochim. Biophys. Acta 810, 62–72.
[10] Salerno, J.C., Bolgiano, B., Poole, R.K., Gennis, R.B. and Ingledew, W.J. (1990) J. Biol. Chem. 265, 4364–4368.
[11] Salerno, J.C. and Ingledew, W.J. (1991) Eur. J. Biochem. 198, 789–792.
[12] Anraku, Y. (1988) Annu. Rev. Biochem. 57, 101–132.
[13] Puustinen, A., Finel, M., Haltia, T., Gennis, R.B. and Wikström, M. (1991) Biochemistry 30, 3936–3942.

[14] Minghetti, K.C., Goswitz, V.C., Gabriel, N.E., Hill, J.J., Barassi, C.A., Georgiou, C.D., Chan, S.I. and Gennis, R.B. (1992) Biochemistry 31, 6917–6924.
[15] Shapleigh, J.P., Hosler, J.P., Tecklenburg, M.M.J., Kim, Y., Babcock, G.T., Gennis, R.B. and Ferguson-Miller, S. (1992) Proc. Natl. Acad. Sci. USA 89, 4786–4790.
[16] Minagawa, J., Mogi, T., Gennis, R.B. and Anraku,Y. (1992) J. Biol. Chem. 267, 2096–2104.
[17] Lemieux, L.J., Calhoun, M.W., Thomas, J.W., Ingledew, W.J. and Gennis, R.B. (1992) J. Biol. Chem. 267, 2105–2113.
[18] Gennis, R.B. (1992) Biochim. Biophys. Acta 1101, 184–187.
[19] Matter, M.W., Springer, P., Hensel, S., Buse, G. and Fee, J.A. (1993) J. Biol. Chem. 268, 5395–5408.
[20] Hallén, S., Svensson, M. and Nilsson, T. (1993) FEBS Lett., in press.
[21] Saraste, M., Raitio, M., Jalli, T., Chepuri, V., Lemieux, L. and Gennis, R.B. (1988) Ann. NY Acad. Sci. 550, 314–324.
[22] Sone, N., Shimadu, S., Ohmori, T., Souma, Y., Gonda, M. and Ishizuka, M. (1990) FEBS Lett. 262, 249–252.
[23] Gai, W.-Z., Sun, S.-M., Sone, N. and Chan, S.H.P. (1990) Biochem. Biophys. Res. Commun. 169, 414–421.
[24] Capaldi, R.A. (1990) Annu. Rev. Biochem. 59, 569–596.
[25] Pan, L.-P., Hazzard, J.T., Lin, J., Tollin, G. and Chan, S.I. (1991) J. Am. Chem. Soc. 113, 5908–5910.
[26] Hill, B.C. (1991) J. Biol. Chem. 266, 2219–2226.
[27] Stowell, M.H.B., Larsen, R.W., Winkler, J.R., Rees, D.C. and Chan, S.I. (1993) J. Phys. Chem. 97, 3054–3057.
[28] Capaldi, R.A. (1990) Arch. Biochem. Biophys. 280, 252–262.
[29] Babcock, G.T. and Wikström, M. (1992) Nature 356, 301–309.
[30] Bisson, R., Steffens, G.C.M., Capaldi, R.A. and Buse, G. (1982) FEBS Lett. 144, 359–363.
[31] Millett, F., de Jong, C., Paulson, L. and Capaldi, R.A. (1983) Biochemistry 22, 546–552.
[32] Taha, S.M. T. and Ferguson-Miller, S. (1992) Biochemistry 31, 9090–9097.
[33] Bolgiano, B., Salmon, I., Ingledew, W.J. and Poole, R.K. (1991) Biochem. J. 274, 723–730.
[34] Bolgiano, B., Salmon, I. and Poole, R.K. (1993) Biochim. Biophys. Acta 1141, 95–104.
[35] Ohnishi, T. and Trumpower, B.L. (1980) J. Biol. Chem. 255, 3278–3284.
[36] Rodkey, F.L. and Ball, E.G. (1950) J. Biol. Chem. 182, 17–28.
[37] Ksenzhek, O.S., Petrova, S.A. and Kolodyazhny, M.V. (1982) Bioelect. Bioenerg. 9, 167–174.
[38] Trumpower, B.L. (1990) J. Biol. Chem. 265, 11409–11412.
[39] Larsen, R.W., Pan, L.-P., Musser, S.M., Li, Z. and Chan, S.I. (1992) Proc. Natl. Acad. Sci. USA 89, 723–727.
[40] Trumpower, B.L. and Berry, E.A. (1985) J. Biol. Chem. 260, 2458–2467.
[41] Sone, N., Sekimachi, M. and Kutoh, E. (1987) J. Biol. Chem. 262, 15386–15391.
[42] Puustinen, A., Morgan, J.E., Verkhovsky, M., Thomas, J.W., Gennis, R.B. and Wikström, M. (1992) Biochemistry 31, 10363–10369.
[43] Matsushita, K., Shinagawa, E., Adachi, O. and Ameyama, M. (1990) Proc. Natl. Acad. Sci. USA 87, 9863–9867.
[44] Lauraeus, M., Haltia, T., Saraste, M. and Wikström, M. (1991) Eur. J. Biochem. 197, 699–705.
[45] Santana, M., Kunst, F., Hullo, M.F., Rapaport, G., Danchin, A. and Glaser, P. (1992) J. Biol. Chem. 267, 10225–10231.
[46] Anemüller, S. and Schäfer, G. (1989) FEBS Lett. 244, 451–455.
[47] Anemüller, S. and Schäfer, G. (1990) Eur. J. Biochem. 191, 297–305.
[48] Lübben, M., Kolmerer, B. and Saraste, M. (1992) EMBO J. 11, 805–812.
[49] Anemüller, S., Bill, E., Schäfer, G., Trautwein, A.X. and Teixeira, M. (1992) Eur. J. Biochem. 210, 133–138.
[50] Zimmerman, B.H., Nitsche, C.I., Fee, J.A., Rusnak, F. and Münck, E. (1988) Proc. Natl. Acad. Sci. USA 85, 5779–5783.
[51] Fee, J.A., Zimmerman, B.H., Nitsche, C.I., Rusnak, F. and Münck, E. (1988) Chem. Scripta 28A, 75–78.
[52] Mather, M.W., Springer, P., Hensel, S., Buse, G. and Fee, J.A. (1993) J. Biol. Chem. 268, 5395–5408.
[53] Garcia-Horsman, J.A., Barquera, B. and Escamilla, J.E. (1991) Eur. J. Biochem. 199, 761–768.
[54] de Vrij, W., Heyne, R.I.R. and Konings, W.N. (1989) Eur. J. Biochem. 178, 763–770.
[55] Sone, N. and Yanagita, Y. (1982) Biochim. Biophys. Acta 682, 216–226.
[56] Ishizuka, M., Machida, K., Shimada, S., Mogi, A., Tsuchiza, T., Ohmori, T., Souma, Y., Gonda, M. and Sone, N. (1990) Biochemistry 108, 866–873.
[57] Lauraeus, M., Haltia, T., Saraste, M. and Wikström, M. (1991) Eur. J. Biochem. 197, 699–705.
[58] Saraste, M. (1990) Quart. Rev. Biophys. 23, 331–366.
[59] Fujiwara, T., Fukumori, Y. and Yamanaka, T. (1992) J. Biochem. 112, 290–298.
[60] Sone, N. and Fujiwara, Y. (1991) FEBS Lett. 288, 154–158.